Mass spectrometric studies of RNA modification patterns in mammals

Dissertation

zur Erlangung des Doktorgrades

der Naturwissenschaften

Vorgelegt beim Fachbereich 14

Der Johann Wolfgang Goethe-Universität

In Frankfurt am Main

von

Paria Asadi Atoi

aus Savadkoh, Iran

Frankfurt 2023

(D 30)

Vom Fachbereich 14, der Biochemie, Chemie und Pharmazie

Johann Wolfgang Goethe - Universität als Dissertation angenommen.

Dekan:

Prof. Dr. Clemens Glaubitz

Gutachter:

1.Gutachterin: Prof. Dr. Stefanie Kaiser (geboren Kellner)

2.Gutachter: Prof. Dr. Jens Wöhnert

Datum der Disputation: 02.06.2023

Erklärung

Except where stated otherwise by reference or acknowledgment, the work presented was generated by myself under the supervision of my advisor **Prof. Dr. Stefanie Kaiser** during my doctoral studies. All contributions from colleagues are explicitly referenced in the thesis.

The material listed below was obtained in the context of collaborative research:

Figure 3. 13: Proteomics differential volcano plot of cortex and liver for the 100 highest NAA or NAG, collaboration partner: **MSc. Gregor Ammann**, Goethe Universität, contribution: providing proteomics data, my contribution: supporting corresponding RNA data.

Figure 3. 21 Quantification of RNA modifications in pulse-chase NAIL-MS experiment after AlkBH3 KD, collaboration partner: **Dr. Felix Hagelskamp**, LMU München, contribution: providing NAIL-MS RNA data, my contribution: supporting protein western blot data, and partly cell culture experiments.

Figure 3. 23 Quantification of RNA modifications in the pulse-chase NAIL-MS experiment after AlkBH1 knockdown. collaboration partner: **Dr. Felix Hagelskamp**, LMU München, contribution: providing NAIL-MS RNA data, my contribution: supporting protein western blot data, and partly cell culture experiments.

Figure 3. 25 Turnover rates of different RNA species during the pulse-chase NAIL-MS experiment after AlkBH5 knockdown. collaboration partner: **Dr. Kayla Borland**, LMU München, contribution: providing NAIL-MS RNA data, my contribution: supporting protein western blot data, and partly cell culture experiments.

Figure 3. 26 Quantification of RNA modification m^6A in the pulse-chase NAIL MS experiment after AlkBH5 KD. collaboration partner: **Dr. Felix Hagelskamp**, LMU München, contribution: providing NAIL-MS RNA data, my contribution: supporting protein western blot data, and partly cell culture experiments.

Figure 3. 27 Quantification of m^6A modification in mRNA in the pulse-chase NAIL MS experiment after AlkBH5 KD. collaboration partner: **Dr. Kayla Borland**, LMU München, contribution: providing NAIL-MS RNA data, my contribution: supporting protein western blot data, and partly cell culture experiments.

……

Paria Asadi Atoi

I humbly dedicate this dissertation to the brave women of my homeland, Iran.

woman, life, freedom

زن، زندگی، آزادی

Acknowledgments

[redacted]

Table of Contents

List of publications

"Benefits of stable isotope labeling in RNA analysis." **Asadi Atoi P**, Barraud P, Tisne C, Kellner S. *Biological Chemistry*. **2019** Jul 1;400(7):847-65.

"Strategies to Avoid Artifacts in Mass Spectrometry-Based Epitranscriptome Analyses." Kaiser S, Byrne SR, Ammann G, **Asadi Atoi P**, Borland K, Brecheisen R, DeMott MS, Gehrke T, Hagelskamp F, Heiss M, Yoluç Y. *Angewandte Chemie International Edition*. **2021** Oct 25;60(44):23885-93.

"Profiling and dynamics study of organ- and RNA species-specific modifications in mouse tissues." **Asadi Atoi P**, Kaiser S, *et al*., in progress.

Abbreviations

(D)MRM	(Dynamic) multiple reaction monitoring
°C	Degree celcius
µg	Microgram
µL	Microlitre
µm	Micrometre
3D	3-dimensional
A	Adenosine
Å	Angstrom (unit)
ac^{4}C	N4-acetylcytidine
Acm D	Actinomycin D
AlkB	α-ketoglutarate-dependent dioxygenase AlkB
AlkBH	α-ketoglutarate-dependent dioxygenase AlkB Homologue
Am	2'-O-methyladenosine
Arg	Arginine
ASCC3	Activating signal co-integrator 1 complex subunit 3
Asp	Aspartic acid
BHT	Butylated hydroxytoluene
bp	Base pair
e.g.	For example
C	Cytidine
CIP	Calf intestinal phosphatase
Cm	2'-O-methylcytidine
Cys	Cysteine
D	Dihydrouridine
i.e.	That is
DMEM	Dulbecco's Modified Eagle Medium
DMSO	Dimethyl sulphoxide
DNA	Deoxyribonucleic acid
dNTP	Deoxyribonucleoside-5'-triphosphate
DTT	Dithiothreitol
E. coli	Escherichia coli (lat.)
EDTA	Ethylenediaminetetraacetate
eq	Equivalent
ESI	Electrospray ionisation
esiRNA	Endoribonuclease-prepared siRNA
FBS	Fetal bovine serum
FTO	Fat mass and obesity-associated protein
G	Guanosine
Glu	Glutamic acid
Gly	Glycine
Gm	2'-O-methylguanosine
GTP	Guanosine triphosphate
h	Hours
HEK	Human embryonic kidney cells
HeLa	Henrietta Lacks cells
His	Histidine
hm^{5}C	5-hydroxymethylcytidine
HPLC	High performance liquid chromatography

I	Inosine
IVT	In vitro transcription
KD	Knockdown
kDa	Kilo-Dalton
ctrl	Control
LC	Liquid chromatography
LC-MS/MS	Liquid chromatography coupled with tandem mass spectrometry
LSU	Large ribosomal subunit
M	Molar
m/z	Mass-to-charge ratio
m^1A	1-methyladenosine
m^1G	1-methylguanosine
$m^{22}G$	2,2-dimethylguanosine
m^3C	3-methylcytidine
m^5C	5-methylcytidine
m^5Cm	5,2'-O-dimethylcytidine
$m^{66}A$	6,6-dimethyladenosine
m^6A	6-methyladenosine
m^7G	7-methylguanosine
MALDI	Matrix-Assisted Laser Desorption Ionisation
METTL	Methyltransferase-like
min	Minute
Mio	Million
miRNA	Micro RNA
mL	Millilitre
mm	Millimetre
MMS	Methyl methanesulphonate
mRNA	Messenger RNA
MS	Mass spectrometry
n.s.	Not significant
NAIL-MS	nucleic acid isotope labelling coupled mass spectrometry
ng	nanogram
Nm	Nucleoside with methylation at O-2´position
NMR	nuclear magnetic resonance
NTP	Nucleosidetriphosphate
NSUN2	NOP2/Sun RNA methyltransferase 2
nts	Nucleotides
LOD	Limit of detection
LOQ	Limit of quantification
P	Phosphorylated
PBS	phosphate-buffered saline
PTC	peptidyl transferase center
PCR	polymerase chain reaction
p-value	Significance value
Q	Queuosin
QQQ	Triple quadrupole
Rib.	Ribose
RNA	Ribonucleic acid
rNTP	Ribonucleoside 5'-triphosphate
ROS	Reactive oxygen species
RP	Reversed phase
rpm	Revolutions per minute

rRNA	Ribosomal RNA
Rt	Retention time
S. cerevisiae	Saccharomyces cerevisiae (lat.)
scr.	Scramble
SEC	Size exclusion chromatography
SILAC	Stable isotope labelling of amino acids in cell cultures
SILIS	Stable isotopes labelled internal standard
siRNA	Small interfering RNA
snoRNA	Small nucleolar RNA
SPD	Snake venom phosphodiesterase
SSC	Saline sodium citrate
SSU	Small ribosomal subunit
TEA	Triethylamine
THU	Tetrahydrouridine
ToF	Time of flight
Tris	Tris(hydroxymethyl)aminomethane
TRMT	tRNA methyltransferase
tRNA	Transfer RNA
U	Uridine
U/µL	Enzymatic units per microlitre
Um	2'-O-methyluridine
UV	Ultraviolet radiation
Val	Valine
x g	Several times the acceleration due to gravity
yW	Wybutosin
α-KG	α-ketoglutarate
Ψ	Pseudouridine

Abstract

RNAs are key players in life as they connect the genetic code (DNA) with all cellular processes dominated by proteins. The dynamics study of RNA modifications has become an important part of epitranscriptomics field, as they are reversible and dynamically regulated far more than originally thought. Several evidences portrait a catalog of RNA modifications and their links to neurological disorders, cancers, and other diseases. Therefore, a deeper investigation of RNA modifications dynamics including their specific profile, biosynthesis, maturation and degradation is required for pioneering disease diagnostics and potential therapeutics development.

Mammalian tissues reveal diverse physiology and functions, despite sharing identical genomes and overlapping transcription profiles. So far, most research on this diversity were referred to variable transcriptomic processing among tissues and differential post-translational modifications that tune the activity of ubiquitous proteins to each tissue's needs. However, study of epitranscriptome dynamics relevance to tissues' functions is not yet revealed. There are a few reports on mouse RNA modification profiles, which are focused on only one type of RNA and limited types of modifications. The first part of my dissertation aims to generate a comprehensive tissue-specific as well as RNA species-specific investigation of all existing RNA modifications, as well as investigating potential codon as an effector of translation diversity among tissues. Using isotope dilution mass spectrometry, I created a library including absolute quantification of 24 tRNA modifications, and up to 22 rRNA modifications. I find an almost identical pattern of modifications in 28S- and 18S-rRNA subunits, but different levels of most modifications in 5.8S-rRNA or tRNA among highly metabolic active organs to *e.g.* heart or spleen. The findings suggest a high degree of similarity between quantities of modifications between presented data to all previous literature, confirming that it is a suitable model to study the tissue-based RNA modification patterns.
The most noticeable difference exhibited was tRNA modifications, which suggests a discerning tRNA engagement in translation between different organs. This can be a good start for investigation of codon bias in enriched genes of specific tRNA modifications among different tissues that may cause differential translation pattern, causing organs diversity. Moreover, 5.8S rRNA data showed an organ-specific pattern, which proposes functional diversity of this rRNA subunit among different organs. Future studies must investigate the possible implications of organ-specific 5.8S rRNA modifications functions, to elucidate the core of the observed variations.

Abundance of RNA modifications is carefully regulated in cells. Part of this regulation is achieved by activity of enzymes removing RNA modifications, named RNA erasers. Literature has provided proof of demethylation activity of AlkBH family on different types of RNA. For instance, AlkBH5 is known to remove m^6A in mRNA, and both AlkBH3 and AlkBH1 are reported to demethylate m^1A and m^3C in tRNA. So far, RNA erasers are mainly studied *in vitro* and direct *in vivo* studies are missing.

Mass spectrometry is a promising approach in the identification and quantification of many RNA modifications. However, mass spectrometric analysis by nature, offers only a static view of nucleic acid modifications, and fails to account for their cellular dynamics. **N**ucleic **A**cid

Isotope **L**abeling coupled **M**ass **S**pectrometry (**NAIL-MS**) was developed as a powerful technique which differentiates among remaining, co-transcriptional and post-transcriptional incorporation of a target RNA modification. This temporal resolution captures the dynamic nature of RNA modifications, and offers absolute and relative quantification of all existing nucleosides in any given RNA sequence, including different isotopologues and isotopomers.

The objective of this study was to uncover the first "direct" *iv vivo* data on AlkBH1, 3 and 5 activities in demethylating each of their specific substrates. I investigated the RNA modification changes through pulse-chase experiments in collaboration with my colleagues **Dr. Kayla Borland** and **Dr. Felix Hagelskamp**. A remarkable observation was that AlkBH3 protein -but not AlkBH1- was overexpressed under methylating reagent treatment *in vivo*. These findings suggest that AlkBH3 -but not AlkBH1- is a methylation damage induced enzyme, that potentially triggers ASCC-AlkBH3 alkylation repair complex after aberrant methylation damage by MMS treatment. However, using NAIL-MS method, we could not detect any significant effect on demethylation activity of the enzymes in tRNA, rRNA or mRNA towards the possible substrates m^6A, m^1A, m^3C, m^5C and m^7G *in vivo*. These distinct outcomes can be partially explained by probable existence of other unidentified demethylases that compensate for AlkBHs demethylation activity; or more probably, demethylation may still arise by remaining active AlkBHs to restore the original levels of the observed RNA modifications, since a stronger KD or a complete knockout of AlkBHs genes was not possible. Further research on fully knocked out AlkBHs genes can provide stronger evidence on unidentified demethylation activities in HEK cells.

Inspired by the recent study of Wollen *et al.* on AlkBH3 partnership with ASCC3 in demethylating MMS-induced m^1A and m^3C from mRNA, I aimed to follow up the connection of *in vivo* AlkBH3 demethylation activity to aberrant methylation stress, triggering ASCC-AlkBH3 alkylation repair complex in human HEK cells, in collaboration with **Dr. Marie Luise Winz** (JGU Mainz).
The findings indicate a connection between MMS stress to a significant increase in the amounts of m^1A and m^3C. Interestingly, m^7G (the main damage in RNA of *E. coli* and yeast) was not increased in the mRNA. My data suggests no significance in methylation repair of KD AlkBH3 or ASCC3 cells, and therefore supports the existence of other unidentified demethylation pathways that compensate for the absence of AlkBH3 or ASCC3. This demonstrates that the complex machinery of aberrant methylation stress-response in human cells, might provide a recompense for AlkBH3 absence by other unidentified demethylases or at least, by remaining active AlkBH3 and thus restoring the original levels of the observed RNA modifications.
Given the study's methodology, it was impossible to follow the methylation damage removal for longer time points than 4 h after stress. Future studies must investigate the possible implications of complete knockout of AlkBH3 gene, during a longer post-methylation stress time.

Another helpful feature of dynamic NAIL-MS is the opening to follow up the dynamics of external RNA sequences within cells, by differentiating between the isotopic labeled native RNA and the unlabeled synthetic RNA. Angiogenin (ANG) is a stress-induced ribonuclease that shows functions in pathophysiology of neurodegenerative disorders, such as Parkinson's disease (PD). Under stress conditions, ANG cleaves tRNA into stress induced tRNA halves (tiRNA). So far, very little is known about functions and dynamics of tiRNAs. Drino *et al*. have identified and characterized native tRNA-Gly_{GCC} derived stress induced halve (tiRNA). Their

study suggested existence of m^2G and Um on the 5´-tiRNA$^{Gly}_{GCC}$ but no m^1G, m^7G, m^2G, $m^{22}G$, Am, and m^6A from the precursor tRNA^{Gly}. The research in this chapter aimed to investigate tRNA fragments (tRFs) stability in context of modification status. I specifically studied the 5´-tiRNA$^{Gly}_{GCC}$ Um modification incorporation relationship to its stability *in vivo,* focusing on a method development for including only biological uptake and exclude biological as well as technical variables that can cause concentration/dilution effects. In order to overcome the uncontrollable variations of sample preparation and analysis, I introduced a new technical standard namely **S**table **I**sotope **L**abelled **I**n **V**itro **T**ranscribed technical internal standard (**SIL-IVT**), by in vitro transcription of a stable isotopologues of the target analyte: ^{13}C-nucleobases and ribose labeled tRNA$^{Val}_{AAC}$. Finally, inspection of modification incorporation effect on 5´-tRF$^{Gly}_{GCC}$ stability in HEK cells was performed, using 4 biological replicates of each modified or unmodified synthetic tRF$^{Gly}_{GCC}$ transfection into HEK cells. My data suggested no significance in the temporal stability between 4-Um modified or unmodified constructs, as both remained in cells for at least 24 h post-transfection phase. This chapter's outcome provides information about model tiRNA stability in cells which can shed light to its functional relevance.

Briefly, numerous mechanisms behind RNA modification dynamics and differences in modification profiles is observed through the application of NAIL-MS. This powerful method allowed me to profile all RNA modifications existing in several tissues in mouse, which opens a door to further investigating epitranscriptome regulations connection to tissues diversities, and much more. The knowledge of mentioned investigated mechanisms could be useful for initiating clinical purposes due to the increasing interest in RNA modifications and their far-reaching influences in diseases and therapeutics potential.

Zusammenfassung (Kurzversion)

RNAs spielen eine Schlüsselrolle im Leben, da sie den genetischen Code (DNA) mit allen zellulären Prozessen verbinden, die von Proteinen beherrscht werden. Die Untersuchung der Dynamik von RNA-Modifikationen ist zu einem wichtigen Teil der Epitranskriptomik geworden, da sie reversibel sind und weitaus stärker dynamisch reguliert werden als ursprünglich angenommen. Es gibt zahlreiche Belege für eine Vielzahl von RNA-Modifikationen und ihre Verbindung zu neurologischen Störungen, Krebs und anderen Krankheiten. Daher ist eine genauere Untersuchung der Dynamik von RNA-Modifikationen, einschließlich ihres spezifischen Profils, ihrer Biosynthese, Reifung und ihres Abbaus, für eine innovative Krankheitsdiagnostik und die Entwicklung potenzieller Therapeutika erforderlich.

Gewebe von Säugetieren weisen trotz identischer Genome und überlappender Transkriptions-profile unterschiedliche Physiologie und Funktionen auf. Die meisten Forschungsarbeiten zu dieser Diversität bezogen sich bisher auf die unterschiedliche transkriptomische Verarbeitung in den verschiedenen Geweben und auf unterschiedliche posttranslationale Modifikationen. Die Untersuchung der Epitranskriptomdynamik, die für die Funktionen der Gewebe relevant ist, ist jedoch noch nicht bekannt. Der erste Teil meiner Dissertation zielt darauf ab, eine umfassende gewebespezifische sowie RNA-Spezies-spezifische Untersuchung aller vorhandenen RNA Modifikationen zu erstellen. Zudem, soll ein potenzieller Codon-bias als Ursache für Translations-unterschiede zwischen den Geweben untersucht werden Mit Hilfe der Isotopenverdünnungs-Massenspektrometrie habe ich eine Bibliothek (Datenbank) erstellt, die die absolute Quantifizierung von 24 tRNA-Modifikationen und bis zu 22 rRNA-Modifikationen umfasst. Es zeigt sich ein fast identisches Muster von Modifikationen in den 28S- und 18S-rRNA-Untereinheiten, aber unterschiedliche Niveaus in 5,8S-rRNA oder tRNA in hochgradig stoff-wechselaktiven Organen, z. B. Herz oder Milz. Die Ergebnisse deuten auf eine große Die Ergebnisse deuten auf eine große Übereinstimmung zwischen den Modifikationsmengen der präsentierten Daten und der gesamten bisherigen Literatur hin, was bestätigt, dass es sich um ein geeignetes Modell zur Untersuchung der gewebebasierten RNA-Modifikationsmuster handelt. Die auffälligsten Unterschiede waren in tRNAs zu finden, was ein guter Ausgangspunkt für die Untersuchung, ob tRNA-Mods über Interaktionen mit dem Codon-Usage-Bias verschiedener Gene zu unterschiedlichen Translationsmuster führen können. Darüber hinaus zeigten die 5.8S rRNA-Daten ein organspezifisches Muster, was auf eine funktionelle Vielfalt dieser rRNA-Untereinheit in verschiedenen Organen hindeutet.

Die Menge der RNA-Modifikationen wird in Zellen sorgfältig reguliert. Ein Teil dieser Regulierung wird durch die Aktivität von Enzymen erreicht, die RNA-Modifikationen entfernen, die RNA-demethylierenden Enzyme (Erasers). In der Literatur wurde die Aktivität der RNA- Erasers der AlkBH-Familie bei verschiedenen RNA-Typen nachgewiesen. Bislang wurden RNA-Eraser hauptsächlich *in vitro* untersucht, und es fehlen direkte *In-vivo* Studien.

Die Massenspektrometrie ist ein vielversprechender Ansatz für die Identifizierung und Quantifizierung vieler RNA-Modifikationen. Allerdings bietet die massenspektrometrische Analyse naturgemäß nur eine statische Sicht auf die Nukleinsäuremodifikationen und berücksichtigt nicht deren zelluläre Dynamik. Die **N**ucleic **A**cid **I**sotope **L**abeling coupled **M**ass **S**pectrometry (**NAIL-MS**) wurde als leistungsfähige Technik entwickelt, die zwischen

verbleibender, kotranskriptioneller und posttranskriptioneller Inkorporation einer Ziel-RNA-Modifikation differenziert. Diese zeitliche Auflösung erfasst die dynamische Natur von RNA-Modifikationen und bietet eine absolute und relative Quantifizierung aller vorhandenen Nukleoside in einer beliebigen RNA-Sequenz, einschließlich verschiedener Isotopologe und Isotopomere.
Ziel dieser Studie war es, die ersten "direkten" *iv-vivo*-Daten über die Aktivitäten von AlkBH1, 3 und 5 bei der Demethylierung ihrer spezifischen Substrate zu ermitteln. In Zusammenarbeit mit meiner Kollegien **Dr. Kayla Borland** und meinem Kollegen **Dr. Felix Hagelskamp** untersuchte ich die Veränderungen der RNA-Modifikation durch Puls-Chase-Experimente. Eine bemerkenswerte Beobachtung war, dass AlkBH3 – nicht aber AlkBH1 – unter der Behandlung mit dem Methylierungsreagenz in vivo überexprimiert wurde. Diese Ergebnisse deuten darauf hin, dass AlkBH3 ein Enzym ist, das durch Methylierungsschäden induziert wird und möglicherweise den ASCC-AlkBH3-Alkylierungsreparaturkomplex nach eines externen-eingeführten Methyl-ierungsschadens durch MMS-Behandlung auslöst. Mit der NAIL-MS-Methode konnten wir jedoch keine signifikanten Auswirkungen auf die Demethylierungsaktivität auf tRNA, rRNA oder mRNA gegenüber den möglichen Enzymsubstraten m^6A, m^1A, m^3C, m^5C und m^7G in vivo feststellen. Angeregt durch eine aktuelle Studie von Wollen et al. über das Zusammenspiel von AlkBH3 mit ASCC3 bei der Demethylierung von MMS-induziertem m^1A und m^3C aus mRNA wollte ich außerdem in Zusammen mit **Dr. Marie Luise Winz** (JGU Mainz) den Zusammenhang zwischen der In-vivo-Demethylierungsaktivität von AlkBH3 und Methylierungsstress, der den ASCC-AlkBH3-Alkylierungsreparaturkomplex in menschlichen HEK-Zellen auslöst, unter-suchen. Die Ergebnisse deuten auf einen Zusammenhang zwischen MMS-Stress und dem Anstieg der Mengen von m^1A und m^3C hin. Außerdem deuten meine Daten darauf hin, dass die Methylierungsreparatur von KD-AlkBHs-Zellen im Vergleich zu Kontrollzellen keine Rolle spielt, und sprechen daher für die Existenz anderer, noch nicht identifizierter Demethyl-ierungswege oder für die Aktivität der verbleibenden AlkBHs bei der Wiederherstellung der ursprünglichen Mengen der Substratmodifikationen. Weitere Untersuchungen an vollständig ausgeschalteten AlkBHs-Genen könnten weitere Beweise für nicht identifizierte Demethyl-ierungsaktivitäten in HEK-Zellen liefern.

Ein weiteres hilfreiches Merkmal der dynamischen NAIL-MS ist die Möglichkeit, die Dynamik externer RNA-Sequenzen in Zellen zu verfolgen, indem zwischen der isotopenmarkierten nativen RNA und der unmarkierten synthetischen RNA unterschieden wird. Angiogenin (ANG) ist eine Ribonuklease, die unter Stress tRNA in sogenannte Stress-induzierte tRNA-Hälften (tiRNA) spaltet. Bislang ist nur sehr wenig über die Funktionen und die Dynamik von tiRNAs bekannt. Drino *et al.* haben native $tRNA^{Gly}_{GCC}$-abgeleitete tiRNAs identifiziert und charakterisiert. Ihre Studie deutet auf die Existenz von m^2G und Um in der 5'-$tiRNA^{Gly}_{GCC}$ hin. Meine Forschung zielte darauf ab, die Stabilität von tRNA-Fragmenten (tRFs) im Zusammenhang mit dem Modifikationsstatus zu untersuchen. Insbesondere die Beziehung zwischen dem Einbau von Um in 5'-$tiRNA^{Gly}_{GCC}$ und der Stabilität dieser tiRNA *in vivo* wurde untersucht. Ein spezieller Schwerpunkt wurde auf die Entwicklung einer Methode exklusiv für die biologische Aufnahme in die Zelle, ohne Berücksichtigung anderer biologischer oder technischer Variablen, die zu Konzentrations- oder Verdünnungseffekten führen könnten. Um für zufällige Schwankungen bei der Probenvorbereitung und -analyse zu kontrollieren, habe ich einen neuen technischen Standard eingeführt, nämlich **S**table **I**sotope **L**abelled **I**n **V**itro **T**ranscribed technical internal standard (**SIL-IVT**), der durch in vitro

Transkription eines stabilen Isotopologen des Zielanalyten hergestellt wird. Schließlich wurde die Auswirkung des Einbaus von Modifikationen auf die Stabilität von 5'-tRF$^{Gly}_{GCC}$ in HEK Zellen durch Transfektion von modifizierten und unmodifizierten tRF-Konstrukten untersucht. Meine Daten zeigten keine signifikanten Unterschiede in der zeitlichen Stabilität zwischen modifizierten und unmodifizierten 4-Um-Konstrukten, da beide für mindestens 24 Stunden nach der Transfektion in den Zellen verblieben. Die Ergebnisse dieses Kapitels liefern Informationen über die Stabilität von synthetischen tiRNA-Analoga in Zellen, die Aufschluss über ihre funktionelle Bedeutung geben können.

Kurz gesagt, zahlreiche Mechanismen hinter der Dynamik der RNA-Modifikation und Unterschiede in den Modifikationsprofilen werden durch die Anwendung von NAIL-MS beobachtet. Diese vielseitig anwendbare Methode ermöglichte es mir, alle RNA-Modifikationen in verschiedenen Geweben der Maus zu charakterisieren, was Möglichkeiten zur weiteren Untersuchung der Epitraskriptomik in Verbindung mit Gewebseunterschieden und vielem mehr eröffnet. Das Wissen über die genannten untersuchten Mechanismen könnte aufgrund des zunehmenden Interesses an RNA Modifikationen und ihren weitreichenden Einflüssen auf Krankheiten und das therapeutische Potenzial nützlich sein.

Zusammenfassung

RNAs spielen eine Schlüsselrolle im Leben, da sie den genetischen Code (DNA) mit allen zellulären Prozessen verbinden, die von Proteinen beherrscht werden. Die Untersuchung der Dynamik von RNA-Modifikationen ist zu einem wichtigen Teil der Epitranskriptomik geworden, da sie reversibel sind und weitaus stärker dynamisch reguliert werden als ursprünglich angenommen. Es gibt zahlreiche Belege für eine Vielzahl von RNA-Modifikationen und ihre Verbindung zu neurologischen Störungen, Krebs und anderen Krankheiten. Daher ist eine genauere Untersuchung der Dynamik von RNA-Modifikationen, einschließlich ihres spezifischen Profils, ihrer Biosynthese, Reifung und ihres Abbaus, für eine innovative Krankheitsdiagnostik und die Entwicklung potenzieller Therapeutika erforderlich.

Gewebe von Säugetieren weisen trotz identischer Genome und überlappender Transkriptionspro-file unterschiedliche Physiologie und Funktionen auf. Die meisten Forschungsarbeiten zu dieser Diversität bezogen sich bisher auf die unterschiedliche transkriptomische Verarbeitung in den verschiedenen Geweben und auf unterschiedliche posttranslationale Modifikationen. Die Untersuchung der Epitranskriptomdynamik, die für die Funktionen der Gewebe relevant ist, ist jedoch noch nicht bekannt. Der erste Teil meiner Dissertation zielt darauf ab, eine umfassende gewebespezifische sowie RNA-Spezies-spezifische Untersuchung aller vorhandenen RNA Modifikationen zu erstellen. Zudem, soll ein potenzieller Codon-bias als Ursache für Translationsunterschiede zwischen den Geweben untersucht werden Mit Hilfe der Isotopenverdünnungs-Massenspektrometrie habe ich eine Bibliothek (Datenbank) erstellt, die die absolute Quantifizierung von 24 tRNA-Modifikationen und bis zu 22 rRNA-Modifikationen umfasst.

Zu diesem Zweck wurden verschiedene Gewebe von vier Mäusen, darunter drei Männchen und ein Weibchen, lysiert und die Gesamt-RNA extrahiert, die mittels Größenausschluss-chromatographie in 28S-, 18S-, 5.8S-rRNA und tRNA aufgetrennt wurde. Jede isolierte RNA-Spezies wurde dann mittels LC-MS/MS analysiert und mit Prism aufgezeichnet. Alle quantifizierten Modifikationen wurden auf "pro entsprechende 10^3 kanonische Nukleoside" normalisiert, um einen Vergleich zwischen den Geweben für jeden RNA-Typ und umgekehrt zu ermöglichen. Darüber hinaus wurde mit Hilfe der Shotgun-Proteomik die direkte Verbindung zwischen codonreichen Genen spezifischer tRNA-Anticodon-Modifikationen und ihrer entsprechenden Aminosäureproduktion untersucht.

Es zeigt sich ein fast identisches Muster von Modifikationen in den 28S- und 18S-rRNA-Untereinheiten, aber unterschiedliche Niveaus in 5,8S-rRNA oder tRNA in hochgradig stoffwechselaktiven Organen, z. B. Herz oder Milz. Die Ergebnisse deuten auf eine große Die Ergebnisse deuten auf eine große Übereinstimmung zwischen den Modifikationsmengen der präsentierten Daten und der gesamten bisherigen Literatur hin, was bestätigt, dass es sich um ein geeignetes Modell zur Untersuchung der gewebebasierten RNA-Modifikationsmuster handelt.

Die auffälligsten Unterschiede waren in die tRNA-Modifikationen zu finden, was auf eine unterschiedliche Beteiligung der tRNA an der Translation in den verschiedenen Organen hindeutet. Dies ein guter Ausgangspunkt für die Untersuchung, ob tRNA-Mods über Interaktionen mit dem Codon-Usage-Bias verschiedener Gene zu unterschiedlichen

Translationsmuster führen können, die unterschiedliche Translationsmuster verursachen und organspezifische Translations-funktionen auslösen können.

Ich habe mich insbesondere auf tRNA U34-Modifikationen wie mcm^5U und mcm^5s^2U konzentriert, die bei der Dekodierung von NAA- und NAG-Codons helfen. Die Tatsache, dass ich im Durchschnitt 4.55 mcm^5U pro 10^3 nts in tRNA im Kortex, aber nur 2.75 in der Leber beobachtete, löste die Untersuchung möglicher translatorischer Konsequenzen aus, die auf die Hochregulierung von Genen zurückzuführen sind, die für NAA-Codons im Kortex im Vergleich zur Leber angereichert sind, während einer Zusammenarbeit mit meinem Kollegen **MSc. Gregor Ammann**. Obwohl eine direkte Verbindung von mcm^5U-entsprechenden codon-angereicherten Genen zu ihren Aminosäuren nicht möglich war, da keine Aminosäuren-basierte Bibliothek (Datenbank) pro Gewebe in Mäusen vorhanden war.

Darüber hinaus zeigten die 5.8S rRNA-Daten ein organspezifisches Muster, was auf eine funktionelle Vielfalt dieser rRNA-Untereinheit in verschiedenen Organen hindeutet. Zukünftige Studien müssen die möglichen Auswirkungen organspezifischer 5.8S rRNA-Modifikationen untersuchen, um den Bildung der beobachteten Variationen zu klären. Nichtsdestotrotz deutet die Quantifizierung der Modifikationen in der Maus auf Variationen in einigen Modifikationszahlen pro gegebener RNA-Spezies hin, von denen bisher angenommen wurde, dass sie in allen Geweben der Maus konserviert sind. Dies ist ein guter Ausgangspunkt für die Untersuchung von Codon-Bias zwischen verschiedenen Geweben, die zu einer unterschiedlichen Translationsaktivität führen können, die wiederum die Organvielfalt bedingt.

Die Häufigkeit von RNA-Modifikationen wird in Zellen sorgfältig reguliert. Ein Teil dieser Regulierung wird durch die Aktivität von Enzymen erreicht, die RNA-Modifikationen entfernen, den so genannten RNA-Erasers. In der Literatur ist die Demethylierungsaktivität der AlkBH-Familie für verschiedene RNA-Typen nachgewiesen worden. So ist beispielsweise bekannt, dass AlkBH5 m^6A in mRNA entfernt, und sowohl AlkBH3 als auch AlkBH1 demethylieren m^1A und m^3C in tRNA. Bislang wurden RNA-Eraserer hauptsächlich in vitro untersucht, und es fehlen direkte In-vivo-Studien.

Die Massenspektrometrie ist ein vielversprechender Ansatz für die Identifizierung und Quantifizierung vieler RNA-Modifikationen. Allerdings bietet die massenspektrometrische Analyse naturgemäß nur eine statische Sicht auf die Nukleinsäuremodifikationen und berücksichtigt nicht deren zelluläre Dynamik. Die **N**ucleic **A**cid **I**sotope **L**abeling coupled **M**ass **S**pectrometry (**NAIL-MS**) wurde als leistungsfähige Technik entwickelt, die zwischen verbleibender, kotranskriptioneller und posttranskriptioneller Inkorporation einer Ziel-RNA-Modifikation differenziert. Diese zeitliche Auflösung erfasst die dynamische Natur von RNA-Modifikationen und bietet eine absolute und relative Quantifizierung aller vorhandenen Nukleoside in einer beliebigen RNA-Sequenz, einschließlich verschiedener Isotopologe und Isotopomere.

Ziel dieser Studie war es, die ersten "direkten" *iv-vivo*-Daten über die Aktivitäten von AlkBH1, 3 und 5 bei der Demethylierung ihrer spezifischen Substrate zu ermitteln. In Zusammenarbeit mit meiner Kollegien **Dr. Kayla Borland** und meinem Kollegen **Dr. Felix Hagelskamp** untersuchte ich die Veränderungen der RNA-Modifikation durch Puls-Chase-Experimente.

Zu den Experimenten in diesem Kapitel gehören die In-vivo-Knockdowns (KD) der einzelnen Enzyme, die anschließende Belastung der Zellen mit dem Methylierungsreagenz MMS und die Verfolgung der Expressionsniveaus der Enzyme sowie der Veränderungen der RNA-

Modifikation unter den genannten Behandlungen mit Western Blotting und NAIL-MS. Western Blotting wurde in mehreren Schritten etabliert und validiert, um Daten über die in vivo KD der einzelnen AlkBH-Proteine sowie deren Expression unter MMS-Behandlung zu erhalten, wobei HEK-Zellen als eukaryotisches Modell verwendet wurden. Western-Blot-Daten bestätigten die erfolgreiche KD von AlkBH1, 3 und 5 bis zu mindestens 50 %.

Eine bemerkenswerte Beobachtung war, dass AlkBH3 – nicht aber AlkBH1 – unter der Behandlung mit dem Methylierungsreagenz in vivo überexprimiert wurde. Diese Ergebnisse deuten darauf hin, dass AlkBH3 ein Enzym ist, das durch Methylierungsschäden induziert wird und möglicherweise den ASCC-AlkBH3-Alkylierungsreparaturkomplex nach eines externen-eingeführten Methylierungsschadens durch MMS-Behandlung auslöst. Mit der NAIL-MS-Methode konnten wir jedoch keine signifikanten Auswirkungen auf die Demethylierungsaktivität auf tRNA, rRNA oder mRNA gegenüber den möglichen Enzymsubstraten m^6A, m^1A, m^3C, m^5C und m^7G in vivo feststellen. Diese Ergebnisse lassen sich teilweise durch die wahrscheinliche Existenz anderer, noch nicht identifizierter Demethylasen erklären, die AlkBHs-Demethyl-ierungsaktivität kompensieren. Wahrscheinlicher ist jedoch, dass die Demethylierung immer noch durch die verbleibenden aktiven AlkBHs erfolgt, um das ursprüngliche Niveau der beobachteten RNA-Modifikationen wiederherzustellen, da eine stärkere KD oder ein vollständiger Knockout der AlkBHs-Gene nicht möglich war. Weitere Untersuchungen an vollständig ausgeschalteten AlkBHs-Genen können einen besseren Beweis für nicht identifizierte Demethylierungsaktivitäten in HEK-Zellen liefern.

Angeregt durch eine aktuelle Studie von Wollen *et al.* über das Zusammenspiel von AlkBH3 mit ASCC3 bei der Demethylierung von MMS-induziertem m^1A und m^3C aus mRNA wollte ich meine Hypothese weiterverfolgen, dass die In-vivo-Demethylierungsaktivität von AlkBH3 mit Methylierungsstress beim Menschen zusammenhängen könnte, indem der ASCC-AlkBH3-Alkylierungsreparaturkomplex bei abnormen Methylierungsschäden ausgelöst wird. Ziel dieser Arbeit war es, der Zusammenhang zwischen der AlkBH3- oder ASCC3-KD-Wirkung unter MMS-Stress auf ausgewählte Modifikationen in der mRNA zu untersuchen.

In Zusammenarbeit mit **Dr. Marie Luise Winz** (JGU Mainz) wurden HEK-Zellen zunächst mit siRNA behandelt, die entweder auf AlkBH3-, ASCC3- oder ZNF598-mRNA-Transkripte abzielt, und nach erfolgreicher KD wurden die Zellen mit MMS behandelt und zu den Zeitpunkten nach der Belastung geerntet. Anschließend wurde die isolierte mRNA für die Nukleosid-MS-Analyse aufbereitet. Zur Normalisierung wurde die Häufigkeit der Modifikationen auf die entsprechenden Guanosin-Nukleoside bezogen.

Die Ergebnisse weisen auf einen Zusammenhang zwischen MMS-Stress und einem signifikanten Anstieg der Mengen von m^1A und m^3C hin. Interessanterweise war m^7G (der Hauptschaden in der RNA von E. coli und Hefe) in der mRNA des Menschen nicht erhöht. Die Ergebnisse für die gemeinsamen RNA-Methylierungsschäden m^1A, m^3C, m^7G, m^6A und den Nicht-Schaden m^5C als Negativkontrolle deuten darauf hin, dass m^1A und m^3C die wichtigsten Methylierungs-schadensprodukte in menschlicher mRNA nach MMS-Behandlung sind, während sich kein Schaden m^7G in menschlicher tRNA nach MMS-Exposition bildet. Was die Beseitigung von Methylierungsschäden nach der Belastung betrifft, so ist in den Kontrollproben nach 4 Stunden eine Abnahme der Häufigkeit von m^1A und m^3C zu beobachten.

Außerdem deuten meine Daten darauf hin, dass die Methylierungsreparatur von KD-AlkBHs-Zellen im Vergleich zu Kontrollzellen keine Rolle spielt, und sprechen daher für die Existenz anderer, nicht identifizierter Demethylierungswege, die das Fehlen von AlkBH3 oder ASCC3 kompensieren. Dies zeigt, dass die komplexe Maschinerie der abweichenden Methylierungs-stressreaktion in menschlichen Zellen einen Ausgleich für das Fehlen von AlkBH3 durch andere, noch nicht identifizierte Demethylasen oder zumindest durch verbleibendes aktives AlkBH3 bieten könnte, wodurch die ursprünglichen Werte der beobachteten RNA-Modifikationen wiederhergestellt werden. Aufgrund der Methodik der Studie war es nicht möglich, die Beseitigung der Methylierungsschäden über einen längeren Zeitraum als 4 Stunden nach der Belastung zu verfolgen. Zukünftige Studien müssen die möglichen Auswirkungen eines vollständigen Knockouts des AlkBH3-Gens während einer längeren Zeit nach dem Methylierungsstress untersuchen.

Ein weiteres hilfreiches Merkmal der dynamischen NAIL-MS ist die Möglichkeit, die Dynamik externer RNA-Sequenzen in Zellen zu verfolgen, indem zwischen der isotopenmarkierten nativen RNA und der unmarkierten synthetischen RNA unterschieden wird. Angiogenin (ANG) ist eine Ribonuklease, die unter Stress tRNA in sogenannte Stress-induzierte tRNA-Hälften (tiRNA) spaltet. Bislang ist nur sehr wenig über die Funktionen und die Dynamik von tiRNAs bekannt. Drino *et al.* haben native $tRNA^{Gly}_{GCC}$-abgeleitete tiRNAs identifiziert und charakterisiert. Ihre Studie deutet auf die Existenz von m^2G und Um in der 5'-$tiRNA^{Gly}_{GCC}$ hin. Meine Forschung zielte darauf ab, die Stabilität von tRNA-Fragmenten (tRFs) im Zusammenhang mit dem Modifikationsstatus zu untersuchen. Insbesondere die Beziehung zwischen dem Einbau von Um in 5'-$tiRNA^{Gly}_{GCC}$ und der Stabilität dieser tiRNA *in vivo* wurde untersucht. Ein spezieller Schwerpunkt wurde auf die Entwicklung einer Methode exklusiv für die biologische Aufnahme in die Zelle, ohne Berücksichtigung anderer biologischer oder technischer Variablen, die zu Konzentrations- oder Verdünnungseffekten führen könnten.

Die Daten wurden durch Transfektion von nicht modifizierten oder mit Um inkorporierten 5'-tRF^{Gly}_{GCC}-Sequenzen in HEK-Zellen als Modelle für 5'$tiRNA^{Gly}_{GCC}$ gewonnen. Zunächst wurden verschiedene Schritte der Qualitätskontrolle einschließlich Reinheit, Sequenzidentität, Länge und Modifikationsstatus der beiden tRFs bestätigt. Dann wurde eine Methode entwickelt, um die dynamische biologische Aufnahme der RNA innerhalb von 72 Stunden nach der Transfektion zu messen.

Um für zufällige Schwankungen bei der Probenvorbereitung und -analyse zu kontrollieren, habe ich einen neuen technischen Standard eingeführt, nämlich **S**table **I**sotope **L**abelled **I**n **V**itro **T**ranscribed technical internal standard (**SIL-IVT**), der durch in vitro Transkription eines stabilen Isotopologen des Zielanalyten hergestellt wird: ^{13}C-Nukleobasen und Ribose-markierte $tRNA^{Val}_{AAC}$.

Um Fehler bei der Berechnung der relativen Häufigkeit der externen RNA im Vergleich zur RNA der nativen Zellen zu vermeiden, habe ich außerdem versucht, die Schwankungen der Zellzahlen durch Einführung eines Korrekturfaktors für die Zählung der Zellen auszuschließen. Schließlich wurde die Auswirkung des Einbaus von Modifikationen auf die Stabilität von 5'-tRF^{Gly}_{GCC} in HEK-Zellen durch Transfektion von modifizierten und unmodifizierten tRF-Konstrukten untersucht.

Meine Daten zeigten keine signifikanten Unterschiede in der zeitlichen Stabilität zwischen modifizierten und unmodifizierten 4-Um-Konstrukten, da beide für mindestens 24 Stunden

nach der Transfektion in den Zellen verblieben. Obwohl der Einbau von Um in das synthetische 5'-tRF$^{Gly}_{GCC}$-Konstrukt seine zeitliche Stabilität in HEK-Zellen nicht verbesserte, führte es auch nicht zu einem schnelleren Abbau in den Zellen. Dies zeigt, dass der Einbau von Um-Modifikationen in tRF für seine zeitliche Stabilität in Zellen irrelevant ist. Die Ergebnisse dieses Kapitels liefern Informationen über die Stabilität von synthetischen tiRNA-Analoga in Zellen, die Aufschluss über ihre funktionelle Bedeutung geben können.

Diese Studie schließt nicht aus, dass endogen produzierte tiRNAs lokal an bestimmten subzellulären Stellen wirken und die stressbedingte Zellphysiologie auf biologisch und kinetisch sinnvolle Weise beeinflussen. Weitere Untersuchungen der lokalisierten mechanistischen Merkmale der tRFs, einschließlich intrinsischerer tiRNA-Modifikationen, unter Verwendung fluoreszenzmarkierter Konstrukte und Ko-Färbung verschiedener Zellorganellen durch dynamische live-cell imaging in Kombination mit paralleler NAIL-MS-Analyse können die unbekannten Funktionen der tiRNAs auf der Grundlage ihrer Akkumulationsmuster in den Zellen im Laufe der Zeit aufklären.

Kurz gesagt, zahlreiche Mechanismen hinter der Dynamik der RNA-Modifikation und Unterschiede in den Modifikationsprofilen werden durch die Anwendung von NAIL-MS beobachtet. Diese vielseitig anwendbare Methode ermöglichte es mir, alle RNA-Modifikationen in verschiedenen Geweben der Maus zu charakterisieren, was Möglichkeiten zur weiteren Untersuchung der Epitraskriptomik in Verbindung mit Gewebseunterschieden und vielem mehr eröffnet. Das Wissen über die genannten untersuchten Mechanismen könnte aufgrund des zunehmenden Interesses an RNA Modifikationen und ihren weitreichenden Einflüssen auf Krankheiten und das therapeutische Potenzial nützlich sein.

1.Introduction

1.1. Ribonucleic acids properties in living cells

RNA structural face, building block of life

A conceptual scenario states that sometime around 4 billion years ago, there was a form of life on Earth when ribonucleic acid (RNA) or something chemically very similar, performed most of the information processing and metabolic transformations needed for life to emerge from chemistry.[1] By contrast, the awareness that RNA is a good candidate for the beginning of life is an idea only ~50 years old: year 1953, when Francis Crick and James Watson succeeded in structural revelation of deoxyribonucleic acid (DNA) as a double helix shaped from phosphate-sugar chains, and the horizontal pairs of bases holding the chains together.[2] Since then, the term "central dogma" of molecular biology -first spoken by Crick in 1958 and revised later in 1970- states that information cannot be transferred from protein to either protein or nucleic acid, but only *vice versa*. Fundamentally, DNA is transcribed, *i.e.* transferred into RNA, which sequentially serves as a template for translation, *i.e.* translation into proteins.[3] While this provides a highly simplified representation of the equivalent cellular processes, the core statement remains valid to this day.

RNA is a biological polymer, constructed of four nucleobases that make up the polyribonucleotide: adenine, guanine, cytosine, and uracil. DNA also consists of the same four major bases except that thymine substitutes for uracil. Thymine, of course, is actually 5-methyluracil (m^5U). These bases are coupled to the C1' atom of a ribose (deoxyribose in DNA) via a glycosidic bond.
The pyrimidine and purine based nucleosides are interlinked by phosphodiester bonds between the 3' carbon of one nucleotide and the 5' carbon of its neighboring nucleotide.[4] The linked nucleotides via phosphodiester-ribose backbone (or in short phosphate backbone), form a strand of nucleobases. (Fig **1.1**)

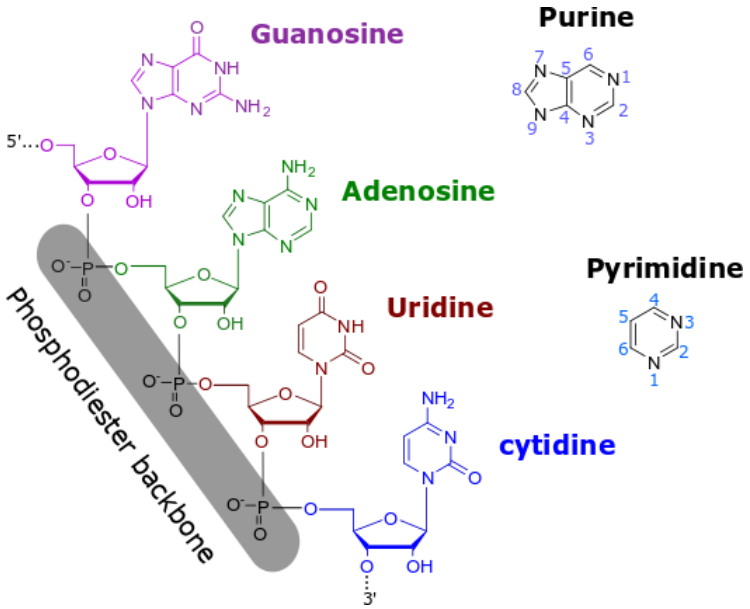

Figure 1. 1 Structure of RNA. The nucleobases from top to bottom (5' → 3') are guanine (G), adenine (A), uracil (U) and cytosine (C). Each nucleoside is shown by a separated color, and phosphate backbone is highlighted in gray. On the right side, the structure and numbering order of the nucleic acid heterocycles are shown.

RNA biological face, genetic code to protein

Genetic information for protein sequence is encoded in DNA, while the actual assembly of amino-acids into proteins occurs in cytoplasmic ribonucleoprotein particles called ribosomes. The fact that proteins are not synthesized directly on genes demands the existence of an intermediate information carrier, known as a stable RNA. Although untranscribed nucleotides in genomes are rare, alternative combinations of exons are widespread. The large proportion of a eukaryotic genome that is transcribed thus produces a huge array of RNA molecules.[5] RNA is not only a messenger operating between DNA and protein, but also numerous non-protein-coding RNA species are generated for transcription of essentially the entire eukaryotic genome, which show complex overlapping patterns of expression and regulation.

The defined apposition of RNA nucleotides forms a primary sequence in different RNA species differing in size, abundance and protein-coding capability. The messenger RNA (mRNA) which serves as a short-term storage of genetic information, consist of several thousand nucleotides which contain the basic blueprint for protein biosynthesis and is a protein-coding RNA species. The term “transcriptome” can be defined as the overall set of RNAs.

Non-protein-coding species (ncRNA) include ribosomal RNAs, which -as assembled ribosomes- are the site of protein biosynthesis. The 28S rRNA is composed of approximately 4700 nucleotides (nts), the 18S rRNA about 1900 nts, 5.8S rRNA 160 nts and 5S rRNA 120 nts. Furthermore, there are the 75-90 nts long transfer RNAs (tRNAs), which act as adapter molecules by reading mRNA codons and delivering amino acids to build protein.[6-8] Small regulatory RNAs, such as microRNA (miRNA, 20–24 nts) and small interfering RNA (siRNA, ~22nt), are also among the non-coding RNAs, that regulate gene expression post-

transcriptionally by binding to specific mRNA targets and promoting their degradation and/or translational inhibition.[9]

However, all these RNA molecules differ not only in their sequential arrangement of the nucleotides which creates their primary structures, but also in their spatial structure, which is determined via folding of these nucleotide chains by hydrogen bonds between the nucleobases, which creates a secondary structure. Formation of the base pairs C-G and U-A (T-A in DNA) is crucial for creation of the secondary structure. Since these interactions were the first structure-determining connections discovered in DNA, they are also referred to as Watson-Crick base pairs, with base pair C-G forming three hydrogen bonds, and the base pair U-A forming two. Similar to DNA, the formation of base pairs in RNA can also lead to the assembly of double-stranded molecules. Hydrogen bonds are also primarily responsible for the subsequent folding into the tertiary structure, but in some cases other interactions such as dipole-dipole and van der Waals forces are also involved.[10]

RNA synthesis and biogenesis

Individual nucleotides are regularly biosynthesized from small metabolites such as CO_2, glutamine, aspartate, glycine, formate and glucose in the cells and subsequently serve the assembly of RNA molecules, according to specific sequential arrangements for each RNA species.[11]
All RNAs in the cell are produced with the help of DNA or RNA binding polymerases. The central event in transcription is the RNA polymerase–catalyzed "copying" the sequence of the template strand of a gene into a revearse-complementary RNA transcript. The polymerase enzymes belong to the subclass of nucleotidyl transferases, since they add a nucleotide to the existing RNA strand by forming a phosphodiester bond. The RNA polymerases are categorized into either DNA-dependent, which produce RNA from a DNA template, or RNA-dependent RNA polymerases. In that case, the polymerases involved in the polyadenylation of mRNAs are the Poly(A) polymerase and polynucleotide phosphorylase, which contributes to both the assembly and disassembly of the poly(A) tail of the mRNA.[12, 13]

One mechanism for regulating gene activity via transcription might involve multiple RNA polymerases with different template specificities. Studies suggest that regulation of RNA synthesis in bacteria may involve regulatory modifications of a single basic polymerase. On the other hand, multiple RNA polymerases are involved in specific transcription of the chief classes of RNA in eukaryotic cells.[14]

The much larger fraction of DNA-dependent RNA polymerases is in turn divided into single enzyme polymerases, such as the T7 bacteriophage polymerase, and the multimeric enzyme complexes. While in prokaryotic organisms, a single RNA polymerase can synthesize the complete transcriptome of all RNAs in a cell, eukaryotes require several RNA polymerases. In 1969, the first chromatographic separation from sea urchins and rat liver by Roeder *et al.* elucidated the existence of RNA polymerase I (pol I) to be responsible for 28S, 18S and 5.8S rRNA synthesis, pol II responsible for mRNAs and small RNAs, and pol III for tRNA, 5S rRNA and some other small RNAs. Plants also possess two other RNA Polymerases namely IV and V, which synthesize siRNAs and thus contribute to gene regulation.[14, 15]

For the transcription of RNA species, different gene segments in the DNA must be targeted by the polymerases. The transcription process for each polymerase can be distributed into the following three steps: initiation, elongation and termination. More precisely, the initiation is the formation of a preinitiation complex (PIC) consisting of the polymerase, the gene promoter sequence and various transcription factors. Elongation, *i.e.* the extension of the new nucleic acid strand, involves in the transcription of the genes into the corresponding RNA sequence. The final step in transcript formation is termination, which occurs when the elongating transcription complex moves into (or, in some cases, beyond) one or more terminator sequences along the DNA template that may serve as transcription regulators within genes or mark the end of a gene or operon. Termination causes the transcription to stop and the polymerase to be detached from the affected gene segment.[16]

Chemical modifications in RNA

For more than half a century, the presence of chemically modified nucleosides in RNA, beyond the basic A, U, C and G including >163 chemically altered residues have been recognized.[17] RNA modifications provide a specific adaptation of RNA molecule to their task in cells. The area around studying RNA modifications, their incorporation into RNA molecules and the molecular effects on RNA epigenetics is known as epitranscriptomics.

Modifications on RNA species can be incorporated either co-transcriptionally -implying that it starts in the nucleus during transcription- *e.g.* the 'life cycle' of an mRNA destined for N6-methyladenosine (m^6A) methylation[18], or post-transcriptionally. Most of the naturally occurring RNA modifications are introduced post-transcriptionally by various enzymes, and modification reactions form very complex pathways, leading to hypermodified residues.[19] Post-transcriptional modifications of RNA introduce a functional diversity that allows the four ribonucleosides to gain diverse functions.

Not all RNA modifications can be biosynthesized by the organisms in which they are found, but can be transported as a nutrient, *e.g.* by the microbiome.[20] Furthermore, some RNA modifications are reversible, *i.e*. the modified residues can get enzymatically demodified, allowing a quick post-transcriptional response to changing cellular or environmental conditions.[21]

These epitranscriptomic modifications can affect the RNA itself (*e.g.* directly affecting the RNA structure) or need specialized readers to fulfill their purpose. Modifications can directly influence RNA structure, by promoting or disrupting certain intramolecular interactions. they can make the RNA molecule more rigid or more flexible. They can also influence RNA interactions with other molecules, in particular proteins. Overall, they contribute strongly to the diversity of functions fulfilled by RNA molecules, especially within complex regulatory networks, where small subtle structural changes can bring about significant changes to cellular metabolism.[22]

The naming of modifications follows a uniform nomenclature, in which each individual atom of the nucleosides is assigned to a fixed number. The pyrimidines (C and U) are numbered

according to the IUPAC nomenclature. The counting method starts in the nucleobase at the nitrogen of the glycosidic bond and is continued in such a way that the heteroatoms located in the ring are assigned the smallest possible numbers. The numbering of purines traditionally starts at the ring nitrogen furthest from the glycosidic bond and ends at the nitrogen of the glycosidic bond (Figure **1.2**). The numbering of ribose follows the IUPAC nomenclature according to the Fischer projection, with each position here additionally given an apostrophe to ensure differentiation between the atoms of the ribose and the nucleobase. Since the phosphate groups of the nucleotides each connect the 5' position of the ribose of one nucleoside to the 3' position of the previous nucleoside, each RNA strand has a 5' end (beginning) and a 3' end (end). The hydroxyl group at the 2' carbon of the ribose remains free (see Figure **1.1**).[23]

For the additional functional groups of the RNA modifications, the abbreviations of the group are placed before the abbreviation of the corresponding canonical nucleoside: m for methyl, s for sulfur, n for amino, and many more (complete list in **Table S1**). A superscript between the two letters indicates the position of the group in the ring (*e.g.* 5-methyl cytidine: m^5C). If there are several groups, they are listed one after the other. If a group appears several times at the same ring position, either a subscript for the number or another version of the superscript is inserted.

(*e.g.* N6,N6-Dimethyladenosine: $m^6{}_2A$ or $m^{66}A$). If the functional group is located on the ribose, the corresponding abbreviation is added only after the abbreviation of the canonical nucleoside (*e.g.* 2'-O-methyluridine: Um). Some modifications have large functional groups or, for other reasons, are difficult to name by the nomenclature described above. Here, particular letters/symbols are sometimes used (*e.g.* pseudouridine: Ψ, queuosine: Q, wybutosine: yW).

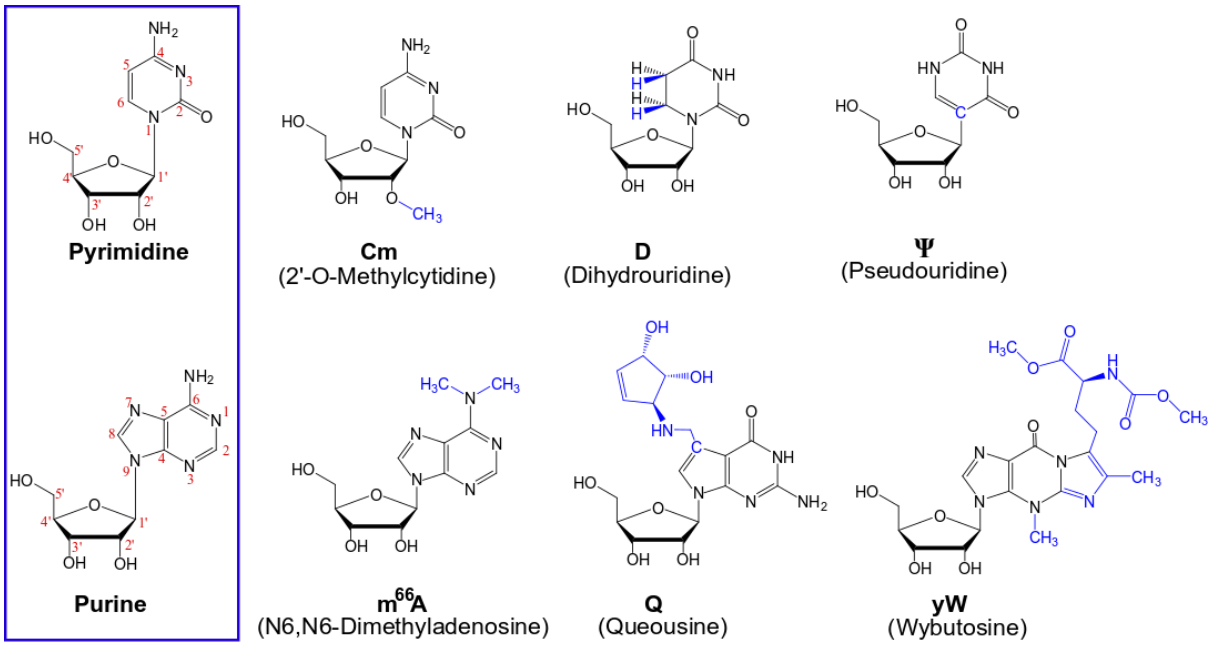

Figure 1. 2 Nomenclature and examples of RNA modifications. The counting method for correct nomenclature of pyrimidine (C and U) and purine (G and A) modifications is indicated in the given box on the left side. Some modifications to illustrate the correct nomenclature are shown on the right side.

The first ever detected RNA modification was Pseudouridine (Ψ) (fig **1.2**).[24] Much evidence exists, that the modifications play a major role in the function of the nucleic acids.

The mitochondrial protein synthesis machinery differs in many ways from translation in the cytoplasm. Mitochondrial RNA (mtRNA) modifications regulate the metabolic reprogramming that is required for the invasion and dissemination of tumor cells from primary tumors.[25] To translate the essential subunits of the respiratory chain complex, the mitochondrial genome contains 22 tRNAs that get modified at 137 positions by 18 types of RNA modifications.[26] The function of these RNA modifications is to determine the accuracy and optimal rate of translation.[27] However, the presented thesis is primarily focused on cytosolic RNA, therefore more detailed structure and function of these RNA species along with their modifications is presented in the following sections.

1.2. RNA molecules structure and functions

tRNA is the most heavily modified RNA with regards to number, density and diversity. After tRNA which contains up to 17% modifications, rRNA with approximately 2% modifications is the next highly modified class of RNAs.[28]

The diversity of RNA molecules is enhanced by a dynamic expansion of RNA modifications or a removal of modifications. Numerous enzymes modify the synthesized RNA strands at specific sites within the sequence. As a result, the modification profile of the RNA is constantly changing by the work of distinctive writer or eraser enzymes. The writer enzymes attach modifications to the RNA or extend modifications, while Eraser enzymes, on the other hand remove RNA modifications. The following sections will focus on tRNA and rRNA molecules structure and functions, as they occupy a major part of my modifications profiling study.

tRNA molecule structure and function

tRNA is a key bridging molecule between the RNA world and protein world. tRNAs are non-coding RNAs with about 70-100 nucleotides and are key players in translation. tRNA is attached to an amino acid which is determined by the mRNA codon, whereas rRNA is required for peptide bond formation between aminoacylated tRNA substrates. In this context, tRNA has two distinct qualities. It carries an anticodon which is reverse complementary to the mRNA codon via hydrogen bonds and from the other side, binds to the corresponding amino acid in a reaction catalyzed by a specific aminoacyl-tRNA synthetase enzyme (fig **1.3 A**).[29]
tRNAs are characterized by a secondary structure made up of three hairpin loops and a terminal helical stem (cloverleaf) which fold into an L-shaped tertiary structure. (fig **1.3**).
A collection of 20 different amino acids, theoretically require a number of 20 different corresponding tRNA molecules. Due to the arrangement of four different bases (C, U, G, and A) in a triplet results however, $4^3 = 64$ different anticodon possibilities exist. tRNAs with distinct anticodons that carry the same aminoacid are called tRNA isoacceptors. To abbreviate each isoacceptors name, the abbreviation of the corresponding amino acid is superscript, followed by its specific anticodon in subscript. For example, for Valine (Val), the tRNA isoacceptor with the anticodon AAC is abbreviated as $tRNA^{Val}_{AAC}$. On the other hand, there

are tRNA molecules that share the same anticodon but have differences in their body sequence, which are called tRNA isodecoders.
Almost all tRNA isoacceptors display a cloverleaf secondary structure, which is subdivided into: the acceptor stem with a CCA residue aminoacyl-tRNA synthetase linked to the 3' end of the tRNA. After the acceptor stem comes the D-arm starting from the 5'-end, the anticodon arm, the variable loop and the T arm (also known as TΨC arm), Each arm consists of a double-stranded stem, in which individual bases pair with each other via hydrogen bonds, and a single-stranded pair with each other, also called a loop. The acceptor stem and the D-arm are mainly involved in correct recognition by aminoacyl tRNA synthetases involved and ensure the loading of the tRNA molecule with the appropriate amino acid. Moreover, the so-called discriminator base, which is located directly 5' upstream to the CCA attachment, and other sequence elements that are typically in the anticodon arm serve for recognition by aminoacyl-tRNA synthetases (Figure **1.3**).[30]

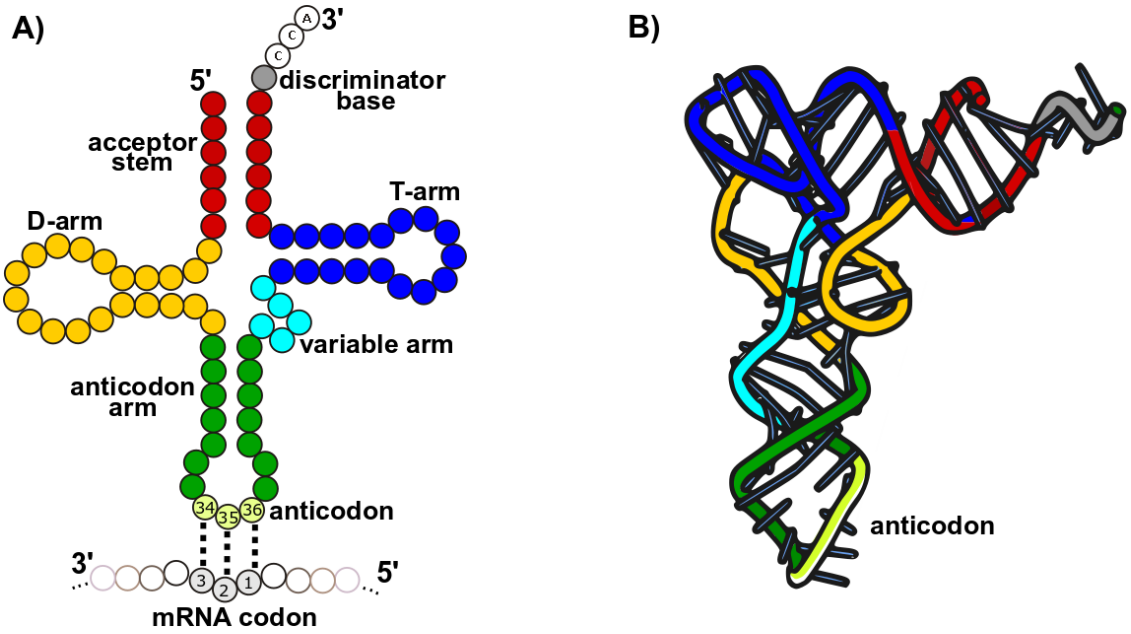

figure 1. 3 The structure of tRNA. (A) Two-dimensional cloverleaf structure of tRNA and the base pairings of the tRNA anticodon with the mRNA codon. **(B)** tRNAs fold into an L-shape in three dimensions, which is maintained by intramolecular base-pairing. Colored in both diagrams: the acceptor stem (red), dihydrouridine (D)-arm (yellow), anticodon stem (dark green), anticodon (bases 34, 35, 36 light green), variable arm (light blue), T-arm (dark blue) and discriminator base (gray).

The T arm is mainly involved in interactions with the ribosome and thus supports efficient translation. For folding into the L-shaped tertiary structure, portions of the D-loop hybridize with the T-loop, which together form the "elbow" domain of the tRNA. The variable loop has a variable length in different tRNA molecules. A continuous numbering of the tRNA molecules is often not possible due to the different length of the variable loop. Instead, individual positions in the D-loop and the variable loop, which are only occasionally represented in tRNA molecules, are skipped during progressive numbering and are numbered with additional letters.

Like the codons of mRNA, the tRNA anticodon consists of three consecutive nucleobases. The anticodon of each tRNA pairs in a reverse complementary manner with the corresponding codon of the mRNA and thus ensures the incorporation of the correct amino acid into the growing polypeptide chain. The anticodon is thus always located at positions 34-36 and other regularly occurring modifications, such as Ψ55 in the T loop, are thus always given the same number. This enables the comparison of the modification profile between different tRNA molecules.
The tRNA anticodon structure is defined by the presence of an array of conserved and semi-conserved nucleotides. Among them, a uridine is recurrently observed at position 33; the base at position 32 is generally a pyrimidine, the bases at positions 37 and 38 are essentially purines, the three bases at the anticodon positions 34, 35, and 36 display a nearly equal proportion of the four nucleotides; positions 34 and 37 accept a large number of modified nucleotides. A very limited number of modified nucleotides are observed at positions 35 and 36. Uridines when present at position 39 are mainly modified into pseudouridines (Ψ).[31, 32]

rRNA molecule structure and function

The ribosome is a ribonucleoprotein complex that conducts one of lifes universal processes: synthesis of proteins. Unlike other cellular polymerases, ribosomes typically contain 50 to 60% RNA as an integral part of its structure. The large ribosomal subunit (LSU) contains the peptidyl transferase center (PTC) and catalyzes transpeptidation.[33] The small ribosomal subunit (SSU) contains the decoding center and reads messenger RNA (mRNA). Much of ribosomal function is performed by ribosomal RNAs (rRNAs), while the ribosomal proteins act primarily as structural stabilizers.[34, 35]

In prokaryotic cells (both eubacteria and archaebacteria), ribosomes contain three ribosomal RNA molecules, usually 5S, 16S, and 23S rRNA, which contain about 120, 1540, and 2900 nucleotides respectively. In eukaryotic ribosomes, the three core classes of rRNA are usually called 5S, 18S, and 28S rRNA. Most eukaryotic cytoplasmic ribosomes contain a 5.8S rRNA as well, which corresponds to the 160 nts at the 5' terminus of prokaryotic 23S rRNA. Some insects also have a 2S rRNA subunit which corresponds to the 3' side (~25 nts) of 5.8S rRNA. Particular regions of rRNA show extremely high sequence conservation. One can think of "typical" 16S-like and 23S-like rRNAs to have about 1500 and 2900 nucleotides respectively, and the other types as variants of those. Typical rRNAs would comprise those of eubacteria, archaebacteria, chloroplasts, and plant mitochondria; the variant types would include eukaryotic cytoplasm and the remaining mitochondrial rRNAs.
Eukaryotic ribosomes are much bigger and more complex than their bacterial counterparts, containing additional rRNA in the form of expansion segments (ES) as well as many additional r-proteins and r-protein extensions.[35]

The binding sites for the aminoacyl-tRNA (A site), peptidyl-tRNA (P site), and deacylated tRNA (exit or E site) on the bacterial ribosome are composed predominantly of rRNA.[36] This is conserved in archaeal and eukaryotic ribosomes, suggesting that the basic mechanism by which the ribosome distinguishes the cognate tRNA from the near or noncognate tRNAs at the A site during decoding is also likely to be conserved. Nevertheless, many r-proteins encroach on the tRNA-binding sites and appear to play important roles in decoding, accommodation,

and stabilization of tRNAs.[37] These r-proteins may be responsible for the slightly different positioning of tRNAs on the eukaryotic ribosome compared with the bacterial ribosome.

At the PTC of the LSU, the CCA endings of the A- and P-tRNAs are stabilized by interaction with the conserved A- and P-loops of the 23S rRNA,[38] thus positioning the α-amino group of the A-tRNA for nucleophilic attack on the carbonyl of the peptidyl-tRNA.
A high sequence and structural conservation of the PTC and the tRNA substrates among archaeal and bacterial ribosomes is observed with eukaryotic ribosomes, which suggests that the mechanism of peptide bond formation is similar. Nevertheless, the varying specificity for binding of antibiotics to the PTC of bacterial *vs* eukaryotic LSU indicates that subtle differences do in fact exist.[39]

In eukaryotes, translation initiation generally requires a scanning mechanism that starts at the 5′-7-methyl-guanosine (5′-m^7G) cap of mRNA and proceeds to the appropriate AUG start codon, often the first AUG codon encountered by the initiation machinery.[40]

As the nascent polypeptide chain (NC) is being synthesized, it goes through a tunnel within the LSU and appears at the solvent side, where protein folding occurs. Cryo-EM reconstructions and X-ray crystallography structures of bacterial, archaeal, and eukaryotic cytoplasmic ribosomes have revealed the universality of the dimensions of the ribosomal tunnel.[41, 42] growing evidence indicates that the tunnel plays a more active role in regulating the rate of translation, in providing an environment for early protein folding events, and in recruiting translation factors to the tunnel exit site.[43] Folding of NCs within the tunnel may have implications for not only protein folding, but also downstream events, such as recruitment of chaperones or targeting machinery.[44, 45]

In eukaryotes, the start codon is identified through base-triplet scanning by the initiator-tRNA bound 40S ribosomal subunit (43S complex), starting from the usually m^7G-capped 5′ end until the correct AUG start codon is found and the 48S initiation complex is formed. At least 13 initiation factors are involved in translation initiation which results in the formation of the 80S initiation complex on joining of the 60S ribosomal subunit (figure **1.4**).[40, 46]

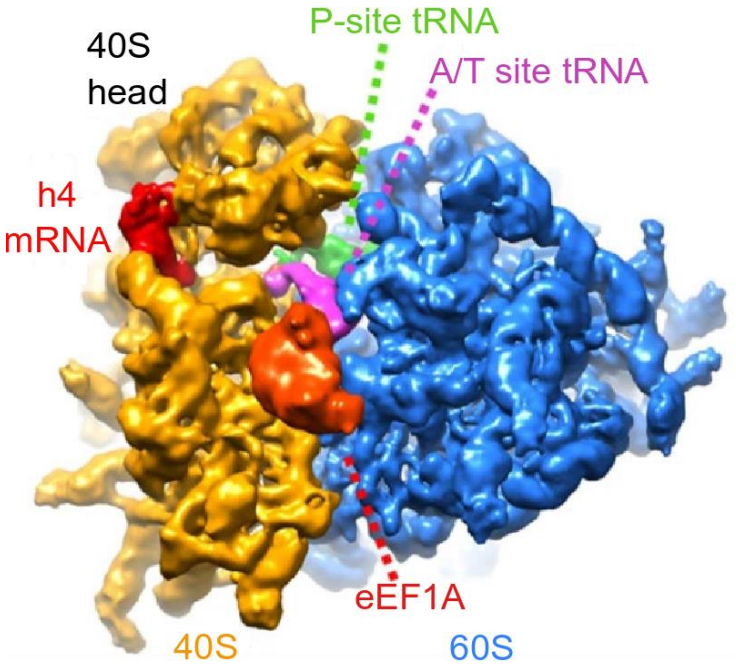

figure 1. 4 Overview of eukaryotic translation assembly, including mRNA-helix 4 (h4)/rRNA 80S complex stalled in the pre-translocation state with mRNA (red), eEF1A (red), A/T-site tRNA (purple), P-site tRNA (green), 60S ribosomal subunit (blue) and 40S ribosomal subunit (orange). structure adapted from Martin *et al.*[47]

The work cycle during which a new amino acid is incorporated on the growing polypeptide chain, so called elongation cycle, is a repetitive multistep process covering aminoacyl-tRNA (A-tRNA) selection, peptide bond formation, and the mRNA-tRNA translocation. This process requires a fine balance between rate and fidelity.[48] It has been estimated that proteins are synthesized *in vivo* at a rate of 15–20 amino acids per second, with an estimated error rate of below ~10^{-4} .[49] The ribosome achieves this balance by working in coordination with elongation factors EF-Tu and EF-G during the A-tRNA delivery and tRNA translocation steps, respectively.

During termination of translation in eukaryotes, a guanosine triphosphate (GTP)-binding protein, eRF3, functions within a complex with the tRNA-mimicking protein, eRF1, to decode stop codons. tRNA-mimicking protein co-operates with the GTPase and with the functional sites on the ribosome.[50] The post-termination complex is then disassembled, enabling its constituents to participate in further rounds of translation.[51]

1.3. Roles of selective eukaryotic RNA modifications

This chapter will focus more strongly on modifications of each major RNA species including mRNA, rRNA, and tRNA. Since the modification profile of tRNA and rRNA molecules have been investigated more extensively in eukaryotic organisms in this work, the focus will be placed on modifications that are more increasingly found on these molecules in eukaryotes. however, some examples of other highly conserved RNA modifications will also be addressed.

Roles of mRNA modifications

While the first chemical modifications on mRNA were identified >40 years ago, their functional significance has only recently begun to uncover. On the 5´terminus 7-methylguanosine (m^7G) is linked to the first transcribed nucleotide via a 5′ to 5′ triphosphate bridge. The first transcribed nucleotide is methylated on the O-2´position of the ribose (Nm). Internal mRNA modifications described to date in mammals include: N^1 and N^6-methyladenosines (m^1A, m^6A, m^6Am), 3- and 5-methylcytosines (m^3C, m^5C), 5-hydroxymethylcytosine (hm^5C), pseudouridine (Ψ), 2′-O-methylation (Nm), and 4-acetylcytidine (ac^4C). Figure **1.5** shows a schematic view of all mRNA modifications.

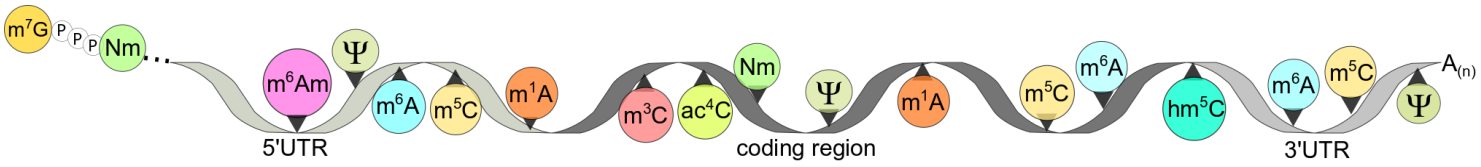

Figure 1. 5 schematic overview of mRNA modifications.

In eukaryotic cells, the mature mRNA, has a three-way structure consisting of a 5´ untranslated region (5´ UTR), a coding region consisted of many triplet codons that each encode an amino acid and a 3´ untranslated region (3´ UTR) (**fig 1.5**).[52]

mRNA as a major product of polymerase II (pol II) is marked during transcription by the addition of a methylated guanosine cap structure to the 5′ terminus. The mRNA cap blocks 5′-3′ exonuclease-mediated degradation and recruits specific RNA processing, export and translation factors. Removal of the cap (decapping) initiates degradation of mRNA. Thus the cap is mechanistically involved in every stage of the mRNA lifecycle.[53]

In mammals, the first existing cap nucleotide is 7-methylguanosine (m^7G), which is linked to the first transcribed nucleotide with a 5′ to 5′ triphosphate linkage. It is methylated on the ribose 2´ position (stands for $m^7GpppNm$, where N is the first transcribed nucleotide). $m^7GpppNm$ was first assumed to exist on all mRNA. Though, due to developments in biochemistry, their organ-specific and cell-specific amounts have been detected. This suggests different regulation of mRNA cap formation in diverse cell lines and/or in response to particular signaling pathways. In addition, second transcribed nucleotide Nm and first nucleotide Am are also readily observed.
Transcription start site influences the cap structure by determining the first transcribed nucleotide. The series of modifications which are detected on internal positions of RNA may also be present on the cap guanosine and cap proximal nucleotides. Yet, the enzymes that have been demonstrated to methylate the cap and neighboring nucleotides are specific for the cap structure, and it is unlikely that enzymes which modify internal residues will also modify the cap.

The occurrence of m^6Am at the 5′ end of transcripts, a reversible modification which is erased by FTO, influences mRNA stability. Another modification affecting adenine is m^1A prevalent

in nuclear mRNAs near translation start codons and also found in mitochondrial mRNA at coding sequence (CDS) and 3′ untranslated regions (UTR)s. Similar to other modifications, m^1A deposition is dynamically regulated by several proteins. Currently, its molecular function remains unknown, although its characteristic localization at 5′ UTRs could suggest a role in translation.[54] While altered activity or expression of its writers, erasers, or substrates is associated with diseases, whether altered m^1A deposition patterns in mRNAs can cause similar pathological outcomes is yet to be revealed.

While m^5C occurrence has been long established in abundant noncoding RNAs, its presence in coding RNAs has recently been shown. Detection approaches exploit the reactivity of unmethylated cytosines to bisulphite or enrich for methylated RNAs.[55] Initial transcriptome-wide profiles have identified hundreds to thousands of m^5C sites in mRNAs. NSUN2 and DNMT2 deposit this modification in mRNA, TET1/TET2/TET3 m^5C erasers demethylate it.[56, 57] Only recently, Aly/REF export factor (reader) has been reported to bind m^5C, indicating a role in nuclear export.[56] Occurrence of m^3C in mRNA deposited by METTL8 has also been described. However, further molecular and functional significance remain undetermined. Uridine is also a target of modifications in a reaction catalyzed by pseudouridine synthases (PUSs) to generate Ψ, the C5-glycosyl isomer of uridine, is the most common modified nucleotide found in RNA throughout all kingdoms of life and the first to be discovered in 1951.[56] In mRNAs, Ψ residues have been detected without positional bias in 5′ UTRs, coding sequences, and 3′ UTRs, which due to extra hydrogen bond donor at the new N1 position, brings stability to tertiary structure of RNA, and for function of the spliceosome.[58] Ψ deposition is regulated in response to environmental signals.[59] Ψ presence alters base-pairing interactions, affecting RNA structures, as well as mRNA coding.

After m^6A deposition on mRNA, carried out by the METTL3/METTL14 methyltransferase complex, functional consequences are orchestrated by a plethora of reader proteins. On the other hand, the discovery of the m^6A eraser, FTO,[60] provided the first evidence of reversible posttranscriptional modifications in mRNAs and reinvigorated interest in mRNA modifications. Since then, complex networks of coordinated writers, erasers, and readers that determine the prevalence and distribution of mRNA modifications have been identified.
As the most prevalent internal modification on eukaryotic mRNA, m^6A participates in almost all steps of RNA metabolism including mRNA translation, degradation, splicing, export and folding. Roles of m^6A in regulation of various cancers have also been reported.[61]

4-acetylcytidine (ac^4C) is similarly described as an mRNA modification that is catalyzed by acetyltransferase NAT10 in human and yeast. In 2018, Arango *et al*. indicated that ac^4C is present in more than 4,000 regions of human transcriptome. In HeLa cells, ac^4C is mainly enriched in the CDS region, and gradually decreases along with the 5′ to 3′ end of the gene transcript.[62] in yeast mRNA, the content of ac^4C was considerably increased under oxidative stress. ac^4C helps the correct codon reading during translation and improves translation efficiency and the stability of mRNA.[63]

Finally, although current epitranscritome studies have primarily focused on base modifications, the ribose can be methylated at the 2′ position to form Nm nucleosides, recently identified in more than 2,000 protein-coding transcripts. Functionally, 2′-O-methylation in coding regions induces ribosome stalling by disrupting codon reading.[64]

Roles of tRNA modifications

tRNA displays a highly conserved secondary and tertiary structure and as mentioned before, the owns the highest number of post-transcriptional modifications among all RNAs. Post-transcriptional modifications of tRNAs are critical for all core aspects of tRNA function, such as stability, folding, and decoding.

Most tRNA modifications were discovered in the 1970s. However, the near-complete description of the genes required to introduce the full set of modifications in both yeast and *Escherichia coli* is relatively recent. Approximately 85 different modifications have been identified in tRNA molecules, with the great majority found at positions 34 and 37 in the anticodon stem loop (ASL), while new ones are still being discovered. These modifications concentrate in two hotspots: the anticodon loop and the tRNA core region, where the D- and T-loop interact with each other, stabilizing the overall structure of the molecule. These modifications can cause large rearrangements as well as local fine-tuning in the 3D structure of a tRNA.[65]

Although the standard rules of the Watson-Crick pairing (A-U, G-C) strictly govern the interaction between base pairs, 1/36 and 2/35, the 3/34 base pairing can be nonstandard (wobble interaction). Therefore, one tRNA molecule can often decode several codons.

In both eukaryotes and bacteria, the pyrimidine-ending codons are generally read by a tRNA harboring a modified G at position 34 (except for Cys and Ser). G34 is often modified to the Gm or Q (and Q derivatives) wobble pairing with U3 or C3. The purine-ending codons are read either by a single tRNA carrying a modified U at position 34 (reading A3 or G3 and mostly used by bacteria) or by two tRNAs, one harboring a modified U and one harboring a C (generally unmodified), reading G3. U34 is often modified to derivatives of xnm^{5}U in bacteria and xcm^{5}U in eukaryotes (reading A3) but can also be doubly modified for added specificity. The oxygen at position 2 of the uracil ring is then replaced by a thio- or seleno- group (cmnm^{5}s^{2}U or mnm^{5}se^{2}U) or a methyl group is added on the 2-hydroxyl of the ribose (cmnm^{5}Um or ncm^{5}Um).

Position 37, which is on the 3 side of the anticodon (also called the dangling base) is also often modified. As a rule, when position 36 is an A or U, position 37 is modified. This diverse set of modifications mainly stabilizes the first base pair of the codon-anticodon interaction, especially A-U and U-A pairs, and thereby contributes to accurate decoding by reducing frameshifts.[66]

Studies showed roles of specific modifications in translation accuracy and efficiency. Lack of several modifications such as Q34, mnm^{5}s^{2}U34, m^{1}G37, yW37, and t^{6}A37 has been associated with increased frameshift phenotypes.[67] The generally accepted model is that nucleoside modifications, mainly those involving positions 34 and 37, contribute to accurate decoding by ordering the ASL and stabilizing the codon-anticodon interactions, therefore preventing ribosome pausing and slippage of the peptidyl-tRNA.[37]

tRNA molecules fold into the so-called L shape and the major interactions maintaining the L

shape occur at the elbow of the tRNA molecule, where the D loop -containing the modification dihydrouridine (D)- and the TΨC loop -containing m^5U and Ψ modifications- meet.
Ψ in tRNA can alter RNA structure, increase base stacking, improve base-pairing, and rigidify the sugar-phosphate backbone.[68, 69] Ψ55 is found in nearly all organisms, and nearly all tRNA isoacceptors, and contributes to the formation of a tertiary base pair with G18 in the D-loop. The improved base stacking may be the most important contribution of Ψ to the stabilization of tRNA structure.[69]

Methylations are the simplest and most frequent modifications found in tRNAs, and they can occur at every position of the target nucleotide. Methylations destabilize Watson-Crick interactions and lead to large structural changes in the global tRNA fold.[70] m^1A9 in human mitochondrial $tRNA^{Lys}$ is a classic example of a methylation that affects tRNA structure, as the methylation displaces the structural equilibrium from an alternative hairpin structure to the functional cloverleaf structure.

An example in the variable loop is 7-methylguanosine (m^7G) modification, which is found widely in eubacteria, eukaryotes, and a few archaea. In most cases, the m^7G modification occurs at position 46 and is a product of tRNA (m^7G46) methyltransferase. The m^7G46 modification forms a tertiary base pair with C13-G22, and stabilizes the tRNA structure.[71]

Collectively, modifications participate in the stabilization of the tRNA molecule *in vivo*, and some of their important structural functions include restriction of nonfunctional alternative folding, cooperative binding of Mg^{2+}, and thermal stabilization. Mg^{2+} and polyamines are important for proper tRNA folding and structure stabilization, and modifications are important players in RNA-Mg^{2+}/polyamine interactions. For example, m^5C in yeast $tRNA^{Phe}_{GAA}$ enhances Mg^{2+} binding,[72, 73] while branched pentamines inhibit m^5C formation in specific tRNAs.[74] Several modifications such as ac^4Cm, m^1Im, Gm, and $m^{22}Gm$ are involved in thermal stabilization of tRNA.[75]

Every tRNA isoacceptor is fine-tuned to be specifically recognized by its cognate aminoacyl-tRNA synthetase (AARS) and isoacceptor-specific modifications can have very important roles in this process. For instance, uridine-5-oxyacetic acid (cmo^5U) in the wobble position of *E. coli*, which is known to extend Us coding capacity to base-pairing not only with A and G but also with U, was present in $tRNA^{Leu}_{UAG}$, but not in $tRNA^{Leu}_{CAG}$.[76]

Other components of the translation apparatus require the presence of modifications to recognize tRNAs. m^5U54 affects the structure of the tRNA TΨC loop, changing the binding interface contacts and thereby altering recognition by EF-Tu.[77]
tRNA thiolations can also act as an antideterminant in tRNA editing. Moreover, maturation of tRNAs can be very complex with spatial separations of the different steps. For example, in yeast, pre-$tRNA^{Phe}_{GAA}$ is exported from the nucleus and then spliced and partially modified in the cytoplasm. The partially modified (or apomodified) tRNA is then imported back into the nucleus, where the m^1G37 modification is introduced by Trm5. The tRNA is then exported back to the cytoplasm, where the yW machinery finishes the maturation process.[78]

Rapid tRNA decay (RTD) system acts selectively on mature tRNA isoacceptors lacking certain pairs of modifications and targets the tRNAs for 5´-3´ degradation. Mature $tRNA^{Val}_{AAC}$ lacking

both m^5C and m^7G46 and mature $tRNA^{Ser}_{CGA}$ and $tRNA^{Ser}_{UGA}$ lacking both Um44 and ac^4C12 are rapidly degraded at 37°C, which proved thermal stability roles of these modifications.[79]

tRNA modification profiles are influenced by parameters such as growth temperature or rate. For example, when thermophiles are grown at high temperature, their tRNA modifications are increased.[80] Moreover, exposure to chemicals such as H_2O_2 or methyl methanesulfonate (MMS) is associated with an increase or decrease of specific sets of tRNA modifications.[65] For instance, modifications such as Cm, m^5C, and $m^{22}G$ in Saccharomyces cerevisiae, showed an increase following H_2O_2 exposure but decreased or were unaffected by exposure to MMS, arsenite, and hypochlorite.[81] In contrast, ms^2C found in 2-thiocytidine (s^2C) containing tRNAs of *E-coli*, namely $tRNA^{Arg}_{CCG}$, $tRNA^{Arg}_{ICG}$, $tRNA^{Arg}_{UCU}$ and $tRNA^{Ser}_{GCU}$ at low abundances, is not formed by natural tRNA methyltransferases action, but during exposure to chemical methylating agent MMS.[82]

Apart from described roles of mentioned tRNA modifications, naturally occurring modifications functions in cell processes can be summarized to: extension and restriction of base-pairing capacity, stability of codon-anticodon interaction, reading frame maintenance, natural suppression of stop codons, effects on initiation of translation, intermediary metabolism, cell cycle control, antibiotics production, cell division, UV sensitivity, mutation frequency, and more.[83] In case of misregulations of tRNA modifications, such as tRNA hypomodification and tRNA-modifying-enzyme deregulation, several diseases may occur, where proteostasis is affected; namely, neurodegenerative and metabolic diseases, as well as several types of cancer.

Roles of rRNA modifications

Ribosomes are composed of a highly conserved catalytic rRNA core and dozens of auxiliary proteins. Dozens to hundreds of residues are modified across ribosomes from different domains of life, with *E. coli* rRNA harboring 36 modifications,[84] yeast 112, and human 228.[85]

In terms of density of modificational pattern, rRNA is only second to tRNA. The content of post-transcriptional modified nucleotides in rRNA is usually ~2% or less in case of prokaryotes. rRNAs are extensively modified throughout their transcription and subsequent maturation in the nucleus and cytoplasm. rRNA modifications, which are installed by either snoRNA-guided or stand-alone enzymes, commonly stabilize the structure of the ribosome. However, they also cluster at functionally important sites of the ribosome, such as peptidyltransferase center (PTC) and the decoding center (DC), where they enable efficient and accurate protein synthesis. The recent identification of sites of substoichiometric Nm and Ψ has overturned the view that all rRNA modifications are constitutively present on ribosomes, highlighting nucleotide modifications as an significant source of ribosomal heterogeneity.

A core set of rRNA modifications is conserved across the three domains of life, and these modifications typically cluster around the functional centers of the ribosome.[28] There is a remarkable diversity of modifications that adorn the ribosome, including diverse forms of methylation, acetylation, and pseudouridylation.

In recent years, it has become clear that ribosomes are considerably more heterogeneous than previously thought. Specifically, it was shown that ribosomes can differ in their primary rRNA sequence, in the composition of ribosomal proteins, as well as in the post-translational modification profiles of the ribosomal proteins.[86]

While the mechanisms regulating partial modification and the functions of specialized ribosomes are largely unknown, changes in the rRNA modification pattern have been observed in response to environmental changes, during development, and in disease. This suggests that rRNA modifications may contribute to the translational control of gene expression.[28]

Several studies over the years show rRNA modifications are dispensable partially, whereas the rRNA modifying enzymes are not, which suggest broad roles of ribosome modifying enzymes include modification dependent functions and modification independent ones.[86] In principle, both modification-dependent and independent roles can manifest in the broad range of functional outcomes associated with disruption of diverse rRNA modifying enzymes, including aberrant assembly, structures, or translational activity, as well as reduced translational output, reduced amino acid incorporations, increased stop codon read-through, and modulation of frameshift rate.[28, 87] Yet, due to the subtlety of the phenotypes and the difficulties in dissecting them, the functions of most modifications remain to a large extent elusive.

the majority of sites reported to be either substoichiometric or dynamically regulated in human and yeast are modified either with Ψ or with 2′-O-methylation. Given that these modifications are guided by snoRNAs, it is tempting to speculate that the substoichiometric modifications associated with a subset of them may reflect this snoRNA-mediated biogenesis.[86]

Ψ in rRNA is normally clustered in the PTC, the DC and the region above the A-site of the ribosome, and the sites where ribosomal subunits interact,[88, 89] which suggest their functional significance on rRNA processing, protein synthesis, and cell growth.[89]

Nm in rRNA is located in proximity of the PTC and the DC.[90] It is notable that relative abundance of individual Nm sites is strongly conserved between human and mouse, which proves correspondences in regulating the structure and function of the ribosome.[91] the quantities of each modification in 28S and 18S-rRNA are mostly conserved among different domains of life, which can be referred to similar ribose assembly and hence function during translation in all organisms.

highest abundant modifications in smrRNA including 5.8S and 5S rRNA are Ψ, and ribose 2′-O-methylations rather than base modifications, due to their functional releavance in rRNA biogenesis such as compromising protein synthesis, as well as ribosome translocation.[92, 93]

Helm lab recently investigated distinctive modifications as co-varying rRNA marker modifications, appeared in small RNA fractions following rRNA degradation.[94] Among them, $m^{66}A$ is confirmed to occur almost exclusively in 18S rRNA. m^3U as counterpart, is typical for the large subunit 28S rRNA. Ribose methylations occur in rRNA at high frequency. Am, which is not known to occur in tRNA and mRNA, can also be a marker for rRNA from either 28S or 18S subunit.

The existing modifications in 28S and 18S rRNA are expected to function in constitution of the PTC, DC of the LSU rRNA, interaction of LSU rRNA with both mRNA and the ASL of tRNA and peptide bond formation. As the case of Ψ, which helps the stabilization of local secondary or tertiary structure through RNA-RNA or RNA-protein interactions.[95]

1.4. RNA modifications dynamics: writers, erasers

The structural diversity of the modified nucleosides which provides regulatory potential to sort groups of RNAs for organized metabolism and functions, is orchestrated by so called modification "effectors", including different classes of "writer" and "eraser" enzymes that alter the modification level, as well as binding proteins "readers" that recognize the chemical marks, as individual modifications can be recognized by readers, which initiate a corresponding molecular reaction.

In this section, an example of a set of effectors on m^6A are presented together with their corresponding diseases associated with their misregulation. A few more modifications effectors are also mentioned, and further discussion of AlkBH erasers family is followed, as the focus of this thesis is on three members of this family.

m^6A is installed on mRNA co-transcriptionally by a complex composed of multiple subunits with a stable core complex formed between methyltransferase-like 3 (METTL3) and methyltransferase-like 14 (METTL14). the former as the catalytic subunit and the latter as an essential component to facilitate RNA binding.[96] Further studies characterized a handful of additional subunits and revealed how they contribute to the activity and specificity of the writer complex. Wilms tumor 1-associating protein (WTAP) binds to METTL3/14 and is required for optimal substrate recruitment and METTL3/14 localization, Vir like m^6A methyltransferase associated (VIRMA) is critical for deposition of m^6A specifically to the 3'UTR, Zinc finger CCCH-type containing 13 (ZC3H13) facilitates nuclear localization of the writer complex, KIAA1429 guides the methyltransferase components to specific RNA region,[97] and RNA binding motif protein 15/15B (RBM15/15B) is reported to bind U-riched regions and may facilitate methylation of certain RNAs.[98]

In the nucleus, m^6A can be recognized and directly bound by m^6A readers YTHDC1, HNRNPA2B1, and IGF2BP1/2/3. In the cytoplasm, m^6A can be recognized and bound by m^6A readers YTHDF1/2/3, YTHDC2, eIF3, and IGF2BP1/2/3. Recognition and binding of m^6A by different readers in the nucleus or cytoplasm mediate divergent biological functions.

m^6A demodification in mRNA and other types of nuclear RNA is dynamically regulated by erasers fat mass and obesity-associated (FTO) or AlkBH5, both of which are localized primarily in the nucleus. FTO has also been reported to regulate the adipogenesis via regulating alternative splicing of adipogenic transcription factor RUNX1T1 (Runt-related transcription factor 1) in an m^6A depend manner.[99] FTO is the first RNA demethylase identified, which apart from removing the methyl group of internal m^6A in mRNA, demethylates m^6Am, a modification found on the second base adjacent to the 5´cap (cap-m^6Am) in mRNAs.[100] Moreover, FTO possesses effective demethylation activity towards m^1A in specific tRNAs and m^6Am in some snRNAs.[101] Figure **1.6** shows a simplified view of m^6A effectors.[102]

AlkBH5 was the second recognized m^{6}A demethylase, which showed modulation activity towards mRNA export and RNA metabolism by reducing the m^{6}A amount in nuclear speckles.[103] Inactivation of AlkBH5 causes male infertility in mice through appropriate m^{6}A methyl removal in the nuclei of spermatocytes, vital for correct splicing and production of longer 3′-UTR mRNAs, and its failure leads to aberrant splicing and accumulation of shorter transcripts.[104] DDX46, one member of DEAD-box (DDX) helicases, has shown to inhibit antiviral native responses by recruiting AlkBH5 and capturing selected antiviral transcripts in the nucleus through erasing their m^{6}A modification.[105]

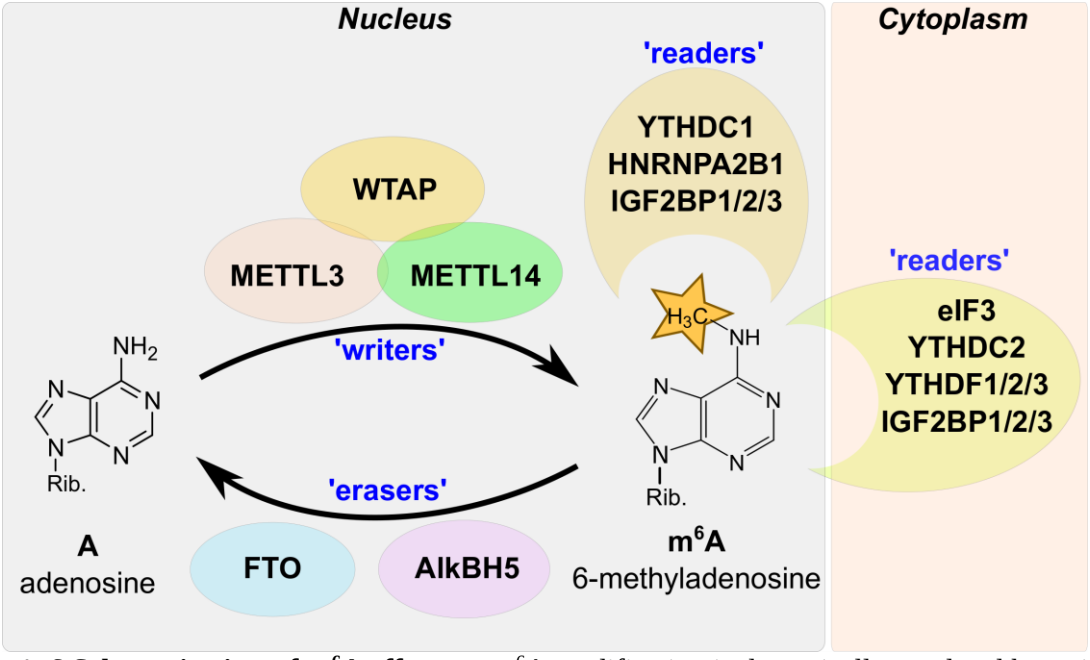

Figure 1. 6 Schematic view of m^{6}A effectors. m^{6}A modification is dynamically regulated by writers (METTL3 and METTL14 complex, with Wilms tumor 1-associating protein (WTAP)) and erasers (fat mass and obesity-associated (FTO) or AlkBH5), both of which are localized primarily in the nucleus. In the nucleus, m^{6}A can be recognized and directly bound by m^{6}A readers YTHDC1, HNRNPA2B1, and IGF2BP1/2/3. In the cytoplasm, m^{6}A can be recognized and directly bound by m^{6}A readers YTHDF1/2/3, YTHDC2, eIF3, and IGF2BP1/2/3. Recognition and binding of m^{6}A by different readers in the nucleus or cytoplasm mediate divergent biological functions.

RNA m^{6}A modification has been recognized to play important roles for regulating RNA splicing, translation, stability, translocation, and high-level structure.[98, 106]
Numerous studies focusing on m^{6}A RNA methylation have verified that the regulators of m^{6}A are involved in various human diseases, including nonalcoholic fatty liver disease,[107] azoospermia,[108] heart failure,[109] especially in human cancers.[110]

m^{5}C is another modification that exists in multiple RNA species, including mRNAs, tRNAs, rRNAs, and ncRNAs, also broadly distributed from archaea, prokaryotes to eukaryotes.
In mRNA, m^{5}C is enriched around 5′UTR and 3′UTR, and conserved in tRNAs and rRNAs. It is dynamically regulated by its related enzymes, including methyltransferases (NSUN, DNMT, and TRDMT family members), demethylases (TET family and AlkBH1), and binding reader proteins (ALYREF and YBX1). So far, accumulative studies have revealed that m^{5}C participates in a variety of RNA metabolism, including mRNA export, RNA stability, and translation.

Writers of m^5C in mRNA include NSUN2 which maintains mRNA stability, and TRM4A/TRM4B which regulate cell proliferation in root apical meristem and the sensitivity to oxidative stress.
In cytoplasm tRNA, NSUN2 places $m^5C48/49/50$ on human and mouse, NSUN6 writes m^5C on human $tRNA^{Cys}$ and $tRNA^{Thr}$, DNMT2 places the m^5C38 in human $tRNA^{Asp}$, and TRM4A/TRM4B on *Arabidopsis thaliana*. In mitochondrial tRNA, NSUN2 places $m^5C48/49/51$ in mammalian cells, while NSUN3 places m^5C34 the on mt-$tRNA^{Met}$. These modifications potentially influence the translation of mt-tRNA. rRNA m^5C is placed by NSUN1 on human 28S at m^5C4447, NSUN5 on human and mouse 28S rRNA, and NSUN4 on human mt-12S rRNA.
While TET1/TET2/TET3 demethylate m^5C in mRNA, which has associations to mRNA degradation, the best characterized tRNA demethylase of m^5C is AlkBH1 for m^5C34 in $tRNA^{Leu}$ and mt-$tRNA^{Met}$.[111]

Ψ synthases are grouped into six families based on sequence homology: TruA, TruB, TruD, RluA and RsuA are named after their bacterial representative; the sixth family, the Pus10 family is present in human, eukaryotes and archaea and does not have significant sequence homology to the other five families.[112] In eukaryotes pseudouridylation is carried out by site-specific Ψ synthases (e.g. Pus1 and Pus10), or by Cbf5 (dyskerin in human), which functions as part of a small nucleolar ribonucleoprotein (snoRNP) complex with a guide RNA conferring site-specificity.[113]

Inosine is an abundant RNA modification in the human transcriptome and is essential for many biological processes in modulating gene expression at the post-transcriptional level.[114] Adenosine deaminases acting on RNA (ADARs) catalyze the hydrolytic deamination of adenosines to inosines (A-to-I editing) in double-stranded regions.[115] Both ADAR and ADARB1 (also known as ADAR2) are essential enzymes in mouse.[116]

AlkBH erasers family

The human homologues of the bacterial ferrous (II)/α-ketoglutarate-dependent dioxygenase AlkB (AlkBH) family consists of nine homologous enzymes (AlkBH1-8, FTO) whose catalytic activity depends on Fe^{2+} and α-ketoglutarate (α-KG). Even though the paralogs share a homologous catalytic core, different combinations of substrates lead to different functions, which are obvious characteristic of the AlkBH family.[117] This section is more focused on three members of the AlkBH family, namely AlkBH1, AlkBH3, and AlkBH5, as their functions are investigated in this thesis.
The first discovered homologue was bacterial AlkB in 1983, in the context of cell sensitivity to methylating reagents, such as methyl methanesulfonate (MMS). It was suggested that it serves as a repair enzyme for cell stress, and that damaged nucleobases.[118]

Iron(II) and 2-oxoglutarate (2OG) dependent oxygenases form a ubiquitous family of oxidative enzymes that catalyze a diverse range of reactions, most commonly hydroxylations, but other types of reaction including desaturations, epimerisations and rearrangements have also been observed. The exact mechanism follows: a reductive activation of an oxygen molecule is coupled to the decarboxylation of the α-ketoglutarate to succinate. The Fe(II) ion in the active site of AlkB coordinates with two histidine and one aspartate residues of the enzyme. Upon

binding of the α-ketoglutarate and oxygen, an Fe(IV) oxo complex is formed, which is capable of hydroxylating the methyl group of a nucleobase (The adenine N1 methyl group in Figure **1.7**). With the release of a formaldehyde molecule, the canonical nucleobase, in this case adenine, is recovered.[119]

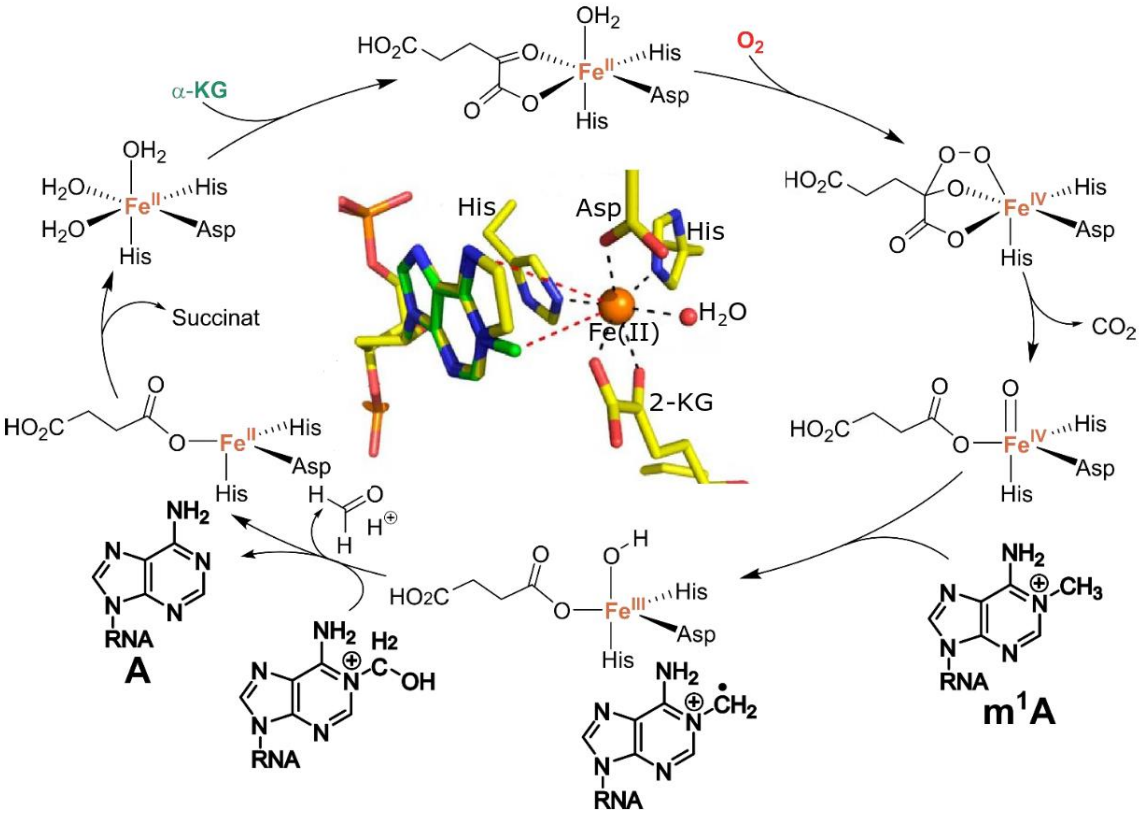

Figure 1. 7 active demethylation of the RNA modification m[1]A by the AlkB enzyme family.

The stepwise demethylation is shown with structural formulas highlighted in bold. The reaction cycle of the iron complex in the catalytic center is shown both structural-mechanistic (adapted from described by [119]), and crystallographic. The active site of AlkB family showing the octahedral coordination around the central metal ion and the relative position of the example substrate m[1]A, shown overlaid. The histidine (His) and aspartate (Asp) residues are abbreviated and the iron (II) ion is colored orange. The red sphere denotes a water molecule crystalized at the molecular oxygen binding site.[120]

Previous discovery of AlkBH5 as mRNA m[6]A and m[6]Am demethylase have shown significant effects on mRNA export and RNA metabolism, and the assembly of mRNA processing factors in nuclear speckles.[60, 103]

AlkBH1 is responsible for the demethylation of m^1A_{58} in tRNA molecules. It was the first identified human methyl eraser. The amount of existing tRNA is adjusted by the removal of m[1]A molecules, thereby regulating the translation initiation.[121] AlkBH1 is also known as the methyl remover of m[3]C in mRNA of mammals,[122] m[5]C in mt-tRNA^{Met} [123, 124] and m[6]A in bubbled or bulged DNAs.[123]

AlkBH3 is also a single-stranded DNA and RNA repair enzyme, which is known to remove m^1A in mRNA, as well as m^1A and m^3C, and potentially m^6A in tRNA,[125-127] although the functional relevance of which still requires further investigations.[121, 126]

While the corresponding writers for most RNA modifications are already known, the research field around erasers is still comparatively young.[128] Both classes of enzymes attack intervene in the targeted adaptation of the modification profile and could thus be of great relevance for future applications in research and medicine.

The interaction between writers and erasers is extremely dynamic and is constantly adapted by the cell to internal and external influences. For each RNA molecule, a modification profile is created that is specifically adapted to the respective situation.

Alteration of RNA modification patterns is well understood and is associated with various human diseases such as cancer. A diverse possibility of diseases is extremely high due to the high number of modifications. An overview of the literature on selected RNA modifications and their AlkBH demethylation partners along with their target RNA sites is presented in Table **1.1**.
Several studies provided association of AlkBH family with tumor stage and subclasses. Compared to the normal tissue, almost all ALKBH homologous are associated with tumor stage except AlkBH5 and FTO. On account of the advance stage which indicates progression, AlkBH1, AlkBH4, AlkBH6, and AlkBH8 may be the potential biomarker for predicting tumor progression.[129] In general, dysregulation or inactivity of AlkBH enzymes correlates with diverse diseases.[130]

Table 1. 1 Correlations of RNA modifications and diseases related to AlkBH enzymes.

RNA modification	Eraser enzyme	Target RNA	Associated disease	References
m^1A	AlkBH1	A58 tRNA	Cervix Cancer	131
	AlkBH3	mRNA (5′UTR near Start codon)	Pancreatic Cancer	132
m^3C	AlkBH1	C32 tRNA	Hepatocarcinoma	122
		C34 mt-tRNA	Hepatocarcinoma	122
m^5C	AlkBH3	C32, C47 tRNA	Cervix Cancer	133
m^6A	AlkBH5	mRNA	Pancreatic Cancer AML Glioblastoma Breast Cancer	134,135 136 137 138
	FTO	mRNA	Glioblastoma Cervix Cancer AML Melanoma Gastric Cancer Breast Cancer	139 139 140 141 142 143
mcm^5s^2U	AlkBH8	tRNA	Breast Cancer	144

Cell stress, and its impact on RNA modifications

The modification profile of RNA molecules based on how it depends on writer and eraser enzymes is built up from cellular (endogenous) to external (exogenous) effects, which ensures the molecular mechanisms are adapted to these different situations.

In homo sapiens, cell stress gets triggered through different stress factors, such as high-energy radiation like UV light or by physical or psychological stress, as well as infections.[145] At the molecular level, this is usually demonstrated by chemical modification of various macromolecules of cells. DNA damage is one of the most critical types of these changes, which in case of not getting recognized and repaired by the cells, can trigger different types of diseases. Approximately 90 percent of all human cancers have an environmental cause (non-genetic inheritance) predominantly through lifestyle choices (smoking, diet, UV radiation) while the remaining due to infections and chemical exposure.[146] Nonetheless, the focus of this section is on different types of stress factors affecting RNA.

Several types of cellular stress factors such as hypoxia, nutrient deprivation, heat shock, inducers of reactive oxygen species (ROS), or direct damage by various chemicals are important stimuli of disease signaling in cells. Oxidative stress is the cellular state in which levels of ROS override the antioxidant defense mechanisms of the cell.[147] They cause damage to RNA molecules by oxidizing the nucleosides.

On the other hand, a common methyl group donor in the cell is the cofactor S-adenosylmethionine (SAM), which at high concentrations could trigger spontaneous, unwanted methylations. Normally, SAM is a donor which provides the methyl groups for histone or nucleic acid modification and phosphatidylcholine production, which may generally be required for stress-responsive transcription. Studies show transcriptional responses to bacterial or xenotoxic stress fail with low SAM.[148] Cell death and neurodegenerative conditions have been linked to oxidative stress and imbalance between generation of free radicals and antioxidant defenses. Multiple sclerosis, stroke, and neurodegenerative diseases have been associated with reactive oxygen species and nitric oxide.[149]

Compared to DNA modifications by ROS, less is known about the effects of oxidative damage to RNA. Purified RNA appears to have greater oxidative stability than DNA. Studies that compared the cleavage of DNA and RNA by photo-oxidants showed that the C-H bond cleavage in RNA was more difficult to occur compared to DNA. Moreover, induction of tRNA fragmentation commonly involves transient exposure of cultured cells to oxidizing agents such as As[III] or H_2O_2 in the high micromolar concentration range. Oxidative RNA damage involves modifications of bases and ribose, base excision, and strand break. Oxidative RNA adducts including 8-oxoguanosine, 8-hydroxyadenine, and 5-hydroxycitosine have been described.[150] Oxidative damage to protein-coding RNA and non-coding RNA could potentially cause errors in protein synthesis and modification of gene expression.[146]

Recent studies have revealed that tRNA modifications can be dynamically altered in response to levels of cellular metabolites and environmental stresses. Importantly, we now understand that deficiencies in tRNA modification can have pathological consequences, which are termed

'RNA modopathies'. Dysregulation of tRNA modification is involved in mitochondrial diseases, neurological disorders and cancer.[151, 152]

The ring nitrogens of the RNA nucleobase are particularly vulnerable to methylating agents, but exocyclic amine- or keto- groups might also be affected. They are mainly nucleophilic and therefore represent a suitable target for methyl group donors. Methyl methanesulfonate (MMS) is an alkylating agent that acts on DNA and RNA by preferentially methylating adenine and guanine bases. Studies verified that MMS treatment mediated distinctly increased m^1A, m^3C and m^7G in HeLa cells total RNA, specially m^1A and m^3C were induced at more than twofold higher density in mRNA.[153] MMS is largely used in basic genome stability research and as a model for mechanistic studies to understand how alkylating agents work. Nevertheless, MMS exerts additional actions, such as oxidation and acetylation of proteins.[154]

Alkylation damage in DNA and RNA is repaired by at least three different mechanisms, such as homologous recombination or non-homologous end joining in DNA double-strand breaks, or nucleotide or base excision repair. Repair mechanisms also attack the damage directly and remove it enzymatically, including damage reversal by oxidative demethylation of different base methylations by AlkB homologues.[155] One interesting example of MMS-induced methylation damage repair has confirmed that ASCC-ALKBH3 repair pathway is exquisitely specific to alkylation damage in human cells, and hypothesized that AlkBH3 is a methylation damage induced enzyme, that triggers ASCC-AlkBH3 alkylation repair complex after certain aberrant methylation damages such as MMS treatment.[156]

On the other hand, under hypoxia conditions, deletion of AlkBH5 has been shown to promote cell proliferation and differentiation in mouse cerebellum by destroying the balance of RNA m6A methylation in different cell fate determination genes.[157] AlkBH5 has been identified to be highly expressed in male mice testes, ablation of which shows increased m^6A in mRNAs mainly leading to testicular atrophy, remarkably reduced rate of breeding and decreased fertility in mice.[103]

tRNA-derived stress-induced halves (tiRNA)s are the result of tRNA hydrolysis in the anticodon loop, which is performed by members of two nuclease families (RNase A and RNase T2). Angiogenin (ANG), a member of the RNase A family, is the main nuclease of various redundant nucleases capable of tRNA hydrolysis.[158] tiRNAs have been detected in almost every cellular context, during various developmental stages and importantly, during exposure to defined stress conditions.[159] Specifically, the production of tiRNAs has been reported after starvation,[160] oxidative stress,[161, 162] nutritional deficiency,[163] hypoxia and hypothermia,[158, 164] heat shock and gamma-irradiation.[162, 165, 166] Upon stress, ANG phosphorylation causes the dissociation from its inhibitor RNH1,[167] and the activation of its catalytic activity results in targeting of pyrimidine-purine dinucleotide sequences, preferentially in the loop structures of tRNAs.[162, 168-170]

In general, the consequences of such damage to RNA molecules are extremely diverse. Often, they are based on the disruption of base pairing and trigger diseases such as cancer or neurological defects. Due to the high exposure to diverse stressors, the cell has therefore developed several mechanisms to repair DNA and RNA damage.

1.5. Processing of tRNA molecules, tRNA fragments

Because the structure of tRNAs is crucial for their function in translating the nucleic acid code into polypeptides, accurate tRNA intron processing is an essential process. Interestingly, tRNA splicing is not carried out by the spliceosome, rather the tRNA intron excision and exon ligation processes are catalyzed by protein-only complexes.[171, 172] Another interesting facet of tRNA biology emerges from examination of the isodecoder families in which tRNA introns are found to reside. Analysis of the genomic tRNA database shows in higher eukaryotes, all of the tRNA genes of a particular isodecoder family tend to contain an intron.[173]

Interestingly, considering sequence similarity among tRNA genes, the introns within a given isodecoder family are not well conserved. In addition, introns of different isodecoders typically do not share similarity; that is, a tRNA intron in a particular organism is unlikely to share similarity with any other tRNA intron in the same organism. However, there is evidence for sequence conservation between introns of the same tRNA gene in closely related species.[173]
In striking contrast to pre-messenger RNA splicing, the removal of introns from pre-tRNA transcripts is spliceosome-independent. These processing events are carried out by a series of protein-catalyzed reactions. The splicing can be split into two distinct activities: cleavage and ligation. In order for a pre-tRNA to be spliced, it must first be recognized by the endonuclease complex.[174]

tRNA-derived fragments (tRF)s are among the oldest small RNAs in all domains of life and are generated by the cleavage of tRNAs. Evolving studies have begun to reveal the versatile roles of tRFs in fundamental biological processes, including ribosome biogenesis, gene silencing, retrotransposition, and epigenetic inheritance, which are engrained in tRFs sequence conservation, RNA modifications, and protein-binding abilities.[175]

Here a summary of the mechanisms of tRFs biogenesis and the impact of RNA modifications is presented, with an extra attention drawn to tRNA-derived stress-induced halves (tiRNAs), which is partially investigated in this thesis.

As previously described in figure **1.3**, the L-shaped structure is overall tightly condensed but has two relatively exposed sites: the anticodon at one end of the L and the tRNA elbow at the bending site of the L, where the D-loop and the T-loop meet and interact with each other. The exposed sites of the tRNA structure could be ‘points of attack’ in an ancient cellular (and perhaps early proto-cell) environment, being fragmented by either nonspecific stress signals such as radiation and ROS, specific recognition by enzymes or ribozymes, or a combination of both.[175]

This observation may support the assumption that, in early life forms, the biogenesis of tRFs directly originated from tRNA degradation processes starting with these loops, perhaps including multistep degradation and the generation of different intermediates,[176] accompanied by regulatory elements such as RNA modifications and specific RNases targeting these loops (fig **1.8**) that emerged during evolution.

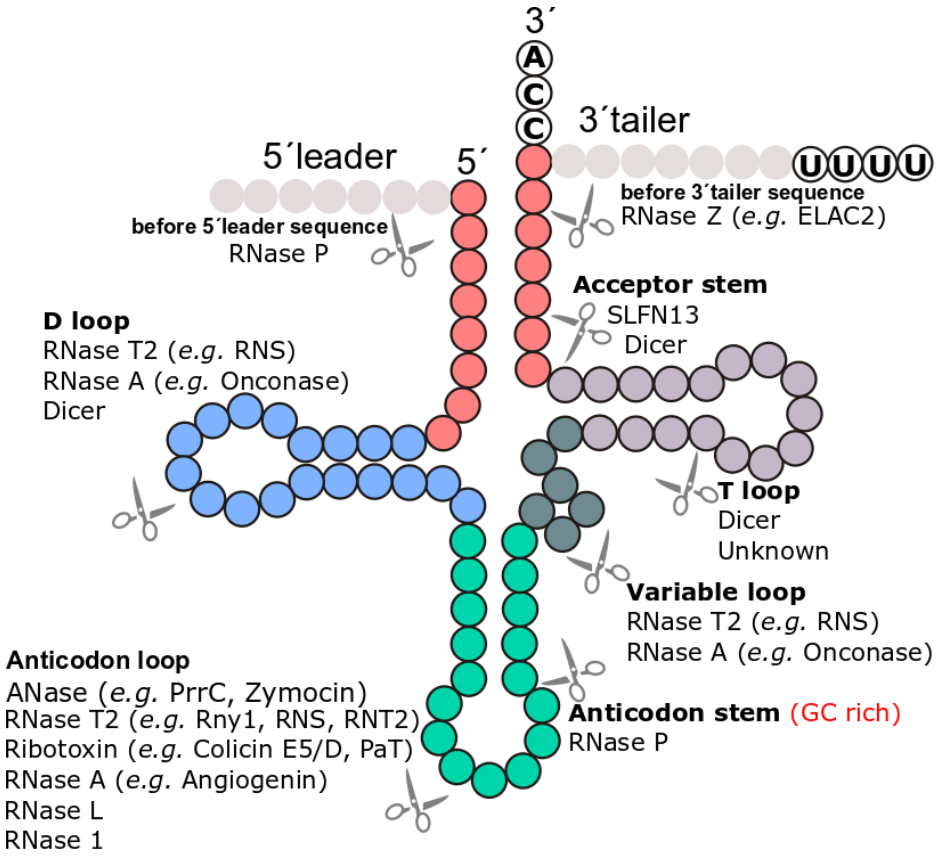

Figure 1. 8 The biogenesis of tRNA-derived fragments (tRFs) is rooted in tRNA structure, regulated by tRNA modifications and RNases. known RNases for tRF biogenesis include Dicer,[177, 178] RNase 1,[179] RNase P,[180] and others reviewed in [181].

Notably, tRNA cleavage can also occur independently of the loop site, such as by targeting a specific tRNA stem position by RNase P that recognizes a specific (*e.g.* GC-rich) sequence,[180] or more generally, by enzymes targeting double-stranded (ds) RNA regions. For example, although it is well-known that the RNase Dicer cleaves dsRNAs to generate siRNAs and miRNAs, Dicer is also responsible for the biogenesis of some tRFs from tRNAs.[177, 178] Since tRFs are present in all domains of life, whereas Dicer has not been identified in prokaryotes,[182] this supports the notion that Dicer-based canonical small RNAs (*i.e.* siRNAs and miRNAs) emerged later than tRFs during evolution, and Dicer may have recognized the ds stem region in a tRNA-like structure when it first emerged. Currently known enzymes that cleave tRNA (and pre-tRNAs) to generate tRFs are well-summarized in a recent review,[181] and are shown in figure **1.8**. The list of enzymes mediating tRFs biogenesis is expected to expand in the future.

Both tRFs and their precursor tRNAs are heavily modified. It has been demonstrated that DNMT2- and NSUN2-dependent addition of an m^5C modification to several tRNAs (*e.g.* $tRNA^{Asp}$, $tRNA^{Val}$, $tRNA^{Gly}$, and $tRNA^{Leu}$) increases tRNA stability in flies and mice, whereas deletion of Dnmt2 and/or Nsun2 abolishes m^5C on these tRNAs, making them more likely to be cleaved into tRFs under stress conditions.[183, 184] The queuosine (Q) modification by QTRT1 occurs in the wobble anticodon position of several tRNAs ($tRNA^{His}$, $tRNA^{Asn}$, $tRNA^{Tyr}$, and $tRNA^{Asp}$) and protects tRNAs against cleavage into tRFs in human HEK293T cells.[185] Interestingly, recent reports showed that C38 Q-modified tRNA promotes DNMT2-mediated

m^5C on C38 of $tRNA^{Asp}$;[20, 186] these discoveries resonate with findings that the establishment of one RNA modification can depend on the existence of another.[187] Recent evidence also shows that deletion of AlkBH1,[188] or AlkBH3,[126] increased the levels of m^1A in tRNAs, preventing tRNA cleavage and resulting in less tRFs production. TRMT10A-mediated m^1G modification also leads to increased $tRNA^{Gln}$ stability and less production of tRF^{Gln} .[189] Moreover, 2′-O-methylation of C34 in human $tRNA^{Met}$ can prevent site-specific cleavage of $tRNA^{Met}$ by angiogenin (ANG) and reduce tRF production.[190]

ANG is a member of RNase A superfamily, a stress-activated ribonuclease that cleaves tRNA within anticodon loops to produce 35-45 nucleotide-long tRNA-derived stress-induced halves (tiRNAs). tiRNAs are of major interest as they were shown to accumulate in neuronal diseases with RNA modification enzyme participation. tiRNAs can be classified in 5´tRNA halves and 3´tRNA halves. The AlkBH3 mediated m^1A demethylated tRNA was shown to be more sensitive to ANG cleavage, followed by generating tiRNAs which are conserved among species, and function as strengthening the ribosome assembly and prevent apoptosis triggered by cytochrome c (Cyt c).[126] Moreover, distinct 5´tiRNAs were found to inhibit protein translation in an eIF2α-independent manner, while some isoacceptors 3´ tiRNAs showed strong affinity to Cyt c in apoptosis inhibition.[191]

Notably, previous reports connected tRNA fragmentation to stress granule (SG) formation, specifically after 5′ tiRNAs were transfected into immortalized cells, which resulted in the induction of SG formation.[162, 192, 193] However, recently it was proven by Schaefer lab that tRNA fragmentation and stress granule (SG) formation are not co-current events, which suggests that tiRNAs are produced after cells responded to oxidative stress through SG formation. They also pointed towards a disconnect between the low levels of specific 5´tiRNAs in As[III]-stressed cells and their assumed role in suppressing protein synthesis in a general translation inhibition.[194] These contradictory results proved that tiRNAs serve specific, likely localized, mechanistic purposes which are 'masked' by the deleterious effects of massive oxidative damage in cells stress response. These findings underline the fact that we still know very little of dynamics and functional relevance of tiRNAs.

Drino *et al*. have identified and characterized 5´-$tiRNA^{Gly}_{GCC}$ by naturally cleaving mature tRNA using overexpression of human ANG, and absolute quantification of modifications in full-length tRNAs resulting 5′ tiRNAs. Their study suggested existence of m^2G and Um on the 5´-$tiRNA^{Gly}_{GCC}$ but not m^1G, m^7G, m^2G, $m^{22}G$, Am, and m^6A from the targeted tRNA isoacceptor.[195] Considering this, it would be possible to explore the tiRNA modification incorporation relationship to their stability *in vivo*, which is the focus of this thesis. Therefore, two 33-nucleotides long 5´-tRF^{Gly}_{GCC} sequences including unmodified and position 4-Um modified were used as models for 5´$tiRNA^{Gly}_{GCC}$ in this study. Further information on the study is presented in the third section of chapter **3**.

RNA interference

RNA interference (RNAi) is a remarkable endogenous regulatory pathway that can bring about sequence-specific gene silencing. If harnessed effectively, RNAi could result in a potent targeted therapeutic modality with applications ranging from viral diseases to cancer.

RNAi can be effective when short (~22nt), double-stranded fragments of RNA - known as small interfering RNAs (siRNAs)- are loaded into the RNA-induced silencing complex (RISC), where the strands are separated, and one strand guides cleavage by Argonaute of target mRNAs in a sequence homology-dependent manner.[196]

The major barrier to realizing the full medicinal potential of RNAi is the difficulty of delivering effector molecules, such as small interfering RNAs (siRNAs) *in vivo*. An effective delivery strategy for siRNAs must address limitations that include poor stability and non-targeted biodistribution, while protecting against the stimulation of an undesirable innate immune response. The design of such a system requires rigorous understanding of all mechanisms involved.[197]

A potent gene-silencing agent has no utility if it cannot be delivered to its intended cell type, tissue, or organ. Delivery of genetic material *in vivo* is the biggest obstacle faced by siRNA therapies.[198, 199] Also virus-based delivery systems, while efficient, may be fatally flawed due to the safety concerns they raise as they induce mutations and trigger immunogenic and inflammatory responses.[200] As a result, extensive work has been done to develop efficacious non-viral delivery systems, including direct chemical modification of siRNA, liposome formulations, nanoparticles, and targeting moieties. These novel strategies provide ways to safely overcome obstacles facing siRNA. Further discussion on siRNA silencing effect along with transfection reagent choices are presented in chapter **3**, specifically subsections **3.2.1** and **3.3.1**.

1.6. Detection of RNA and RNA modifications

Types of detection methods

Improving our understanding of nucleic acids, both in biological and synthetic applications, remains a bustling area of research for both academic and industrial laboratories. Studying RNA includes many different aspects of RNA biology, including single-cell gene expression, translation (the translatome), RNA structure (the structurome), and elusive function of RNA modifications, which help with better understanding of their molecular causes and effects, and as a result connecting them to human diseases. As nucleic acids research evolves, so must the analytical techniques used to characterize them. The detection, localization, and quantification of RNA modifications have evolved extensively during the past decades.

A powerful analytical technique during the past decade, is RNA sequencing (RNA-seq), which has been widely used as an essential tool for transcriptome-wide analysis of differential gene expression and differential splicing of mRNAs. Sequencing offers the advantage that the sequence information is preserved, hence allows a clear positional assignment of the of the corresponding modification within the transcriptome, but it does not deliver any information about the chemical nature of it. The method suffers from that structurally alike modifications often cannot be distinguished from one another.[201] Exciting new applications are being discovered, such as spatial transcriptomics (spatialomics). Accompanied by new long-read and direct RNA-seq technologies and improved computational tools for data analysis, innovations in RNA-seq are funding to a fuller understanding of RNA biology, from questions such as

when and where transcription arises to the folding and intermolecular interactions that govern RNA function.

NMR spectroscopy is a very powerful method for structural studies of RNA. Due to RNAs rather uniform negatively charged surface, their flexibility and tendency to conformational heterogeneity, RNAs are in general less pliable to structural studies with X-ray crystallography than proteins. NMR in contrast can deal with more dynamic molecules very well and this intrinsic property places NMR at a central location for structural studies of RNAs. However, NMR studies of RNAs suffer from two major problems, which become even more striking when the size of the RNA increases, namely chemical shift overlap of resonances and line broadening leading to complete signal loss. The different strategies involving isotope labeling, promises to reduce difficulties associated with chemical shift overlap and rapid signal decay.[202, 203]

Many RNA modifications, such as thiolation, amino acid addition, and even methylations lead to a change in the chemical reactivity of the RNA. The resulting differential reactivity of modified nucleosides is exploited for their detection by sequencing but also by mass spectrometry. Mass spectrometry of RNA modifications can be performed on full-length RNA (top-down MS), partial RNA hydrolysates (oligonucleotide MS), or complete hydrolysates (nucleoside MS). Figure **1.9** summarizes the strengths (outside) and weaknesses (inside) of current methods for RNA modification analysis, with regard to discovery and chemical characterization of novel RNA modifications, impact of RNA modifications on RNA structure/stability, location of modification within the sequence, identity and chemical structure of modification (especially isomer discrimination), quantity of modification, and dynamics of RNA modifications.[204]

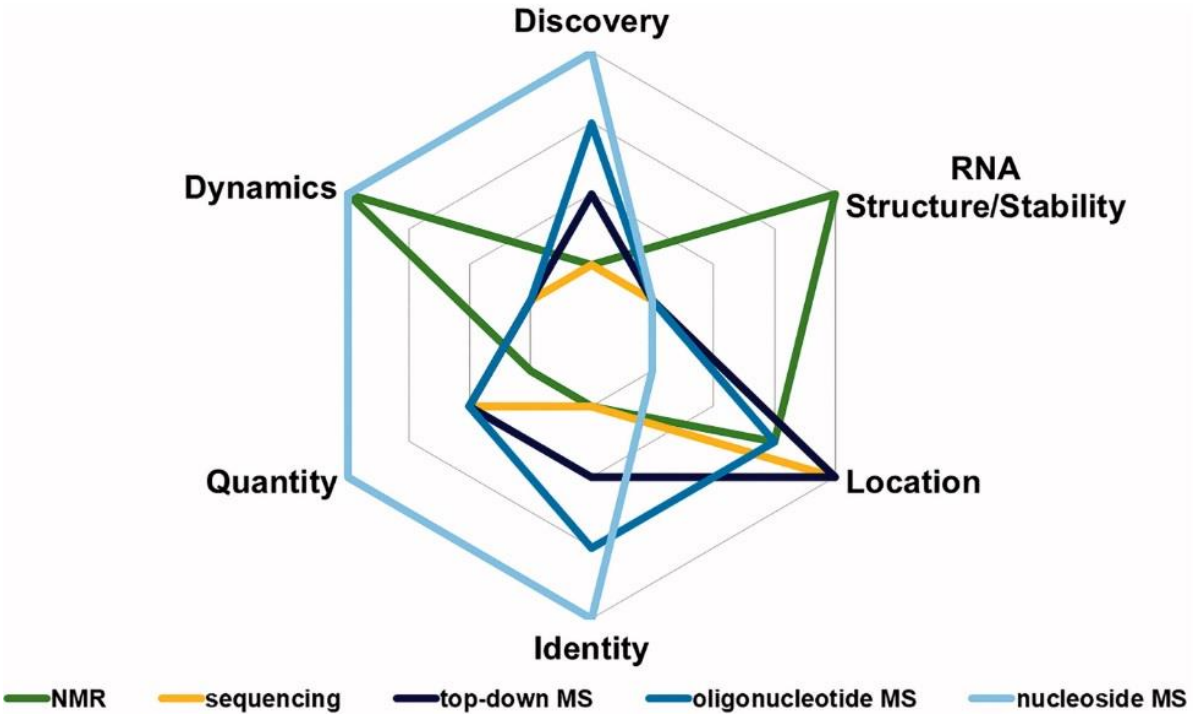

Figure 1. 9 Strengths (outside) and weaknesses (inside) of current methods for RNA modification analysis. Figure adapted from yoluc *et al.* review.[204]

Interestingly, NMR, MS, and sequencing analyses complement each other as they conquer the major pitfalls of the other two. For example, mass spectrometry is ideally suited to clearly identify the chemical nature of the modified nucleoside even with trace amounts of sample load. MS and sequencing are orthogonal techniques that benefit from each other while NMR analysis adds information on the structural impression of an RNA modification.

I discuss the basic principles of MS analyses, with the main focus on the most recent advances in this field, as nucleoside LC-MS/MS is the method of choice for RNA modifications analyses performed in this thesis.

The disadvantage of nucleoside MS is that it depends on the complete enzymatic digestion of the RNA and thus all sequence information and the location of the modified nucleoside remains unknown.

Isotope labeling of biomolecules as a tool for analysis

Studies on RNA and its modifications have evolved in the last decades and the sensitivity and depths of analyses have improved. One key aspect of this development is the use of stable isotopes as probes, labels or standards. These stable isotopes comprise deuterium (hydrogen-2), carbon-13, nitrogen-15, oxygen-18, fluorine-19 and sulfur-34. MS and NMR spectroscopy are the key tools with breakthrough developments that intensively engage in the analysis of stable isotope labeled RNA. Current stable isotope labeling techniques such as metabolic labeling, enzymatic labeling and chemical synthesis are normally used to provide stable isotopes of RNA molecules.

Challenges of RNA structural analysis by NMR due to the mentioned problems of chemical shift overlaps and line broadening leading to signal loss, have been solved by several isotope labeling strategies, such as deuteration, segmental isotope labeling or site-specific labeling.

RNA isotope labeling can be divided into radioactive labeling (*e.g.* with phosphorus-32 or tritium) and stable isotope labeling. While radioactive labeling is still a valuable technique, no technological improvements were made in the last decades. Contrariwise, stable isotope labeling has boosted the methodological possibilities of many techniques. Stable isotopes became quantitatively available for basic research in the 1940s as recently reviewed.[205]

In 1992, The first ever stable isotope labeling of RNA was done metabolically. Bacteria were cultured in the presence of carbon-13 (^{13}C) and nitrogen-15 (^{15}N) containing nutrients and the isotopes were found to be incorporated into the nascent RNAs by the bacterial metabolism.[206] From this RNA, stable isotope labeled nucleotides were isolated and used for enzymatic production of an RNA transcript of interest. In this case, the isotope label is distributed equally throughout the transcript. Later techniques, such as position selective labeling of RNA (PLOR), allowed site-specific incorporation of stable isotope labeled nucleosides.[207, 208] The site-specific incorporation is often crucial to the success of the subsequent application and solid-phase synthesis is a key tool in that respect. In summary, stable isotope labeling techniques can be divided into (I) metabolic approaches, (II) enzymatic techniques and (III) solid phase synthesis.

Metabolic labeling, also referred to as biosynthetic labeling, relies on simple organisms, which are able to incorporate stable isotope labeled nutrients into their biomolecules. The first studies

were conducted in bacteria such as Escherichia coli, where growth media with a single carbon or nitrogen source were used. With isotopically labeled glucose or ammonium sulfate as nutrients a complete labeling of the nucleic acids with ^{13}C and ^{15}N was achieved.[206] Later, stable isotope labeling was achieved in Saccharomyces cerevisiae,[209-211] and other organisms. Metabolic labeling has also proven to be a fundamental tool for the identification of bacterial communities that share similar metabolic pathways using RNA-stable isotope probing (RNA-SIP).

These approaches are uniform labeling approaches, as all carbon and nitrogen atoms become labeled. By combining bacterial knockout strains with differentially labeled nutrients such as 1,3-$^{13}C_2$-glycerol, an atom-specific isotope labeling becomes possible and, *e.g.* all carbons, except C_4' become carbon-13 labeled.[212] Both NMR and MS studies commonly use metabolic labeling, but the *in vivo* production of labeled RNAs is a key tool to NMR.

In 1992, Pardi and coworkers established the field by feeding E. coli with ^{13}C-glucose and ^{15}N ammonium sulfate.[206, 213] These early techniques used a single carbon or nitrogen source in the bacterial growth media. From these nutrients, the cell formed the amino acids glycine, aspartic acid and glutamine, which are in combination with the carbon donor tetrahydrofolate (THF), carbon dioxide (CO_2) and the phosphoribosylpyrophosphate (PRPP) building block the main components during nucleotide biosynthesis.

Carbon-13 labeled PRPP, THF, CO_2, aspartic acid and glycine are formed from $^{13}C_6$-glucose metabolism which leads to the incorporation of carbon-13 into the nucleotides. ^{15}N-ammonium sulfate as a nutrient leads to ^{15}N-labeled aspartic acid, glutamine and glycine, which are the nitrogen donors of nucleotide biosynthesis. In pyrimidines the N1, C4, C5 and C6 positions derive from aspartic acid (Asp), the C2 from CO_2 and the N3 from glutamine (Gln). The N4 of cytidine is incorporated from a glutamine (Gln). Purine position N1 and the exocyclic N6 of adenine are from aspartic acid (Asp). Position C4, C5 and N7 are from glycine (Gly). Positions N3, N9 and the exocyclic N2 position of guanine are from glutamine (Gln). Positions C2 and C8 are from THF and the remaining position C6 derives from CO_2 incorporation. After *de novo* nucleotide synthesis, dNTPs and rNTPs are used for DNA synthesis and RNA transcription and stable isotope labeled nucleic acids become available.

Uniform labeling with stable isotopes is commonly used in MS to identify and study modified nucleosides. The complete substitution of all, e.g. carbon or nitrogen atoms by stable isotope labeling has become a key tool for sum formula generation and is very helpful for structure prediction and verification by MS.[209, 210, 214, 215] Quantification of modified nucleosides requires the availability of stable isotope labeled internal standards. Due to the high chemical diversity, metabolic labeling is an optimal tool for their production.[209, 210, 216-218]

For a long time, no stable isotope labeled internal standards for oligonucleotide MS (oligo-MS) were available and the technique was limited to non-quantitative statements about the localization of modified nucleosides. The main challenge is that it is not possible to predict and synthesize all possible oligonucleotides as stable isotope labeled standards.

An interesting approach for RNA modification analysis of oligonucleotides was described as the comparative analysis of ribonucleic acid digests (CARD). This approach employs isotope labeling during RNase digestion, which allows the direct comparison of a tRNA of unknown modification status against a reference tRNA, whose sequence or modification status is known. The reference sample is labeled with ^{18}O during RNase digestion while the candidate

(unknown) sample is labeled with ^{16}O. These RNase digestion products are combined and analyzed by mass spectrometry. CARD approach for RNA modification analysis simplifies the determination of differences between reference and candidate samples, providing a route for higher throughput screening of samples for modification profiles, including determination of tRNA methylation patterns.[219]

The technique was further improved in 2017, when upon the original $^{18}O/^{16}O$ labeling CARD method was developed in Limbach lab, namely stable isotope labeling comparative analysis of RNA digests (SIL-CARD) approach.[220] For Characterization of *in vivo* RNA sample, it was directly compared with a reference RNA, the sequence of which was known. This reference is in vitro transcribed using a $^{13}C/^{15}N$ isotopically enriched nucleoside triphosphate (NTP). The two RNAs were digested with an endonuclease, the specificity of which matches the labeled NTP used for transcription. Overall, SIL-CARD simplifies data analysis and enhances quantitative RNA modification mapping by mass spectrometry.

Similarly, stable isotope-labeled ribonucleic acid as an internal standard (SILNAS) allowed the determination and quantification of all modified nucleosides in *Schizosaccharomycespombe*

rRNAs and generated the first complete modification maps of eukaryotic rRNAs at single-nucleotide resolution.[85] Quantitative analysis of dsRNA is also possible by using metabolically prepared RNA form *E. coli*.[221]

Specifically, for absolute quantification of nucleosides, stable isotope labeled compounds are necessary to overcome the limitations of MS. In quantification, the signal intensity of an analyte must correlate with its concentration or amount of analyte, but in addition on a multitude of other parameters such as salt load, ionization properties of the analyte, instrument parameters and so on. These detection fluctuations make quantification by MS a challenging task, which can only be done by using stable isotope labeled internal standards (SILIS) of the analyte of interest. Our lab has reported metabolic isotope labeling to produce isotopically labeled internal standards in bacteria and yeast. These can be used for the quantification of at least 26 different modified nucleosides. It is explained in detail how these internal standards are produced and show their mass spectrometric characterization. These internal standards provide quantification of the modification content of RNA species from bacteria and various eukaryotes. It was confirmed that the origin of the internal standard has no impact on the quantification result.[222] Knowledge on the absolute abundance of, e.g. modified nucleosides in an RNA of interest is crucial to the field and allows studies of RNA modification function and impact.[211, 222]

More detailed information is presented in my review on recent progress in the analysis of RNA modification and structure on the basis of stable isotope labeling techniques.[223]

"Benefits of stable isotope labeling in RNA analysis" **Asadi-Atoi, P.**, Barraud, P., Tisne, C. and Kellner, S. *Biol. Chem.* **2019** Jun 26;400(7):847-865.

Declaration of contribution: The research, all graphs and tables were generated by me, the manuscript was written and completed by cooperation of all authors.

Mass spectrometry for the investigation of RNA modifications

Even with the ever-rising number of sequencing techniques, which detect modified nucleosides in whole transcriptomes, MS remains the key technique for characterization of modified nucleosides. RNA MS analytics can be subdivided into two principles. The first uses enzymes, which partially digest RNA into smaller oligonucleotides. Here, some of the sequence context surrounding a modified nucleoside remains and the technique is used to place modified nucleosides in known and unknown RNA sequences. The second relies on complete enzymatic digestion of the RNA into the nucleoside building block and is highly sensitive. This technique is commonly used for detection, quantification or discovery of modified nucleosides. Especially for quantification, stable isotope labeled compounds are necessary to overcome the limitations of MS.

For quantification, the signal intensity of an analyte must correlate with its concentration or amount. In MS, as mentioned before, the signal intensity is affected by other parameters such as salt load, ionization properties of the analyte, instrument parameters and so on, which can only be overcome by using SILIS of the analyte. Knowledge on the absolute abundance of, e.g. modified nucleosides in an RNA of interest is crucial to the field and allows studies of RNA modification function and impact.

Depending on the sample preparation of the target RNA, MS analysis can be subdivided into three categories: Top-Down MS, Oligonucleotide MS and Nucleoside MS.

Top-down MS

In top-down MS, unhydrolyzed intact RNA molecule is ionized and the total mass is analyzed, so that the sequence information and exact position of RNA modifications would not be lost. With this approach, determination of oligonucleotides mass for tRNA isoacceptors and 5S rRNA along with identification of potential modification sites were performed, using tandem mass spectrometry (MS/MS).[224, 225]

A good assessment of the top-down MS method quality is the sequence coverage, which can be verified by fragmentation and the generation of overlapping ion series. It was possible to detect a 39 nucleotide long RNA with full sequence coverage, while each of the 37 phosphodiester linkages in this molecule was cleaved at least once and the two complementary partial fragments could be detected by MS, using radical transfer dissociation (RTD).[226]

One advantage of the top-down approach is that digestion steps are avoided and the sequence information of the RNA is completely preserved. On the other hand, very pure RNA sample is required for this purpose (no cell extracts), or otherwise the data analysis would be too complex, which is considered a disadvantage. Furthermore, this type of MS requires very expensive instruments, sophisticated software and still, the differentiation of mass-identical RNA modifications, such as m^1G and m^2G, or Ψ from U is very difficult.

Oligonucleotide MS

Oligonucleotide MS is based on the partial digestion of RNA and the reconstruction of the entire sequence by identifying fragments in which modifications may be partially present in context. The oligonucleotides can be separated chromatographically via HPLC prior to MS and fragmented individually into smaller units or single nucleosides in the collision cell of MS/MS. This method, introduced by McCloskey is able to detect the complete modification profile of mRNA, a mixture of many tRNA isoacceptors, rRNA and snoRNA, with assignment to specific sequence sites within oligonucleotides, using selective RNase cleavage.[227]

Sequence-specific RNases that create 5-15mer RNA fragments, are helpful for generating oligonucleotides that are easier to ionize. Usually, a combination of several RNases are used. For instance, RNase T1, Colicin E5 or MazF, are usually used together to digest RNA for analysis, to achieve higher sequence coverage. It is possible to use different RNases at different frequencies on the same RNA molecule and thus gain oligonucleotides of different sizes.[228]

Still, the differentiation of detected modifications with the same mass within the oligonucleotide is not possible. Therefore, recording MS/MS spectra and the corresponding subsequent software analysis play a key role in the identification and localization of a modification. Through softwares such as RNAModMapper (RAMM) and Nucleic-AcidSearchEngine (NASE), modifications mapping from a few nano grams of a RNA species mixture to be mapped within the sequence .[229, 230] As mentioned in the previous section, suitable isotope labeling strategies can support modification assignment to distinguish mass-identical RNA modifications.[231]

The more complex the RNA mixture, the greater the probability of co-eluting fragments and the number of oligonucleotides to be detected in the MS, especially in light of different abundances of individual fragments. Intensive sample preparation steps or orthogonal LC/LC approaches are required to reduce sample complexity and facilitate detection. Separation of oligonucleotides was thus improved using the 2D LC technique.[232]

Co-eluting RNA fragments in LC of complex RNA mixtures, is a challenge in the separation prior to oligonucleotide MS. Laboratory-intensive sample preparation steps or orthogonal LC/LC approaches are necessary to recompense for this issue. In recent years the separation of oligonucleotides has been improved using the 2D LC technique.[232, 233]

Liquid chromatography for oligonucleotide MS is usually performed on a reverse phase (RP) column. However, due to the hydrophilicity of the negatively charged phosphodiester backbone of the oligonucleotides, the material of the column is modified with ion-pairing reagents, so called ion-pair reversed-phase high-performance liquid chromatography (IP-RP-HPLC), to act as a pseudo-ion-exchange column for better retention of the RNA fragments. The most commonly used ion pair reagents, or modifiers, are triethylamine (TEA) or hexafluoroisopropanol (HFIP), which interact with the nonpolar column material via their alkyl radicals, but at the same time include polar or ionic groups that interact with the negative RNA.[234, 235] The use of a modifier, like HFIP, is required to overcome the reduced MS sensitivity for electrospray ionization typical with ion-pair reagents.[235] Although high concentrations of HFIP can also lead to ion suppression.[236] Moreover, the choice of ion-pair reagent can affect the degree of ion suppression and that the optimal ion-pair reagent and modifier system can depend on the type and content of the oligonucleotide.[237]

To circumvent the problem of ion pair reagent usage, other chromatography methods have developed, such as usage of hydrophilic interaction liquid chromatography (HILIC) columns, which are run with aqueous ammonium acetate buffer and acetonitrile, without the addition of ion-pair reagents.[238, 239]

Nucleoside MS

With the development of thermospray and electrospray ionization, the analysis of nucleosides became possible by liquid chromatography coupled-mass spectrometry (LC-MS).[240] In this method, there is no sequence information, since RNA goes through total hydrolyzation by enzymatic digestion, and the resulting single nucleosides mixture is directly separated by LC followed by sensitive detection in the mass spectrometer.

The RNA of interest is hydrolyzed by a mixture of enzymes consisting of a nuclease, phosphodiesterase and alkaline phosphatase, which was developed by Crain *et al.*[241] Besides the loss of sequence information, total digestion has other disadvantages. For example, contaminated RNA after digestion can distort the modification content in the RNA of interest. MS artifacts can also arise from different choices of digestion protocol, which must be identified.[242, 243]

Like oligonucleotide MS, nucleoside MS requires a prior separation of the modifications, by a prior chromatography. In most cases, RP-HPLC is used, which leads to a separation of a large number of RNA modifications in only 12 minutes run time.[240]

To produce gas-phase ions from RNA molecules, two ionization methods have proven to be suitable: MALDI (matrix assisted laser desorption/ionization), which makes it possible to ionize RNA up to 150 kDa ,[244, 245] and ESI (electrospray ionization).[246]

MALDI is often used for the analysis of macromolecules such as oligonucleotides. However, ionization in MALDI-MS usually transfers a charge, thus the analyte becomes unstable.[247] On the other hand, the spectra can be evaluated more easily due to simpler mass assignment. MALDI is usually coupled with a high-resolution TOF detector (time of flight). ESI-MS is more cost-effective than MALDI, is gentler on the analytes and has the advantage of modular coupling with an upstream reverse phase (RP) HPLC, on which small analytes, such as nucleosides, can be separated chromatographically and thus do not increase the complexity of the sample.[248] In LC-ESI-MS, a low-resolution triple quadrupole mass spectrometer (QqQ) is usually used. Its high sensitivity, as well as the regulation of different voltages are ideally suited for the simultaneous and accurate detection of multiple nucleosides and isotopologues with tuned fragmentation and mass-specific filtering.[249, 250]

For high-resolution mass spectrometers, a time of flight (TOF) or an orbitrap is usually used as mass analyzers. On the other hand, the highest sensitivity can be achieved by a triple quadrupole mass spectrometer (QQQ). After ionization in the source, the ions are filtered via a first quadrupole on the basis of their mass-to-charge ratio (m/z). After selection of the so-called precursor ions, these are transferred to the collision cell, where collision with an inert gas (often nitrogen) releases product ions (CID, collision induced dissociation). With a few exceptions (e.g. Ψ), the charged nucleobase is thus obtained in nucleoside analysis via this mass transfer. This is filtered again by setting the appropriate m/z ratio via a second quadrupole

and thus passed on to the detector. There, the incoming ion triggers a chain reaction via a signal amplifier and is then detected in the form of individual released electrons. This measurement mode is called dynamic multiple reaction monitoring (D-MRM). In a fraction of a second, the electronics of the individual components can be changed in such a way that in a single second over 50 different mass transitions can be detected. The targeted selection of individual ions eliminates background noises and thus achieves a high sensitivity. With combination of an upstream HPLC with ESI source, simultaneous quantification of several small molecules (in here nucleosides) is possible.[251] The general setup of a triple quadrupole mass spectrometer is shown in figure **1.10**.

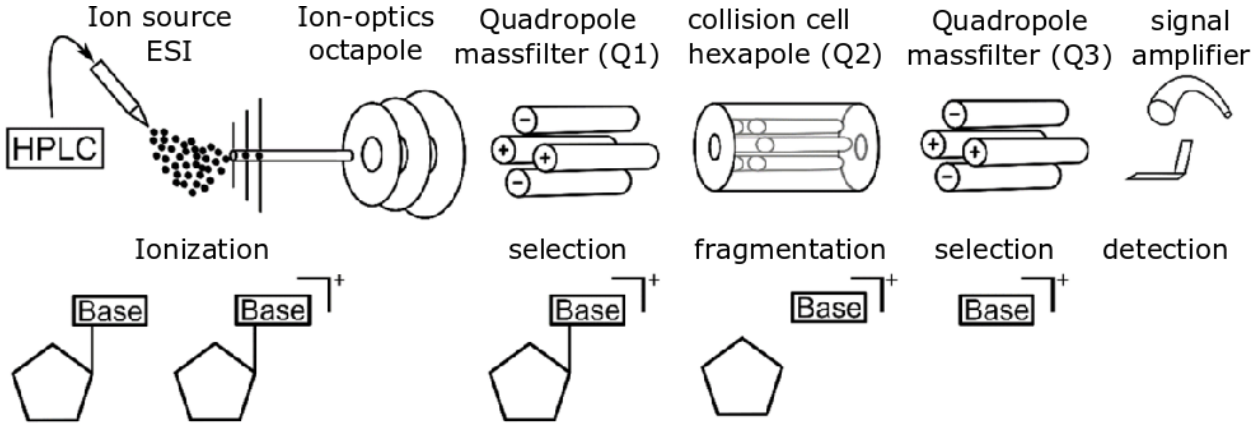

Figure 1. 10 Structure of an LC-MS/QQQ system.

Markedly, mass spectrometry overall is not a quantitative method. Nonetheless, it has the capacity to become a quantitative method, with the help of including internal standards and calibration curves, which includes dilutions of a nucleoside mixed with a constant amount of an internal standard and then measured.[252, 253] The equal amount of internal standard is added to the samples, allowing the amount of nucleoside in each sample to be determined via the calibration line. The internal standard should ensure that error effects such as ion suppression or deviating ionization properties have no influence on the outcome and is therefore, in the best case, an isotopologue of the analyte nucleoside.[222, 253] With these, absolute quantification of over 170 modified nucleosides has been easily accessible in our lab.

NAIL-MS

RNA has the option for removal of an unwanted modification: the RNA itself is degraded and a new RNA is transcribed. This potential competition between these two processes makes it difficult to study the dynamics of RNA modifications. Although we have seen many studies in the last few years, which claim that mRNA is enzymatically demodified, no solid *in vivo* proof has yet been presented. Due to limited number of tools to study the dynamics of RNA modifications and in addition, the complex process of finding biological consequences to RNA modifications, studying time-based modifications removal by RNA degradation and transcription of new RNA molecules has been a challenge. Currently, quantitative MS of RNA

modification profiles was used to claim an active demodification *in vivo*.[254] However, the absolute number of a modification within an RNA does not reflect the origin of the modification. For example, the decrease in modification density can be explained by enzymatic demodification processes but also by increased degradation of modified RNA or even by increased transcription of the RNA, without it being modified. *Vice versa*, an increase in modification density can be explained by additional modification events in the original RNA or by increased degradation of non-modified RNAs.

Our lab, headed by Prof. Dr. Stefanie Kaiser presented the establishment and application of a technique, which overcomes these current limitations by utilizing metabolic stable isotope labeling. The technique is termed nucleic acid isotope labeling coupled MS (NAIL-MS). The principle of NAIL-MS for analysis of dynamic (de-)modification processes relies on a pulse-chase type experimental set-up. The cells are grown in a particularly labeled growth media and upon exposure to a pulse, *e.g.* RNA damaging agent, the media is exchanged to a differently labeled media. With this principle, it is possible to study the fate of the RNA present during the pulse and chase their behavior. It is also possible to study the kinetics and behavior of the newly transcribed RNAs and observe their modification status over time. The pre-requisites, labeling techniques and necessary validation experiments of NAIL-MS studies has been very well described in recent methods papers.[211, 255] Other NAIL-MS capabilities include tracking modification dynamics, or comparative/comparative studies similar to experiments performed in proteomics in the context of SILAC. In addition, biosynthetic production of internal standards in the form of SILIS in multiple model organisms is possible. The advantages of the application of NAIL-MS as well as first successes have already been published in several papers,[222, 256] some of which are also part of the present dissertation.

2.Research goal

RNA molecules dynamically change their modifications density, by incorporating new modifications and removal of unwanted modifications. This dynamic process is known to associate with some neurological diseases, several types of cancer, and mental disabilities. Moreover, RNA molecules are constantly degraded and a new RNA is transcribed in cells. These two processes make the study of RNA modifications dynamics complicated.

Absolute or relative abundance of individual modified nucleosides in specific RNA types of mice has been investigated by many scientists in different contexts. However, exploration of tissue-specific or RNA molecules specific modification levels has not been broadly reported, noting there are a few reports focused on only one type of RNA and limited types of modifications. With the goal of creating a tissues- and RNA species-wide modifications library, one can refer them to potential organs function- or RNA type- specific function through linking to transcription dynamics as well as translational pattern. First, absolute quantification of all existing RNA modifications for each RNA species should be plotted, so that comparison among abundance of each RNA modification in different tissues, as well as each tissues RNA species modifications becomes available. After validation, codon bias inquiry on the modifications is possible. I aimed connecting a specific tRNA anticodon modification between cortex and liver to their corresponding amino acids abundances to signal the translational consequence. A grasp of tissue or RNA species specificity, transcriptional phase dynamics, translation patterns and possible gender specificity of modifications, are the main goals of the first chapter.

So far, quantitative mass spectrometry (MS) of RNA modifications was the method of choice, to prove RNA demethylation *in vivo*. However, this statement is not conclusive, since absolute quantification with MS *per se*, offers a static view by giving the absolute number of a modification, which does not reflect its origin. Expressly, the "decrease" in modification density can be explained by enzymatic demodification processes, but also by degradation of modified RNA or even by dilution effect, due to increased transcription of new RNA, without carrying that modification. Similarly, an "increase" in modification density can be derived from either additional modification events in the original RNA or by increased degradation of non-modified RNAs. Therefore, a method is required to include distinctive original or new transcripts as well as enzymatic or damage-induced modifications.

To overcome the mentioned limitations of MS, establishment and application of NAIL-MS was developed, utilizing metabolic stable isotope labeling in eukaryotic cell culture. NAIL-MS provides the study of RNA fate present during the pulse, and chase their behavior. It is also a promising tool in studying kinetics and behavior of the newly transcribed RNA and observe their modification status over time.

The abundance of modifications is carefully altered in cells. This regulation is achieved by transcriptional speed, abundance of RNA writers and activity of RNA erasers. So far, RNA erasers are mainly studied *in vitro* and *in vivo* studies are absent. The goal in this regard was to investigate RNA eraser enzymes AlkBH1, 3 and 5 *in vivo* activity in demethylating each of their specific methylated ribonucleotide substrates in HEK cells. To investigate such activity, experiments including *in vivo* knock down of each enzyme are required to compare the absolute

amounts of the target modifications in presence and absence of the AlkBH protein, Moreover, stressing the cells by MMS methylating reagent, and following up enzymes expression levels, as well as RNA modification changes under mentioned treatments would shed light to modifications dependence on the enzyme activity. The goal of studying AlkBHs expression levels as well as analysis under MMS treatment was followed. I aimed *in vivo* study of AlkBH1, 3 and 5 activities in tRNA, rRNA and mRNA. All analyses are provided by either nucleoside LC-MS/MS for RNA or western blot for protein molecules.

Under stress conditions, human angiogenin enzyme (ANG) is known to cut tRNA into stress induced halves (tiRNA). So far, there is very little known about functions or dynamics of these tiRNAs in cells. Studies on their stability are commonly done with synthetic tiRNAs, which neglect the native modification status of tiRNAs, which emerge often from modified tRNAs. Drino *et al*. study suggested existence of m^2G and Um on the 5´-tiRNA$^{Gly}_{GCC}$ but no other modification from the precursor tRNA. Interestingly, in other context Um modification is expected to help with thermal and conformational stability of tRNA and its fragments in cells. Yet, no studies exist which focus on its function in tiRNA. Dynamic NAIL-MS has the potential to close this gap by following up the dynamics of synthecic, but (un-)modified RNA sequences within cells, by differentiating between the isotopic labeled native RNA and the unlabeled synthetic RNA. This feature would allow the study of tRNA fragments (tRFs) stability with focus on modification incorporation effect. In order to account for only biological uptake and exclude biological as well as sample preparation and analysis variables that can cause concentration/dilution effects, introduction of a new technical standard is required. Information about model tiRNA stability in cells as well as modification incorporation effect on temporal stability, can shed light to its functional significance.

3. Results and discussion

3.1. Profiling RNA modifications in mouse tissues by NAIL-MS

Despite sharing identical genomes and overlapping transcription profiles, mammalian tissues reveal diverse physiology and function. This specification arises from orchestrated gene transcription, epitranscriptomic processing of RNA and differential post-translational modifications that tune the activity of proteins to each tissue's needs.

Absolute or relative abundance of individual modified nucleosides in specific RNA types of mice has been investigated by many scientists in different contexts.[257, 258] However, exploration of tissue-specific RNA modification levels of different RNA species has not been well established, noting there are a few reports focused on only one type of RNA and limited types of modifications .[259, 260]

With the goal of creating a tissues- and RNA species-wide modification library, flash frozen mouse organs from three male and one female mice including heart, liver, cortex, lung, spleen, olfactory bulb and kidney were used.

I aimed to create tissue and RNA type modification profiles in order to refer them to potential organs function- or RNA type- specificity by linking to transcription dynamics as well as translational dynamics. figure **3.1** shows the concept of this project.

Our powerful NAIL-MS technique allows absolute and relative quantification of all existing nucleosides in any given RNA sequence. Using NAIL-MS, I provided a dataset of 24 tRNA modifications, and up to 22 rRNA modifications profiles. Tissue or RNA species specificity, transcriptional phase dynamics, translation patterns and possible gender specificity of modifications, are presented and discussed in the following chapters.

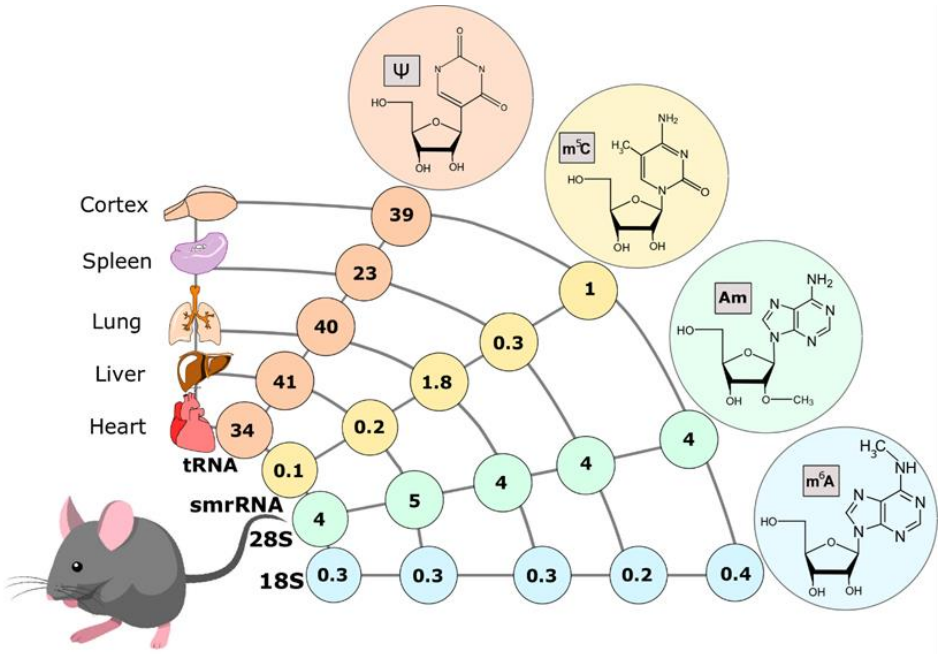

Figure 3. 1 Concept of profiling RNA modifications in different RNA types of mouse organs. All modifications are analyzed by NAIL-MS absolute quantification, in which quantified amount of each modified nucleoside is normalized to per 10^3 canonical nucleosides.

Total RNA was extracted from flash frozen mouse organs using phenol/chloroform-based isolation. RNA easily fragments in the presence of RNases but also chemically due to elevated pH or bivalent cations. Thus, it is important to check the length of total RNA after RNA isolation, as recently suggested by a study from the Helm lab.[94] I separated and analysed total RNA of each tissue by size exclusion chromatography (SEC), using a 300 Å SEC column. **Figure 3.2**, shows exemplary chromatograms of liver and spleen total RNA.

Based on total RNA chromatograms, there was no visible sign of *e.g.* rRNA fragmentation, as the example of liver chromatogram shown in figure **3.2.A** left side, shows a sharp separated peak with a good resolution between each RNA species at their expected retention time (Rt 4-5 min). Thus I moved on to isolate 28S and 18S rRNA, 5.8S-rRNA which contains 156 nt, and tRNA using established SEC protocols.[261, 262] All tissues total RNA showed a similar chromatographic pattern as the liver example, apart from spleen (figure **3.2.B** left side), which showed peak splitting for tRNA. This issue affected the precision of quantified spleen tRNA modifications, which will be discussed later.

Afterwards, I moved on to a second round of SEC, to isolate 28S- from 18S-rRNA using a 1000 Å SEC column, as viewed on the right side chromatograms of figure **3.2**. Comparing liver, which shows two distinctive peaks for respectively 28S and 18S to spleen rRNA chromatogram, a low resolution as well as peak splitting is observed for spleen; which makes it hardly definable as separated 28S and 18S peaks (**3.2**.B right). However, a good precision of quantified rRNA modifications between spleen replicates was observed. (fig **S1.4.** nested graphs).

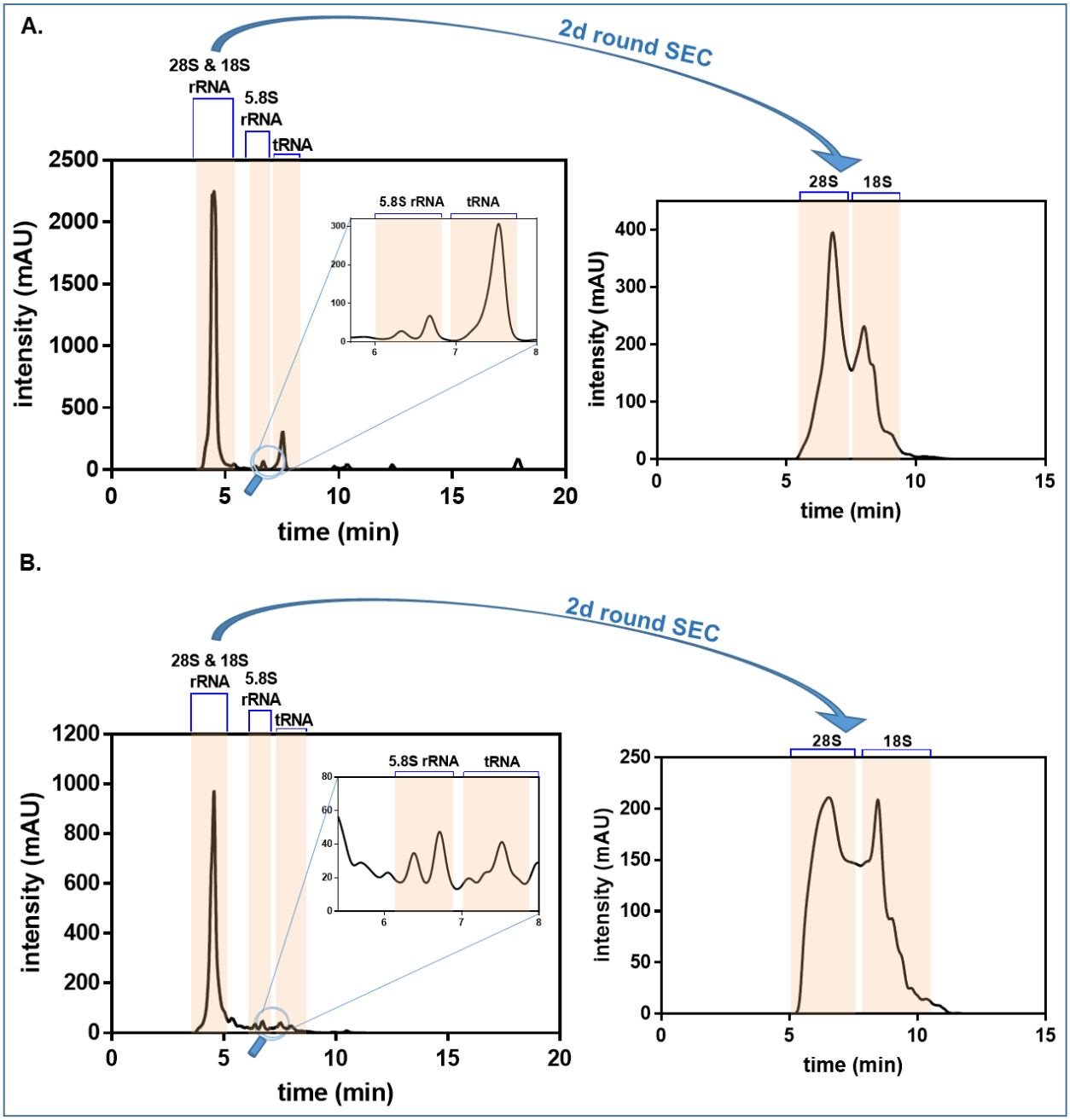

Figure 3. 2 SEC chromatograms for mouse replicate #2b in liver **(A)** or spleen **(B)**: total RNA separation of mouse by 300 Å column (left) and further separation of 28S and 18S by 1000 Å column (right).

As all tissues total RNA (apart from spleen) showed a similar chromatographic pattern as the liver example, total RNA samples integrity was proven unharmed by storage at -20°C for a 3-5 weeks of storage before analysis. Further separation of rRNA 28S and 18S was successful for other tissues (SEC not shown) just like the liver, apart from Spleen tRNA (fig.**3.2**.B).

I further investigated of the integrity and purity of isolated smrRNA, using RNA nano chip gel electrophoresis. Figure **3.3** shows the example of mouse #2b gel electrophoresis image of all tissues smrRNA after SEC collection. Given the fact that all bands (apart from olfactory bulb, which showed some impurities) show only one peak at around 160 nucleotides, which is

referred to the size of 5.8S RNA, as well as a single band at the same size on the gel image, it was confirmed that smrRNA collected fractions were composed of only 5.8S rRNA, which stayed intact during SEC isolation. After running such quality controls, absolute quantification protocol was in order, which is discussed further.

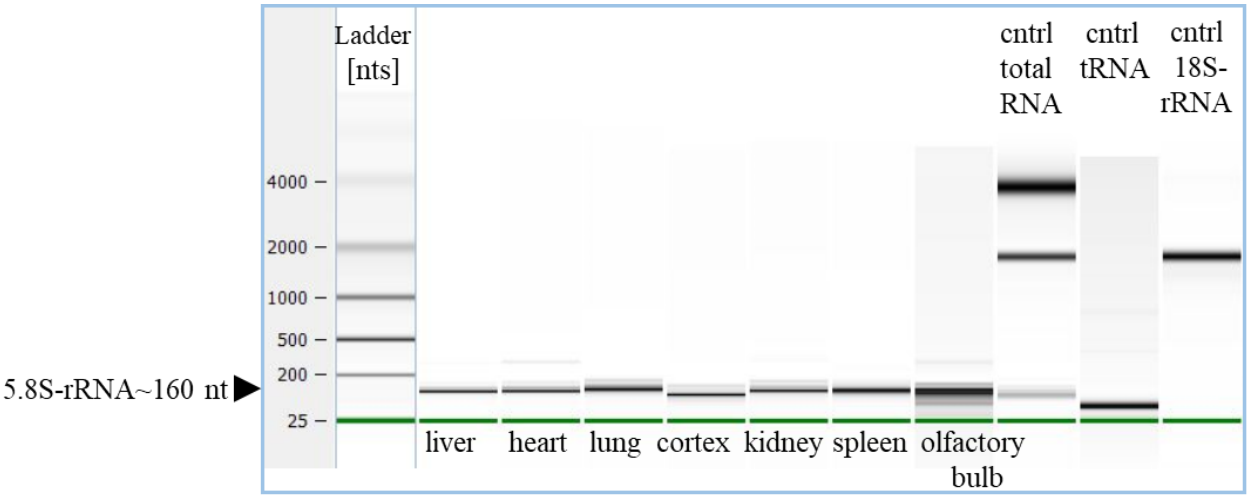

Figure 3. 3 Purification quality test of eluted 5.8S-rRNA of mice tissues. verified by Bionalyzer RNA Nano chip gel electrophoresis of mouse #2b.

3.1.1. Absolute quantification of RNA modifications in mouse tissues by NAIL-MS

Kaiser lab has established protocol for LC-MS/MS quantification of modified nucleosides.[222] I have adapted the existing protocol and utilized it to screen the modification profile of all isolated RNAs from all tissues in at least 4 technical replicates.

Figure **3.4** shows a schematic workflow for the analysis of mouse RNA tissues. After complete hydrolysis of the RNA into nucleosides, enzymes were removed by 10kDa molecular-weight-cut-off filtrations (MWCO). Subsequent analysis by targeted triple-quadrupole mass spectrometry in the presence of metabolically produced SILIS revealed the absolute abundance of canonical and modified nucleosides.

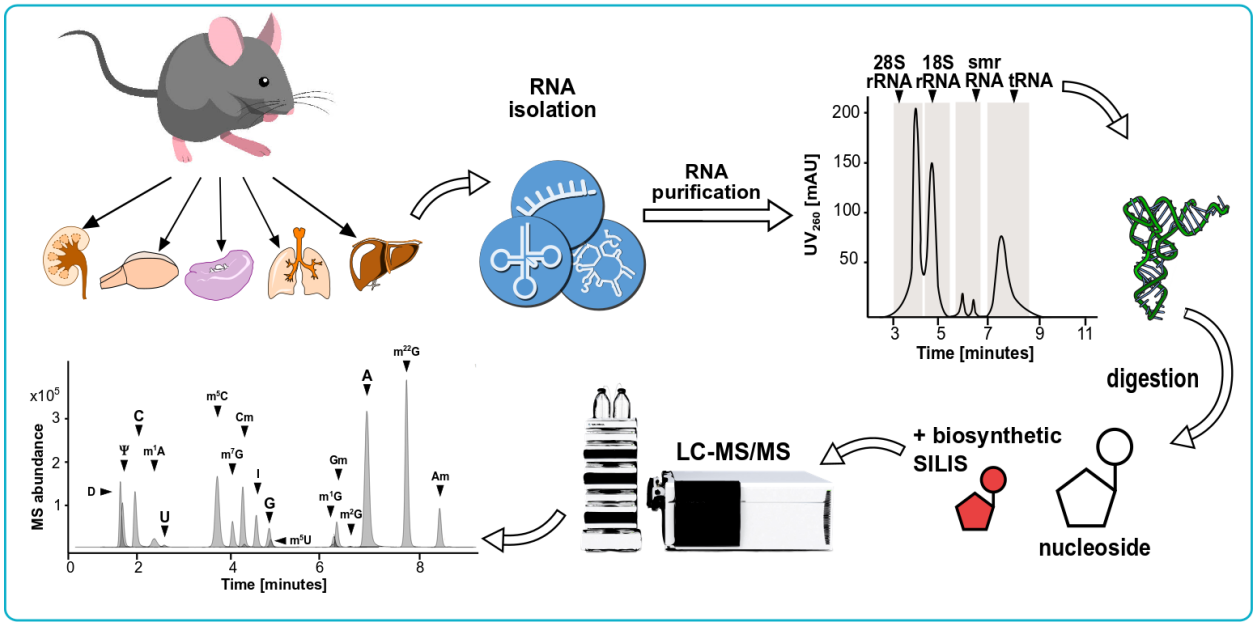

Figure 3. 4 General workflow and graphs for quantification of RNA modifications in mouse. To analyze RNA modifications, different mouse organs from four biological replicates (n=1 ,2 ,3 male and n=4 female) were divided into 4 technical replicates, then lysed by tissue ruptor and total RNA content was isolated through phenol/chloroform based extraction. RNA was separated into 28S ribosomal RNA (rRNA),18S-rRNA, small ribosomal RNA (5.8S-rRNA), and transfer RNA (tRNA) through size exclusion chromatography (SEC). The RNA samples were enzymatically digested into single nucleosides and analyzed by liquid chromatography–mass spectrometry (LC-MS/MS). Quantification was performed using rRNA or tRNA *S. cerevisiae* stable isotope labeled internal standard (SILIS), and analysis of serial diluted synthetic standard nucleosides as external calibration curve. The lines between four technical replicates of each mouse modification reflect the average.

In order to simplify the comparison of modification abundances for all RNA species among tissues, an identical normalization factor of modified nucleoside per 10^3 canonical nucleosides was used for the left y-axis. To get a better impression on the stoichiometric distribution of RNA modificaitons within the respective RNA, the abundance of modifications per RNA molecule was calulcated and is indicated by the right y-axis (fig **3.5-3.8**) The order of modifications is from highest to lowest abundant of liver tRNA (figure 3.5 A) throughout all RNA graphs, as shown in figure **3.5-3.8**.

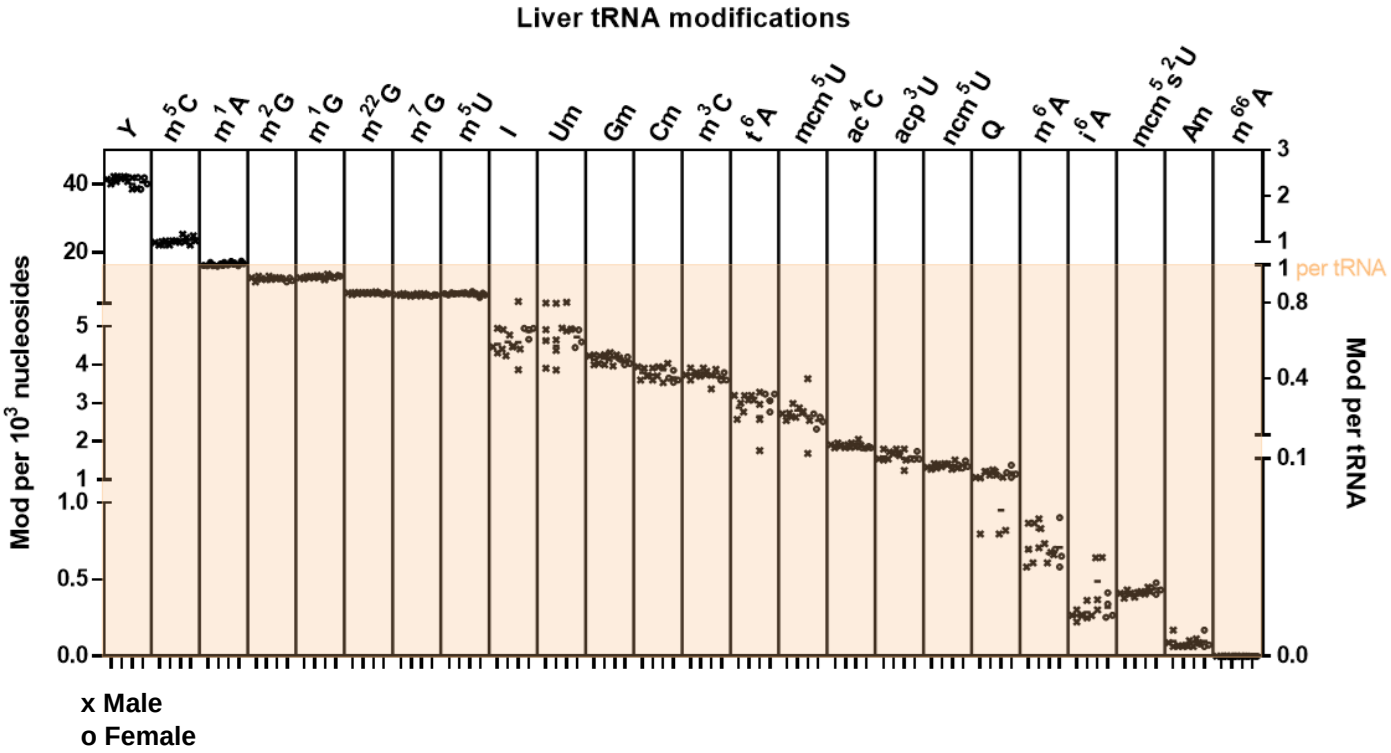

Figure 3.5 Nested graph of absolute quantified mice liver tRNA modified nucleosides. The modifications order is from highest to lowest abundant in tRNA. The left Y axis shows modifications absolute amounts normalized to each 10^3 nucleosides, and the right Y axis shows them per tRNA molecule.

As expected, the highest chemical diversity and abundance of modifications can be found in tRNA (fig **3.5**). Ψ is the most abundant modification, followed by m^5C and m^1A. All in all, the stoichiometries are reasonable with more than *e.g.* 2 Ψ per tRNA, as Ψ is located in all tRNAs at least once and sometimes up to 4 Ψ can be found in certain tRNA isoacceptors. On the other hand, less than 1 *e.g.* m^3C per tRNA, is found, which is reasonable as only 12 tRNAs out of 47 carry m^3C.

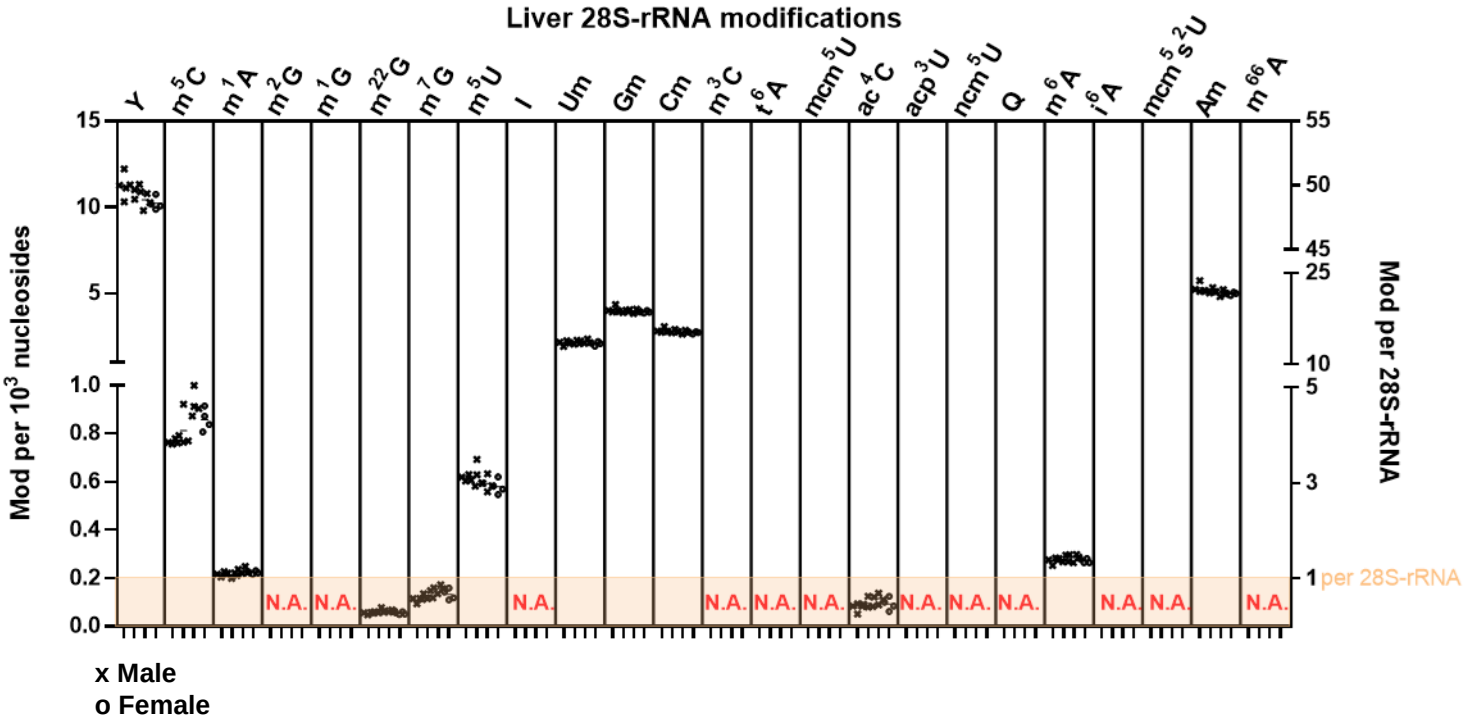

Figure 3.6 Nested graph of absolute quantified mice liver 5.8S-rRNA modified nucleosides. The modifications order is adapted from highest to lowest abundant in tRNA. The left Y axis shows modifications absolute amounts normalized to each 10^3 nucleosides, and the right Y axis shows them per 5.8S-rRNA molecule. Not analyzed modifications are abbreviated as (N.A.) on the graph.

Confident that our quantitative analysis is reasonable for tRNA (a detailed comparison with the literature is discussed later in this chapter), I analyzed the SEC-purified 5.8S-rRNA. As shown in figure **3.6**, the abundance and chemical diversity of modifications in 5.8S-rRNA is lower than tRNA (fig **3.5**). Moreover, the highest abundant modifications in 5.8S-rRNA are Ψ, and ribose 2′-O-methylations (Nm), which is reported in the literature.[263, 264] On the other hand, ~3 I per 10^3 nts was quantified in this study in average for all tissues, which is not so far reported in literature.

Judging from the absence of tRNA-specific anticodon loop modifications like mcm^5U and i^6A ,[265, 266] we are confident that the 5.8S-rRNA fraction is not contaminated with tRNA. While most analyzed modifications are below the LLOD or are present in sub-stoichiometric quantities, 6-methyladenosine (m^6A), and 4-acetylcytidine (ac^4C) appear to be present slightly above background, which are not reported to exist in the 5.8S-rRNA fraction so far.

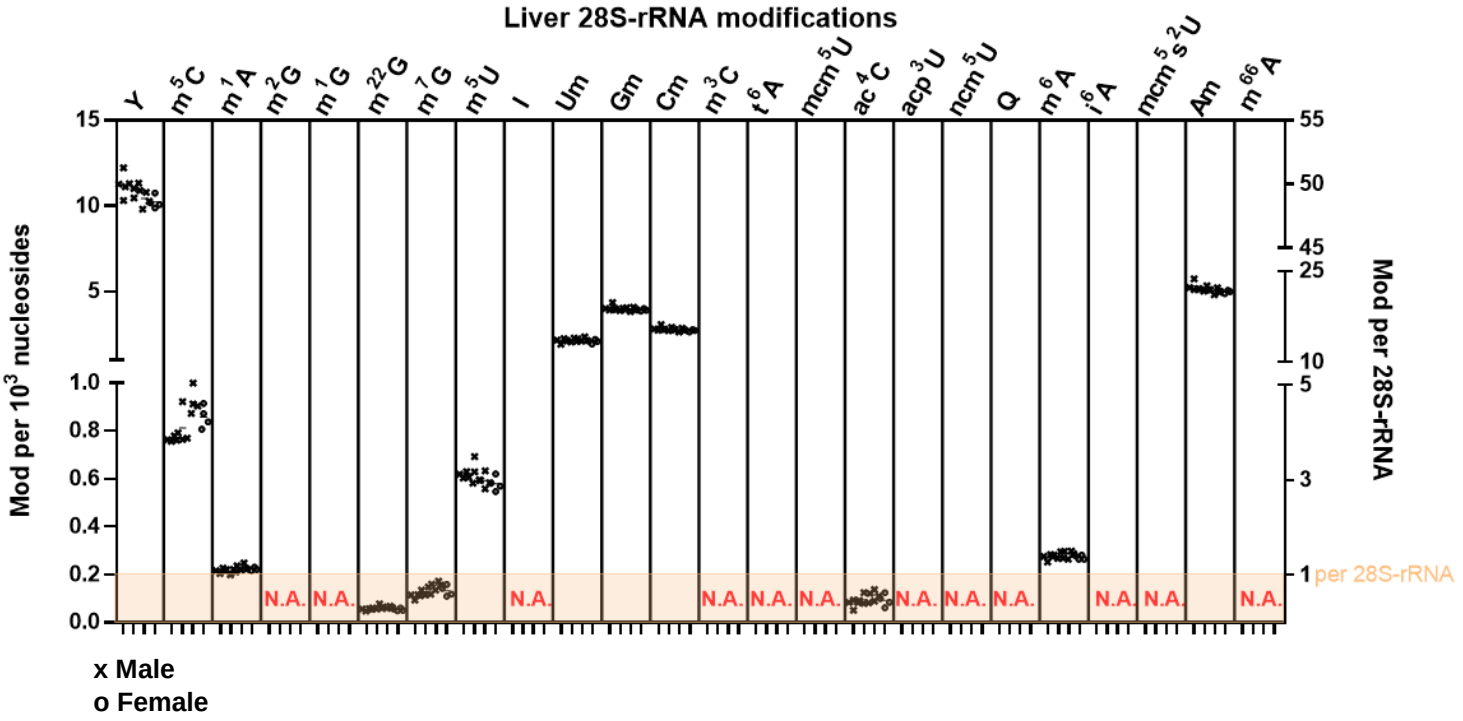

Figure 3.7 Nested graph of absolute quantified mice liver 28S-rRNA modified nucleosides. The modifications order is adapted from highest to lowest abundant in tRNA. The left Y axis shows modifications absolute amounts normalized to each 10^3 nucleosides, and the right Y axis shows them per 28S-rRNA molecule. Not analyzed modifications are abbreviated as (N.A.) on the graph.

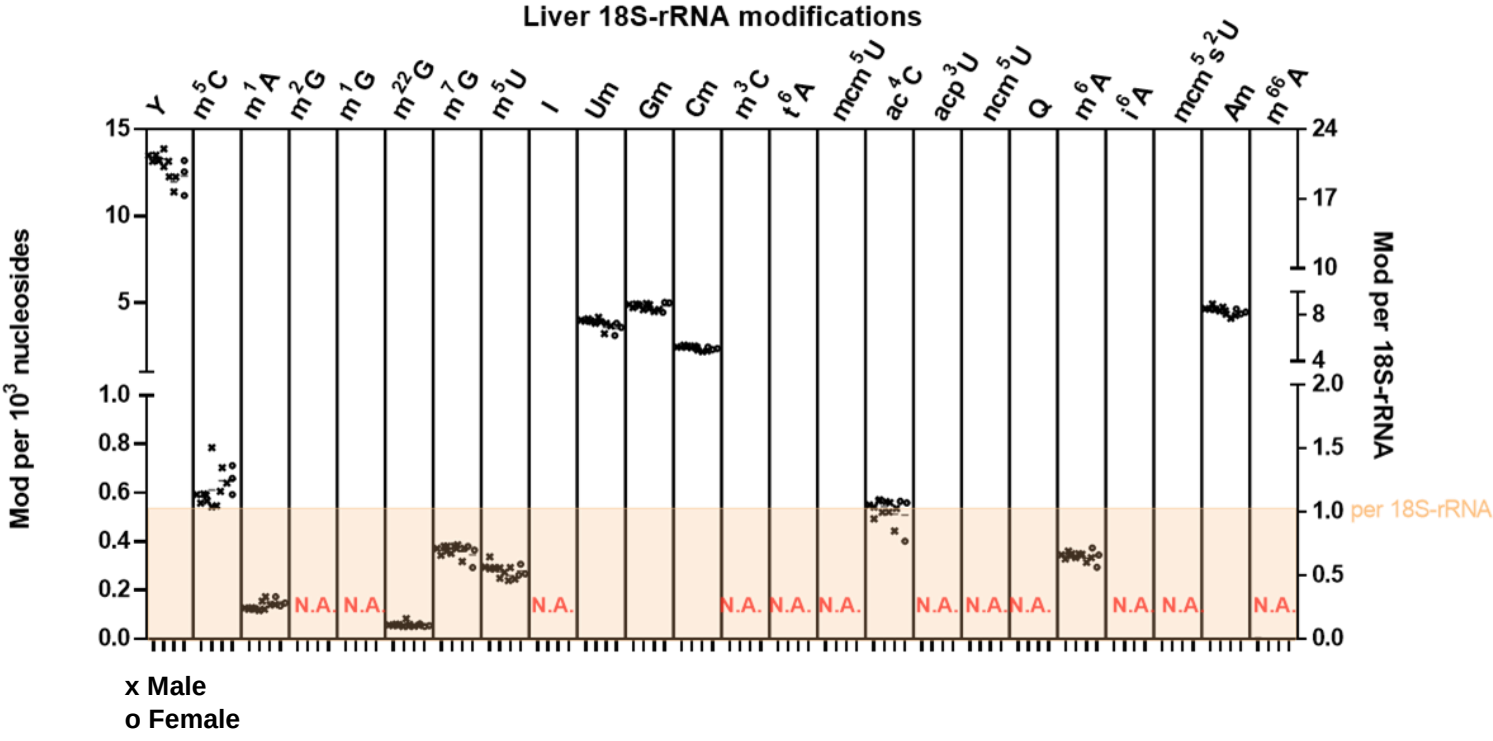

Figure 3.8 Nested graph of absolute quantified mice liver 18S-rRNA modified nucleosides. The modifications order is adapted from highest to lowest abundant in tRNA. The left Y axis shows modifications absolute amounts normalized to each 10^3 nucleosides, and the right Y axis shows them per 18S-rRNA molecule. Not analyzed modifications are abbreviated as (N.A.) on the graph.

The modification profiles of 28S rRNA and 18S rRNA are similar to the 5.8S rRNA fraction and mainly show high abundance of Ψ and Nm (fig **3.7** and **3.8**). In addition, we detect m^5C, m^1A and m^6A in 28S rRNA which is in good accordance with human 28S rRNA reported in literature.[17]

In 18S rRNA, we detect ac^4C, m^7G and m^6A which is also in accordance with expectation.[85] In addition, we detect low amounts of m^5U, which probably hails from mitochondrial rRNA co-eluting with our rRNA fractions.[267] One unique 18S rRNA modification N6,6-dimethyladenosine ($m^{66}A$) could not be analyzed in my samples. Due to the degradation of its SILIS counterpart, $m^{66}A$ was not quantifiable in any of the analyzed samples.

This is of high importance due to its suitability as a marker of 18S rRNA contamination in other RNA preparations such as tRNA or mRNA.[94] As a side note, based on my colleague **Gregor Ammann's** experience, loss of $m^{66}A$ from samples is caused by the use of sample preparation (MWCO filtration) commonly for enzyme removal prior to MS.[243] Thus, the use of MWCO filtration is not recommended if the $m^{66}A$ abundance is of interest. Inosine (I), is another modification that is not analyzed in 28S and 18S rRNA, due to co-elution issue with Adenosine signals for these sample sets. It is however expected to exist in low amounts in these rRNA species, as reported to have rare or below detection limit amounts in them.[94]

Moreover, due to the unavailability of synthetic standards for other potential Ψ modifications in rRNA such as Ψm or $m^1Ψ$, these modifications could not be quantified in this study. As shown in figure **3.5-8**, the technical and biological fluctuation is very small among the replicates. The nested graph of all other tissues can be found in **supplementary figure 1**.

3.1.2. Comparison of modification levels between different types of RNA

Comparison of modified nucleoside quantities between different types of RNA within a unique tissue, reveals important information on identification of candidate modifications for specific RNA type markers, as Helm lab approved $m^{66}A$ and Am as rRNA marker modifications.[94] The importance of marker modifications lies in excluding RNA species contamination with one another, to assess RNA purification protocols, as well as account for RNA degradation effects. Moreover, comparison of modification extent in each types of RNA, can reveal their functional relevance. To enable such a comparison, exemplary modification profile of each studied RNA type in mouse liver are plotted together in figure **3.9**, based on the average values for all 16 replicates.

As shown in figure **3.9**, for the highest abundant modifications like Ψ, the abundance is ~4 times higher in tRNA than all rRNAs. The same pattern exists for all studied tissues (**Supplementary Figure 2**). This is in accordance with the known functions of Ψ: In tRNA, Ψ alters structure, increases base stacking, improves base-pairing, and rigidifies the sugar-phosphate backbone.[69, 68] Ψ in rRNA is clustered in the peptidyl transferase center (PTC), the decoding center (DC) and the region above the A-site of the ribosome, and the sites where ribosomal subunits interact ,[88, 89] which suggest its functional significance on rRNA processing, protein synthesis, and cell growth.[89]

Another example is inosine. Several potential functions for post-transcriptional adenosine-to-inosine (A-to-I) RNA editing are already discovered in tRNA, such as enlarging the codon recognition capacity during protein synthesis and amino acid alterations.[268] My data shows ~6 I per 10^3 nts in tRNA and ~4 I per 10^3 nts in 5.8S-rRNA in average for all tissues (fig **3.9**). Given the fact that there is so far no literature report on the quantities of I in 5.8S-rRNA, inosine functional significance in 5.8-rRNA remains an open question for further study.

The consistency of modification amounts in all of my RNA datasets, confirms the fact that tRNA modifications are crucial for accurate and efficient translation of the genetic code, as well as tRNA folding or stability in all body organs, and therefore tRNA is the heaviest modified RNA molecule in all studied tissues.

My data shows a good correlation between 2′-O-methylated modifications (Nm) among different RNAs. In most of reports on Nm is found at positions 32 or 34 and mainly, U, C or G are methylated. I observed only low amounts of Am in tRNA among all investigated RNAs, as it is known to be absent in tRNA and considered as a 28S and 18S-rRNA fragment marker.[94]

Evidently, there is a kinetic preference of inosine formation through A-to-I editing over Am formation from adenosine at position 34 in tRNA.[269] Moreover, there are less enzymatic pathways leading to Am production than other Nms,[270] which can correlate to low amounts of Am in tRNA. Nm in rRNA is located in proximity of the PTC and the DC.[90] Notably, relative abundance of individual Nm sites is strongly conserved between human and mouse,[91] which has correspondence to universal regulation of the structure and function of ribosome in higher eukaryotes.

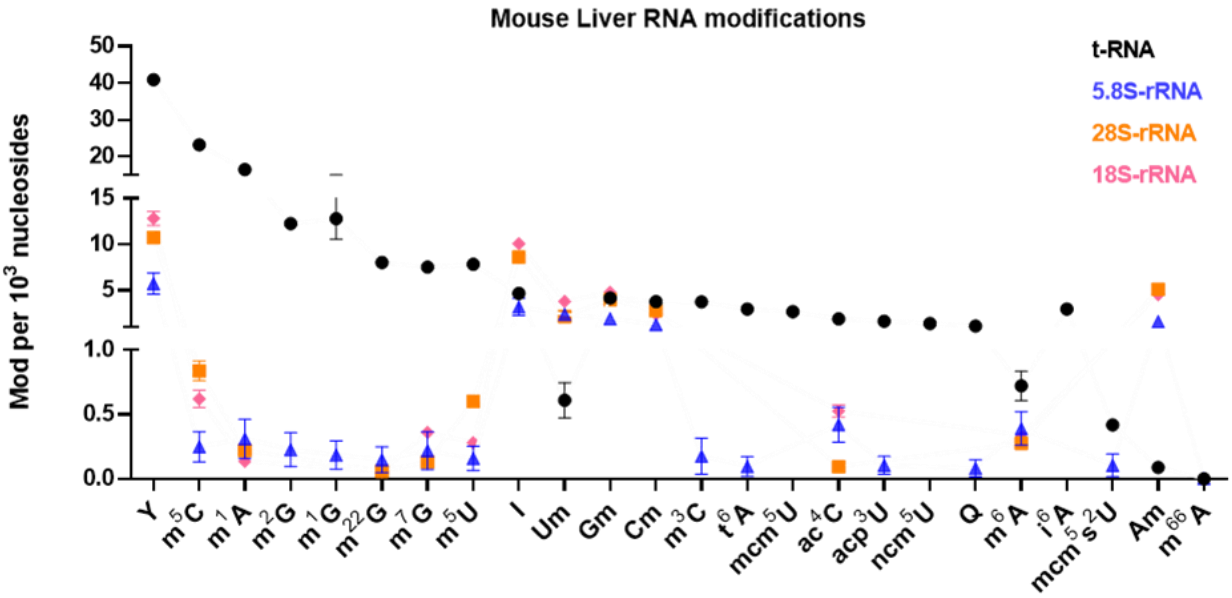

Figure 3. 9 modification profile of each studied RNA type in mouse liver, based on the average values for all 16 replicates. Error bars reflect the standard deviation. Symbles on the corresponding X axes only belong to analyzed modification amounts above LOD.

In the case of specific tRNA anticodon loop uridine modifications, previous studies in Byström lab revealed functional peculiarity of mcm^5U, mcm^5s^2U, and ncm^5U role in reading codons for some tRNA isoacceptors.[265] For instance, $tRNA_{mcm^5UCU}^{Arg}$ species decodes in the split codon box AGN (N: A or G) for arginine, whereas $tRNA_{mcm^5UCC}^{Gly}$ decodes in the glycine family codon box GGN. There are no reports on the existence of mcm^5s^2U, mcm^5U, or ncm^5U on rRNA so far, which is also confirmed by my data, that showed below detection limit signals for these modifications in rRNA.

3.1.3. Organ-specificity investigation of RNA modifications

Exploration of tissue-specific RNA modification levels of different RNA species has not been well established, noting there are a few reports focused on only one type of RNA and limited types of modifications.[259] For instance, Carell lab focused on tRNA modification density correlation with translational Efficiency, by comparing modification differences between mouse and pig organs.[260] In a recent study by Helm lab, fate of rRNA and tRNAs after organismal death via detection of their characteristic modifications was punctuated.

In order to take an initiative step in accounting for mammalian tissue-specific physiology and function, resulted from dynamic epitranscriptomic regulation, I provided a comparative plot of modification profiles between different mouse tissues for each RNA type, based on the average values of all four mice replicates (fig **3.10**). Interestingly, while tRNA of highly metabolic active organs such as liver, cortex and lung are highly modified and almost identical, a muscle tissue such as heart, shows lower levels of modifications (fig **3.10.**A).

Moreover, mitochondrial gene expression and thus transcript abundance varies between tissues based on tissue-specific energy demand. As provided by a study of Mercer *et al*. on the human mitochondrial transcriptome, in heart, mitochondrial transcripts comprise almost 30% of total mRNA content of cells, whereas it is only ∼5% of total mRNA in tissues with lower energy demand such as lungs.[271] My results on mice post-transcriptional modifications are derived from the total cellular RNA content which includs mitochondrial RNA.

My data show higher amounts of modifications for lung than heart. This trend challenges a direct relevance of post-transcriptional modifications to the energy-demand by the means of mitochondria transcriptome content. Although mitochondrial DNA comprises 0.1–2% of the total DNA in most mammalian cells, the RNA modification differences coming from mitochondrial content, might not be detectable.[272]

Quantities of modifications in mouse spleen tRNA, is the lowest among all tissues (fig **3.10.A**), with the exception of i^6A and Am, which is related to the poor isolation of Spleen tRNA from total RNA by SEC (fig. **3.2.**B). Am in spleen and olfactory bulb tRNA is surprisingly higher than the otherwise more modified-tRNAs from organs such as liver. Regarding the SEC trace in fig **3.2**, I observed stronger RNA fragmentation for spleen and thus my data confirms the report from the Helm lab, which claims that Am is an indicator of rRNA fragmentation.[94]

In contrast, i^6A, shows an opposite trend in higher modified tissues than less modified ones. As seen in figure **3.7.**A, spleen and heart which have the least amount of modifications, show the highest amount of i^6A compared to liver or lung, which is in a good correlance with Carell

2012 paper comparison as well (fig **3.8**). This effect can be due to i^6A helping translation fidelity in absence of other anticodon loop modifications.

In eukaryotes, Q is fully dependent on diet or on gut microbiome in multicellular organisms.[185] Interestingly the occurrence of Q in spleen tRNA is ~0.63 per 10^3 nts whereas ~1.2 in all the rest of tissues. Similarly, another helpful modification for codon reading namely ncm^5U shows the lowest abundance in spleen, which can suggest less need for diverse anticodon loop modifications in spleen.

As shown in figure **3.7.**B, 5.8S-rRNA of olfactory bulb shows a distinct profile with higher modification quantities than the rest of compared organs, although with a lower precision. Moreover, the amount of ribose methylations in 5.8S-rRNA such as Am, show unique amounts for each organ, which suggests 2′-O-methylation in 5.8S-rRNA can have organ-specific functions further than just RNA stability.[75] Nevertheless, the quantities of each modification in 28S and 18S-rRNA are mostly undistinguishable among all investigated tissues (fig **3.7.**C & D), which can be referred to a conservative ribose assembly and hence function during translation in all tissues.

Due to lack of quantifiable amounts after SEC elution for purified olfactory bulb 28S and 18S rRNA, this organ was not analyzed in those two RNA types, also Kidney modifications are absent in tRNA and 5.8S-rRNA measurments, due to the same issue.

A.

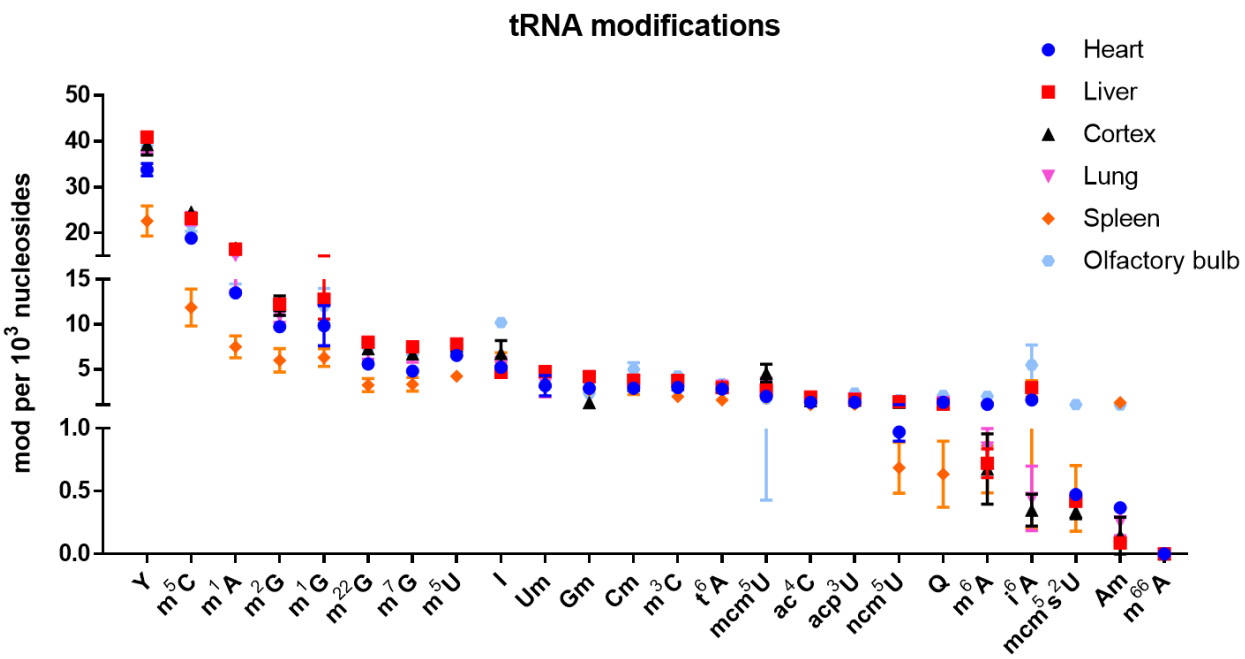

B.

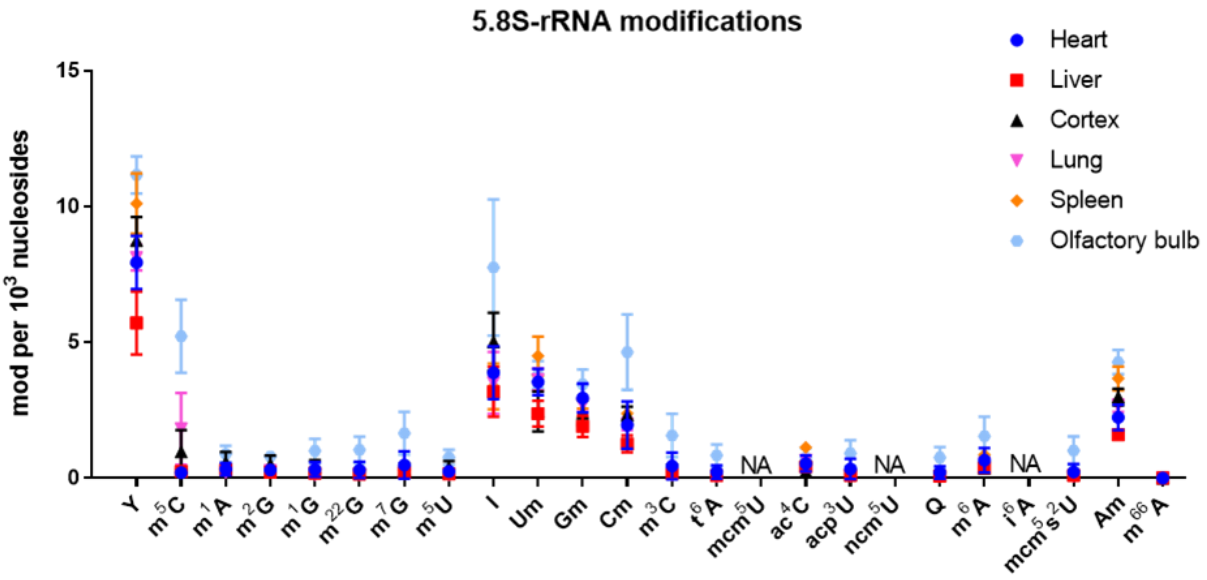
5.8S-rRNA modifications
mod per 10^3 nucleosides
15
10
5
0
Heart
Liver
Cortex
Lung
Spleen
Olfactory bulb
NA
NA
NA
Y
m^5C
m^1A
m^2G
m^1G
$m^{22}G$
m^7G
m^5U
I
Um
Gm
Cm
m^3C
t^6A
mcm^5U
ac^4C
acp^3U
ncm^5U
Q
m^6A
i^6A
mcm^5s^2U
Am
$m^{66}A$

C.

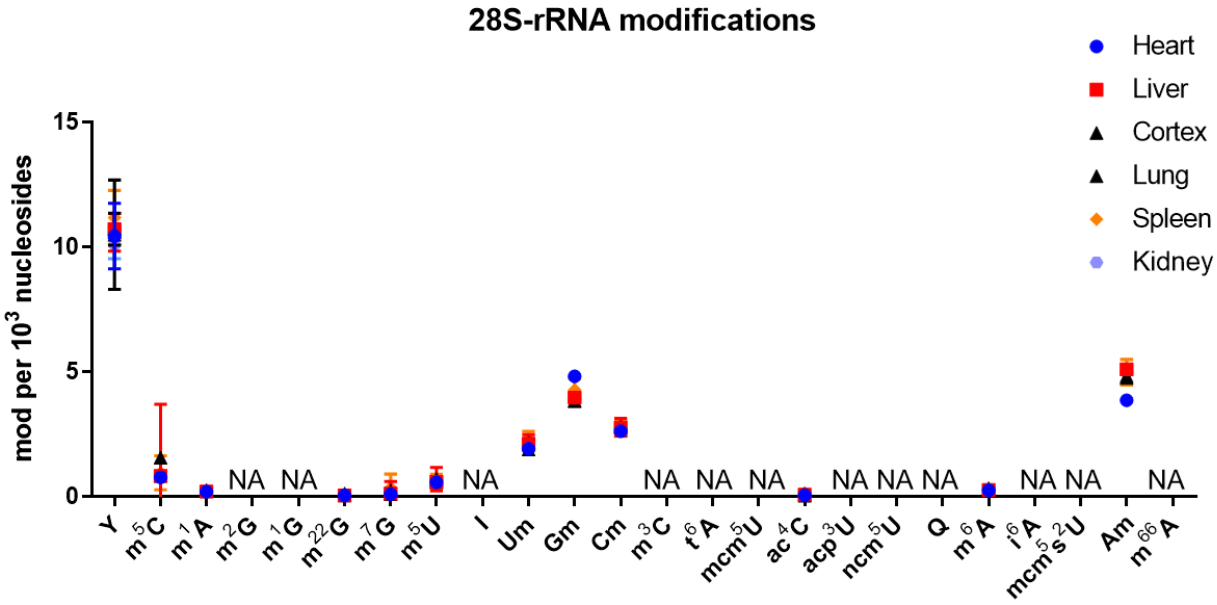
28S-rRNA modifications
mod per 10^3 nucleosides
15
10
5
0
Heart
Liver
Cortex
Lung
Spleen
Kidney
NA NA NA NA NA NA NA NA NA NA NA NA NA NA
Y
m^5C
m^1A
m^2G
m^1G
$m^{22}G$
m^7G
m^5U
I
Um
Gm
Cm
m^3C
t^6A
mcm^5U
ac^4C
acp^3U
ncm^5U
Q
m^6A
i^6A
mcm^5s^2U
Am
$m^{66}A$

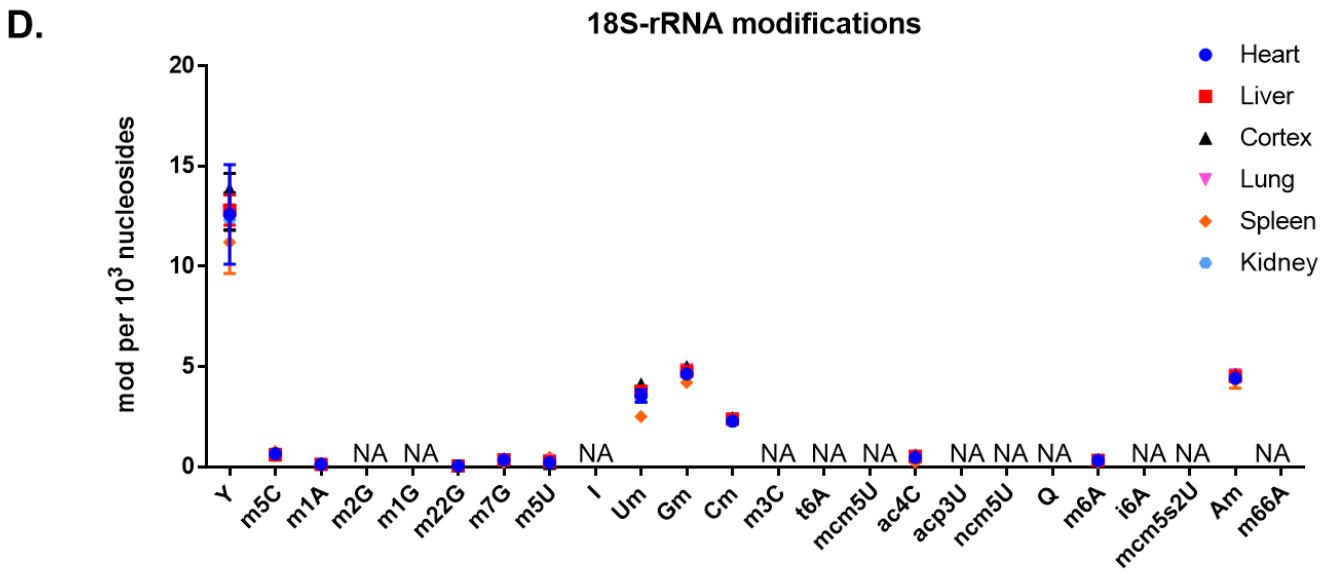

Figure 3. 10 Comparison of each RNA modifications in different mouse tissues. (A) Overlaid mouse tRNA modification profiles and (B) Overlaid mouse 5.8S-rRNA modification profiles of heart, liver, cortex, lung, spleen and olfactory bulb. (C) 28S-rRNA modification profiles and (D) and 18S-rRNA modification profiles for heart, liver, cortex, lung, spleen and kidney. Data points are the averaged for 16 replicates, and error bars reflect the standard deviation. Modification amounts below LOD or not analyzed (NA) are labeled on the corresponding X axes.

3.1.4. Comparison of RNA modification levels to previous studies

In order to validate the profiling data, I compared my results to published studies on mouse similar RNA types and tissues. Starting based on chronology, from the Carell lab in 2012 on the counterpart tRNA modifications and organs, including m^2G, m^1A, m^1G, $m^{22}G$, t^6A, i^6A, and Am; in lung, liver, heart and spleen.[260]

A quantitative comparison for the seven tRNA modifications is shown in Figure **3.11** adapting to their Y-axes normalization 'per 10^3 tRNAs'. The detected quantities of modified nucleosides from purified tRNA are in accordance with the reported values in lung, liver and heart, except for m^2G, which has a higher abundance in their study. The quantified values for spleen are lower for us compared to the literature (fig **3.11** bottom right), which might be due to contamination of spleen tRNA with an unknown RNA as seen in the SEC trace in fig. **3.2**.

They created chemically synthesized isotope-labeled derivatives of 11 tRNA modifications, with isotope labels only on the nucleobase modification sites and not on the nucleoside itself, as internal standards. Their external calibration included 6 dilutions, separately measured on LC–MS for each investigated modified nucleoside. For data visualization, they used normalization factor of modification per 10^3 tRNA molecules in their data analysis, and therefore, so did I.

Figure **3.11** shows the quantified values for the matching organs tRNA modifications of this study compared to theirs. Overall, my data for tRNA modifications is in good agreement with the absolute quantities determined by the Carell lab using eleven synthetic stable isotope labeled standards (fig **3.8**).[260] The detected quantities of modified nucleosides from purified tRNA are mostly in accordance with the reported values in heart, liver and lung, except for m^2G (fig **3.11**). However, the quantified values for spleen show more variance (fig **3.11**-below right).

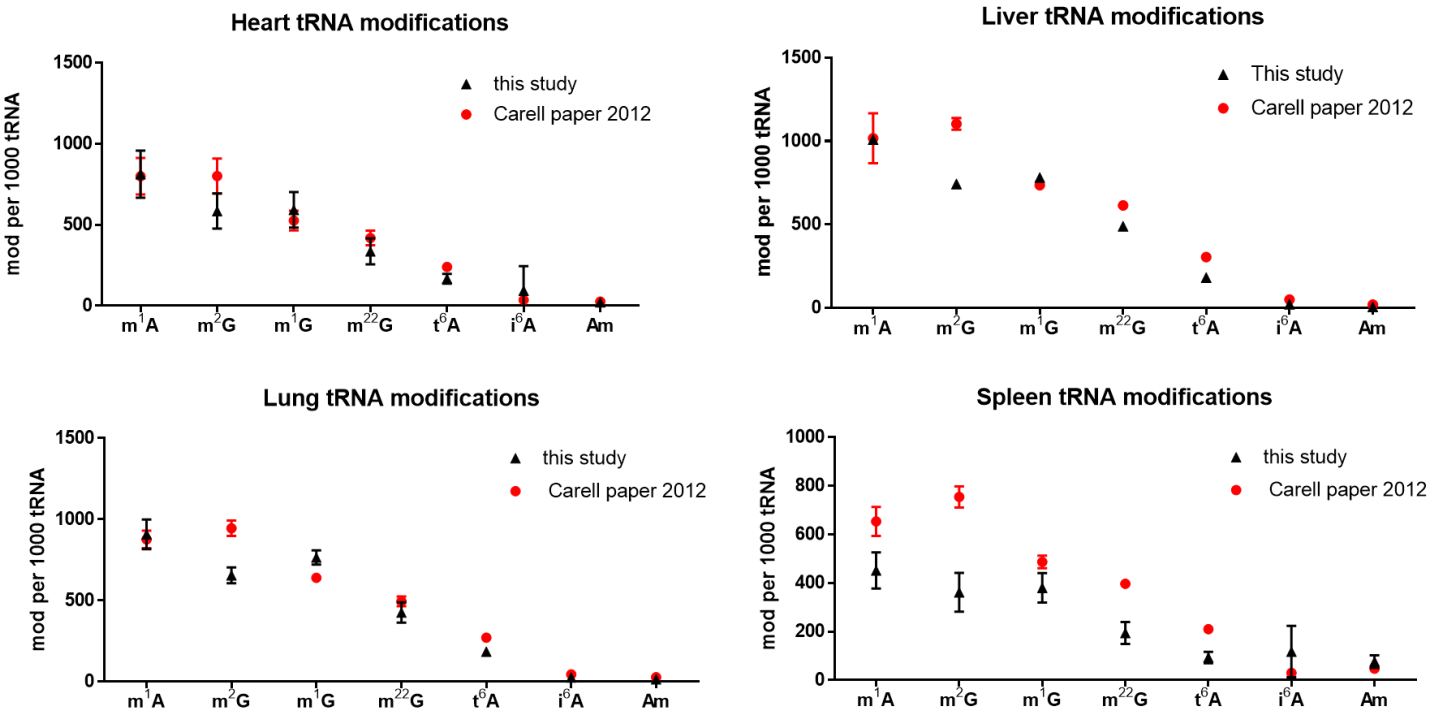

Figure 3. 11 Comparison of absolute quantified modifications between Carell *et.al.* paper to this study for matching mouse organs tRNA including: heart, liver, lung and spleen. The average of n =5 biological replicates and 2 technical replicates is compared to n=4 biological replicates with 4 technical replicates in this study.[260]

Furthermore, I compared my results to another study from our lab in 2019 on tRNA modifications in mouse liver by Borland *et al.*, including Y, m^2G, m^1A, m^5C, m^1G, $m^{22}G$, m^7G, m^5U, Um, t^6A, Gm, m^3C, I, Cm, ac^4C, mcm^5s^2U, m^6A, i^6A, Am and $m^{66}A$, by using the identical method for absolute quantification analysis, serial dilutions of nucleosides synthetic standards as external caliberation curve and addition of yeast tRNA SILIS to each sample as internal standard.[222]

As viewed in figure **3.12.**A, m^5C, m^1A, m^5U and m^2G modifications show significantly higher abundance in my study than the previous one. Nevertheless, my data matches to Carell data (fig **3.11**) and Helm data (fig **3.12.**B), besides I had in total 16 replicates (including 4 biological, each having 4 technical replicates) compared to 3 biological replicates in Borland paper.

Finally, the comparison to Helm 2022 study was performed.[94] They used 2 biological replicates, each having 3 technical replicates. In addition, they also used biosynthetically produced SILIS, similar to my experiments (fig **3.12.**B). For direct data comparison, I performed the same '% per adenosine' normalization and plotted their results alongside mine. For most modifications, a high degree of similarity was found.

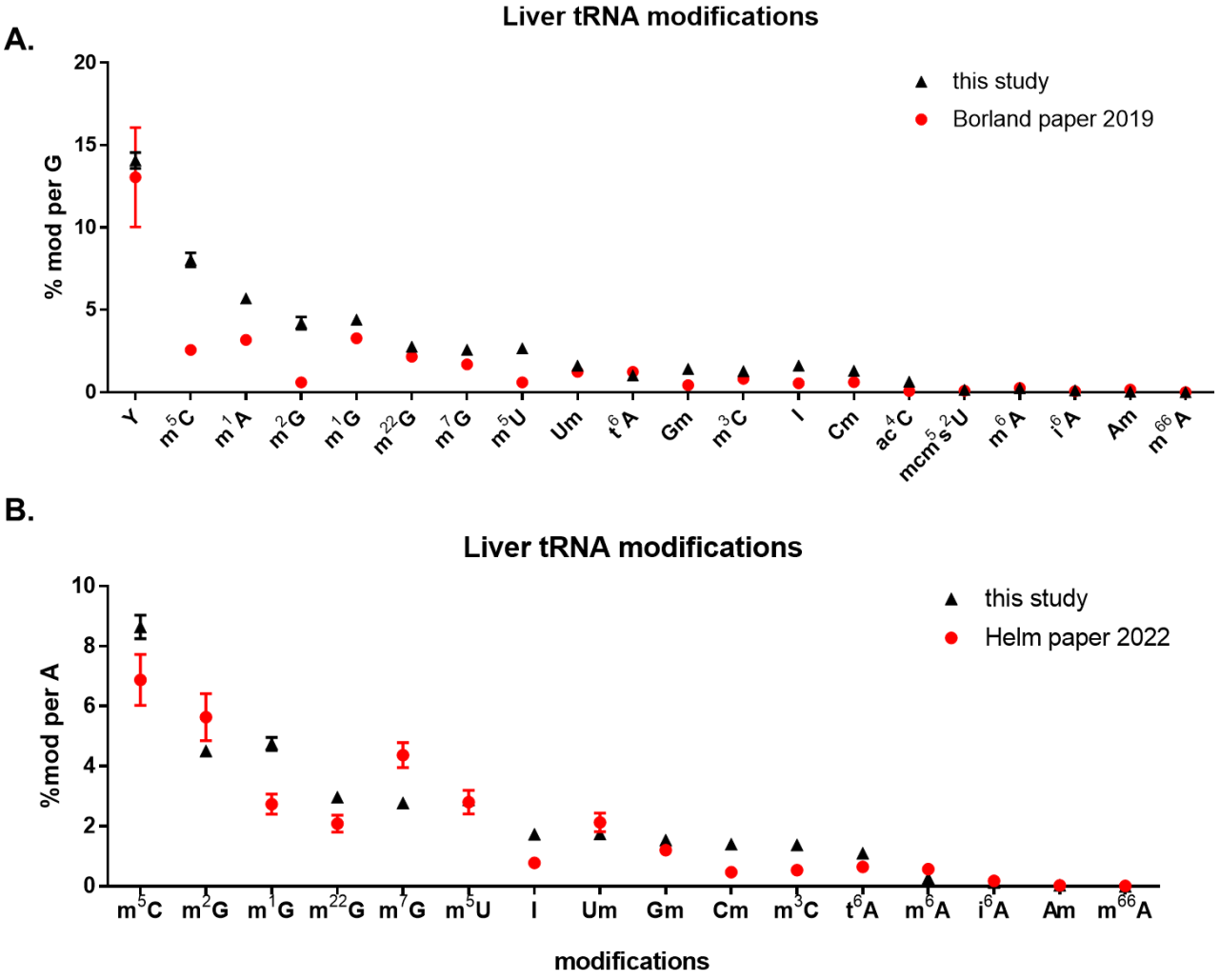

Figure 3.12 Comparison of absolute quantified modifications between **(A**) Borland *et.al.* paper,[222] and **(B)** Richter *et al*. paper,[94] to this study for matching mouse liver modifications. The average of n = 3 replicates is compared to total 16 replicates of our study.

3.1.5. translational consequences of mouse RNA modifications

Mammals have more than 30,000 protein-encoding genes.[273] So far, studies have focused on tissue-specific pattern of mRNA expression as a clue on protein-encoding human and mouse genes in several tissues.[274] However, enlarging the protein expression scopes to post-transcriptional RNA modification effects on organ-specific functions has not yet been explored. Studies have focused on the connection between codon usage to translation

elongation rates and co-translational protein folding, with preferred codons enhancing translational efficiency and folding fidelity.[275, 276]

We tried another approach in order to have an objective view to this connection. NAA and NAG codons code for either Lysine, Glutamine or Glutamic acid, and tRNA U34 modifications such as mcm^5U and mcm^5s^2U help with decoding NAA and NAG codons.[265, 277] Given the fact that I observed in average 4.55 mcm^5U per 10^3 nts in cortex tRNA, but only 2.75 in liver (fig **3.7.**A), we got curious to know if there is an upregulation of genes enriched for NAA codons in cortex compared to liver. My colleague MSc. **Gregor Ammann**, measured the protein content gained from these two tissues using shotgun proteomics in label-free quantification mode, and MaxQuant software for data analysis.

He afterwards wrote a program to count all NAA codons for >27000 mouse genes, then divided the counts of NAA codons by mRNA length. He spotted the 100 proteins that contain the highest number of NAA codons (normalized to mRNA length) and compared it with our mouse proteomics data, in which ~3000 proteins were detected. He then highlighted all proteins from the top 100 list that also appear in the proteomics dataset.

Finally, he summarized these findings in a differential volcano plot, as seen in figure **3.10**. The red labeled proteins in fig **3.10.**A contain many more NAA codons, and in fig **3.10.**B contain many more NAG codons compared to unlabeled proteins.

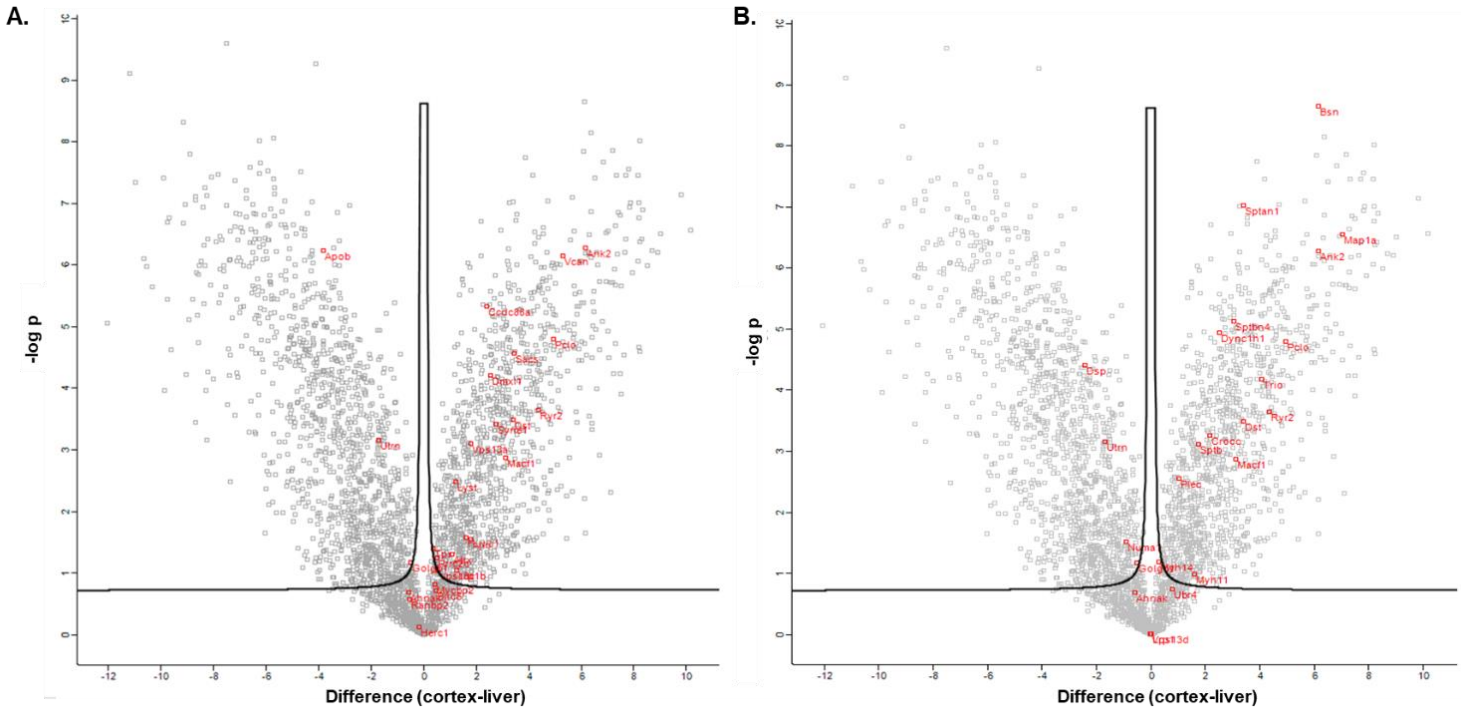

Figure 3.13 Proteomics differential volcano plot of cortex and liver for the 100 highest NAA (A) or NAG (B) codon-containing proteins compared to unlabeled proteins. On each volcano plot, left side shows upregulation in liver and right side upregulation in cortex. The red labeled proteins are enriched for more NAA codons compared to unlabeled proteins (Data provided by MSc. Gregor Ammann).

As shown in figure **3.10.**A, there is a clear trend of the red labeled proteins containing many more NAA codons towards the cortex side than liver, which is expected, if there is a direct connection to cortex containing more mcm^5U than liver, and therefore more amino acids with NAA codons.

However, the same approach was used for NAG codons-enriched genes which showed a very similar pattern (fig **3.13.**B). This is potentially due to introduction of a bias towards proteins that contain more of these amino acids by dividing the number of codons to mRNA length. This dataset, does not match to the hypothesis that mcm^5-modification enhances the translational efficiency of only AA-ending codons, and not AG ending ones.

It is still possible that the cortex proteome is enriched for some amino acids *e.g.* lysine, Glutamine or Glutamic acid containing proteins compared to liver, owing to mentioned codon-enrichment bias. However, such an approach requires a library of amino acids ratio per tissue in mice, instead of proteins, which is already vastly studied.[278-280] Since it is too complicated to refer a single anticodon-endorsing modification to a whole biosynthesized body of a protein, further study on translational consequences of organ specific post-transcriptional modifications is therefore not yet imaginable.

Moreover, there can be other reasons for organ specific post-transcriptional modification differences, which is hypothesized in its dependence to transcriptional dynamics. Repaying to the organ-specific mouse RNA modifications comparison study (figure **3.10**), it can be interpreted that fluctuations in analysis of modification numbers per given RNA species can follow, depending on 'when' during RNA maturation process it is isolated from the cells. This might be a consequence of transcription phase, subjected to transcription-dependent pathways or enzymatic post-modifying pathways involved in incorporating each modification.

Further investigation of temporal RNA modifications in the themes of maturation, stress dependence, and modification re-profiling with transcription dependence can add to this interesting hypothesis, using proteome and oligonucleotide MS experiments.

To recapitulate, I provided the first comparative RNA modifications profile between different mouse tissues and RNA types, to account for dynamic epitranscriptome regulations connection to tissue-specific physiology and function. Interestingly, while 28S- and 18S-rRNA subunits showed almost identical modification patterns between the studies tissues, 5.8S rRNA data showed an organ-specific pattern, which proposes functional diversity of this rRNA subunit among different organs. Moreover, tRNA of highly metabolic active organs such as liver, cortex and lung showed higher levels of most modifications than heart, which may have a functional reliance.

A direct data comparison to three previous studies on similar tissues and RNA species was also performed, which showed a high degree of similarity for most modifications between my data and existing literature.

The fact that I observed more mcm^5U in cortex tRNA than liver, triggered the investigation of potential translational consequences, due to upregulation of genes enriched for NAA codons in cortex compared to liver. Although a direct connection of mcm^5U corresponding codon-enriched genes to its amino acids was not possible due to absence of an amino acids based library per tissue in mice. As tRNA U34 modifications such as mcm^5U and mcm^5s^2U help with

decoding NAA and NAG codons, and NAA and NAG code for either Lysine, Glutamine or Glutamic acid, I emphasize that such amino acids library would help with elucidation of differential post-translational modifications that tune the activity of proteins to each tissue's needs.

Notably, fluctuations in analysis of modification numbers per given RNA species can depend on 'when' during RNA maturation process it is isolated from the cells. This might be a consequence of transcription phase, subjected to transcription-dependent pathways or enzymatic post-modifying pathways involved in incorporating each modification.

Further investigation of temporal RNA modifications in the themes of maturation, stress dependence, and modification re-profiling with transcription dependence can add to this interesting hypothesis, using proteome and oligonucleotide MS experiments.

3.2. Eraser enzymes *in vivo*

As shown for murine tissue RNAs, the abundance of modifications is carefully regulated in cells. The regulation is achieved by transcriptional speed, abundance of RNA writers and activity of enzymes removing RNA modifications, named RNA erasers. So far, RNA erasers are mainly studied in vitro and in vivo studies are lacking.

The goal in this chapter is to investigate RNA eraser enzymes AlkBH1, 3 and 5 *in vivo* activity in demethylating each of their specific methylated ribonucleoside substrates. Experiments include *in vivo* knock down of each enzyme, then stressing the cells by MMS methylating reagent, and following up enzymes expression levels, as well as RNA modification changes under mentioned treatments. Figure **3.14** shows the general concept of *in vivo* experimental workflow as well as analysis by either nucleoside LC-MS or western blot.

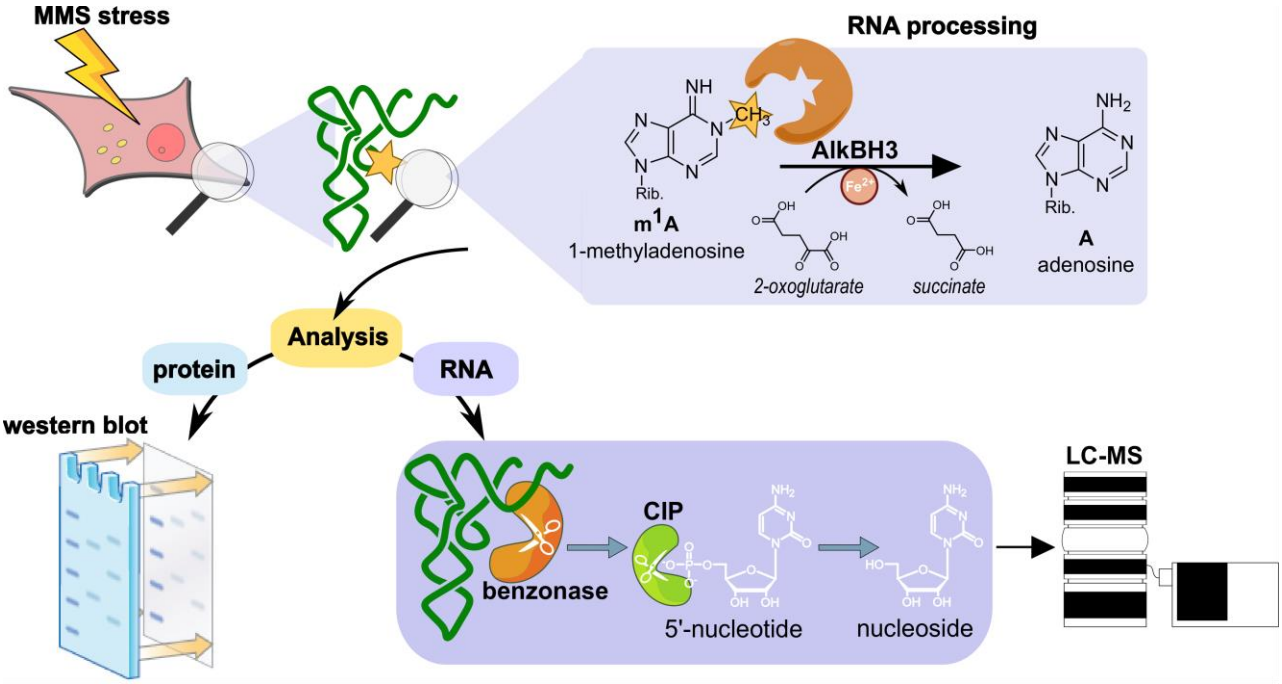

Figure 3. 14 General workflow of investigating eraser enzymes activity under MMS stress *in vivo*. Cells after *in vivo* work up such as MMS stress (with or without silencing AlkBH eraser enzymes) are divided into two portions, one for protein analysis of AlkBHs using western blot and the other for RNA analysis, which includes enzymatic hydrolysis to single nucleosides for LC-MS analysis of RNA modifications that are substrates for each AlkBH enzyme.

3.2.1. Establishment and validation of western blotting for detection of AlkBHs

Since the introduction of western blotting by Towbin *et al.*,[281] it has been intensely used as not only a semi-quantitative method, but also quantitative methods for analysis of specific proteins in complex cell homogenates.[282] Yet, the RNA-focused Kaiser lab did not have this technology available at the art of my PhD. However, this technological gap needed to be overcome to merge the RNA data with investigation of RNA eraser enzymes *in vivo* expression levels, in order investigate their knock down extend by small interfering RNA (siRNA) transfection. Therefore, I started establishing and validating western blotting for protein detection and semi-quantification, aiming for AlkBH1, 3 and 5 proteins as specific, under study targets. Apart from common basic validation steps for the technique, such as selecting the most compatible primary and secondary antibodies as well as detection protocol, I focused on selecting the optimized biological and technical factors that could affect the proteins gain, expression or detection efficiency; such as cells harvesting style, siRNA construct for transfection, transfection reagent, and housekeeper protein.

Effect of cells harvesting on AlkBHs protein detection in western blot

Harvesting of cells in cell culture experiments, may affect the isolation efficiency of specific target proteins and therefore detection sensitivity in western blot analyses. For instance, usage of trypsin affects protein gains, as it cleaves proteins on the C-terminal sides of lysine and arginine residues .[283, 284] Different types of harvesting were investigated on HEK cells, to validate the efficiency of relative gained target protein (ALKBH) to the housekeeper tubulin.

AlkBH1 was used as the target protein for this experiment. Cells were grown on p40 dishes in standard DMEM (D6546, from Sigma-Aldrich) modified with 10% fetal bovine serum and 2 mM L-glutamine (GlutaMax, Gibco) medium, then harvested using different techniques at 40 h post-seeding. Cells were detached resulting in a cell suspension in different ways including: vigorous pipetting with PBS, pipetting with freshly exchanged medium, scratching by cells scraper with PBS, cells scraper with freshly exchanged medium, or addition of trypsin. Each cells suspension was then centrifuged and the isolated cells pellet was directly lysed with fresh radioimmunoprecipitation assay (RIPA) buffer, followed by downstream western blotting sample preparation. Figure **3.15A** shows 30µg loaded total protein lysate for western blot, targeting tubulin and AlkBH1.

Based on figure **3.15A**, the highest abundance of AlkBH1 normalized band intensity is achieved by pipetting compared to all tested harvesting styles. For further comparison, I designed an experiment more similar to a true biological experiment and I included MMS treatment as stressor, harvested by either trypsinisation or simple pipetting and quantified AlkBH1 and the housekeeper protein.

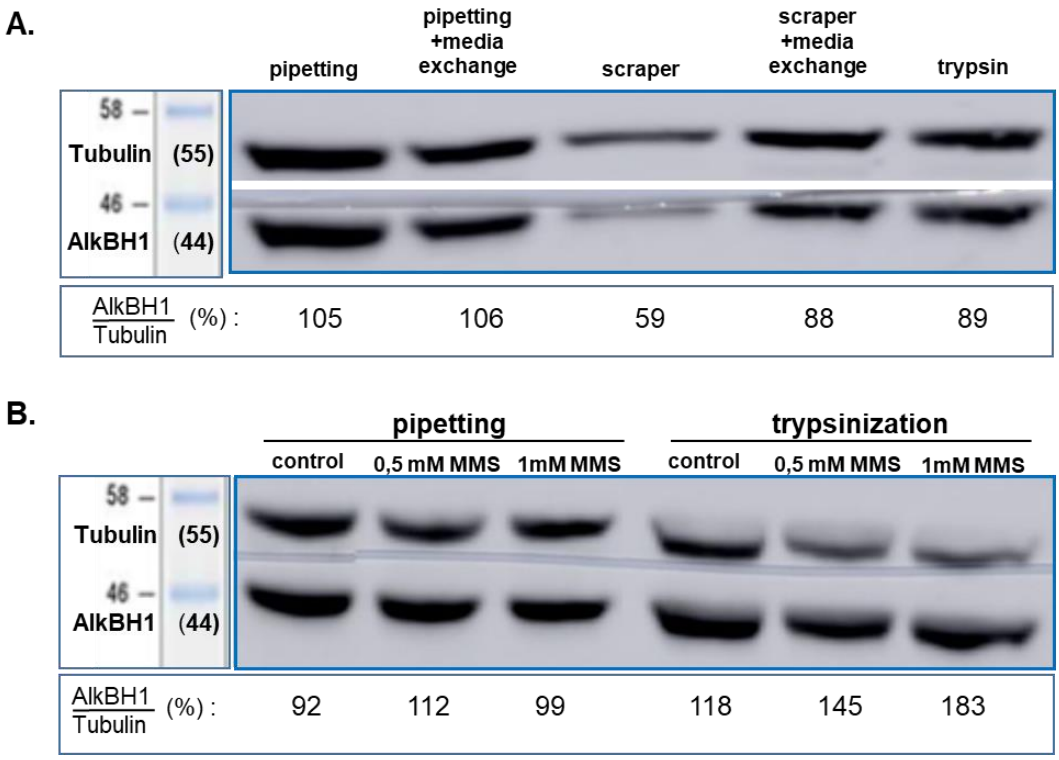

Figure 3. 15 Comparison of gained protein of AlkBH1 and Tubulin in western blot. (A) between different styles of cell harvesting, and (B) between pipetting and trypsinization with and without inclusion of MMS stress effect. The relative band intensities of AlkBH1 normalized to tubulin as the housekeeper protein were quantified using ImageJ software.

As portrayed in figure **3.15.B**, comparison between relative band intensities shows an MMS dependent loss of the housekeeper protein tubulin under MMS treatment using trypsinisation but not using pipetting. Thus, the harvesting method impacts the interpretation of AlkBH1 quantification, as an upregulation of AlkbH1 appears to be detectable using trypsinisation but not by pipetting. This data indicates that trypsin is not a good candidate for cell harvesting protocols aiming for proteomics. My conclusion is supported by the fact that trypsin is one of the most important peptidases in the digestion process.[283, 285] Thus, the necessity of a better loading control for western blot normalization is inevitable, due to several drawbacks that cause expression changes of a single housekeeper protein such as tubulin through the experiment.[286] The housekeeper protein optimization is followed up in figure **3.19**.

Impact of MMS stress on AlkBH1 and AlkBH3 expression

MMS stress is one of the most used chemical methylation stresses on cells. With the goal to study the stress response in human cells, our lab designed pulse-chase experiments to study the temporal placement of modified nucleosides in tRNA and 18S rRNA, caused by dynamic MMS stress.[287] Moreover, studies have provided evidence on increased binding of ASCC3 to mRNA after MMS treatment, which associates with AlkBH3 to facilitate unwinding and efficient demethylation of m^1A and m^3C in DNA and RNA.[153, 156] Yet, no direct evidence for AlkBH3 demethylation activity in vivo has been presented.

To follow up on this hypothesis, I investigated the potential link between MMS stress and expression of AlkBH3 compared to AlkBH1 protein. As shown in figure **3.16** western blots, 1h of 1mM MMS treatment in both biological replicates of the experiment causes an obvious overexpression (OE) of AlkBH3, but not AlkBH1. Normalized bands quantification shows up to 58% OE of AlkBH3 with 1mM MMS (fig. **3.14.**B).

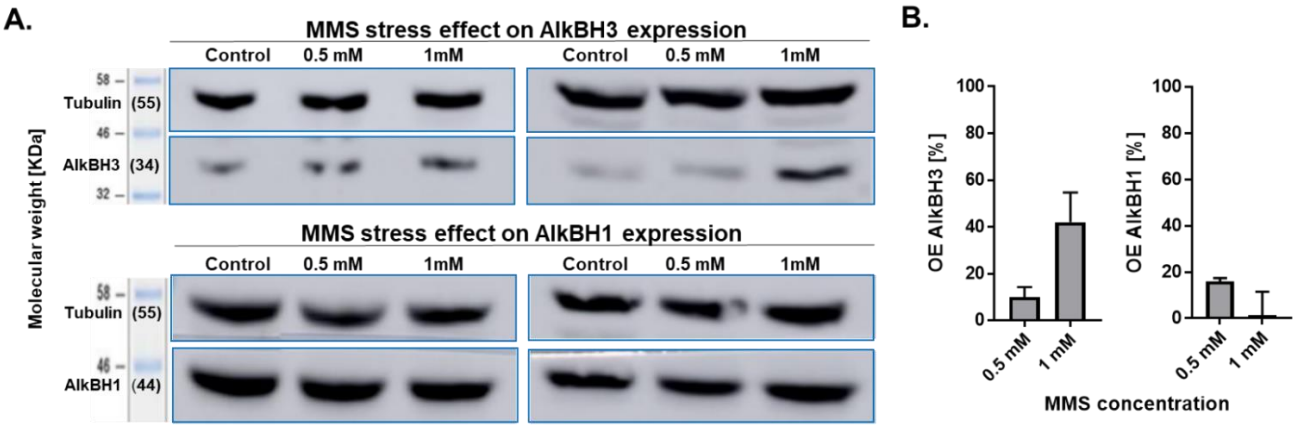

Figure 3. 16 Western blot of MMS concentration impact on AlkBH1 and AlkBH3 expression levels. (A) two biological replicates (left and right boxes) of each enzyme protein are shown. HEK cells were treated with an increasing concentration of MMS, ordered from left to right 0 mM (control), 0.5 mM and 1 mM for 1h. Upper blotted membrane shows AlkBH3 expression levels and the lower blot AlkBH1, the upper bands for each blot show tubulin, which is used as the housekeeper. The bands of AlkBH1 and 3 are normalized to tubulin bands for semi-quantitation using ImageJ software. (B) Calculated over expression (%) compared to control bands for AlkBH3 (left bar graph) and AlkBH1 (right bar graph). The bars are plotted based on the mean of two replicates and error bars represent standard deviation.

My data supports the hypothesis that AlkBH3 is a methylation damage induced enzyme, that triggers ASCC-AlkBH3 alkylation repair complex after certain aberrant methylation damages such as MMS treatment.[156]

Influence of siRNA vs. esiRNA sequence selection on AlkBHs transcription silencing

To close in on the experimental proof on in vivo AlkBH3 RNA demethylation under MMS stress, a successful knockdown (KD) of the AlkBH proteins *in vivo* is needed to identify RNA modifications that are differentially abundant in the KD samples in contrast to the transfection controls (scrRNA).

In the case of AlkBH5, HEK 293 cells were seeded in unlabeled medium, treated with siRNA against AlkBH5 mRNA, then incubated to induce KD of AlkBH5 at the transcript and protein levels. As seen in figure **3.17**, three constructs of 21 nts long siRNAs, namely si-1, si-2 (siRNA sequences can be found in table **5.6**), and combination of si-1 and 2 were transfected, but no decrease in the amount of AlkBH5 was observed. Therefore, I tried another silencing strategy: using endoribonuclease-prepared siRNA (esiRNA, sequence information in table **5.6**), which is a heterogeneous mixture of siRNAs that all target the same mRNA sequence, causing multiple silencing. As seen in fig **3.17** right blot, esiRNA provides down to 50% KD of AlkBH5

(right side bar graph). Based on this result, silencing with esiRNA was chosen for all forthcoming KD experiments.

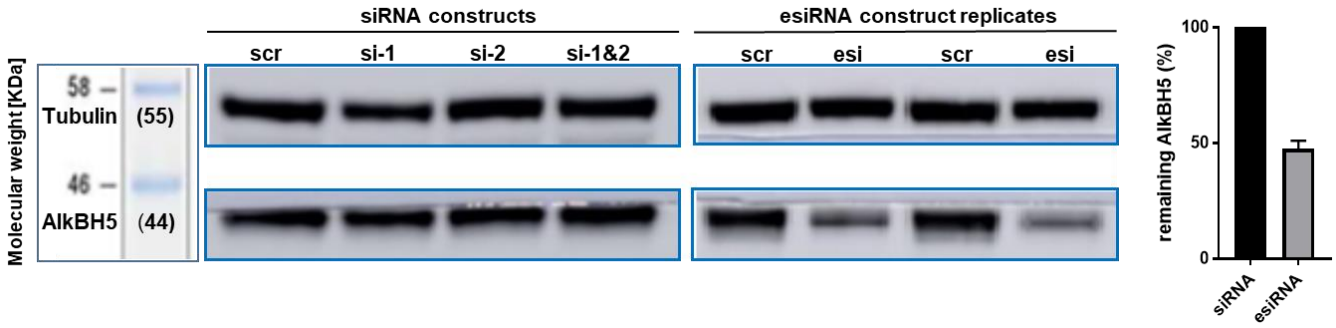

Figure 3. 17 Comparison of different constructs of siRNA on silencing AlkBH5 protein expression to esiRNA transfection to HEK 293 cells. Two constructs of 21 nts siRNA targeting AlkBH5 mRNA transcript namely si-1 or si-2 and their mixture were transfected (left blot) compared to AlkBH5 esiRNA. The bar graph shows % remaining normalized AlkBH5 after silencing, based on the mean value for siRNA constructs (black bar) or esiRNA replicates (gray bar), the error bars represent standard deviation.

Impact of transfection reagents on AlkBHs silencing efficiency

All transfections of this chapter were so far performed by JetPRIME (JP) reagent. Based on the fact that compared to cationic lipofection, cationic polymers such as JP produce less cytotoxicity but show lower efficiency,[288] I was curious to know to what extend is the transfection efficiency altered between Lipofectamine 2000 (LP2000) and JP.
In order to compare them, esiRNA targeting AlkBH5 transcript was transfected with each reagent into HEK 293 cells. Figure **3.18** shows western blot results for both reagents. As shown in the bar graph, the band for LP2000 transfection shows only 9% higher efficiency of silencing. As the JP workflow is better compatible with my envisioned NAIL-MS experiments (1 h vs. 6 h transfection phase and lower probability of induction of de novo nucleotide synthesis), I continued all future experimental steps with JP.

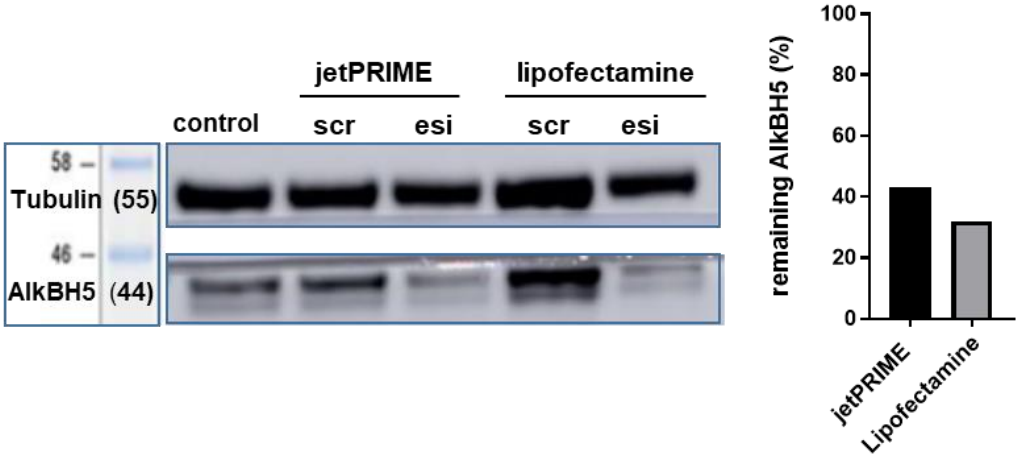

Figure 3. 18 Comparison of transfection efficiency between transfection reagents lipofectamine 2000 (LP2000) and JetPRIME (JP), based on KD extend of AlkBH5. The % remaining AlkBH5 was measured by relative expression difference of esiRNA transfected vs. scrRNA into HEK cells, band intensity quantification was performed by ImageJ.

Effect of loading control choice in western blot quantification of AlkBHs

The disadvantage of using a single housekeeper protein like tubulin as loading control in western blotting, has been described in fig. **3.13** where I found changed tubulin abundance upon MMS treatment. Thus, I searched for a better loading control. In order to do so, I compared normalization of my target protein to tubulin *vs.* to the whole protein lysate as the final western blotting validation step.

Given the fact that whole lysate protein staining does not interfere with antibody affinity of target proteins (AlkBH1 in this case), one can easily use whole protein lysate as loading control. As shown in figure **3.19**, normalization to both tubulin and whole lysate show around 50% KD, which is not considerably different, but as discussed before, the housekeeper proteins such as actin, tubulin, or GAPDH are prone to expression fluctuations under experiments biological or technical errors, therefore normalization to whole cell protein content is chosen for this study.

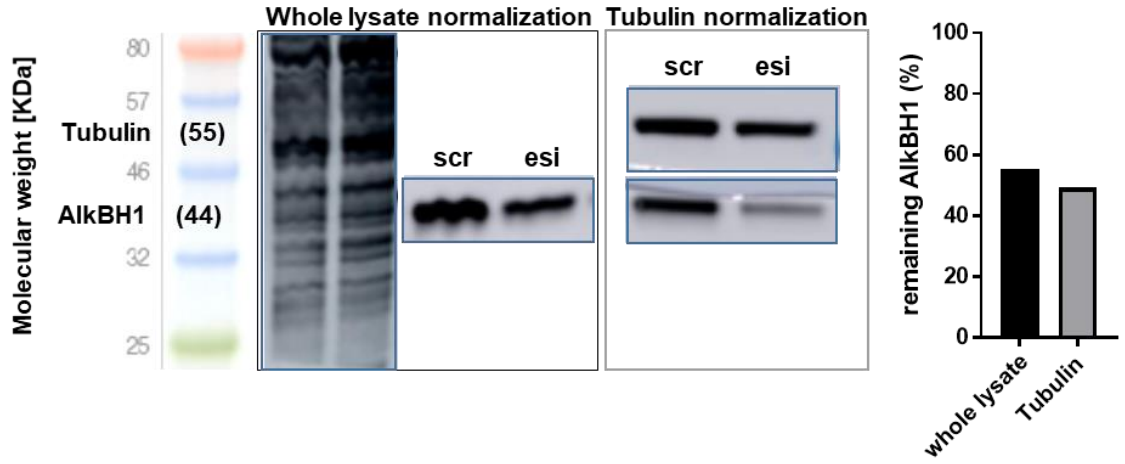

Figure 3. 19 Comparison of AlkBH1 KD quantification based on normalization to whole cell lysate using No-stain™ protein labeling reagent (Invitrogen™ by Thermo fisher) [left box] or tubulin as housekeeper [right box]. The bar graph on the right side shows % remaining AlkBH1 protein based on relative quantified band intensities for esiRNA transfection into HEK 293 cells vs. scrRNA, using ImgeJ software.

3.2.2. Influence of AlkBHs knockdown on RNA modifications

In order to follow up the AlkBHs KD effect on their target RNA modifications, NAIL-MS experiments for detection of RNA modification dynamics was performed in a joint project with my colleague **Dr. Felix Hagelskamp**. For this purpose, AlkBH protein expression was silenced *in vivo* in order to investigate RNA modifications that are differentially abundant in the KD samples compared to the transfection controls. A significant increase of a modification in KD sample means that it is a potential substrate for corresponding AlkBH enzyme. In addition to *in vivo* confirmation of RNA modifications dependence on a single AlkBH enzyme, a possible compensation of the KD by other demethylases should also be investigated.

Through a pulse-chase NAIL-MS experiment, HEK 293 cells were seeded in unlabeled medium, transfected with esiRNA against corresponding AlkBH mRNA to induce KD of the

AlkBH at the transcript and protein levels, and finally harvested after incubation with isotope-labeled NAIL-MS medium for 0 or 8 hours. Harvested cells were divided into two parts, one for RNA sample preparation of RNA modification analysis, and the other for western blot analysis of the enzyme KD. After 8 hours in stable isotope-labeled NAIL-MS medium, the RNA of HEK 293 cells consists of three different nucleoside species: the unlabeled (old), the isotopically labeled (new), and post-methylated. These can be detected separately in the mass spectrometer due to their different masses.
The RNA data for this section is provided by my colleague **Dr. Felix Hagelskamp** [Massenspektrometrische methoden zur untersuchung enzymatisch modifizierter RNA. Ludwig-Maximilians-Univerität München, 2021 (Dissertation)].

Influence of AlkBH3 knockdown on RNA modifications in the NAIL-MS context

The purpose in this section is to explore whether tRNA or rRNA substrates, such as m^1A and m^3C, are more abundant in AlkBH3 KD samples than in controls, which indirectly gives information about possible RNA modifications that are demethylated by AlkBH3 in the cytosol. For pulse-chase NAIL-MS experiment, HEK 293 cells were seeded in unlabeled medium, transfected with esiRNA targeting AlkBH3 transcript and finally harvested after incubation with isotope-labeled NAIL-MS medium at 0 and 8 hours. The western blot shown in **figure 3.20** determines the KD degree of AlkBH3 protein.

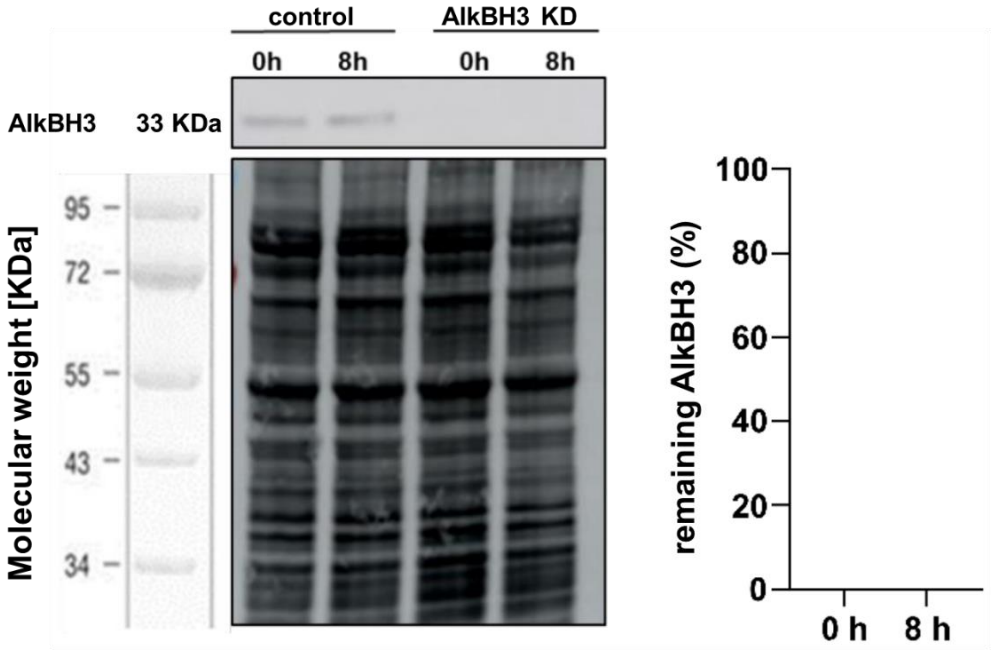

Figure 3. 20 Western blot of the AlkBH3 KD pulse-chase NAIL MS experiment. The whole protein lysate of the four collected samples were separated by electrophoresis and later stained. Based on relative quantification of AlkBH3 band intensities by ImageJ, the efficiency of KD was calculated compared to transfection control, and plotted in the right bar graph.

In AlkBH3 KD samples, compared to the transfection controls taken at the same time, no bands for AlkBH3 were detected. This corresponds to a knockdown efficiency of 100%. However, the amount of AlkBH3 in unstressed cells seems to be very low, as only a very weak band is detectable for the protein, it is possible that a small, undetectable amount of AlkBH3 is present in cells after esiRNA knockdown.

After purification of 28S rRNA, 18S rRNA and tRNA, the RNAs were digested to nucleosides and MS analysis was performed. Figure **3.21** shows the abundance of m^1A or m^3C in both original and newly transcribed RNA within the 8 hours of incubation. Here, we did not detect any in vivo activity of ALKBH3 against these substrates as the quantities of these modifications were unchanged.

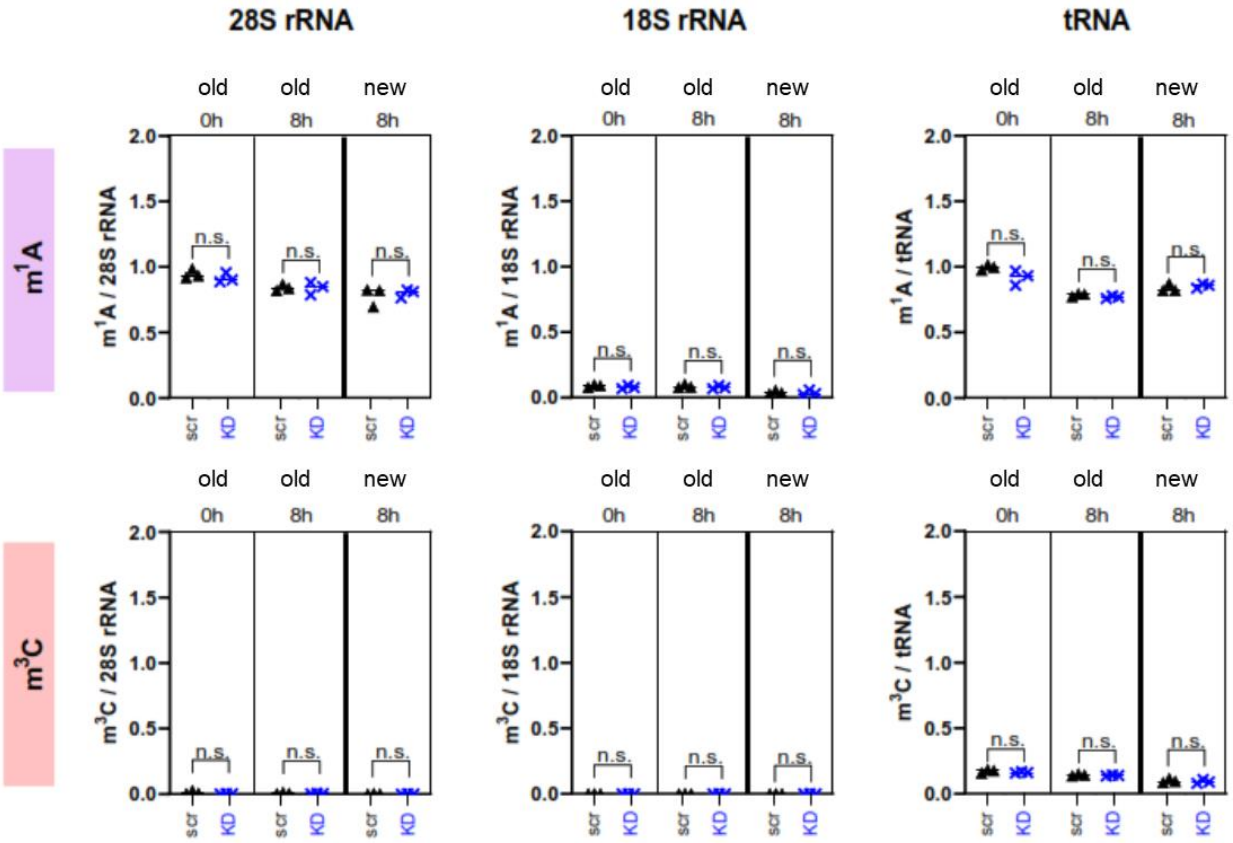

Figure 3. 21 Quantification of RNA modifications in pulse-chase NAIL-MS experiment after AlkBH3 KD, performed by Dr. Felix Hagelskamp. The boxplots demonstrate the absolute values for m^1A (first row) and m^3C (second row) per respective RNA molecule (left column: 28S rRNA; middle column: 18S rRNA; right column: tRNA). Each boxplot is divided into three columns, with the old, unlabeled nucleosides before changing the medium (t = 0h, 64 hours after seeding), in the middle the old, unlabeled nucleosides after incubation with stable isotopically labeled medium (t = 8 h, 72 h after seeding) and on the right new, labeled nucleosides are shown after 8 hours of incubation. At each time point, RNA was isolated from both AlkBH3 knockdown probes (KD, blue) and the transfection controls (scr: scramble control, black). All values are from n=3 biological replicas. The two-way analysis of variance determines the significance, which is placed over the data points (n.s.= not significant).

The same result was obsereved from comparison of AlkBH3 KD to control for m^6A, m^5C and m^7G modifications in the three RNA species (data not shown).
AlkBH3 *in vivo* KD shows no effect on the levels of expected AlkBH3-substrate modifications.[127] Our data suggests that neither m^1A nor m^3C are AlkBH3 targets in HEK 293 cells or potentially, are compensatory maintained at the same level by either remaining active AlkBH3 (since a complete knockout of AlkBH3 gene was not possible here) or other undefined demethylases.

Influence of AlkBH1 knockdown on RNA modifications

With the purpose to explore whether AlkBH1 has tRNA or rRNA as substrates, we investigated whether m^1A, m^3C, or m^6A are more abundant in AlkBH1 KD samples compared to controls. For this purpose, HEK 293 cells were seeded in unlabeled medium, transfected with esiRNA against AlkBH1 mRNA to induce KD at the transcript and protein level and finally harvested after incubation with isotope-labeled NAIL-MS medium for 0 or 8 hours.

To verify the KD of AlkBH1 protein, cell samples were analyzed using western blot (figure **3.22**). After 8 hours (72 hours after seeding), 58% of the AlkBH1 in the KD sample remained compared to the simultaneously collected transfection control, which corresponds to a 42% knockdown of AlkBH1.

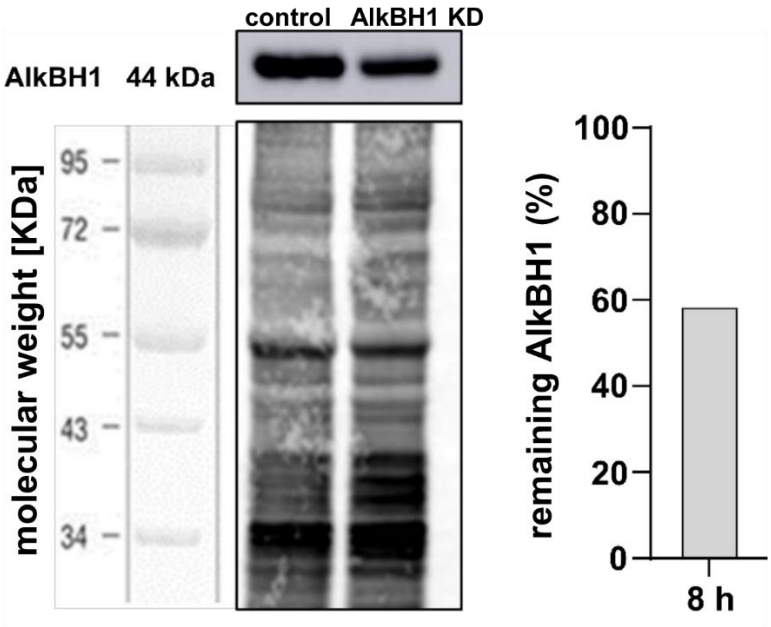

Figure 3. 22 Western blot of AlkBH1 KD pulse-chase NAIL-MS experiment. The whole protein lysate of the two collected samples were separated by gel electrophoresis and later stained. Based on relative quantification of AlkBH1 band intensities by ImageJ, the efficiency of KD was calculated and plotted in the right bar graph, compared to transfection control.

To investigate the effects of AlkBH1 knockdown on RNA modifications, isolated total RNA at each of the two time points was separated into 28S rRNA, 18S rRNA and a total tRNA by

SEC, and after digestion to nucleosides and MS analysis, absolute quantification of m^1A, m^3C, m^5C, m^7G, and m^6A was performed by **Dr. Felix Hagelskamp**.

As shown in **Figure 3.19**, there is no difference in the amounts of modifications m^1A or m^3C in the newly transcribed RNA within the 8 hours of incubation, nor in the original RNAs. Similar results were obtained for m^6A, m^5C and m^7G (data not shown).

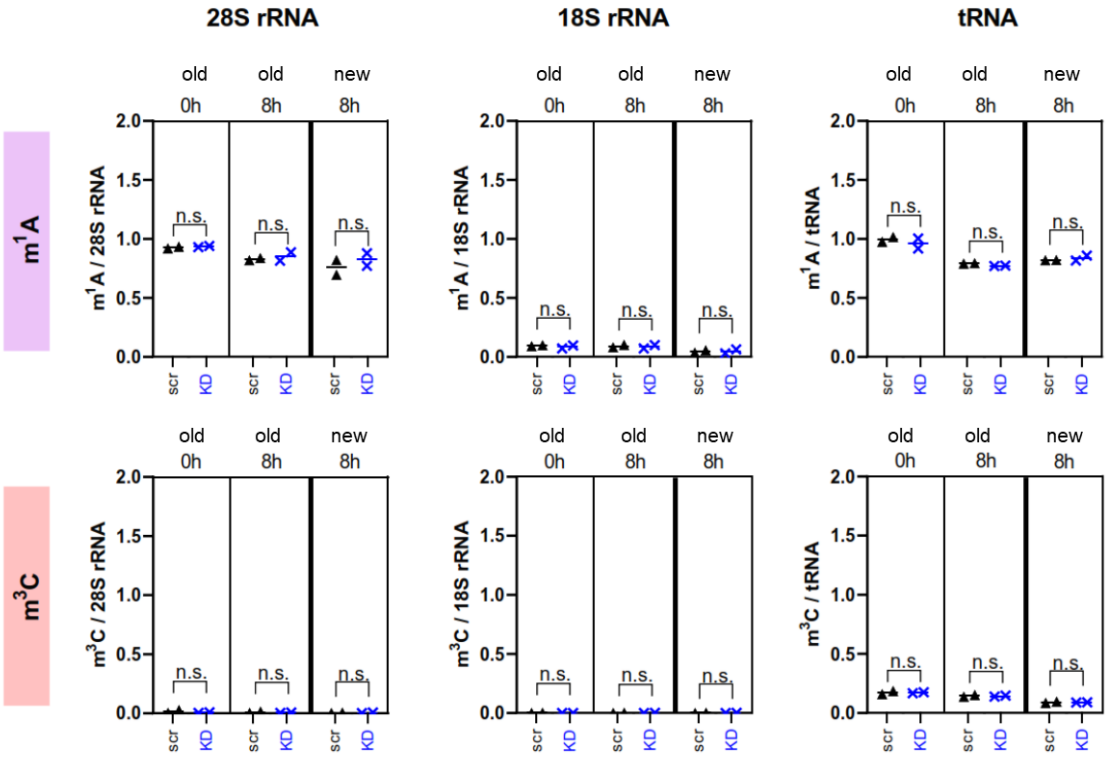

Figure 3. 23 Quantification of RNA modifications in the pulse-chase NAIL-MS experiment after AlkBH1 knockdown, performed by Dr. Felix Hagelskamp. The boxplots demonstrate the absolute values for m^1A (first row) and m^3C (second row) per respective RNA molecule (left column: 28S rRNA; middle column: 18S rRNA; right column: tRNA). Each boxplot is divided into three columns, with the old, unlabeled nucleosides before changing the medium (t = 0h, 64 hours after seeding), in the middle the old, unlabeled nucleosides after incubation with stable isotopically labeled medium (t = 8 h, 72 h after seeding) and on the right new, labeled nucleosides are shown after 8 hours of incubation. At each time point, RNA was isolated from both AlkBH1 KD probes (blue) and the transfection controls (scr: scramble control, black). All values are from n=3 biological replicates. The two-way analysis of variance determines the significance, which is placed over the data points (n.s.= not significant).

In summary, there is no difference in the abundance of the five RNA modifications in AlkBH1 KD samples in contrast to the transfection controls.
On one hand, with AlkBH1 absence *in vivo*, other unidentified demethylases might compensate for its demethylation activity. Even more probably, demethylation may still arise by remaining active AlkBH1 to restore the original levels of the observed RNA modifications, since a stronger KD or a complete knockout of AlkBH1 gene was not possible.

On the other hand, plausible mitochondrial demethylation of AlkBH1 due to the small amount of mitochondrial to cytosolic RNA could not be detected, due to the RNA isolation method limitations.

Influence of AlkBH5 knockdown on RNA modifications

The design of the NAIL-MS experiment makes it possible to study the degradation as well as the synthesis of the different RNA species and RNA nucleosides over time and thus discover kinetic differences between eraser enzymes KD and control samples. According to the literature, AlkBH5 is supposed to indorse demethylation of m^6A in mRNA.[103] To discover a possible regulatory network of modifications influenced by AlkBH5, my former colleague **Dr. Kayla Borland** isolated and analyzed the mRNA from the pulse-chase NAIL-MS experiment, while **Dr. Felix Hagelskamp** investigated AlkBH5 KD effect on rRNAs and tRNA in HEK cells.

The successful knockdown of AlkBH5 at the protein level was confirmed by western blot. Three biological replicates (total of 6 protein lysate samples) of the 8h time point were analyzed. **Figure 3.24** shows up to 56% AlkBH5 protein remaining in the KD samples, implying ~44 % KD.

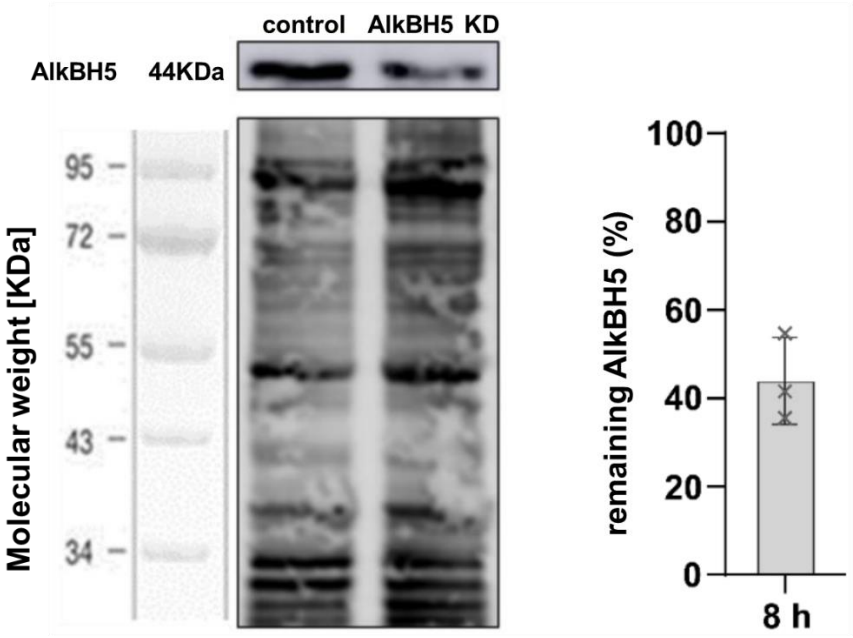

Figure 3. 24 Western blot of the AlkBH5 KD pulse-chase NAIL-MS experiment. The protein lysate of the six collected samples at 8h was separated by gel electrophoresis and later stained (only two exemplary bands are shown here). From the intensities of the bands, the efficiency of the knockdown compared to the transfection control is shown in the bar graph on the right side, from n=3 biological replicates. The error bars reflect standard deviation.

Dr. Felix Hagelskamps data showed no difference in the level of modifications between control nucleosides to the unlabeled nucleosides right after transfection (before exchanging the unlabeled medium to isotope-labeled medium). This was true for 8 RNA modifications

including Nm and m^5C, m^7G and m^3C, and ac^4C in tRNA, 28S and 18S rRNA species (data not shown).

However, after medium exchange, newly synthesized RNA molecules were prepared from isotopically labeled nucleosides, hence the ratio of unlabeled nucleosides by all nucleosides can stand as a measure of how fast the already existing RNA molecules were degraded. Guanosine was chosen as the canonical nucleoside for the degradation or turnover rates shown in Figure **3.25**. All data in this figure are provided by **Dr. Kayla Borland** and **Dr. Felix Hagelskamp**.

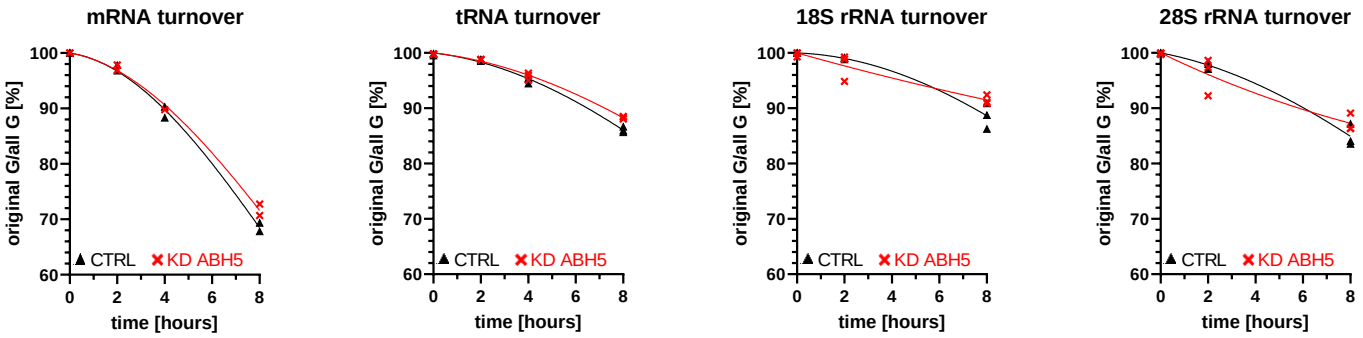

Figure 3. 25 Turnover rates of different RNA species during the pulse-chase NAIL-MS experiment after AlkBH5 knockdown. The RNA was isolated from AlkBH5 KD samples (red) and from transfection controls (black). All values were from n=3 biological replicates. The turnover rates of mRNA were analyzed by **Dr. Kayla Borland** and tRNA, 28S- and 18S rRNA were analyzed by **Dr. Felix Hagelskamp**.

It is notable that at the time of the medium exchange, pre-existing mRNA was degraded faster than the other RNA species. This can be explained by the shorter half-life of mRNA compared to for example tRNA. After 8 hours only 70 % of the unlabeled mRNAs are still present. 28S rRNA, 18S rRNA and tRNA have longer half-lives and only about 10 % of the molecules have been degraded, thus no longer isolated and detected by mass spectrometry.

After considering the kinetics of RNA species in figure **3.25**, kinetics of the m^6A nucleosides were investigated further by **Dr. Hagelskamp**. As shown in figure **3.26**, m^6A shows a static density over the time course of the NAIL-MS experiment. While m^6A cannot be detected in tRNA, it was found in both rRNA species (28S and 18S) in both original and new transripts arguing for their co-transcriptional placement. Importantly, KD of AlkBH5 does not impact the abundance of m^6A in tehse RNAs, which is in accordance with expectation.

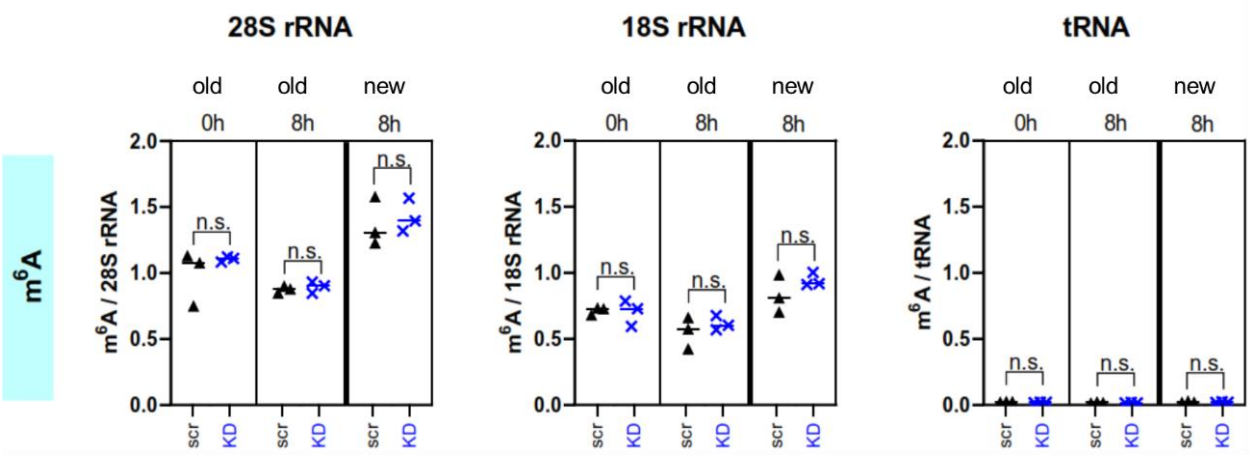

Figure 3. 26 Quantification of RNA modification m^{6}A in the pulse-chase NAIL MS experiment after AlkBH5 KD. The boxplots show the absolute values for m^{6}A per respective RNA molecule (left column: 28S rRNA; middle column: 18S rRNA; right column: tRNA). Each boxplot divides into three columns: the old, unlabeled nucleosides on the left before the medium exchange (t = 0 h, 64 h after seeding), in the middle the old, unlabeled nucleosides after incubation with stable isotope-labeled medium (t = 8 h, 72 h after seeding) and on the right new, labeled nucleosides after 8 h incubation. At each time point, RNA from both AlkBH5 KD samples (blue) and transfection controls (scr. for scramble control, black) were isolated. All values were from n=3 biological replicates. The two-way analysis of variance determines significance, which is entered above the data points (n.s.= not significant).

To determine m^{6}A abundance as the major substrate of AlkBH5 in mRNA, m^{6}A was analyzed by **Dr. Kayla Borland** from isolated mRNA. Then again, no significant levels in the AlkBH5 knockdown samples compared to control were observed for m^{6}A (figure **3.27**). Thus, AlkBH5 KD did not show any significant effect on the modification density of m^{6}A, m^{3}C, m^{5}C and m^{7}G in tRNA, 18S and 28S rRNA, nor m^{6}A in mRNA.

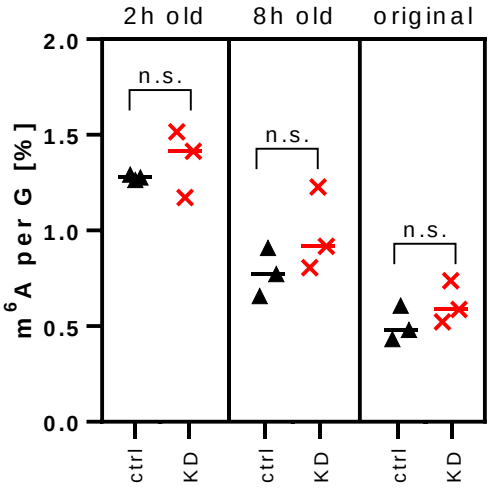

Figure 3. 27 Quantification of m^{6}A modification in mRNA in the pulse-chase NAIL MS experiment after AlkBH5 KD. The boxplot shows the absolute values for m^{6}A per G (%). The boxplot is divided into three columns: the old, unlabeled nucleosides on the left before the medium exchange (t = 0 h, 64 h after seeding), in the middle the old, unlabeled nucleosides after incubation with stable

isotope-labeled medium (t = 8 h, 72 h after seeding) and on the right original, D_3-labeled nucleosides remaining from before the incubation. At each time point, mRNA from both AlkBH5 KD samples (blue) and transfection controls (scr. for scramble control, black) were isolated. All values were from n=3 biological replicates. The two-way analysis of variance determines significance, which is entered above the data points (n.s.= not significant).

In summary, there was no difference in the abundance of the RNA modifications considered as AlkBH5 targets, in AlkBH5 KD samples in contrast to the transfection controls. The complex machinery of higher eukaryotic cells such as human cells, might provide the compensation for AlkBH5 absence by other unidentified demethylases or at least, by remaining active AlkBH5 and thus restore the original levels of the observed RNA modifications. A stronger KD or a complete knockout of AlkBH5 gene was not possible in this study.

3.2.3. Impact of MMS stress on mRNA modifications

In my AlkBH3 KD experiments with unstressed cells, the absolute quantities of described AlkBH3 substrates such as m^1A and m^3C in 28S rRNA, 18S rRNA or tRNA did not change. Yet, I could confirm, that AlkBH3 abundance is increased upon methylation stress in human cells. Thus I hypothesize that the *in vivo* demethylation activity of AlkBH3 might be connected to methylation stress in human. Further evidence is provided by the interaction of AlkBH3 and Activating Signal Co-integrator Complex 3 (ASCC3). ASCC3 encodes a 3′-5′ DNA helicase, whose activity is crucial for the generation of single-stranded DNA upon which AlkBH3 preferentially functions for dealkylation. *In vivo*, a loss of AlkBH3 or ASCC3 led to increased m^3dC in DNA.[289]

Intrigued by the recent study of Wollen *et al.* on AlkBH3 partnership with ASCC3 in demethylating MMS-induced m^1A and m^3C from mRNA,[153] I aimed to look for either AlkBH3 or ASCC3 KD effect under MMS stress on selective modifications in mRNA, in collaboration with **Dr. Marie Luise Winz** (JGU Mainz). ZNF598 protein, which acts as the rate-limiting factor for ribosome-associated quality control,[290] was used as a quality control for checking the significance of modifications changes caused by AlkBH3 or ASCC3 inhibition.

In the Winz lab, HEK cells were first treated with siRNA aiming either for AlkBH3, ASCC3 or ZNF598 mRNA transcripts, and after successful KD, cells were treated with 1mM MMS for 1h, and harvested at 0h (time point of MMS removal) or 4h post MMS-stress time points. mRNA was isolated by the Winz lab from each sample, and I performed sample preparation for nucleoside MS analysis.

Influence of AlkBH3 or ASCC3 knockdown on mRNA modifications under MMS stress

I have summarized the results for the common RNA methylation damage marks m^1A, m^3C, m^7G, m^6A and the non-damage m^5C as negative control in **figure 3.28**. For normalization, abundance of modifications is referred to each corresponding guanosine nucleosides.

As known from previous studies in the Kaiser lab,[291] MMS stress causes a significant increase in the amounts of m^1A and m^3C. Interestingly, m^7G, the main damage in RNA of *E. coli* and

yeast was not formed in the mRNA of human. This is in accordance with another report from the Kaiser lab, which reported no formation of damage m^7G in human tRNA following MMS exposure. Regarding methylation damage removal 4 hours after stress removal, a decrease in abundance is visible for m^1A and m^3C in the control samples (fig **3.28.B** and **C**).

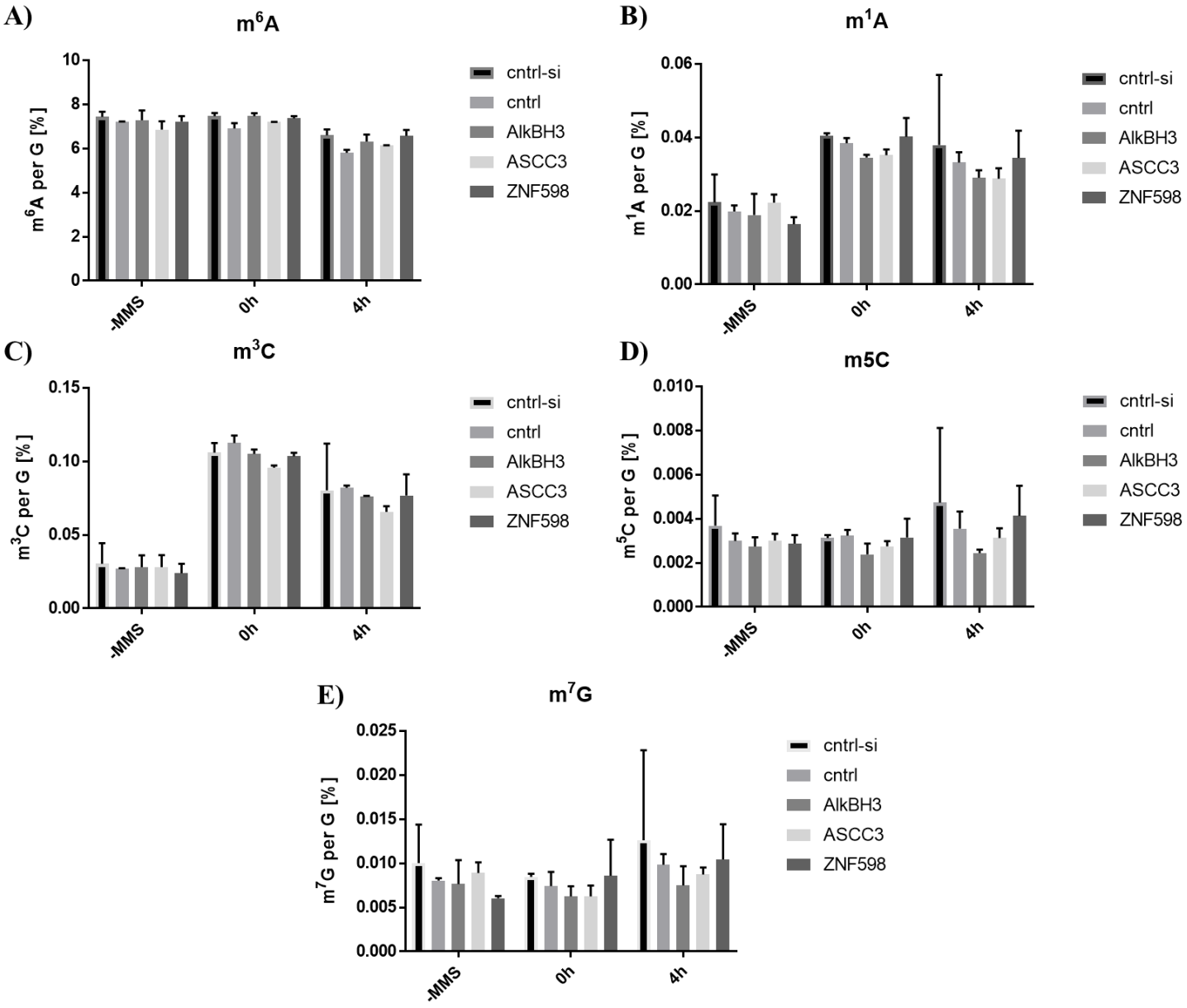

Figure 3. 28 Effects of AlkBH3, ASCC3, or ZNF598 KD on mRNA modifications under MMS Stress. The [cntrl–si] on the plot labels means the control without any transfection; the [cntrl] means with control scrambled RNA (scrRNA) transfection. The bars labeled with each enzymes name mean that enzymes transcript is knocked down. Data is plotted based on the average value of two biological replicates, where the error bars represent standard deviation. Studied modifications are: **(A)** m^6A, **(B)** m^1A, **(C)** m^3C, **(D)** m^5C, and **(E)** m^7G.

Interestingly, comparing the 4h post MMS removal of both m^1A and m^3C modifications bars, absence of AlkBH3 or ASCC3 show slightly but not significantly more demethylation than in control samples, which does not comply with our expectation of AlkBH3 or ASCC3 demethylation role. Moreover, compared to ZNF598 KD, demethylated abundances are not significantly different from AlkBH3 or ASCC3 KD samples, based on paired t-test at significance level of $p<0.05$. This data suggests no significance in methylation repair of knockdown AlkBH3 or ASCC3 cells, and therefore supports the existence of other unidentified demethylation pathways that compensate for the absence of AlkBH3 or ASCC3. Based on literature, it is expected for m^1A and m^3C to return to near pre-treatment levels after 24h post MMS, but not m^7G; which suggests removal of MMS-induced m^7G is likely mediated by mRNA degradation only, as no human RNA m^7G demethylase is known. Thus, removal of m^1A and m^3C may be mediated by combined mRNA degradation and ALKBH3-mediated demethylation.[153] However, this hypothesis cannot be fully studied in this experiment, since it was stopped after 4h post MMS methylation stress.

Based on my data, m^1A and m^3C are the major methylation damage products in human mRNA after MMS treatment. While the abundance of these damages drops 4 hours after stress removal, I find that neither AlkBH3 nor ASCC3 are involved in the demethylation of damaged human mRNA *in vivo*.

To conclude my studies on human RNA erasers, I did not find a difference in the abundance of the RNA modifications considered as AlkBH family members 1, 3 or 5 substrates, in AlkBHs KD samples in contrast to the transfection controls in this chapter. The complex machinery of aberrant methylation stress-response in human cells, might provide a recompense for AlkBHs absence by other unidentified demethylases or at least, by remaining active AlkBHs and thus restoring the original levels of the observed RNA modifications. A complete knockout of AlkBHs gene might show different outcome, though was not possible in this study.

3.3. Effect of modification incorporation on tRF stability *in vivo*

NAIL-MS, as our current analytical toolbox, provides insights on underlying mechanisms into the dynamics of nucleic acid modifications. Dynamic NAIL-MS palse-chase experiments help with following up the dynamics of external RNA sequences within cells, by differentiating between the isotopic labeled native RNA and the unlabeled synthetic RNA. This feature would allow the study of tRNA fragments (tRFs) stability with focus on modification incorporation effect.

Drino *et al*. has identified and characterized native tRNA-Gly_{GCC} derived stress induced halve from isoacceptor Glycine $_{GCC}$ (5´-tiRNA$^{Gly}_{GCC}$), using overexpression of human angiogenin enzyme (ANG), and absolute quantification of modifications in full-length tRNAs resulting 5′ tiRNAs. Their study suggested existence of m^2G and Um on the 5´-tiRNA$^{Gly}_{GCC}$ but no m^1G, m^7G, m^2G, $m^{22}G$, Am, and m^6A from the targeted tRNA isoacceptor.[195] Considering their results, I aimed to study the 5´-tiRNA$^{Gly}_{GCC}$ Um modification incorporation relationship to its stability *in vivo*, which could suggest Um incorporation functional relevance of 5´-tiRNA$^{Gly}_{GCC}$ in cells.

Therefore, two 33-nucleotides long 5´-tRF$^{Gly}_{GCC}$ sequences including unmodified or position 4-Um modified are used as models for 5´tiRNA$^{Gly}_{GCC}$ in this study. This chapter's outcome provides information about model tiRNA stability in cells which can shed light to its functional relevance. Figure **3.29** Shows the concept of the study and it´s experimental design.

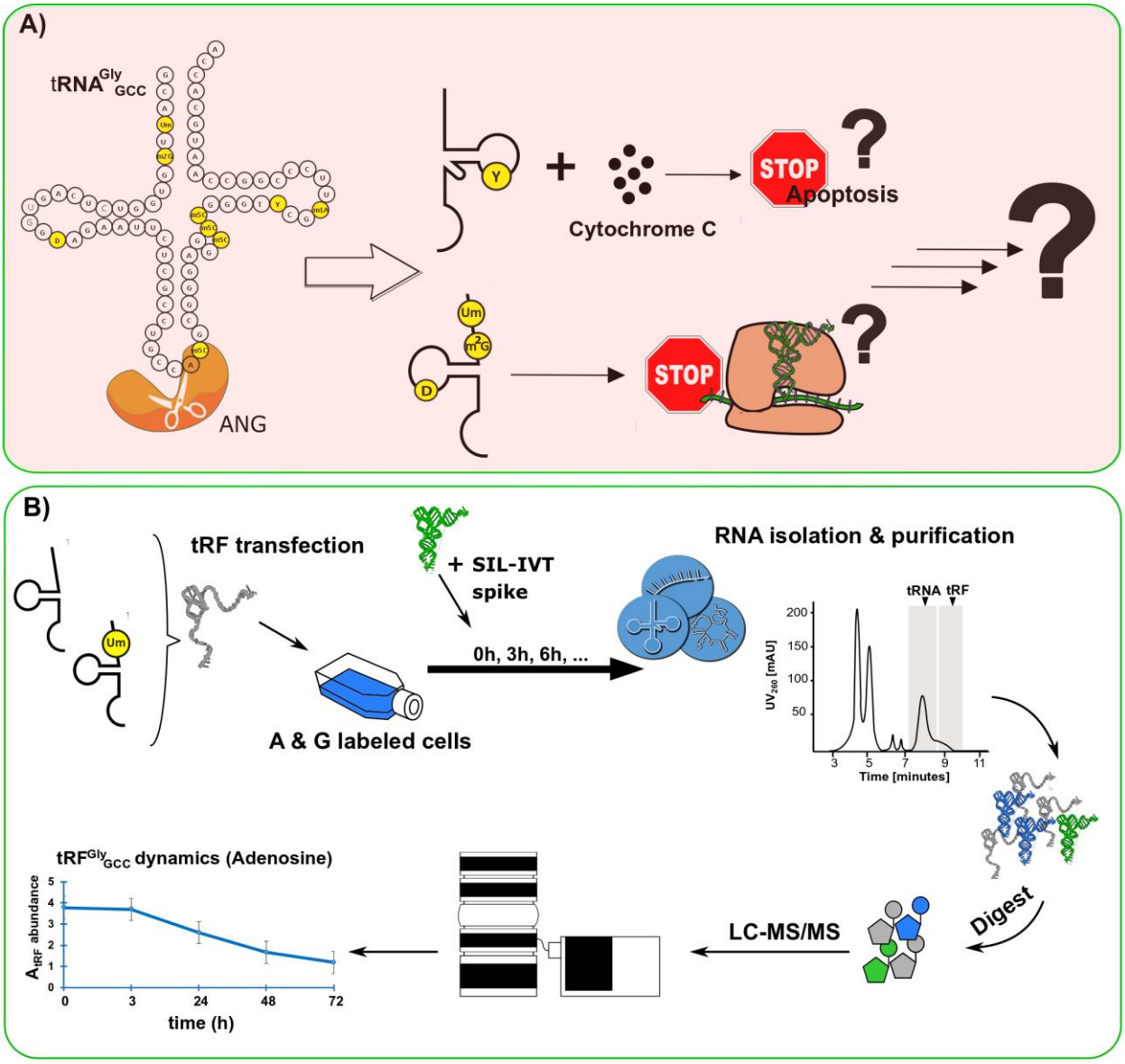

Figure 3. 29 (A) Summary of tiRNA formation from tRNA$^{Gly}_{GCC}$ through ANG cleavage in the anticodon loop and its potential functions. (B) general workflow of tRF *in-vivo* stability study. Synthesized 5´-tRF$^{Gly}_{GCC}$ sequences were transfected into $^{15}N_5$ adenine labeled HEK cells, then lysed with TRI reagent at different post-transfection time points with spiking the technical internal standard (SIL-IVT), and total RNA content was isolated, tRNA and tRF portion were purified together (300 Å column) or separately (130 Å column) by SEC, and digested to single nucleoside building blocks using enzymatic digestion mix. Then samples were subjected to LC-MS/MS analysis. the nucleosides abundances were calculated by Agilent MassHunter Workstation software. Data plotted based on relative abundances of tRF to cells tRNA.

3.3.1. Quality assurance of model synthesized tRF$^{Gly}_{GCC}$

Commercially available 33 nucleotides RNA sequences, which were identical to the unmodified version of 5´-tiRNA$^{Gly}_{GCC}$, or modified with only Um at position 4, without the two CC nucleosides at the 3´end, were used to mimic the 5′ tiRNAs.

In order to confirm purity, sequence identity, length, and modification status of the two tRFs, different steps of quality control were performed. At the first step, 2 ng of the tRF sequences were loaded on high resolution automated electrophoresis (Bioanalyzer). As shown in figure **3.30**, total RNA and total tRNA extracted from HEK cells were used as length controls. The tRFs showed a good purity and their length were ~30 nucleotides which was expected.

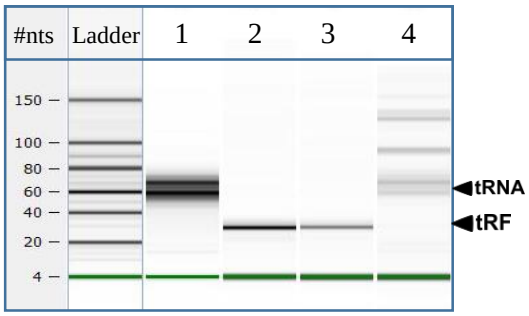

Figure 3. 30 5´tRF$^{Gly}_{GCC}$ quality control by automated gel-electrophoresis system (bioanalyzer small chip). 1: total tRNA, 2: unmodified tRF, 3: Um-modified tRF, 4: total RNA.

Next, the modification status of the unmodified tRF was analyzed by absolute quantification on LC-MS/MS (figure **3.31.**A). For this purpose, tRF was digested to single nucleosides and injected with SILIS, and the amount of modifications per tRF sequence was calculated. As shown in figure 3.3.3, apart from very low amounts of m^5C and I, all other tRNA modifications were below the LOD. The existence of m^5C in synthesized RNA sequence has already been discussed by Helm lab,[292] and existence of inosine can be due to hydrolytic deamination of adenosine under alkaline environment of digestion.[241] However, there is only ~0.01 of these two modifications per tRF sequence, which does not interfere with tRF stability measurements and Um quantification.
In the next validation step, Um modification amount in the two synthesized tRF sequences were absolute-quantified and compared.

Based on figure **3.31.**B, there was no Um detected in the unmodified sequence (SK178), while 0.94 Um per injected tRF molecule was calculated on the modified sequence (SK179), which confirms existence of ~ 1 Um modified nucleoside per tRF molecule.

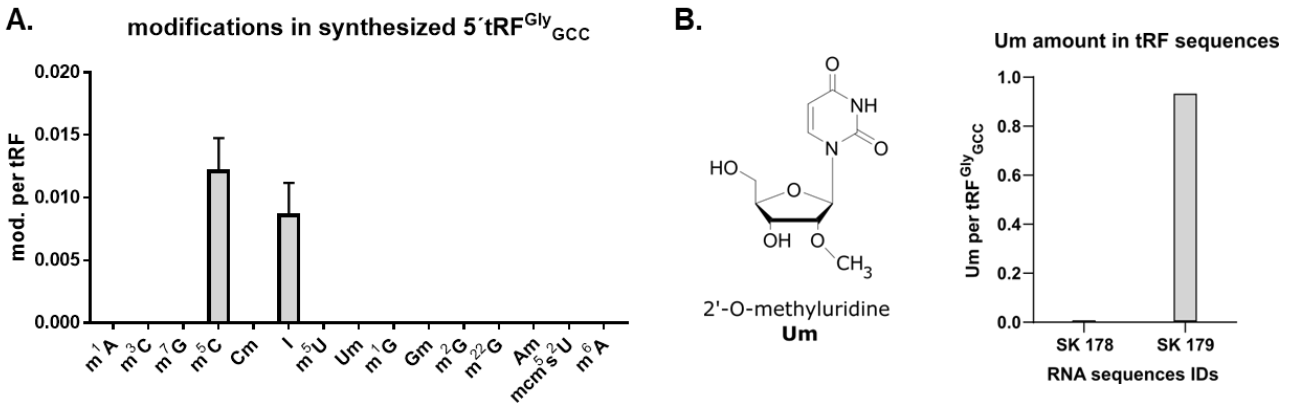

Figure 3. 31 (A) Absolute quantification of modification amounts in synthesized 5´tRF$^{Gly}_{GCC}$ analyzed by LC-MS/MS **(B)** Um modification structure, and analysis of Um amounts in the synthesized tRF molecules by LC-MS/MS absolute quantification. SK178: unmodified tRF$^{Gly}_{GCC}$ and SK179: Um-modified tRF$^{Gly}_{GCC}$.

Quality control is also performed for the sequence composition of synthesized tRF, by quantifying and comparing number of each canonical nucleoside per tRF sequence to the expected values (table **3.1**). Table **3.2** shows a good correlation with the theory with low % error values. Based on the % error values which are ~10% for both sequences, there is a good correlation between the expected number of canonicals to their measured values.

Table 3. 1 Expected number of canonical nucleosides per tRF$^{Gly}_{GCC}$ sequences

identity	ID number	G	A	U	C	SUM
unmodified tRF$^{Gly}_{GCC}$	SK178	11	5	11	6	33
Um-modified tRF$^{Gly}_{GCC}$	SK179	11	5	10	6	32

Table 3. 2 Calculated amount (pmol) of a single canonical nucleoside in the injected RNA molecule, based on dividing the automatically calculated amount by the quantitative MassHunter Software to the corresponding number in injected RNA sequence.

ID number	calculated concentration/number in sequence				% error calculation		
	G	A	U	C	average	error (SD)	% error
SK 178	9,12	9,89	7,44	8,41	8,71	0,90	10,38
SK179	6,82	7,71	6,11	6,41	6,76	0,69	10,27

After quality assurance of the synthesized model tRFs, variable parameters in the cell culture were investigated. First, HEK cells were labeled with $^{15}N_5$ adenine supplemented medium for 7 days (=3 passages). Therefore, monoisotopic labeling efficiency of A and G from cells total RNA was investigated 40 h after the last exchange of the $^{15}N_5$ adenine medium. Total RNA was purified, digested to single nucleosides, and samples were analyzed by LC-MS/MS. Given the fact that 99.6% of naturally occurring nitrogen is ^{14}N and 0.4% ^{15}N, there should be ~2% ^{15}N labeled bases left in unlabeled cells. Based on figure **3.32**, amount of $^{14}N/^{15}N$ labeled was 0.96% for adenosine and 2.4 % for guanosine in labeled cells.

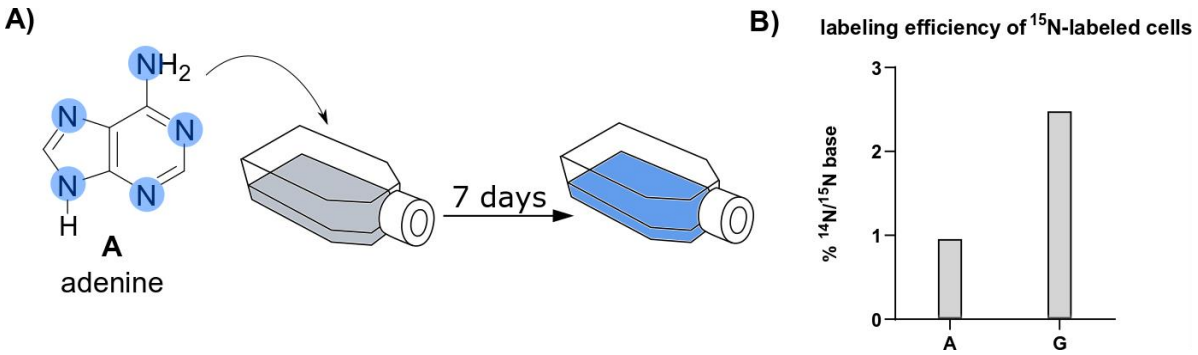

Figure 3. 32 (A) Workflow for labeling HEK cells with $^{15}N_5$ adenine. Cells incubated in special medium: DMEM D0422 + dialyzed FBS + $^{15}N_5$ labeled adenine + unlabeled uridine. **(B) labeling efficiency of $^{15}N_5$ adenine labeled cells.** Total RNA of HEK cells was harvested 40 h after medium exchange. Data is plotted based on percent relative amounts of unlabeled to labeled adenosine and guanosine. Amounts were quantified by Agilent MassHunter Workstation Software for quantitative analysis.

Effect of using FBS in cell culture on tRF transfection experiment

Usage of fetal bovine serum (FBS) is essential in human cell culture due to incorporating undefined composition and variable concentration of metabolites to help cell growth. Different studies have shown cleavage in tRNA anticodon loop to produce tRNA half molecules, is not limited to stress, but also in non-stress conditions. tRNA halves are especially abundant in hematopoietic system including serum, fetal liver and placenta. They were also found in body fluids such as sperm, cerebrospinal fluid and urine, and in extracellular vesicles.[181] This information infers the necessity of investigating tRNA fragments contamination caused by FBS content.

In order to analyze the RNA of FBS, 10 mL of liquid regular or dialyzed FBS was spiked with different amounts of total RNA extracted form HEK cells including: 0 ng (no RNA addition), 100ng, 500 ng, 1000 ng, 5000 ng. Moreover, cell death results in the release of cellular content into extracellular space, including tRFs; which remains stable in cell medium. Therefore, I collected and analyzed cells growth medium including regular FBS after 48h of cells incubation, in order to account for the tRF produced by degradation of dead cells (figure **3.33**.B, fifth lane from left). All samples were freeze-dried by lyophilization, then lysed with 5 mL TRI reagent and precipitated. The gained total RNA recovery was not very good, due to the fact that dried FBS did not dissolve easily in TRI, but formed a big foamy interphase between the aqueous and organic phases, which was reduced by centrifugation, however some sample loss occurred while moving samples to new reaction tubes. The total RNA content were analyzed by bioanalyzer Pico RNA chip (figure **3.33**)

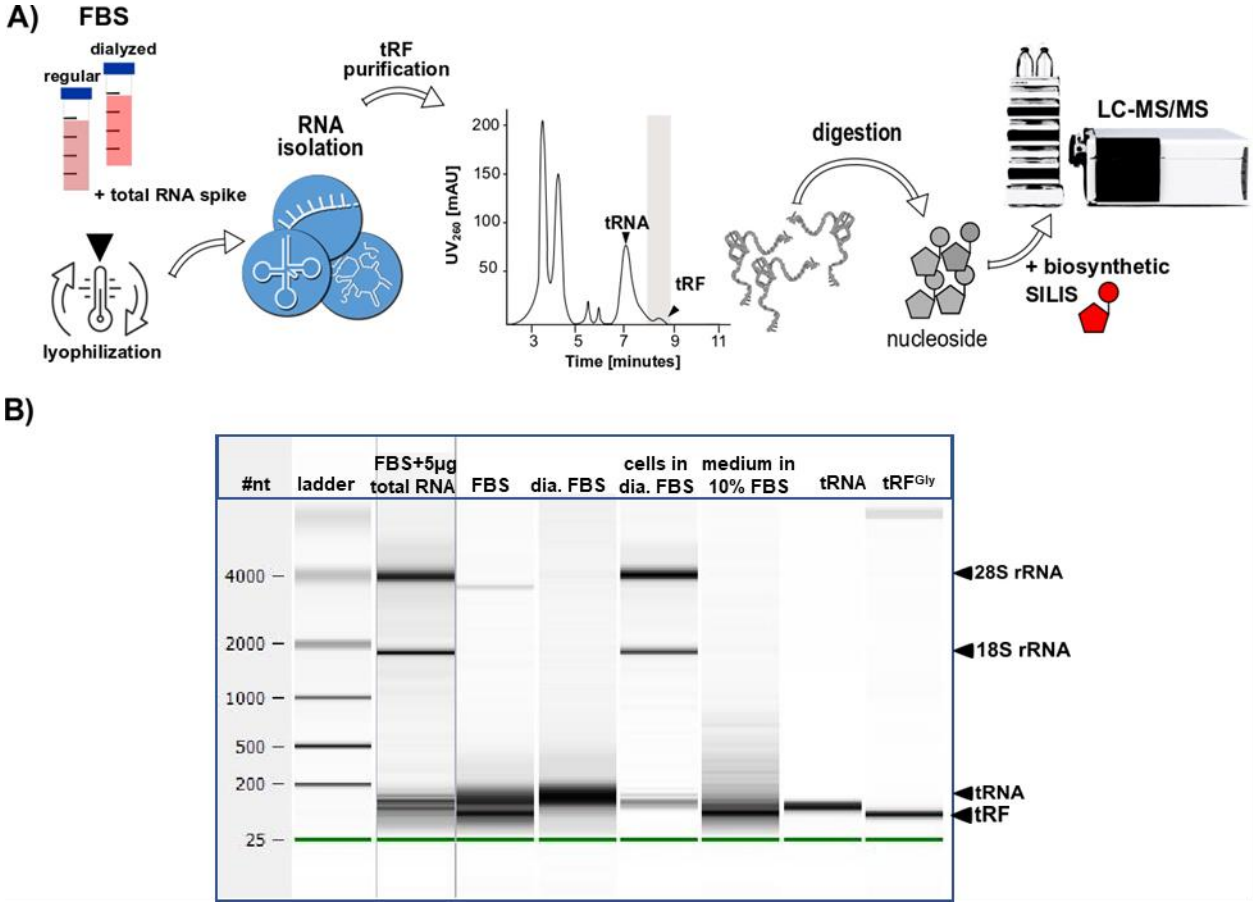

Figure 3. 33 (A) Workflow of FBS extracted tRF modifications analysis. 10 mL of liquid regular or dialyzed FBS were spiked with different amounts of total RNA extracted form HEK cells (only 5 µg is shown). Samples were freeze-dried, then lysed with 5 mL TRI reagent and RNA content was precipitated, isolated using SEC (130 Å column), and digested to single nucleoside building blocks using enzymatic digestion mix. The stable isotope label internal standard (SILIS) was added and the samples, which were subjected to LC-MS/MS analysis. the absolute quantification of nucleosides was calculated by Agilent MassHunter Workstation software and plotted. **(B) Bioanalyzer Pico RNA chip of total RNA extracted from FBS lysis.** Regular FBS is labeled as FBS and dialyzed FBS as dia. FBS.

Due to the RNA extraction hardships, there were no visible traces of added total RNA to the FBS before lyophilization (not shown). Markedly, there was a difference in the traces of regular *vs.* dialyzed FBS as visualized in the bioanalyzer gel image of figure **3.33.B**: in the lane including regular FBS, there is a thick band with a nucleotides length close to the synthesized tRF (~30-50 nt), while this band is absent for dialyzed FBS. Even though there is another thick band in between 100-200 nt for all of the tested FBS compositions, it does not interfere with this study´s target sequence length. This was a good reason for using dialyzed FBS throughout the whole experiments of this chapter.

Moreover, it is important to note that FBS causes RNA contamination in all of our cell culture experiments. Although NAIL-MS evades this issue in isotopic labeled target RNA studies, one can expect some irregularities in the unlabeled RNA experiments analysis in general. Further, the isolation of tRF portion from total RNA of the two types of FBS were processed by SEC, digestion to single nucleosides, and absolute quantification of tRNA modifications by LC-MS/MS (figure **3.34**). For normalization, abundance of modifications is referred to each

10^3 sum of canonical nucleosides. The resulted analysis showed in figure **3.34** provides a good insight into the importance of choosing dialyzed FBS over regular for tRF transfection experiments, as there are different modifications in the regular FBS, but not in dialyzed.

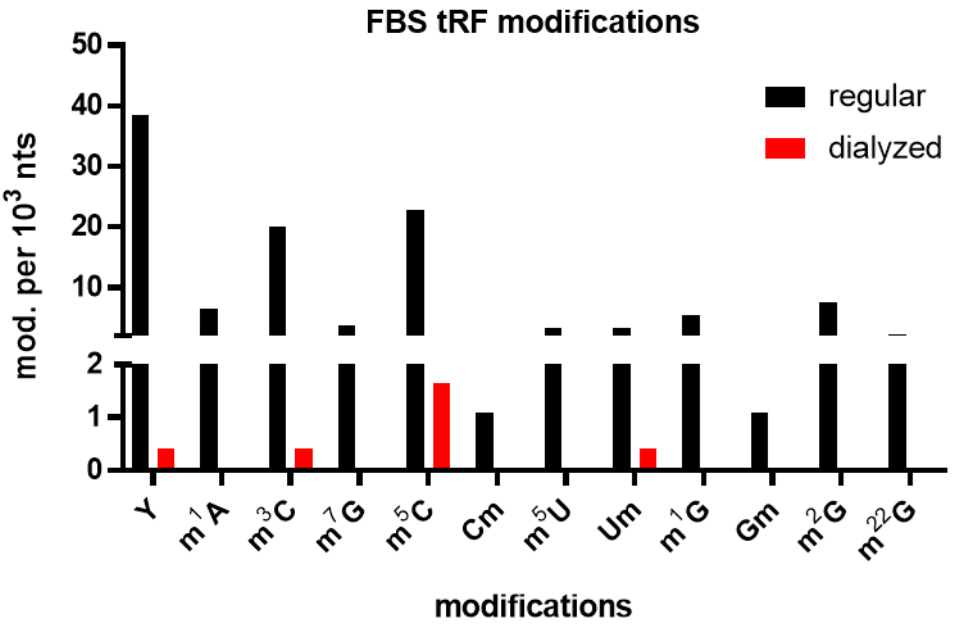

Figure 3. 34 Absolute quantification of purified tRF modifications from cell culture FBS by LC-MS/MS of 100 pmol sample injection.

Based on the visualized data, process of FBS dialysis excludes partial RNA contamination in the oligonucleotide lengths close to tRNA fragments. Culturing HEK cells, we observe higher proliferation rate with regular FBS than dialyzed, potentially due to exclusion of some nutrients desirable to cells in the dialysis process. However, the cells could tolerate dialyzed FBS, as they did the mitosis and kept their oval armed physiology and adherence to the plate surface. Therefore, dialyzed FBS is chosen for the tRF transfection experimental set.

Selection of transfection reagent for tRF experiments

Among different types of transfection reagents for RNA, such as viral or plasmid vectors, liposomal reagents, cationic polymers, nanoparticles, *etc*., two of the common reagents for small RNA delivery into eukaryotic cells are Lipofectamine 2000 (LP2000) and jetPRIME (JP). Lipofection entails cationic liposome-RNA complexes formation, which requires the interaction between positively-charged liposomal molecules and negatively charged nucleic acids, while cationic polymers such as JP form complexes with the negatively charged nucleic acids, which aid in the uptake of the RNA by cells through endocytosis. Compared to viral vectors and cationic lipofection, cationic polymers produce less cytotoxicity but are also compromised with lower efficiency.[288] Based on the fact that JP workflow is better compatible with NAIL-MS and fast compared to LP2000 (1h vs. 6h transfection phase), I decided to compare the transfection efficiency between LP2000 and JP for 5´tRF$^{Gly}_{GCC}$ transfection into HEK cells.

To do so, HEK cells were grown fully $^{15}N_5$-adenine labeled in a 6 well plate, then transfected with the synthesized unmodified tRF using either JP or LP2000 with their manufacturer suggested workflow, and were harvested 1h after the transfection phase by TRI reagent. For the negative controls, only LP2000 or JP were added to the cells without tRF addition, and for the positive controls, the same 'empty transfection' was completed as the negative controls, but the exact transfection amount of tRF (96 pmol) was added to the cell lysate right after addition of TRI.

Figure 3.35 shows the relative abundances based on dividing the unlabeled nucleoside to the sum of unlabeled and cell culture NAIL-MS metabolically labeled of adenosine or guanosine for each condition.

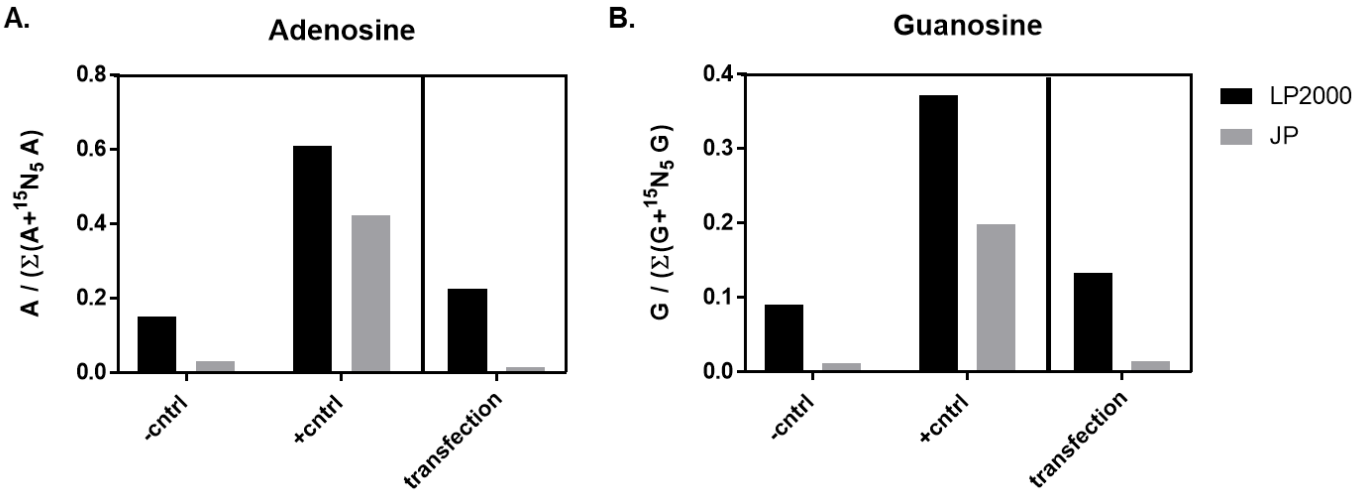

Figure 3. 35 LC-MS/MS data of tRF transfection efficiency. X axis titles from left: negative control, positive control, and transfected tRF with lipofectamine 2000 (LP2000, black) or jetPRIME (JP, gray), based on relative peak areas of unlabeled nucleoside (from transfected tRF) to sum of nucleoside in cells isolated tRNA and tRF for **(A)** adenosine and **(B)** guanosine.

LP2000 showed 36% transfection efficiency based on G and 37% based on A relative abundances compared to the positive control, while JP displayed very poor transfection efficiencies (<7%) in HEK cells. Similar results were obtained when comparing 6h transfection phase + 1h post transfect of LP2000 to 7h of transfection with JP. Based on this outcome, LP2000 was chosen for all upcoming transfection experiments. Absence of FBS in the transfection phase of LP2000 helps to avoid the FBS RNA interference in tRF uptake by cells. However, the presence of 10% serum is necessary for cells survival in post-transfection phase.

3.3.2. Establishment and application of SIL-IVT as technical standard for tRF analysis

The absolute amount of external RNA uptake by the cells during transfection, is affected by variable parameters in cell culture, such as cell numbers, cells viability, growth phase, external stress, and other biological factors; as well as variations in sample preparation and analysis due to different errors caused at each workflow step. Many of these variables can cause concentration/dilution effects which are not due to biological uptake of the transfected RNA.

In order to compensate for the uncontrollable variations throughout the whole workflow including: cell culture, sample preparation, and LC-MS/MS analysis, introduction of an internal standard was needed.

I decided to introduce a technical standard, that would stay inert throughout the sample preparation, while representing the changes to the analyte. Isotopic labeled internal standards have proven to be the best candidates, as stable isotopologues of the target analyte have the same physico-chemical properties and thus can be used to correct for mass spectrometric detection fluctuations. Stable isotopes like carbon-13, nitrogen-15 or oxygen-18 are commonly used to produce the mass of interest.

Apart from SILIS production, our lab had already introduced different types of isotopic labeling namely NAIL-MS for pulse-chase experiments including $^{13}C_6$-glucose, $^{15}N_5$-adenine and $^{13}C_5$ $^{15}N_2$- uridine, or CD_3-methionine metabolic labeling.[287, 293] For a new technical standard production, I needed to consider a different mass transition of nucleosides than in other established techniques *e.g.* SILIS or NAIL-MS, to avoid signals overlapping in the mass spectrometry analysis.

The production of a stable isotopic labeled compound can be done either synthetically or metabolically.[210, 260] From our experience, the target isotopologue of a nucleoside must be at least 3 u heavier compared to the naturally occurring nucleoside to avoid false positive results by the detection of the natural carbon-13 signals. Considering this note, ^{13}C labeling of both nucleobases and ribose, was a good option, given the fact that the m/z for both A and G with this isotopic incorporation, would make a +10 u difference with the unlabeled isotopes, and +5 u difference with the NAIL-MS metabolic labeled nucleosides, coming from the $^{15}N_5$ adenine labeled cells (**Figure 3.36**.B).

(A)

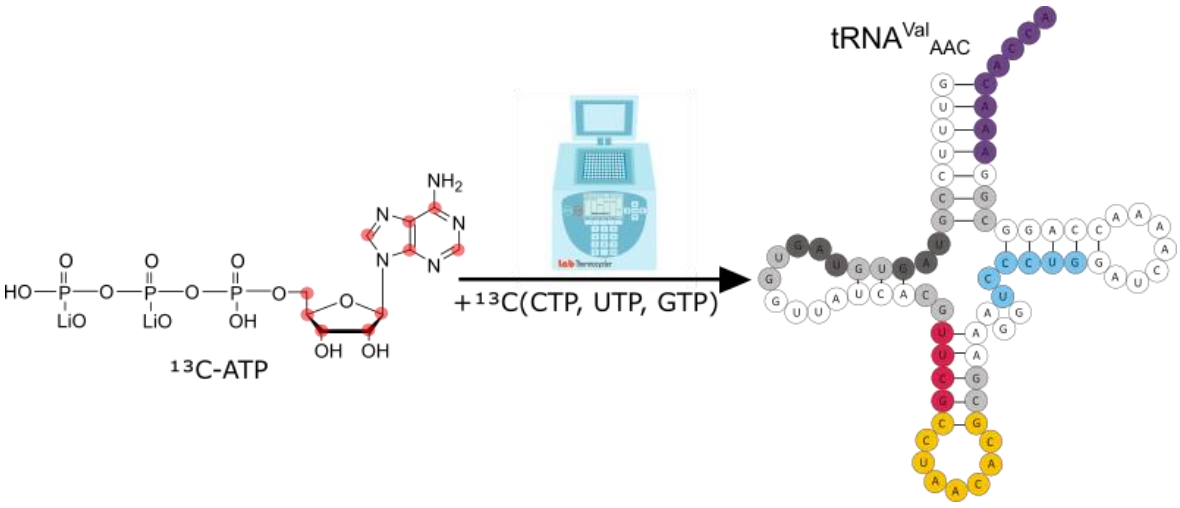

(B)

Compound / m/z	A	A SILIS	A SIL-IVT	A ^{15}N-lab.	G	G SILIS	G SIL-IVT	G ^{15}N-lab.
Precursor Ion	268	283	278	273	284	299	294	289
Product Ion	136	146	141	141	152	162	157	157

Figure 3. 36 (A) in vitro transcription of tRNA$^{val}_{AAC}$ as stable-isotope labeled in vitro transcribed technical internal standard (SIL-IVT). **(B)** mass transitions of precursor and product ions for different labeling status of adenosine and guanosine including the SIL-IVT.

Thus, I decided to use full $^{13}C_{10}$ labeling to create tRNA isoacceptor Valine with the anticodon AAC (tRNA$^{val}_{AAC}$), through in vitro transcription. This new stable-isotope labeled in vitro transcribed technical internal standard (SIL-IVT) has 76 nucleotides, which lies within the size of total tRNA, therefore it has the advantage of going through sample preparation (such as SEC isolation and precipitation steps), together with total tRNA from cells and transfected tRF.

In vitro transcription of tRNA$^{val}_{AAC}$ SIL-IVT was performed using the protocol described by Hagelskamp *et al.*,[261] including amplification of the DNA template with encoded sequence regions for the T7 promoter region (T7 prom), hammerhead ribozyme (hh) and the tRNA sequence by PCR. Next, RNA was generated with T7 RNA Polymerase followed by autocatalytic cleavage of hh. The DNA was digested by DNase I (fig **3.36**.A).

For purification of in vitro transcribed tRNA$^{val}_{AAC}$, preparative gel electrophoresis, with 12% TBE-urea preparative gel was used (**figure 3.37.**A). The gel was then stained with GelRed reagent, and imaged by UV imager at 260 nm. Gel bands of tRNA$^{val}_{AAC}$ were isolated by crush and soak method,[294] and then bioanalyzer small RNA chip was employed for purity control of IVT product tRNA$^{val}_{AAC}$ purified by preparative TBE-urea gel (**figure 3.37.**B). Based on bioanalyzer gel image, the SIL-IVT tRNA$^{val}_{AAC}$ purity is confirmed.

Afterwards, the generated $tRNA^{val}_{AAC}$ SIL-IVTs labeling status was validated by digested nucleosides LC-MS/MS analysis, using MS^2 scan mode analysis, as presented in figure **3.37.**C. The expected peaks for ^{13}C-labeled precursor and product ions were detected for A, G and C but not for U. Next, only ^{13}C-UTP was digested by CIP enzyme to cleave the phosphate group, then checked with MS^2 scan to inspect the incorporation status of ^{13}C-U.

Interestingly, the precursor and product ion signals for purchased ^{13}C-UTP were detected (data not shown). Based on this detection, the incorporation of ^{13}C-U to the tRNA transcription seemed to be questionable. However, since the cells labeling scheme of the upcoming experiments were focused on A and G, absence of SIL-IVT uridine was not going to affect the results of this study.

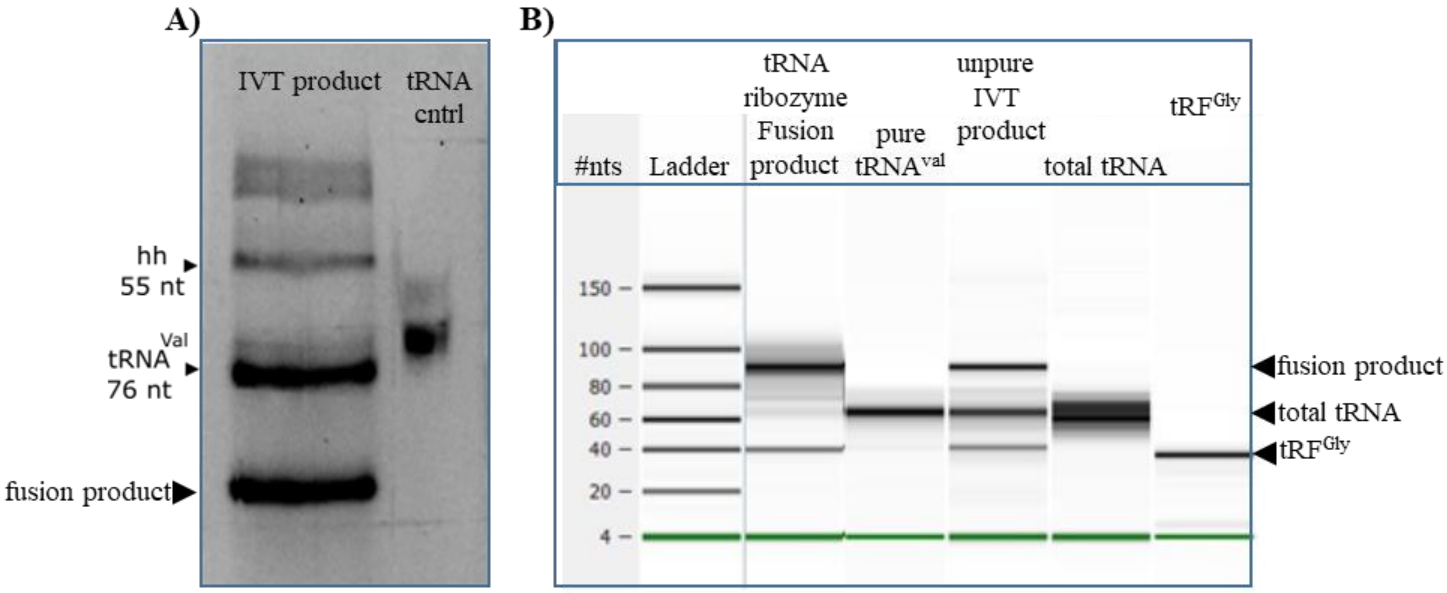

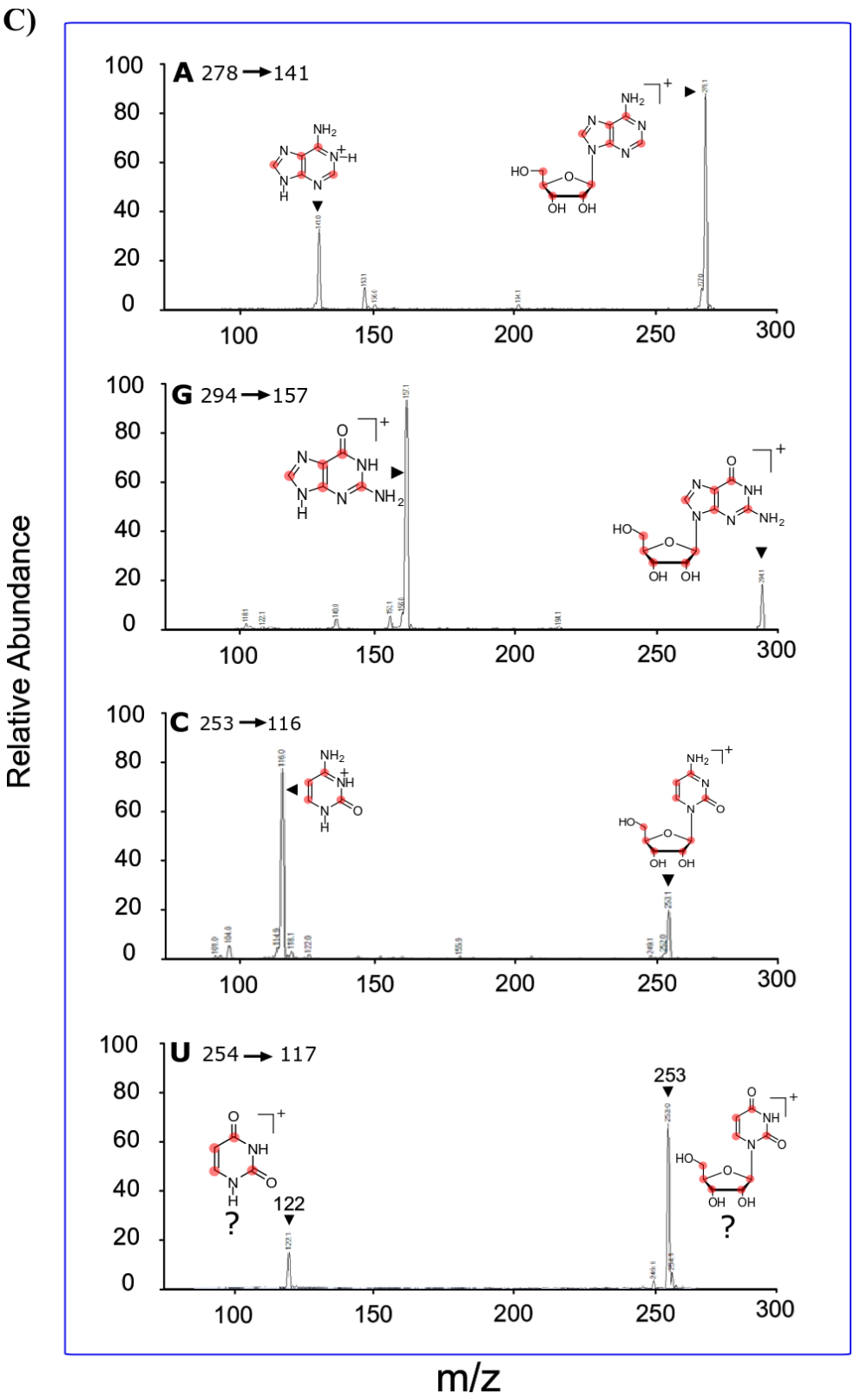

Figure 3. 37 Identity and purification controls of in vitro trascribed tRNA$^{val}_{AAC}$ (A) UV image of tRNA$^{val}_{AAC}$ purification by 12% TBE-urea preparative gel electrophoresis, stained with GelRed (SigmaAldrich), and imaged by UV imager (Bio-Rad universal hood II) at 260 nm. **(B)** Bioanalyzer small RNA chip of IVT product tRNA$^{val}_{AAC}$, purified by preparative TBE-urea gel. **(C)** MS^2 scan of ^{13}C labeled nucleosides from IVT tRNA$^{val}_{AAC}$. The expected MS^2 ion peaks for C, G, and A were detected, but U did not show the MS^2 signals.

Validation of SIL-IVT (^{13}C-tRNA$^{Val}_{AAC}$) for NAIL-MS measurments

With the aim of bringing SIL-IVT in tRF relative abundance calculation, by normalization of unlabeled (transfected) nucleoside to sum of the nucleoside in unlabeled, ^{15}N-labeled (metabolic labeled tRNA) and ^{13}C-labeled (SIL-IVT), validation of SIL-IVT spike-in amount to cell lysate was performed.

First, the amount of SIL-IVT spike-in to cell lysate was optimized to gain a quantifiable peak area compared to ^{15}N-labeled tRNA. Fully A-labeled cells were grown on a 6 well plate, harvested simultanously with TRI reagent, and different amounts of SIL-IVT was added to each lysate. **Figure 3.38**.A shows the sample work-up. Data was plotted based on relative peak areas for ^{15}N-metabolic labeled tRNA nucleoside to the corresponding SIL-IVT nucleosides.

A)

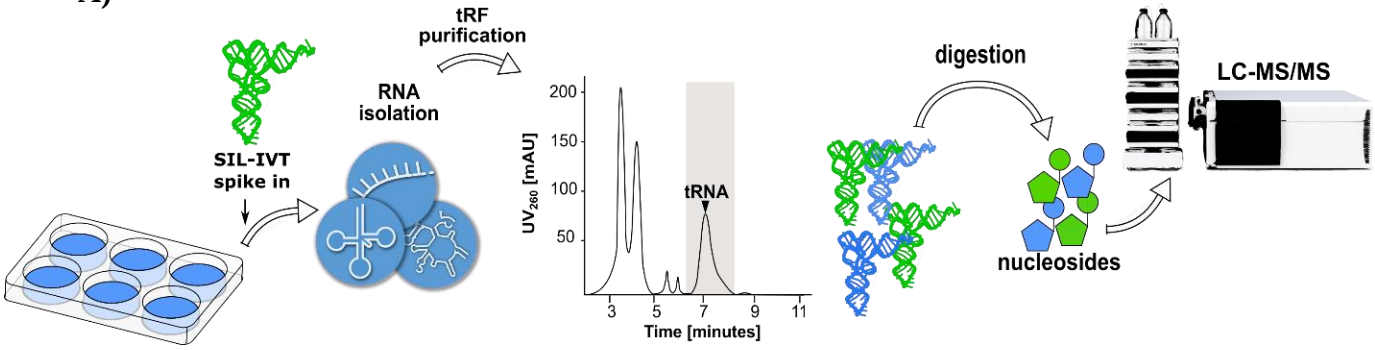

B)

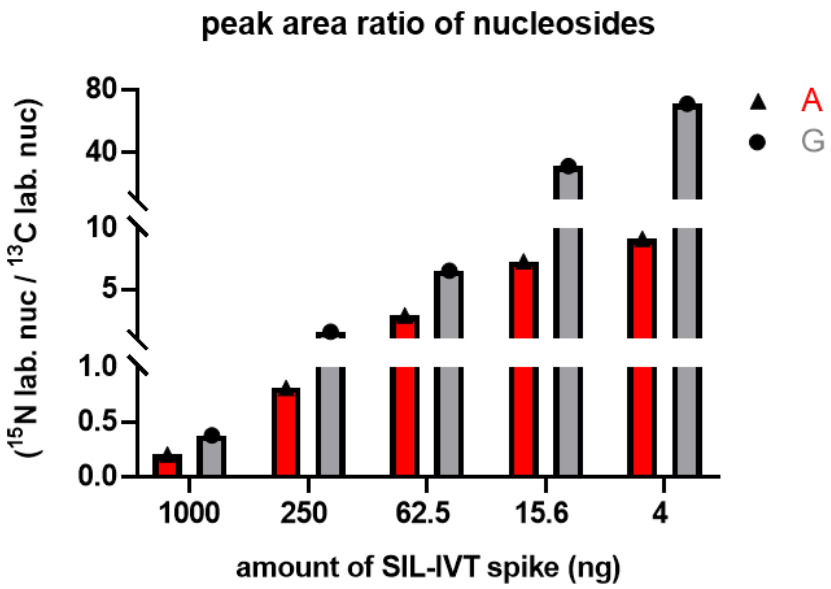

Figure 3. 38 SIL-IVT spike into cell lysates amount optimization (A) workflow and **(B)** comparison of peak area ratio for ^{15}N-labeled nucleoside (nuc) from cells metabolic labeling to ^{13}C-labeled nuc from SIL-IVT with the spike amounts of 1000, 250, 62.5, 15.6 or 4 ng on each well of the 6 well plate.

Based on data shown on figure **3.38.**B, 60 ng was chosen as a good amount of SIL-IVT spike for 6 well plates, as a signal of metabolic labeling of A and G was 5 times higher than the SIL-IVT with cells amount gained from each of a 6 well plate, where both nucleoside species were

easily quantifiable. Given the fact that adenosine ionization efficiency is very high in the positive ionization mode, and the amount of ^{15}N-labeled A is much higher than SIL-IVT A in this experiment, the MS/MS parameters including fragmentor voltage and collision energy were optimized for ^{13}C-labeled species *vs*. ^{15}N-labeled to avoid MS signal suppression on ^{13}C labeled SIL-IVT. Table **3.3** shows the parameters used in the LC-MS/MS method for each labeling type of adenosine.

Table 3. 3 MS/MS parameters used for different labeling schemes of adenosine.

Adenosine type	Fragmentor voltage (V)	Collision Energy (eV)
$^{15}N_5$ (NAIL-MS)	250	25
SILIS	200	20
^{13}C SIL-IVT	110	21
unlabeled	200	20

Using the optimized LC-MS/MS method, the reproducibility of ^{15}N-labeled nucleosides ratio to ^{13}C-labeled species (from SIL-IVT) was investigated for a 6 well plate, to consider the extend of cells number fluctuation between wells of a 6 well plate. Fully metabolic $^{15}N_5$ adenine labeled cells tRNA A & G were harvested for each well plate by TRI reagent, and 60 ng of SIL-IVT was added to each cell lysate, then relative abundances for each nucleoside was plotted (figure **3.39**).

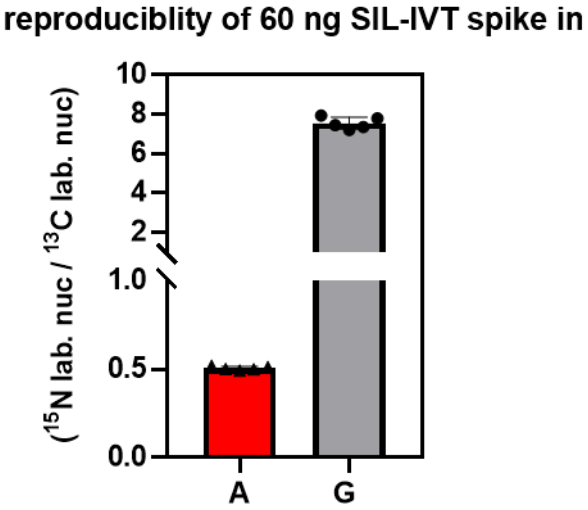

Figure 3. 39 Reproducibility of HEK cells ^{15}N-labeled tRNA to 60 ng ^{13}C-labeled SIL-IVT tRNA$^{Val}_{AAC}$ nucleosides abundances ratio, from spiking into the cells lysate. Data plotted based on relative peak areas. Error bars represent standard deviation for 5 replicates.

Although this data shows very low error bars, one needs to account for cells numbers differences between measurements. After confirming that spiking into the cell lysates is a good way to include my technical internal standard, I tried omitting cell numbers variation by producing a calibration curve based on relative peak areas of [cells nucleoside $^{15}N_5$ labeled / ^{13}C-labeled SIL-IVT] *vs.* [number of cells]. To do so, fully $^{15}N_5$ adenine labeled HEK cells

were grown in to gain 0.5, 1, 2, 3, 4 and 5 million cells by manual counting. Then each cell lysate was spiked with 60 ng SIL-IVT, and the calibration curve (CC) was plotted (figure **3.40**).

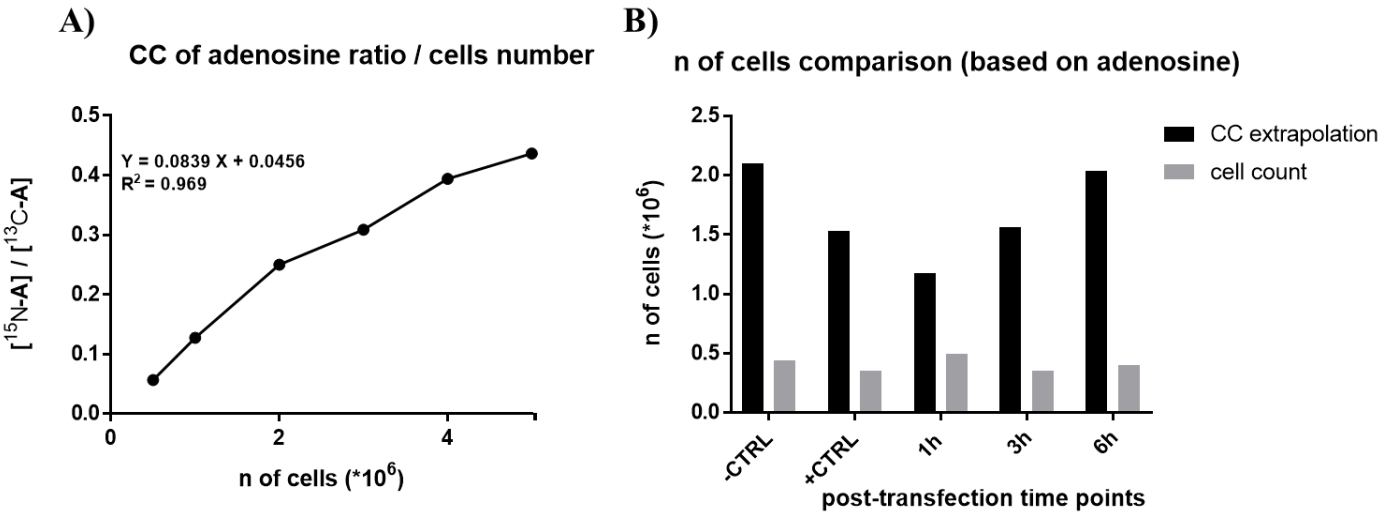

Figure 3. 40 (A) Calibration curve (CC) of [cells adenosine $^{15}N_5$ labeled / ^{13}C-labeled SIL-IVT adenosine] *vs.* [number (n) of cells] and **(B)** Comparison of number of cells between extrapolation into the adenosine plotted CC in (A), to manual cell counting.

Although the data fitting the regression model for the plotted CC is acceptable (R^2 = 0.969) (fig **3.40**A), the trial of extrapolating of gained nucleosides ratio to the number of cells did not match the experimental counted values for cells number. **Figure 3.40.**B shows the example for extrapolation based on adenosine CC. Therefore, The CC was not used and instead, manually cell counting is used and a correction factor for the number of cells for each separated transfection experiment is created for the rest of the experiments.

Finally, the unmodified tRF^{Gly}_{GCC} (SK178) transfection experiment with incorporation of SIL-IVT and cell counting was performed in order to investigate the feasibility of the experimental design. To study the tRF stability in HEK cells, labeled cells grown on 6 wells, were transfected with tRF^{Gly}_{GCC} (SK178), then harvested at different post-transfection phase time points. All lysates were spiked in with 60 ng of SIL-IVT and went through sample processing including total RNA isolation, SEC purification of tRNA+ tRF portion, enzymatic digestion to single nucleosides, and LC-MS/MS analysis.

Figure **3.41** shows the analyzed data of this experiment. Calculation for either adenosine or guanosine nucleoside (nuc) of transfected tRF^{Gly}_{GCC} was done, using MS peak area of unlabeled nuc normalized to the sum of all nucleosides multiplied to SIL-IVT nucleosides peak area, as the following formula:

(1)

$$\text{relative abundance of transfected nuc} = \frac{10^7 * \text{unlab. nuc}}{\sum (\text{unlab.} + {}^{15}\text{N-lab. nuc}) * {}^{13}\text{C-lab. nuc}}$$

For omitting the variations in cell numbers (n) that would affect the ^{15}N-labeled nucleosides gain and therefore final relative abundance of transfected nucleoside, cell number correction factor was used, by dividing the highest counted number of cells among post-transfection time points of the same experimental replicate, to each of the time points count, using formula **(2)**:

(2)

$$\text{cell counting correction factor} = \frac{\text{highest n of cells among time points}}{\text{n of cells from each time point}}$$

Each calculated relative abundance from formula **(1)** was then multiplied to its own counting correction factor. Then all of the relative abundance values for A or G were normalized to the corresponding negative control in order to gain the final values for only transfected tRF based on A and G in the cells (figure **3.41**).

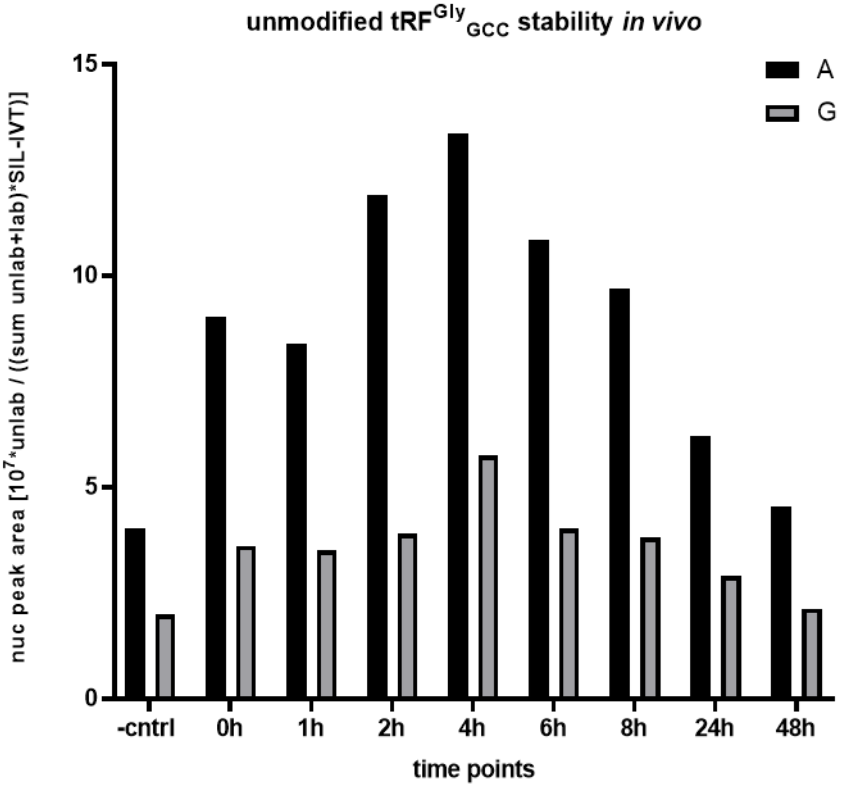

Figure 3. 41 Unmodified tRF$^{Gly}_{GCC}$ stability in HEK cells based on the relative peak areas of transfected unlabeled nucleoside (unlab nuc) to the sum of [(unlab and labeled) * SIL-IVT nuc] for A and G.

The efficiency of transfection was calculated based on highest % relative abundance (in this case 4h post-transfect time point) divided to the positive control for both A and G. Data shows 32.8 % transfection efficiency for A and 39,6% for G. These values are comparable to the previously transfected values without SIL-IVT and counting. Given the fact that several parameters are optimized compared to previous transfection (figure **3.35**), tRF relative amount is still higher than negative control at 48h post-transfection, therefore is considered still present in cells at this time point. Therefore, I decided to continue the time frame of this study till 72h and of course with separated biological replication.

3.3.3. tRF stability dependence on modification incorporation *in vivo*

To inspect the effect of modification incorporation on 5´-tRF$^{Gly}_{GCC}$ stability in HEK cells, 4 biological replicates are provided, which each modified or unmodified synthetic tRF$^{Gly}_{GCC}$ were transfected into HEK cells a week apart form the next corresponding biological replicate.

Data was plotted using relative peak areas as depicted in formulas (1) and (2) to gain the relative abundance of transfected nucleoside (A or G), for each time point and with correction of cell numbers fluctuation. The gained value for each time point is then normalized to the corresponding replicates negative control.

Figure **3.42** shows the comparison of unmodified vs. Um-modified tRF stability based on relative abundance of tRF nucleoside, where the normalized abundance of A or G at each post-transfection time point is compared to their corresponding negative control which is interposed at Y=1 with a red line; implying at Y=1 (negative control), no transfection is occurred. Any values higher than that is considered to come from the transfected RNA.

As seen in the figure, the unmodified tRF A or G, shows an increase from 0 h till 6 h, and then decreases till it exists in cells no longer than 24 h post-transfect. Whereas Um-modified tRF shows the highest amount at 0 h, and keeps decreasing over time till it reaches to negative control at 24 h, again for both nucleosides. Although comparing the matching time points of unmodified to Um-modified nucleosides amounts over time shows no diffenerce at significance level of 0.05 (apart from 6 h for G), the average values show a different trend of degradation over time for unmodified than the Um- modified tRFs A and G. In unmodified tRF, the relative amount keeps increasing till 6 h post-transfection phase and thereafter decreases, while the modified tRF starts degrading right after the transfection phase. This trend is obvious for both A and G.

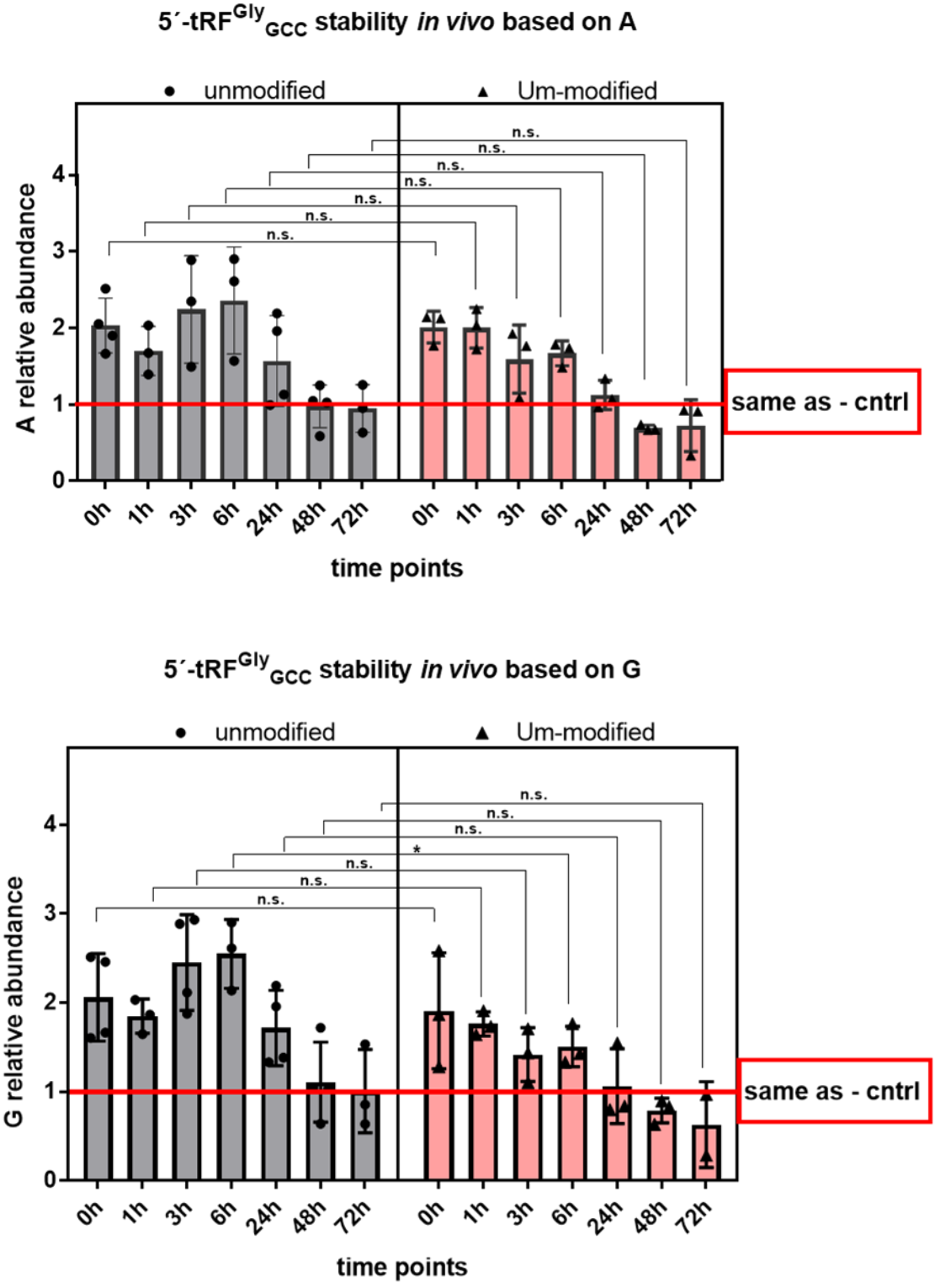

Figure 3.42 Comparison of Um modification incorporation on 5´-tRF$^{Gly}_{GCC}$ stability in HEK cells. Data points are normalized to negative control (red line at Y=1) for A and G. Y=1 represents the nucleoside amount for negative control of each corresponding replicate, which all the rest of time points are normalized to this value. Data plotted for 4 biological replicates and error bars represent standard deviation. Student T-test determines the significance plotted above the data points (n.s.= not significant, *= significant at $p<0.05$).

Comparing the data in fig.**3.42** for unmodified (left side bars) to Um modified (right side bars) group for each time point, no significance in A or G relative abundances is observed, except for 6 h in the case of G. Given the fact that I kept all experimental parameters exactly the same for both transfected RNAs, I hypothesize the stability of 5´-tRF$^{Gly}_{GCC}$ unmodified and the Um-modified might reflect the following biological impact of the modification incorporation:

The stimulation of pattern recognition receptors (PRRs) in cell, triggers the innate immune response by recognition of distinct pathogenic patterns that are not present on self-cells. There are two general classes of receptors recognizing foreign pathogens: toll-like receptors (TLRs) and cytoplasmic receptors.[294] Two types of TLRs that have shown relevance to single-stranded RNA (ssRNA) delivery including TLR7 and TLR8, which respond in a sequence-specific manner, as well as a cytoplasmic PRR namely RIG-I seem to be involved in stimulation of delivered tRFs digestion by lysosome.

Based on the fact that 6 h in G shows a significant difference between the two groups, it might be suggested that recognition of Um modified construct by receptors such as TLRs and RIG-I as a pathogen, happens faster in Um-modified tRF than the unmodified. However, the rest of data time points and the theoretical expectation of Um stabilizing tRNA, do not support this idea.

Since I used LP2000 for all experiments, I do not discuss the features of RNA delivery systems on the nature and degree of immunostimulation. Moreover, Um modification is expected to help with thermal and conformational stability of tRNA and its fragments in cells.[295, 296] Specifically, modifying the 2´ group on the ribose ring of the RNA backbone has shown to reduce or even eliminate the innate immune response by successfully inhibiting TLR7/8-mediated recognition of siRNA without diminishing RNAi potency.[297]

Based on my data, an immediate degradation for both tRF constructs may indicate that Um incorporation on the transfected RNA structure, does not trigger more immunoresponse activity compared to its absence. However, this does not mean the same effect is expected from naturally induced tiRNAs in cells.

Remarkably, regardless of the modification status on the synthetic 5´-tRF$^{Gly}_{GCC}$, the transfected nucleosides A and G are completely vanished at a time point between 24h and 48h post-transfect (marked with the red line = control in figure **3.42**). Therefore, the presented stability provides new insights into time-based relevance of tiRNA function in cells, if not the impact of modification incorporation on these functions. Nevertheless, transfection of synthetic tRF sequences might be a poor surrogate for endogenously produced tiRNAs which contain various modifications and could also be structured,[195] and have unknown functions in the cells, which stops them from degrading very fast through processing of lysosomal enzymes.

To sum up, presented data shows a time-based stability comparison between unmodified *vs.* position 4-Um modified synthetic 5´-tRF$^{Gly}_{GCC}$ (mimicking endogenously produced tiRNA under stress conditions) in HEK cells, which suggests irrelevance of Um modification incorporation on tRF to its temporal stability in cells, while both 4-Um modified or unmodified constructs remain in cells for at least 24h post-transfection phase.

However, mimicking the naturally induced tiRNAs by incorporating only Um on the synthetic 5´-tRF$^{Gly}_{GCC}$, did not help its temporal stability in HEK cells, but caused no faster degradation in cells niether.

Presented tRF data does not exclude the fact that endogenously produced tiRNAs might be acting locally at specific subcellular sites to impact stress-related cellular physiology in a biologically and kinetically meaningful fashion.

In order to further study of localized mechanistic features of the tRFs mimicking tiRNAs, fluorescent tagged tRF sequences can be provided, and transfection of these constructs with co-staining of different cell organelles by dynamic live cell imaging as well as parallel NAIL-MS analysis can elucidate tiRNAs unknown functions, based on their accumulation patterns in cells over time.

4. Conclusion and outlook

Concisely, development of NAIL-MS has drastically empowered the study of RNA modifications dynamics and underlying mechanisms. Applications of NAIL-MS provide the possibility to study RNA fate during pulse-chase experiments, kinetics and behavior of the newly transcribed RNA with their temporal modification status, and tracking modification dynamics, or comparative studies. NAIL-MS combined with metobolic produced internal standard SILIS, delivered the core mass spectrometric analyses for the presented dissertation.

Using NAIL-MS, a library including absolute quantification of 24 tRNA modifications, and up to 22 rRNA of 28S-, 18S- and 5.8S-rRNA subunits in both adult mice genders were provided. A comparison of data among tissues for each RNA type, and other way round was done to investigate potential codon bias alliance to amino acids formation as a signal of translation diversity among tissues. Moreover, quantified data was validated by two approaches: first, normalization of modifications abundances to per RNA molecule, which matched to the expected numbers. Second, comparison to all previously studies of mice RNA modifications in identical RNA types or tissues, which showed a high degree of similarity. This validation confirmed that presented data is a suitable model to study the tissue-based RNA modification patterns. Notably, while an almost identical pattern of modifications in 28S- and 18S-rRNA subunits were observed among studied tissues, higher levels of most modifications in 5.8S-rRNA or tRNA between highly metabolic active organs such as liver or lung were achieved compared to *e.g.* heart or spleen, which may have a functional reliance to epitranscriptome regulation.
Investigation of direct connection between codon-enriched genes of specific tRNA anticodon modifications to their amino acids was also performed, but was not conclusive, due to absence of an amino acids-based library per tissue in mice. Nonetheless, the mouse modifications quantification, suggests variations in some modification numbers per given RNA species, that were previously thought to be conserved among all tissues in mouse. This study is a good start for investigation of codon bias among different tissues that may cause differential translation activity, leading to the organs diversity.

Apart from absolute quantification of modified nucleosides, NAIL-MS provides a chance to determine the temporally dynamic nature of RNA modifications. Following demethylation activity of oxidative demethylase AlkBH family *in vitro*, such as AlkBH5 removing methyl group from m^6A in mRNA, the first *iv vivo* data on AlkBH1, 3 and 5 activities in demethylating each of their specific substrates are created in HEK cells. A successful establishment and validation of western blotting technique as a quantification method to follow the *in vivo* KD of each AlkBH protein, as well as their expression under MMS treatment is presented. The protein data on AlkBHs expressions under MMS treatment, confirmed their KD as well as the fact that AlkBH3 -but not AlkBH1- is a methylation damage induced enzyme, that potentially triggers ASCC-AlkBH3 alkylation repair complex under aberrant methylation damage by MMS treatment. On the RNA part, *in vivo* KD of each enzyme followed by stressing the cells by MMS, showed no significant effect on demethylation activity of the enzymes in tRNA, rRNA or mRNA towards the possible substrates including m^6A, m^1A, m^3C, m^5C and m^7G. Moreover, investigation on AlkBH3 partnership with ASCC3 in demethylating MMS-induced m^1A and m^3C from mRNA, displayed m^1A and m^3C to be the major methylation damage products in

human mRNA after MMS treatment; but again, showed no significance in methylation repair of KD AlkBH3 or ASCC3. Therefore, existence of other unidentified demethylation pathways in incomplete absence of AlkBH3 or ASCC3 is hypothesized. Generally, the complex machinery of aberrant methylation stress-response in human cells, might provide a recompense for AlkBHs absence by other unidentified demethylases or at least, by remaining active AlkBHs after KD and thus restoring the original levels of the observed RNA modifications.

Recalling another novel feature of dynamic NAIL-MS: taking initiative to follow up the dynamics of external RNA sequences within cells, by differentiating between the isotopic labeled native RNA and the unlabeled synthetic RNA. This feature allowed the study of tRNA fragments (tRFs) stability with focus on modification incorporation effect, given there is very little known about tiRNAs functions and dynamics. Quality controls showed promising results on two Um modified or non-modified 5´-tRF$^{Gly}_{GCC}$ sequences. Then, a method was developed to measure the dynamic biological uptake of the RNA within 72 h after transfection, excluding biological as well as sample preparation and analysis variables that can cause concentration/dilution effects. To this regard, a new technical standard namely **S**table **I**sotope **L**abelled **I**n **V**itro **T**ranscribed technical internal standard (**SIL-IVT**), was provided by in vitro transcription of ^{13}C-labeled tRNA$^{Val}_{AAC}$. Moreover, omitting cell numbers variation was done by introducing a cell numbers correction factor. Finally, 4 biological replicates of each modified or unmodified synthetic tRF$^{Gly}_{GCC}$ transfection into HEK cells, suggested irrelevance of Um modification incorporation on tRF to its temporal stability in cells, while both 4-Um modified or unmodified constructs remained in cells for at least 24 h post-transfection phase. Although mimicking the naturally induced tiRNAs by incorporating only Um on the synthetic 5´-tRF$^{Gly}_{GCC}$, did not help its temporal stability in HEK cells, but caused no faster degradation in cells neither. This outcome provided the first insights about model tiRNA stability in cells which can shed light to its functional relevance.

Briefly, numerous mechanisms behind RNA modification dynamics and diversity in modification profiles is observed through applications of NAIL-MS. This powerful method allows further investigation of so far unknown epitranscriptome regulations, which are potential enterprises in clinical field for faster disease diagnostics, as well as creating targeted and more efficient RNA- based therapeutics.

5. materials and methods

5.1. Materials

Salts, reagents, isotopes and nucleosides

All salts (unless otherwise stated) were obtained from Sigma Aldrich (Munich, Germany) at molecular biology grade unless stated otherwise. Isotopically labeled compounds: ^{15}N-NH_4Cl (≥98%) and L-methionine-methyl-D_3 (98%) from Sigma-Aldrich. $^{13}C_6$-glucose (≥99%) and $Na_2{}^{34}SO_4$ (≥99.1%) from Eurisotop (Saarbruecken, Germany). 1,3-$^{15}N_2$-uracil (98%) from Cambridge Isotope Laboratories (Tewksbury, MA, USA). All solutions and buffers were made with water from a Millipore device (Milli-Q, Merck). Nucleosides: adenosine (A), cytidine (C), guanosine (G), uridine (U) and N_2-methylguanosine (m^2G) from Sigma Aldrich. 1-Methyladenosine (m^1A), 7-methylguanosine (m^7G), N3-methylcytidine (m^3C), N6-methyladenosine (m^6A), 2′-O-methylcytidine (Cm), 2′-O-methylguanosine (Gm), 1-methylguanosine(m^7G), 5-methylcytidine (m^5C), 5-methyluridine (m^5U) were purchased from Carbosynth (Newbury, UK).

Specific laboratory equipement

Injection vial for HPLC and LC-MS: 0.3 mL PP snap ring micro vial, 32 × 11.6 mm, transparent, VWR (Radnor, PA, USA), Cat. No. 5480120. Injection vial cap: 11 mm snap ring cap, tr., natural rubber/TEF, 60°, 1.0 mm, VWR (Radnor, PA, USA), Cat. No. 548-0014. Fraction collector glass vial: 1.5 mL screw vial, 32 × 11.6 mm clear, VWR (Radnor, PA, USA), Cat. No. VWRI548-0018. Glass vial cap: 8 mm PP-screw cap black hole, VWR (Radnor, PA, USA), Cat. No. VWRI548-3322. Culture tube: centrifuge tube 50, TPP (Trasadingen, Switzerland), Product No.91050.

Table 5. 1 list of devices

Device	Description
CO_2 incubator	Thermo Scientific Heracell™ VIOS 160i CO_2 incubator
automated cell counter	Invitrogen Countess® II automated cell counter
Laminar flow hood	Thermo Scientific Safe 2020
Microscope	Zeiss Axiovert 200
water bath	Memmert WNB22
Ultra-low freezer box	FRYKA freezer box B 35-85 F210101

HPLC	Agilent 1100 HPLC system
LC-MS/MS	Agilent 1260 Infinity II LC System Agilent 6470A Triple Quadrupole with Jet Stream ESI source
SpeedVac	Genevac EZ-2 Plus Evaporating System
Nanophotometer	Implen NanoPhotometer® N60
Bioanalyzer	Agilent 2100 Bioanalyzer
Thermocycler	SensoQuest Labcycler
Thermal shaker	CellMedia TS basic
Centrifuges	Eppendorf 5417R / Hettich Rotina 380 R
UV gel imager	Bio-Rad universal hood II (serial no. 76S/07708)
Blotting imager	Amersham Imager 680 blot and gel imager
Voltmeter (PAGE)	Pharmacia Biotech Electrophoresis Power Supply EPS 600
Voltmeter (NB & WB)	BioRad PowerPac™ HC High-Current Power Supply
UV Crosslinker	Stratagene Stratalinker® UV Crosslinker 1800

Stock solutions and media for cell culture

- "Basic medium": 44 mL DMEM D6546, 5 mL FBS (non-dialyzed or dialyzed), 1 mL L-glutamine (50×)
- "unlabeled NAIL-MS medium": 42.4 mL DMEM D0422, 5 mL dialyzed FBS, 1 mL L-glutamine (50×), 1 mL adenine (50×), 500 µL uridine (100×), 100 µL L-methionine (500×), 40 µL cystine (1250×).
- "stable isotope labeled $^{15}N_5$ adenine labeled medium": 42.4 mL DMEM D0422, 5 mL dialyzed FBS, 1 mL L-glutamine (50×), 1 mL $^{15}N_5$-adenine (50×), 500 µL uridine (100×), 100 µL (D_3)-L-methionine (500×), 40 µL cystine (1250×).
- "Trypsin stop medium" *: 45 mL DMEM D6546 or DMEM D4022, 5 mL FBS (non-dialyzed OR dialyzed).
- "Thawing medium": 39 mL DMEM D6545, 10 mL FBS (not dialyzed), 1 mL LGlutamine (50×).
-"Cryopreservation medium" (2×): 8 mL FBS (not dialyzed), 2 mL DMSO.

* Trypsin stop medium is used to deactivate the protease activity of trypsin during cell passage was prepared from the medium and FBS appropriate to the experiment and FBS.

Table 5. 2 Preparation of stock solutions for use in cell culture. Aliquots of glutamine, uridine and FBS were stored at -20 °C. All other stock solutions were stored at 4 °C. Weights are given for the respective concentrations of unlabeled components.

Stock solution	Recipe
200 mM glutamine (50×)	292 mg in 10 mL MilliQ water
325 mM cystine (1250×)	157 mg in ~ 1 M HCl (1 mL HCl conc. + 11 mL MilliQ water
100 mM methionine (500×)	153 mg in 10 mL MilliQ-water
5 mM adenine (50×)	6.8 mg in 10 mL MilliQ water
20 mM uridine (100×)	24.4 mg in 5 mL MilliQ water

When the isotopically labeled components were used, the weights were adjusted accordingly. All stock solutions were sterile filtered after preparation and aliquoted if necessary. The necessary dilution in cell culture medium is indicated in parentheses.

SEC buffer

7.7 g NH_4OAc (molecular biological quality) was added to a clean 1 L laboratory threaded bottle and filled up with 1000 mL highly pure water, so that a 100 mM solution was available.

AlkBHs storage buffers

- AlkBH1 storage buffer (50 mL): final concentrations: 20 mM TrisHCl (pH 7,5), 10% Glycerol (v/v), 250 mM NaCl.

- AlkBH3 storage buffer (50 mL): final concentrations: 20 mM TrisHCl (pH 8,0), 10% Glycerol (v/v), 2 mM DTT, 100 mM NaCl.

- AlkBH5 storage buffer (50 mL): Final concentrations: 25 mM TrisHCl (pH 8,0), 10% Glycerol (v/v), 2 mM DTT, 150 mM NaCl.

LC-MS/QQQ (Nucleoside-MS) buffer

To a clean 1 L laboratory threaded bottle, 0.385 g NH_4OAc (LC-MS grade, ≥ 99%, VWR), was added and filled up till 1000 mL with ultrapure water (final concentration 5 mM). To set the correct pH (5.3), 65 µL of acetic acid (HiPerSolv CHROMANORM for LC-MS, acetic acid 99%, VWR Chemicals) was added.

RIPA lysis buffer

3 mL sodium chloride 5 M was measured out and added to 5 mL Tris-HCl 1 M, pH 8.0, 1 mL nonidet P-40, 5 mL sodium deoxycholate (10 %), and 1 mL SDS (10%). The mixture was placed in a 100 mL Duran bottle, which was filled up to 100 mL with ultrapure H_2O. (salts and detergents were purchased from Sigma Aldrich.)

Towbin transfer buffer (Western Blot)

30.0 g of Tris base was dissolved in MilliQ H_2O, and added to 144.0 g of glycine, and 10.0 g of SDS. H_2O was added to reach 1000 ml total volume. The pH of the buffer was 8.3. Running buffer was stored at room temperature and diluted to 1× before use for SDS-PAGE. (salts were purchased from Sigma Aldrich.)

Tris-Buffered Saline (TBS) buffer

To prepare 10× TBS wash buffer stock solution, 24 g Tris and 88 g NaCl were dissolved in 900 mL of MilliQ water and then pH was adjusted to 7.6 with final volume to 1 L. The prepared stock buffer was diluted to 1:10 v/v to reach 1× buffer for use. (salts were purchased from Sigma Aldrich.)

Tris-buffered saline with 0.1% Tween® 20 detergent (TBST) buffer

100 mL of 10× TBS buffer (described above) was added to 1 mL Tween® 20 detergent (Sigma Aldrich) and 900 mL of MilliQ water was added to reach 1× TBST buffer.

Loading buffer for denaturing RNA PAGE

90 mL formamide was added to 10 mL 10× TBE buffer. Blue loading dye: one spatula tip bromphenolblue and xylenxyanol were added.

Western blot blocking solution

Compartments: 1× TBS, 0.1% Tween-20, and 5% w/v nonfat dry milk bovine (Sigma Aldrich): for 150 mL, 15 mL 10× TBS was added to 135 mL water and mixed. 7.5 g nonfat dry milk was added and mixed well. While stirring, added 0.15 mL Tween-20.

12% TBE-urea gel

12% TBE-urea gel was manually casted, using the casting recipe by the manufacturer (Carl Roth ROTIPHORESE®DNA sequencing system). 24 mL of gel concentrate was mixed with 21 mL of gel diluent, and 5 mL of buffer concentrate to yield a urea concentration of 50% (w/v). To start the gel polymerization, 100 µL of APS (100 g/L) was added to 10 mL of this mixture. The solution was mixed, and then 10 µL of TEMED was added. After remixing, the solution was quickly placed between the previously installed glass plates in the gel casting stand at room temperature and polymerized with a ten-pocket comb for 20 min. Polymerized gels were wrapped in moist cellulose paper until use and stored at 4 °C in a sealable plastic bag (maximum 1 month).

Table 5. 3 List of antibodies used for western blotting.

Antibody name	class	Host/isotype	target organism	company
AlkBH3 AB	polyclonal	Rabbit / IgG	Human	Invitrogen
AlkBH5 AB	monoclonal	Rabbit	Human, Mouse and Rat	abcam
AlkBH1 AB	Polyclonal	Rabbit / IgG	Human	Invitrogen
β/Tubulin AB	Polyclonal	Rabbit / IgG	Bovine, Human, Mouse, Plant, Rat	Invitrogen
HRP conjugate anti-Rabbit IgG (H+L) (Secondary AB)	Polyclonal	Goat / IgG	Rabbit	Invitrogen

5.2. Cell culture methods

HEK 293 cells were received from DSMZ, Braunschweig, Germany. Cells were cultured in water vapor saturated atmosphere under 10% CO_2 at 37 °C.
Media and solutions were warmed to 37 °C before use. For subcultivations, confluence level was determined by microscopic observation.

Cryopreservation of cell lines

for cryopreservation of HEK-293 cells, they were cultured in 2× T75 cell culture flasks cultured and then trypsinized (3 mL trypsin per T75 flask). In each case, 12 mL of standard medium was added, the cells resuspended and the concentration is determined. Cells were centrifuged (130×g, 3 min) and in the corresponding quantity standard medium resuspended to a concentration of 4×10 cells/mL. The same amount of 2× Cryo stock was carefully added to obtain a final concentration of 2×10^6 cells/mL. 1 mL of each cell suspension was transferred to cryotubes and stored overnight at -70°C in a freezing container filled with isopropanol (Thermo Scientific™ Mr. Frosty™). Cells were transferred to a liquid nitrogen tank the next day.

Revitalization of cell lines

For revitalization of cell lines, 1 mL of frozen cell suspension was stored at 37°C as quickly as possible. This was carefully transferred into 5 mL of prewarmed thawing medium and then centrifuged (130× g, 3 min). The cell pellet was resuspended in thawing medium and placed in a T25 cell culture flask for culturing. For a following subcultivation, thawing medium was again used. Subcultivation Cells adhering to the cell culture flask were carefully rinsed with 5 mL of PBS in order to get rid of dead cells on the one hand, and on the other hand to inhibit the influence of serum on the trypsin activity. Subsequently, the cells were incubated for 2 min in 1 mL trypsin at 37°C. Cells were mixed with 4.5-7 mL quenching medium (depending on the desired subcultivation).
Cell suspension was homogenized and then 1 mL of it was centrifuged (130×g, 3 min). The cell pellet was resuspended in 5 mL fresh medium and cultured in a T25 cell culture flask. It was always a subcultivation aimed at a confluency level ~90%. Subcultivations were usually made every Monday, Wednesday and Friday.

Stress experiments

For the seeding of cells for MMS stress experiment, the cell density was determined using the automatic cell counter. After cultivation for at least 24 h but at most 48 h, the respective stress factor was added by a corresponding change of the medium. A PBS rinse step was omitted unless otherwise noted, when due to the experimental design a renewed change of medium was necessary. Thereby, it was always necessary to care that the original medium is completely removed.

Transfection experiments

5´-tRF$^{Gly}_{GCC}$ transfection:

- lipofectamine 2000 (LP2000): on 6 wells, 96 pmol (= 1.2 µg) 5´-tRF$^{Gly}_{GCC}$ was transfected based on manufacturer´s scaling-down protocol (Thermo Fisher, Waltham, MA, USA) of LP2000; 0.96 µL of 100 mM tRF was added in 223.86 µL $^{15}N_5$ adenine labeled Serum-free (SF, all compartments as stated in materials section, except for FBS) medium. The mixture was mixed with 4.82 µL LP2000 in 220 µL $^{15}N_5$ adenine labeled SF medium for 20 min at room temperature. Then this 0.45 mL mixture was added to 0.55 mL stable isotope labeled $^{15}N_5$ adenine labeled medium, and cells medium was replaced with this 1 mL medium. 4 h later, 1 mL 2× serum supplemented labeled medium was added to cells, and at different time points cells were washed gently with PBS. 100 µL of cells suspension was separated for counting, which was performed by manual counting using Fuchs-Rosenthal counting chamber (Roth, Karlsruhe, Germany), and the rest of cells suspension was centrifuged 130× g for 3 min, the supernatant PBS was removed, and cells pellet was directly lysed with TRI reagent.

- JetPRIME: 0.96 µL of 100 mM tRF was added to 195 µL jetPRIME buffer, and this mixture was added to 4 µL jetPRIME reagent, and incubated for 10 min at room temperature. The mixture was added to the cells labeled medium. cells were washed gently with PBS as described above, and harvested with TRI at different time points.
Negative and positive controls: for negative control, 0.96 µL of PBS was used instead of tRF with the above workflow, as for positive controls, only 0.96 µL of 100 mM tRF was added to the TRI-lysed labeled cells.

Table 5. 4 Oligonucleotide sequences of tRF$^{Gly}_{GCC}$.

Sequence identity	Sequence (5´to 3´)
unmodified tRF$^{Gly}_{GCC}$	[Phos]-GCAUUGGUGGUUCAGUGGUAGAAUUCUCGCCUG
Um-modified tRF$^{Gly}_{GCC}$	[Phos]-GCA**Um**UGGUGGUUCAGUGGUAGAAUUCUCGCCUG

Knockdown of AlkBH enzymes in vivo by si/esiRNA transfection:

For the knockdown of AlkBH1 (Art.-No.: EHU135521-50µg, Sigma Aldrich, Munich, Germany), AlkBH3 (part no.: EHU06458-50µg, Sigma Aldrich, Munich, Germany) or AlkBH5 (part no.: EHU021751-50µg, Sigma Aldrich, Munich, Germany) and a control (art.

no.: EHUFLUC-50µg, Sigma Aldrich, Munich, Germany), the corresponding "mission esiRNAs" were purchased. Furthermore, transfection reagent (Art.-No.: 114-07, Polyplus Transfection, Illkirch, France) was acquired. First, 0.7 million HEK 293 cells per T25 cell culture flask containing 5 mL of "unlabeled NAIL-MS" medium was seeded. 24 hours later (30% confluence), 250 µL transfection mix was prepared according to **Table 5.4**. esiRNA was mixed with jetPrime buffer, vortexed for 10 sec,
And then jetPrime reagent was added, pretexted for 10 sec and incubated for 10 min. The mix was then pipetted to the cells, making sure that it was only added dropwise, and well distributed into the cell culture flask with gentle swirling.

Table 5. 5 Transfection mix for knockdown of AlkBH enzymes in vivo. This is a recipe for the transfection of a T25 cell culture flask. In the following NAIL-MS experiment, two bottles were transfected with the same esiRNA. To avoid pipetting errors, each transfection mix was therefore prepared with 2× of the component stock concentration volume.

Component	Stock concentration	**Volume**
jetPrime™ Buffer		227.5 µL
jetPrime™ Reagent		10 µL
esiRNA	200 ng μL^{-1}	12.5 µL

Table 5. 6 siRNA or esiRNA transfected sequences for silencing AlkBHs experiments of this thesis. Sequences refer to complementary DNA (cDNA) of the corresponding transfected RNA. ID Nr.: ID number in the oligonucleotide database of the AK Kaiser (2022)

ID Nr.	identity	mRNA target	nts	Sequence (5´to 3´)	source
SK109	siRNA	AlkBH1_1	21	GGAUGACCAGAAUAGCGAA[dT][dT]	Sigma
SK110	siRNA	AlkBH1_1_as	21	UUCGCUAUUCUGGUCAUCC[dT][dT]	Sigma
SK111	siRNA	AlkBH1_2	21	CCCGAGAGAUUCAAUGGUA[dT][dT]	Sigma
SK112	siRNA	AlkBH1_2_as	21	UACCAUUGAAUCUCUCGGG[dT][dT]	Sigma
SK113	siRNA	control siRNA	21	UUCUCCGAACGUGUCACGU[dT][dT]	Sigma
SK114	siRNA	control siRNA_as	21	ACGUGACACGUUCGGAGAA[dT][dT]	Sigma
SK115	siRNA	AlkBH3_1	21	GAGAGAAGCUUCACUGAAA[dT][dT]	Sigma
SK116	siRNA	AlkBH3_1_as	21	UUUCAGUGAAGCUUCUCUC[dT][dT]	Sigma
SK117	siRNA	AlkBH3_2	21	GAAAGAAGCUGACUGGAUA[dT][dT]	Sigma
SK118	siRNA	AlkBH3_2_as	21	UAUCCAGUCAGCUUCUUUC[dT][dT]	Sigma
SK119	siRNA	AlkBH5_1	21	ACAAGUACUUCUUCGGCGA[dT][dT]	Sigma
SK120	siRNA	AlkBH5_1_as	21	UCGCCGAAGAAGUACUUGU[dT][dT]	Sigma
SK121	siRNA	AlkBH5_2	21	GCGCCGUCAUCAACGACUA[dT][dT]	Sigma
SK122	siRNA	AlkBH5_2_as	21	UAGUCGUUGAUGACGGCGC[dT][dT]	Sigma
-	esiRNA (cDNA target seq.)	AlkBH1	291	TTGCTGTCATTCAGCTTTGGACAGTC CGCCATCTTTCTCCTGGGTGGTCTTC AAAGGGATGAGGCCCCCACGGCCAT GTTTATGCACAGTGGTGACATCATGA TAATGTCGGGTTTCAGCCGCCTCTTG AACCACGCAGTCCCTCGTGTCCTTCC AAATCCAGAAGGGGAAGGCCTGCCT CACTGCCTAGAGGCACCTCTCCCTGC TGTCCTCCCGAGAGATTCAATGGTAG AGCCTTGTTCTATGGAGGACTGGCA	Sigma

				GGTGTGTGCCAGCTACTTGAAGACC GCTCGTGTT	
-	esiRNA (cDNA target seq.)	AlkBH3	468	GCCAGACCTGGAAGAACAAAGAGCA TCATCTCTCTGACAGAGAGTTTGTGT TCAAAGAACCTCAGCAGGTAGTACG TAGAGCTCCTGAGCCACGAGTGATT GACAGAGAGGGTGTGTATGAAATCA GCCTGTCACCCACAGGTGTATCTAGG GTCTGTTTGTATCCTGGCTTTGTTGA CGTGAAAGAAGCTGACTGGATATTG GAACAGCTTTGTCAAGATGTTCCCTG GAAACAGAGGACTGGCATCAGAGAG GATATAACTTATCAGCAACCAAGAC TTACAGCATGGTATGGAGAACTTCCT TACACTTATTCAAGAATCACTATGGA ACCAAATCCTCACTGGCACCCTGTGC TGCGCACACTAAAGAACCGCATTGA AGAGAACACTGGCCACACCTTCAAC TCCTTACTCTGCAATCTTTATCGCAA TGAGAAGGACAGCGTGGACTGGCAC AGTGATGATG	Sigma
-	esiRNA (cDNA target seq.)	AlkBH5	497	TTCAAGCCTATTCGGGTGTCGGAACC AGTGCTTTCCCTGCCGGTGCGCAGGG GAAGCGTGACTGTGCTCAGTGGATA TGCTGCTGATGAAATCACTCACTGCA TACGGCCTCAGGACATCAAGGAGCG CCGAGCAGTCATCATCCTCAGGAAG ACAAGATTAGATGCACCCCGGTTGG AAACAAAGTCCCTGAGCAGCTCCGT GTTACCACCCAGCTATGCTTCAGATC GCCTGTCAGGAAACAACAGGGACCC TGCTCTGAAACCCAAGCGGTCCCAC CGCAAGGCAGACCCTGATGCTGCCC ACAGGCCACGGATCCTGGAGATGGA CAAGGAAGAGAACCGGCGCTCGGTG CTGCTGCCCACACACCGGCGGAGGG GTAGCTTCAGCTCTGAGAACTACTGG CGCAAGTCATACGAGTCCTCAGAGG ACTGCTCTGAGGCAGCAGGCAGCCC TGCCCGAAAGTCTACCCGCCGCCCTC CTGGGAACTCTGGCTC	Sigma

After a transfection incubation time of 24 h, the old medium was removed and new "unlabeled NAIL-MS" medium prewarmed to 37 °C was added to the cells without "unlabeled NAIL-MS" medium was added to the cells. 16 hours later, this medium was removed, a 5 mL PBS buffer wash step was performed, and a T25 per knockdown assay was harvested with 1 mL TRI Reagent® and transferred to an Eppendorf microreactor for isolation of total RNA. The remaining cell culture flask was washed with 5 mL of new "stable isotope-labeled NAIL-MS" medium. After 8 hours, these cell culture flasks were also prepared for isolation of total RNA using TRI Reagent. In the case of protein knockdown efficiency analysis by western blot in

addition to RNA analysis, the cells did not have to be washed directly after removal of the medium.
the cells were not washed directly with TRI Reagent® but with 1 mL of trypsin. After an incubation period of 2 min, the cell suspension was placed in 1 mL "trypsin stop" medium and incubated at 2000× g at room temperature, centrifuged for 2 min in two micro reaction tubes. After aspiration of the medium, a cell pellet was stored at -80 °C for further western blot analysis and the other was included in 1 mL of TRI Reagent®.

5.3. Biochemical methods

Cell lysis and RNA purification
Cells were directly harvested on cell culture dishes using 1 mL TRI reagent for T25 flasks or 0.5 mL TRI reagent for smaller dishes. The total RNA was isolated according to the supplier's manual with chloroform (Roth, Karlsruhe, Germany). tRNA, 28S and 18S rRNA were purified by size exclusion chromatography (AdvanceBio SEC 300 Å, 2.7µm, 7.8 × 300 mm for tRNA and BioSEC 1000 Å, 2.7 µm, 7.8 × 300 mm for 28S and 18S rRNA, Agilent Technologies) according to published procedures. The RNA was resuspended in water (35 µL).

Cell lysis for protein analysis
Collected cell pellet was directly lysed with RIPA buffer at 4°C (~30-100 µL depending on the size of pellet) and kept the test tube on ice. Constant agitation was maintained through occasionally pipetting up and down or flicking the test tube every 5 min for 30 min. Then it was centrifuged at 14´000 rpm for 15 min at 4°C.
The supernatant was transferred to a fresh tube on ice while taking care that none of the sticky viscous subnatant was aspirated.
Bradford Assay was performed in order to create a Bovine serum albumin (BSA) caliberation curve, so that all unknown protein concentrations would be calculated using extrapolation in this caliberation curve. For the assay, 1 µL of protein sample was mixed with 49 µL of MilliQ H_2O. The mixture was placed in a cuvette including 950 µL 1× Bradford reagent (Thermo Fisher, Waltham, MA, USA) and the UV absorption rate was measured by BioPhotometer.
Protein samples concentration for each cell lysate was then measured by Bradford assay and calculated using extrapolation in a BSA calibration curve.

Mouse samples RNA extraction

We received flash frozen mouse organs from three male and one female mice including heart, liver, cortex, lung, spleen, olfactory bulb and kidney from a partner lab. Each organ, was divided into four technical replicates by careful cutting to equal sizes, for each mouse (except for olfactory bulb which had one technical replicate of each mouse due to its very small size). Each organ piece was crushed by a tissue ruptor, lysed in TRI reagent and total RNA was extracted using phenol/chloroform-based isolation, which were kept at -20°C until their preparation time for a few weeks.

Lyophilization:
FBS samples were lyophilized to complete dryness using an ALP2000ha 2-4 LSCbasic Lyophilizer (Christ, Osterode, Germany) with condenser temperature of -85°C under high vacuum for four days.

RNA purification by size exclusion chromatography

For the purification of tRNA and total rRNA size exclusion chromatography (SEC) was used. SEC buffer was used as the mobile phase. An AdvanceBio SEC 300 Å 2.7 µm, 7.8 × 300 mm column enabled the Separation of tRNA from total rRNA using isocratic elution at 1 mL/min and a column temperature of 40 °C. After equilibrating the column for up to 100 µg of total RNA was injected for at least 30 minutes. the big rRNA subunits including 28S and 18S rRNA elute from 3.5-4.8 min and the tRNA from 6.9-7-9 min. Times have been adjusted slightly with increasing of the column age. For the purification of 18S rRNA and 28S rRNA, an AdvanceBio SEC 1000Å 2.7 µm, 7.8 × 300 mm column is used. Other parameters are the same as before. 28S rRNA elutes from 5.0-7.2 min and 18S rRNA from 7.5-8.5 min in this case.

For the combined purification of total RNA in both tRNA, 28S and 18S rRNA, the AdvanceBio SEC 1000 Å column using a capillary connector was added after the AdvanceBio SEC 300 Å column in the installed column oven of the Agilent HPLC 1100 system. Other parameters were the same as before, only the run time of the method has been increased to 31 minutes. 28S rRNA eluted from 11.1–12.1 min, 18S rRNA from 12.5–13.5 min and tRNA from 18.5–19.5 min. Using the "tandem" SEC, the yield of 28S and 18S rRNA increased because additional SpeedVac and resuspension steps were eliminated.

An AdvanceBio SEC 130 Å 2.7 µm, 7.8 × 300 mm column was used for the purification of tRF. Separation was performed at a column temperature of 60°C using isocratic elution at 0.5 mL/min in 22 min. The tRNA eluted from 10.5-11.5 min and tRF from 11.8-12.2 min.

The desired RNA fractions were joint and concentrated to 100 µL using a SpeedVac. 2.5× volume of 100% ethanol and 1 µL of GlycoBlue™ (Thermo Fisher, Waltham, MA, USA) were added. After precipitation of the RNA at -20°C overnight, the solution was centrifuged at 12´000× g and 4 °C for at least 30 minutes. The supernatant was removed, the pellet washed carefully with 70% ethanol and centrifuged again (12´000 × g, 4 °C, 5–10 min). After carefully removing the ethanol, the RNA pellet was resuspended in ~ 30 µL of ultrapure water.

In vitro transcription

^{13}C-Isotopic labeled tRNA
The total volume of the T7 *in vitro* transcription was 200 mL. A total of 100 mL PCR product were added to T7 buffer mix and T7 enzyme (TranscriptAid T7 HighYield Transcription Kit, Thermo Fisher Scientific, Waltham, MA, USA) and 1.6 mL of each rNTP (^{12}C-rNTPs were provided by the kit,^{13}C-rNTPs were purchased by Silantes, Munich, Germany, Partnumber.: 121306100). The mixture was incubated for 2 h at 37◦C and 600 rpm. After 2 h incubation, the sample was treated with 2 mL T7 enzyme mix and 5 mL 50mM $MgCl_2$ and incubated for additional 2 h. After another 2 h incubation, the sample was treated again with 2 mL T7 enzyme mix and 5 mL 50 mM $MgCl_2$ and incubated for additional 2 h to improve the yield of the

transcription. The transcription was finished after 6 h. DNA template was removed by addition of 4 mL DNase 1, which is provided in the kit, 1 h at 37◦C. In the next step, $MgCl_2$ was added with a final concentration of 5 mM and the sample was incubated at 60◦C for 1 h to auto-catalytically cleave the precursor *in vitro* transcript into its target tRNA. Prior to RNA precipitation, the sample was centrifuged at 5000× *g* for 5 min at
room temperature to remove the insoluble pyrophosphate of the transcription reaction. The supernatant was precipitated by addition of 0.1 vol. of 5M ammonium acetate and 2.5 vol. of ice-cold ethanol (100%) followed by overnight precipitation.

The transcribed tRNA was purified by 12% acrylamide preparative TBE-urea gel electrophoresis followed by crush and soak method.[294] Before cutting the bands for transcript template and $tRNA^{Val}$, the gel was imaged by gel UV imager (Bio-Rad) at ƛ=260 nm. Afterwards purification efficiency was examined using bioanalyzer electrophoresis.

T7 in vitro transcribed RNA as substrate or internal standard

In vitro transcription was used to synthesize $tRNA^{Val}_{AAC}$ molecule on a µg scale.
First, a polymerase chain reaction (PCR) was performed to generate sufficient DNA template. The components of the PCR were as follow: For $tRNA^{Val}_{AAC}$, a primer with T7 promoter sequence (SK10), a primer that is reverse complementary to the specific tRNA (SK59) and a DNA template (SK80) were required. The components were pipetted according to **Table 5.9.**

Table 5. 7 Preparation of the PCR mix for in vitro transcription. PCR pipetting scheme is shown in the following table. The set containing polymerase and HF buffer (part no.: M0531S, New England Biolabs, Ipswich, MA, USA) and dNTP mix (part no.: N0447S, New England Biolabs, Ipswich, MA, USA) were purchased.

Components	Stock solution	Volume
fusion HF buffer	5×	10 µL
SK10	4 µM	12 µL
SK59	4 µM	12 µL
SK80	0.1 µg/µL	1 µL
fusion Polymerase		1 µL
dNTP Mix		1 µL
MilliQ-Water		till 50 µL

After the polymerase was pipetted last to the batch PCR reaction tube, the mixture was mixed thoroughly by pipetting up and down. The tube was immediately transferred to a thermal cycler and the following program was started as shown in table **5.10**.

Table 5. 8 Protocol of the PCR program for in vitro transcription. The following Instrument parameters set was used: Lid temperature 96 °C, preheating pressure 30 N and preheatingblock temperature 25 °C. After running the fourth step, step 2 was run again. This was repeated thirty times before proceeding to step 5. After completion of the fifth step, the sample was cooled down to 4 °C. Care was taken to ensure that the sample was removed as soon as it reached this temperature and then the program was terminated.

Steps	Temperature	Time	Repeats
1	92 °C	2 min.	1
2	92 °C	15 sec.	30
3	47 °C	20 sec.	30
4	72 °C	30 sec.	30
5	72 °C	10 min.	1
6	4 °C	variable	1

Two identical PCR preparations were transferred from the respective PCR tubes into an Eppendorf microreaction tube. To start the T7 in vitro transcription, the following components from **Table 5.11** were added to the reaction vessel.

Table 5. 9 T7 in vitro transcription. The T7 Transcript Aid HighYield set (part no.: K0441, ThermoFisher Scientific, Waltham, MA, USA) and ^{13}C-stable isotope-labeled ribonucleoside triphosphates (rNTPs) (Art. No.: 121206100, Silantes, Munich, Germany) were purchased.

Components	Stock solution	Volume
T7 Transcription buffer	10×	10 µL
$MgCl_2$	50 mM	3 µL
T7 Polymerase		3.2 µL
rNTPs (4×)		each 1.6 µL
PCR Product		100 µL
MilliQ-Water		till 200 µL

The T7 Transcript Aid HighYield kit contains the T7 Polymerase and the corresponding transcription buffer, as well as individual reaction tubes with CTP, UTP, GTP and ATP. Stable isotope-labeled in vitro transcript ^{13}C-NTPs from Silantes were used. For in vitro transcription, the microreaction vessel was placed in a Heating block at 37 °C and 300 rpm for 2 hours. Thereafter, an additional 1.5 µL T7 polymerase and 5 µL 50 mM $MgCl_2$ were added. With a successful transcription, a slight turbidity of the solution can be observed due to precipitated pyrophosphate. Subsequently, incubation was continued for another 2 hours at the above parameters. After addition of the same amounts of T7 polymerase and $MgCl_2$, it was incubated for 2 hours. The in vitro transcription lasted at least 8 hours and was completed by centrifugation of the excess pyrophosphate and addition of 4 µL DNase I (art. no.: M0303S, New England Biolabs, Ipswich, MA, USA) to the supernatant to terminate. DNase I digestion of the DNA template was performed at 37 °C and 300 rpm for 1 hour. In the final step, the in vitro transcribed RNA was precipitated by ethanol precipitation at -20 °C overnight. 2.5× the volume of 100% ethanol (500 µL) was added to the solution along with 20 µL of 5M NH_4OAc. After centrifuging the solution at 12´000× g and 4 °C for at least 60 min, the RNA pellet was resuspended in ~100 µL of MilliQ water (protocol established by Hagelskamp *et al.*).[261]

TBE-urea PAGE for RNA

Manually polymerized 12% TBE-urea gel was preheated for 20 min at a constant voltage of 200 V. 1-1.5 µg total RNA (7.5 µg for tRNA analysis) in 10 µL volumes were mixed with 10 µL of 2× loading buffer (95% formamide) and then incubated for 1 min at 90 °C. The complete volume (20 µL) was then loaded to the gel pockets of gel. In addition, into at least one free pocket, 6 µL of 2× RNA loading dye (NEB, Ipswich, MA, USA) was added. Running conditions: 275 V, at room temperature, 45-60 min (based on the size of the target RNA, using the length indication of xylene cyanol and bromophenol blue dyes inside the RNA loading dye), in 1× TBE buffer (Roth, Karlsruhe, Germany).

Preparative TBE-urea gel electrophoresis

For purification of tRNA in vitro transcripts from precursor products, preparative TBE-urea gel electrophoresis was used based on Petrov *et al*. so called crush and soak method.[294] A 12% TBE-urea denaturing PAGE was poured, polymerized and pre-ran for 30 min with W power set on 200 V potential and maximum 35 mA current. Meanwhile, the RNA sample were mixed with 2× RNA loading buffer by pipetting 1:1 v/v, and heated up to 70°C for 2 min. After the pre-run, the wells were rinsed extensively with 1× TBE run buffer. Thereafter, the samples were loaded into the wells, and the gel run started with 275 V for 2h. The gel plate was removed from the gel running apparatus.
A metal spatula was used to pry open the top glass plate of the gel. the gel was covered with plastic wrap. Carefully flipped the gel plate to remove the glass plate, and placed the gel on a clean plastic foil. The gel was placed on top of a 'Fluor-coated TLC plate (fluorescent plate) and shined UV light on it with a 260 nm UV lamp in darkness to visualize RNA bands of interest. The band of tRNA was cut using a new, clean razor blade. The gel slice was crushed using the razor blade on the plastic foil, and transferred into a 1.5 mL sample tube. 2× volumes of elution solution (v/w) (0.5 M NH_4OAc) was added to the sample tube, and incubated on a shaker with 500 rpm at room temperature for 3 h. Sample centrifuged at 5000 g for 1 min, the supernatant was collected, while avoiding gel debris pick up. Centrifugation was repeated and recollected the leftover sample. 0.1 v/v of 5 M NH_4OAc was added to the eluted RNA, plus 3× volumes of ethanol. Finally, sample was incubated at -20°C overnight to precipitate the RNA.

SDS-PAGE for proteins

30 µg of total protein content was brought to 10 µL volume by adding ultrapure H_2O. In case of low concentrations, more volume of the sample (up to 30 µL based on gel pocket capacity) was used. Protein samples were never vortexed, mixing was performed by gentle pipetting up and down to avoid degradation. Samples were mixed with 5× loading buffer (2 µL for each 10 µL sample), then incubated on a heater at 70 °C for 10 min.
12% pre-casted Mini-PROTEAN gel (Bio-Rad Laboratories GmbH) was placed into cassette inside the mini PAGE tank and 1× MES-SDS run buffer (NuPAGE™ MES SDS Running Buffer (20×), Thermo Fisher, Waltham, MA, USA) filled the tank till the mark line. The comb was removed and wells were washed with run-buffer 3 times with a syringe. protein samples were loaded into the pockets of the SDS-PAGE gel, along with 5 µL of pre-stained protein ladder as the Molecular weight marker on the first and last pockets. Gel electrophoresis run was set at 200 V constant potential, while checking current and run pattern of pre-stained ladder

every 5 min to ensure a normal run. The gel electrophoresis run was stopped manually at the right time, based on desired target protein (30 – 90 min).

Western-blotting

After SDS-PAGE, the stacking gel on upper section including the wells was cut off. the gel was placed in Towbin transfer buffer, and started rotating on a rotating shaker for 15 min at 100 rpm to equilibrate the gel with the transfer buffer. Meanwhile, Western Blot filter papers (Thermo Fisher, Waltham, MA, USA) were also soaked into Towbin buffer. A nitrocellulose membrane with 0.2 µm pore size (Bio-Rad Laboratories GmbH) was soaked in transfer buffer and shortly after, assembly of the transfer sandwich was performed inside its cassette, by this order from cathode to anode side: fiber pad (sponge), filter paper, gel, membrane, filter paper, fiber pad, while noting no air bubbles trapped between gel and membrane. In case of air bubbles, they were removed through gently applying pressure and dragging it out of the gel-membrane surface. The cassette was placed in the transfer tank and a cooling pack as well as a magnetic stirring bar were added in the tank. The transfer tank was filled with Towbin buffer until the marked 'blotting' line. Transfer occured at 4 °C whilst stirring at a constant current of 70 V for 3 h.
Blocking and antibody incubation was performed afterwards as following: the membrane was removed from the blotting tank, and directly incubated in the blocking solution for 30 min. Membrane was washed 3 times for 5 min with TBS-T buffer on a shaker with ~100 rpm. Primary antibody solutions were prepared in a 50 mL Falcon tube by adding 1/1000 v/v of the respective primary antibody to blocking solution. Membrane was placed into the primary antibody solution against the target protein on a rotary shaker at 4°C overnight. Nitrocellulose membrane was washed 3 times for 5 min with TBS-T buffer. Secondary antibody solution was prepared in a 50 mL Falcon tube by adding 1/10´000 of the secondary antibody stock solution to blocking solution. The membrane was incubated in the secondary antibody solution for 1 h. Membrane was washed 2 times for 5 min with TBS-T buffer and afterwards once with TBS (without tween 20) buffer.
Chemiluminescent detection was performed for detecting the target proteins, by adding substrate to the membrane according to the manufacturer's recommendation (Thermo Fisher, SuperSignal™ West Pico PLUS Chemilumineszenz-Substrat). ImageJ software was used to determine the band intensities of the target proteins for semi-quantification.

RNA concentration determination

RNA yields were determined using a nanophotometer (Implen NanoPhotometer® N60). For this purpose, RNA was resuspended in ultrapure water and 1.5 µL was used for the concentration determination.

Bioanalyzer measurements

After preparation of the respective Agilent RNA Chips (6000 Pico RNA Chip for mRNA or Small RNA Chips for in vitro transcribed tRNA) according to the corresponding instructions, 1 µL of the diluted samples were applied to the respective chip and analyzed with the Agilent 2100 Bioanalyzer and the preinstalled Eukaryote Total RNA Pico Series II.xsy" and "Small RNA Series II.xsy" methods, respectively.

RNA digestion for nucleoside analysis

A digestion master mix can be prepared according to **Table 5.12** for the appropriate number of samples. $MgCl_2$ and Tris are components of the buffer system.
Benzonase and SPD (snake venom phosphodiesterase) are nucleases and CIP (calf intestine phosphatase) is the phosphatase. Pentostatin and THU (tetrahydrouridine) protect the nucleosides from deamination and BHT (butylated hydroxytoluene) acts as an antioxidant. For the master mix shown 15 µL of sample would be digested with 15 µL of master mix. In case of deviating volumes, the amount of $MgCl_2$ and Tris was adjusted accordingly. All other data refer to the digestion of 10 µg RNA and must/can only be adjusted only if the amount of RNA is increased/decreased. After digestion for 2 h at 37 °C, all samples were diluted with half volume of LC-MS buffer (e.g. 30 µL
digest + 15 µL LC-MS buffer). With each sample, 1 µL of SILIS (10×) was co-injected.
(*e.g.* 9 µL sample + 1 µL SILIS). The digestion of a maximum of 3 µg of RNA SILIS was performed according to a 10 µg RNA protocol, optionally with 0.1× volume of theophylline (100 µM) and LC-MS buffer added. Here, the buffer was chosen to achieve a target concentration of 20 ng/µL of RNA.

Table 5. 10 Exemplary master mix for the digestion of RNA. The master mix shown refers to the digestion of 15 µL sample with 15 µL master mix. 10 µg of RNA is digested to nucleosides within 2 h at 37 °C.

Substance	Stock solution	Target concentration	1×	50×
$MgCl_2$	10 mM	→ 1 mM	3 µL	150 µL
TRIS pH = 8	50 mM	→ 5 mM	3 µL	150 µL
Benzonase	1 U/µL	→ 2 U	2 µL	100 µL
CIP (Alk.Phos.)	1 U/µL	→ 2 U	2 µL	100 µL
SPD (PDE1)	0.1 U/µL	→ 0.2 U	2 µL	100 µL
Pentostatin	1 mg/mL	→ 1 µg	1 µL	50 µL
THU	5 mg/mL	→ 5 µg	1 µL	50 µL
BHT	10 mM	→ 10 uM	1 µL	50 µL

5.4. Analytical methods

Synthetic modified nucleosides for preparation of calibration solutions were purchased from: Sigma-Aldrich, Munich, Germany. Nucleoside test mix: inosine (I)
Each nucleoside powder was weighed into a clean tube (5–10 mg per nucleoside) and dissolved in pure water to reach a final concentration of 10 mM. The nucleosides and the test mix were combined to a final concentration of 500 pmol/µL of A, 2000–500 fmol/µL of each modified nucleoside and 1× of the prepared SILIS. The calibration mix was serial diluted 1:5 and 1:10 with 1× SILIS until the lowest calibration concentration of 5 fmol/µL canonical and 5 amol/µL modified nucleoside were reached.10 µL of each calibration solution was injected onto LC-MS/MS. After LC-MS/MS measurement the value of the integrated MS signals of the

unlabeled synthetic nucleosides were set into relation to the integrated MS signals of the heavier SILIS nucleosides.
The results were plotted against the nucleoside concentrations and the regression lines from the diagrams were used to calculate the respective RFN values, necessary for quantification.

Nucleoside mass spectrometry (QQQ)

Nucleosides were separated using a Synergi Fusion-RP column (Synergi® 2.5 µmFusion-RP 100 Å, 150 × 2.0 mm, Phenomenex®, Torrance, CA, USA). LC-MS/QQQ buffer (buffer A) and pure acetonitrile (buffer B) were used as buffers. The gradient started with 100% buffer A for 1 min, followed by an increase to 10% buffer B over a duration of 4 min. Buffer B was then increased to 40% over 2 min and maintained for 1 min before switching back to 100% buffer A over a duration of 0.5 min and re-equilibrating the column for 2.5 min. The total time was 11 min and the flow rate was 0.35 mL/min at a column temperature of 35 °C. the LC system was interfaced with a triple quadrupole mass spectrometer (G6470A, Agilent Technologies) via an electrospray ionization (ESI) source (Jet Stream, Agilen Technologies. The gas temperature (N_2) was 230 °C with a flow rate of 6 L/min. Sheath gas temperature was 400 °C with a flow rate of 12 L/min. Capillary voltage was 2500 V, skimmer voltage was 15 V, nozzle voltage was 0 V, and nebulizer pressure was 40 Psi. The cell accelerator voltage was 5 V. All methods were performed in dynamic multiple reaction monitoring (dMRM) between 1.1 min and 9 min and positive ion mode. Fragmentor voltage and collision energy were optimized specifically for each nucleoside. Optimized parameters, along with retention times and mass transitions of unlabeled and isotopically labeled nucleosides, are in **Table 5.5** for RNA nucleosides. The MS1 resolution was set to "Wide" and MS2 resolution to "Unit" in each case, and the SILIS transition was reported directly as an internal standard in each case.

Calibration

For calibration, synthetic nucleosides were weighed and dissolved in water to a stock concentration of 1-10 mM. Calibration solutions ranged from 0.025 pmol to 100 pmol for each canonical nucleoside and from 0.00125 pmol to 5 pmol for each modified nucleoside. The concentrations of Ψ and D ranged from 0.005 pmol to 20 pmol. Analogous to the samples, 1 µL of SILIS (10×) was co-injected with each calibration. The creation of the calibration curve and the corresponding evaluation of the samples was performed using Agilent's quantitative MassHunter software. The principle of quantification using a SILIS is described in more detail in Borland *et al.*[222]

Normalization / Calculation per RNA molecule

To make different samples quantitatively comparable, the molar amount of each modified nucleoside was referenced to the molar amount of the sum of the injected canonical nucleosides and then reported per 1000 canonical nucleosides unless otherwise indicated. In individual cases, modifications in total tRNA were referenced to 60 canonical nucleosides to indicate the amount of modification in an average tRNA molecule. When the sequence of the RNA molecule was known (e.g., tRF^{Gly}_{GCC}), we normalized to the amount of RNA molecules (n_{RNA})

to obtain the number of modifications per RNA molecule. For this purpose, the calculated amounts of injected canonical nucleosides (e.g., n_C) were divided by their expected amount (#) in the respective RNA molecule according to **Equation 5** and then averaged. The numbers for each canonical nucleoside (#) were taken from the sequence of the RNA molecules.

$$n_{RNA} = \frac{\frac{n_C}{\#C} + \frac{n_U}{\#U} + \frac{n_G}{\#G} + \frac{n_A}{\#A}}{4}$$

The LLOQ was found at the calculated concentration where the peak hight of the analyte is 10-fold higher than the surrounding noise (S/N > 10). The principle of quantification is further described in more detail in Heiss *et al.*[287]

6. Appendix

6.1. Additional data

Supplementary table 1. 1 Abbreviations of all common functional groups in RNA modifications. Abbreviations can be combined to describe more complex RNA modifications.

Abbreviation	full group name
ac	acetyl
acp	amminocarboxypropyl
ca	carboxyl
chm	carboxyhydroxymethyl
cmo	glyoxylat
cmnm	carboxymethylaminomethyl
f	formyl
g	glycinyl
gal	galactosyl
ge	geranyl
glu	glutamyl
hn	hydroxynorvalylcarbamoyl
ho/hm	hydroxy/hydroxymethyl
i	isopentenyl
io	cis-hydroxyisopentenyl
m	methyl
man	mannosyl
mchm	carboxyhydroxymethyl methylester
mcm	methoxycarbonylmethyl
mcmo	glyoxylat methylester
mnm	methylaminomethyl
mo	methoxy
ncm	carbamoylmethyl
n	amino
r(p)	5-O-phosphono-b-D-ribofuranosyl
s	thio
se	seleno
t	threonylcarbamoyl
tm	taurinomethyl

Supplementary table 1. 2 Optimized parameters for RNA nucleoside dMRM method.

Compound group	Compound name	Precursor ion	Product ion	R_t (min)	ΔR_t (min)	fragmentor	Collision Energy
A	A	268,1	136,0	5,3	1	200	20
A	A lab	273,0	141,0	5,3	1	200	20
A SILIS	A SILIS	283,0	146,0	5,3	1	200	20
A SIL-IVT	A SIL-IVT	278,0	141,0	5,3	1	110	21
ac^{4}C	ac^{4}C	286,1	154,0	5	1	85	9
ac^{4}C	ac^{4}C lab	293,0	156,0	5	1	85	9
ac^{4}C SILIS	ac^{4}C SILIS	300,0	163,0	5	1	85	9
acp^{3}U	acp^{3}U	346,1	214,1	2,3	1	95	15
acp^{3}U	acp^{3}U lab	353,1	216,1	2,3	1	95	15
Am	Am	282,1	136,0	6	1	130	17
Am	Am D_3	285,0	136,0	6	1	130	17
Am	Am lab	287,0	141,0	6	1	130	17
Am	Am lab D_3	290,0	141,0	6	1	130	17
Am SILIS	Am SILIS	298,0	146,0	6	1	130	17
C	C	244,1	112,0	2,1	1	200	20
C	C lab	251,0	114,0	2,1	1	200	20
C SILIS	C SILIS	256,0	119,0	2,1	1	200	20
C SIL-IVT	C SIL-IVT	253,0	116,0	2,1	1	200	20
Cm	Cm	258,1	112,0	4,1	1	180	9
Cm	Cm D_3	261,0	112,0	4,1	1	180	9
Cm	Cm lab	265,0	114,0	4,1	1	180	9
Cm	Cm lab D_3	268,0	114,0	4,1	1	180	9
Cm SILIS	Cm SILIS	271,0	119,0	4,1	1	180	9
D	D	247,1	115,0	1,6	1	70	5
D	D lab	254,0	117,0	1,6	1	70	5
D SILIS	D SILIS	258,0	121,0	1,6	1	70	5
G	G	284,1	152,0	4,3	1	200	20
G	G lab	288,0	156,0	4,3	1	200	20
G SILIS	G SILIS	299,0	162,0	4,3	1	200	20
G SIL-IVT	G SIL-IVT	294,0	157,0	4,3	1	200	20
Gm	Gm	298,1	152,0	5	1	100	9
Gm	Gm D_3	301,0	152,0	5	1	100	9
Gm	Gm lab	302,0	156,0	5	1	100	9
Gm	Gm lab D_3	305,0	156,0	5	1	100	9
Gm SILIS	Gm SILIS	314,0	162,0	5	1	100	9
I	I	269,1	137,0	4,1	1	100	10
I	I lab	273,0	141,0	4,1	1	100	10
I SILIS	I SILIS	283,0	146,0	4,1	1	100	10
i^{6}A	i^{6}A	336,3	204,1	8	1	140	17
i^{6}A	i^{6}A lab	341,3	209,1	8	1	140	17
i^{6}A SILIS	i6A SILIS	356,0	219,0	8	1	140	17
m^{1}A	m^{1}A	282,1	150,0	2,2	1,5	150	25
m^{1}A	m^{1}A D_3	285,0	153,0	2,2	1,5	150	25
m^{1}A	m^{1}A lab	287,0	155,0	2,2	1,5	150	25
m^{1}A	m^{1}A lab D_3	290,0	158,0	2,2	1,5	150	25
m^{1}A SILIS	m^{1}A SILIS	298,0	161,0	2,2	1,5	150	25
m^{1}G	m^{1}G	298,1	166,0	4,9	1	105	13
m^{1}G	m^{1}G D_3	301,0	169,0	4,9	1	105	13
m^{1}G	m^{1}G lab	302,0	170,0	4,9	1	105	13
m^{1}G	m^{1}G lab D_3	305,0	173,0	4,9	1	105	13
m^{1}G SILIS	m^{1}G SILIS	314,0	177,0	4,9	1	105	13
m^{1}I	m^{1}I	283,1	151,0	4,8	1	80	12
m^{1}I	m^{1}I D_3	286,1	154,0	4,8	1	80	12
m^{1}I	m^{1}I lab	287,1	155,0	4,8	1	80	12
m^{1}I	m^{1}I lab D_3	290,1	158,0	4,8	1	80	12

m^1I SILIS	m^1I SILIS	298,0	161,0	4,8	1	80	12
$m^{22}G$	$m^{22}G$	312,1	180,0	5,7	1	105	13
$m^{22}G$	$m^{22}G$ D_3	318,0	186,0	5,7	1	105	13
$m^{22}G$	$m^{22}G$ lab	316,0	184,0	5,7	1	105	13
$m^{22}G$	$m^{22}G$ lab D_3	322,0	190,0	5,7	1	105	13
$m^{22}G$ SILIS	$m^{22}G$ SILIS	329,0	192,0	5,7	1	105	13
m^2G	m^2G	298,1	166,0	5,1	1	95	17
m^2G	m^2G D_3	301,0	169,0	5,1	1	95	17
m^2G	m^2G lab	302,0	170,0	5,1	1	95	17
m^2G	m^2G lab D_3	305,0	173,0	5,1	1	95	17
m^2G SILIS	m^2G SILIS	314,0	177,0	5,1	1	95	17
m^3C	m^3C	258,1	126,0	2	1,5	88	14
m^3C	m^3C D_3	261,0	129,0	2	1,5	88	14
m^3C	m^3C lab	265,0	128,0	2	1,5	88	14
m^3C	m^3C lab D_3	268,0	131,0	2	1,5	88	14
m^3C SILIS	m^3C SILIS	271,0	134,0	2	1,5	88	14
m^3U	m^3U	259,1	127,0	4,8	0,6	75	9
m^3U	m^3U D_3	262,0	130,0	4,8	0,6	75	9
m^3U	m^3U lab	266,0	129,0	4,8	0,6	75	9
m^3U	m^3U lab D_3	269,0	132,0	4,8	0,6	75	9
m^5C	m^5C	258,1	126,0	3,8	1	185	13
m^5C	m^5C D_3	261,0	129,0	3,8	1	185	13
m^5C	m^5C lab	265,0	128,0	3,8	1	185	13
m5C	m^5C lab D_3	268,0	131,0	3,8	1	185	13
m^5C SILIS	m^5C SILIS	271,0	134,0	3,8	1	185	13
m^5U	m^5U	259,1	127,0	4,4	1	95	9
m^5U	m^5U D_3	262,0	130,0	4,4	1	95	9
m^5U	m^5U lab	266,0	129,0	4,4	1	95	9
m^5U	m^5U lab D_3	269,0	132,0	4,4	1	95	9
m^5U SILIS	m^5U SILIS	271,0	134,0	4,4	1	95	9
$m^{66}A$	$m^{66}A$	296,0	164,0	7,1	1	130	21
$m^{66}A$	$m^{66}A$ D_3	302,0	170,0	7,1	1	130	21
$m^{66}A$	$m^{66}A$ lab	301,0	169,0	7,1	1	130	21
$m^{66}A$	$m^{66}A$ lab D_3	307,0	175,0	7,1	1	130	21
$m^{66}A$ SILIS	$m^{66}A$ SILIS	313,0	176,0	7,1	1	130	21
m^6A	m^6A	282,1	150,0	6,5	1	125	17
m^6A	m^6A D_3	285,0	153,0	6,5	1	125	17
m^6A	m^6A lab	287,0	155,0	6,5	1	125	17
m^6A	m^6A lab D_3	290,0	158,0	6,5	1	125	17
m^6A SILIS	m^6A SILIS	298,0	161,0	6,5	1	125	17
m^7G	m^7G	298,1	166,0	3,5	1,5	100	13
m^7G	m^7G D_3	301,0	169,0	3,5	1,5	100	13
m^7G	m^7G lab	302,0	170,0	3,5	1,5	100	13
m^7G	m^7G lab D_3	305,0	173,0	3,5	1,5	100	13
m^7G SILIS	m^7G SILIS	314,0	177,0	3,5	1,5	100	13
mcm^5s^2U	mcm^5s^2U	333,1	201,0	6,2	1	92	8
mcm^5s^2U	mcm^5s^2U D_3	336,1	204,0	6,2	1	92	8
mcm^5s^2U	mcm^5s^2U lab	340,1	203,0	6,2	1	92	8
mcm^5s^2U	mcm^5s^2U lab D_3	343,1	206,0	6,2	1	92	8
mcm^5s^2U SILIS	mcm^5s^2U SILIS	347,1	210,0	6,2	1	92	8
mcm^5U	mcm^5U	317,1	185,1	5	1	95	5
mcm^5U	mcm^5U D_3	320,1	188,1	5	1	95	5
mcm^5U	mcm^5U lab	324,1	187,1	5	1	95	5
mcm^5U	mcm^5U lab D_3	327,1	190,1	5	1	95	5
mcm^5U SILIS	mcm^5U SILIS	331,0	194,0	5	1	95	5
ncm^5U	ncm5U	302,0	170,0	2,5	1	85	8
ncm^5U	ncm^5U lab	309,0	172,0	2,5	1	85	8
ncm^5U SILIS	ncm^5U SILIS	316,0	179,0	2,5	1	85	8
Q	Q	410,2	295,1	4,3	1	115	12

t^6A	t^6A	413,1	281,1	5,8	1	130	9
t^6A	t^6A lab	418,1	286,1	5,8	1	130	9
t^6A SILIS	t^6A SILIS	434,0	297,0	5,8	1	130	9
U	U	245,1	113,0	3	1	95	5
U	U lab	252,0	115,0	3	1	95	5
U SILIS	U SILIS	256,0	119,0	3	1	95	5
U SIL-IVT	U SIL-IVT	254,0	117,0	3	1	95	5
Um	Um	259,2	113,0	4,6	1	96	8
Um	Um D_3	262,2	113,0	4,6	1	96	8
Um	Um lab	266,2	115,0	4,6	1	96	8
Um	Um lab D_3	269,2	115,0	4,6	1	96	8
Um SILIS	Um SILIS	271,1	119,0	4,6	1	96	8
Y	Y	245,1	209,0	1,7	1	90	5
Y	Y lab	252,0	216,0	1,7	1	90	5
Y SILIS	Y SILIS	256,0	220,0	1,7	1	90	5

Supplementary figure 1 N**ested graphs of absolute quantified modified nucleosides from mouse organs: (1)** Heart, **(2)** lung, **(3)** cortex, **(4)** Spleen, **(5)** olfactory bulb and **(6)** kidney.

1. Heart (A)

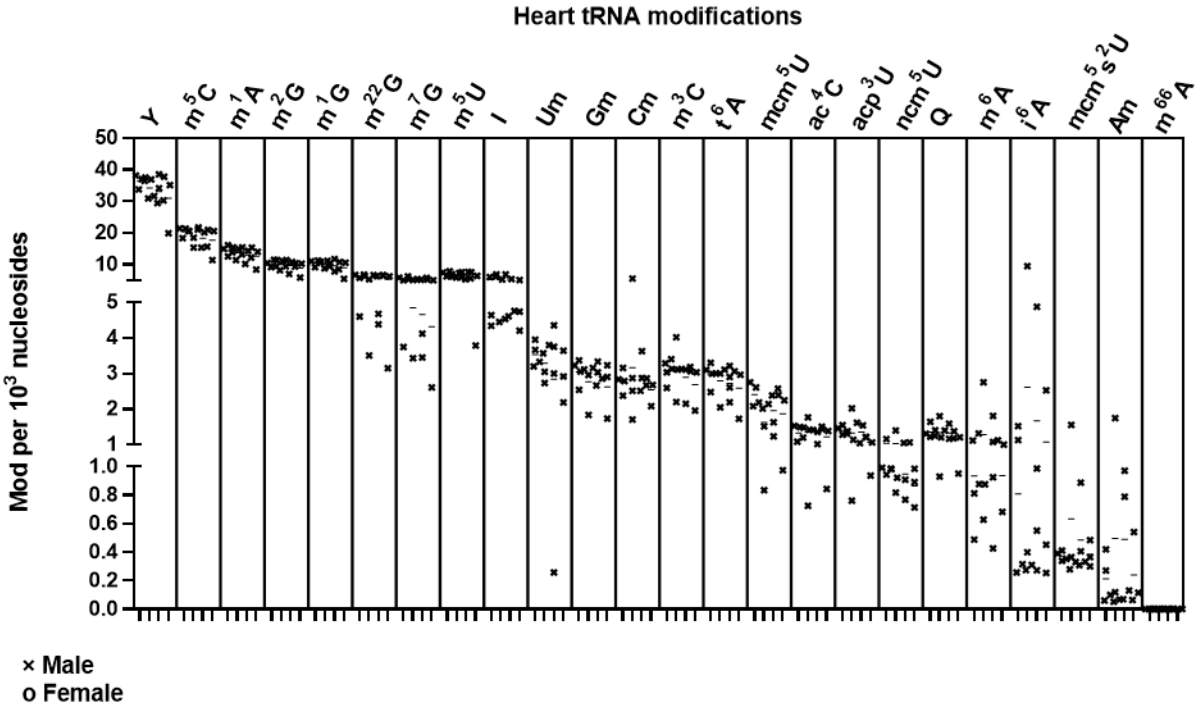

(B)

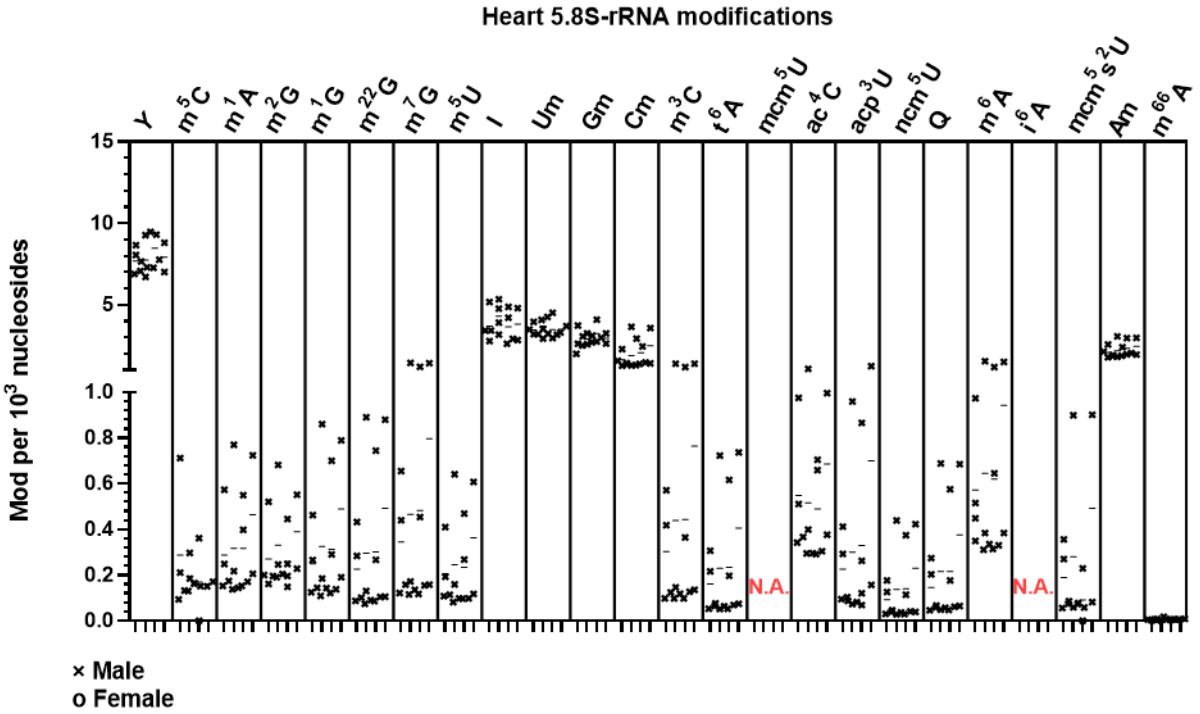

(C)

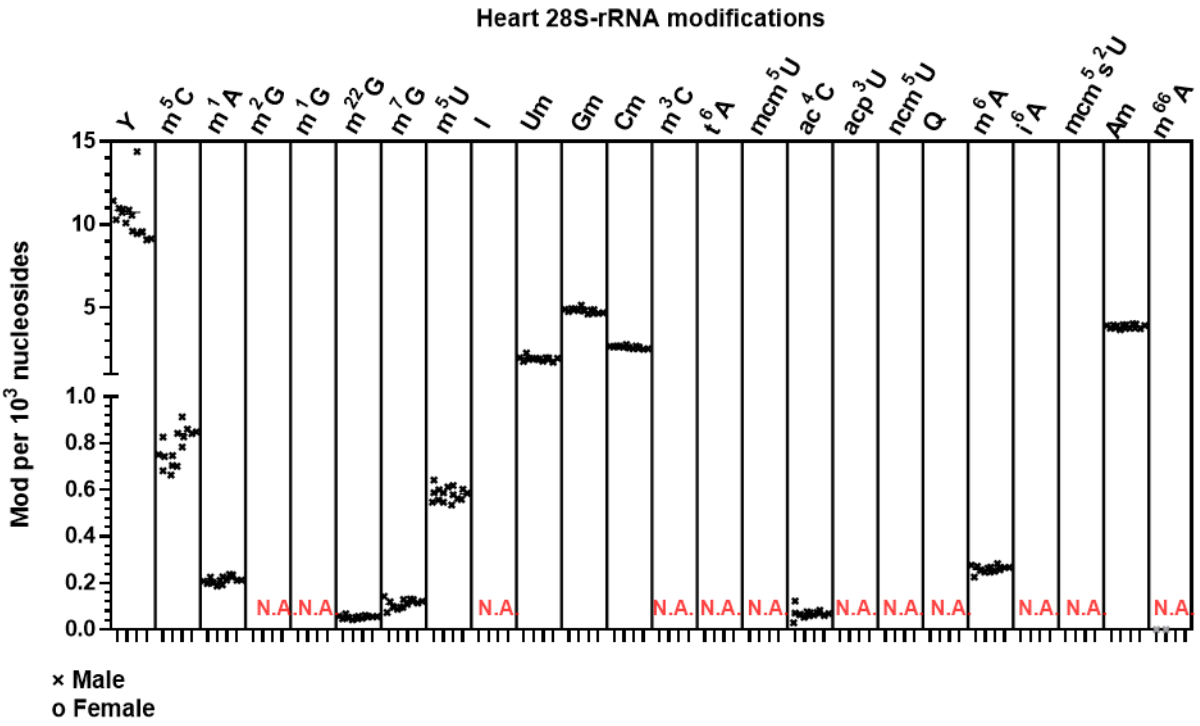
Heart 28S-rRNA modifications
Ψ
m5C
m1A
m2G
m1G
m22G
m7G
m5U
I
Um
Gm
Cm
m3C
t6A
mcm5U
ac4C
acp3U
ncm5U
Q
m6A
i6A
mcm5s2U
Am
m66A
Mod per 10^3 nucleosides
15
10
5
1.0
0.8
0.6
0.4
0.2
0.0
N.A.
× Male
o Female

(D)

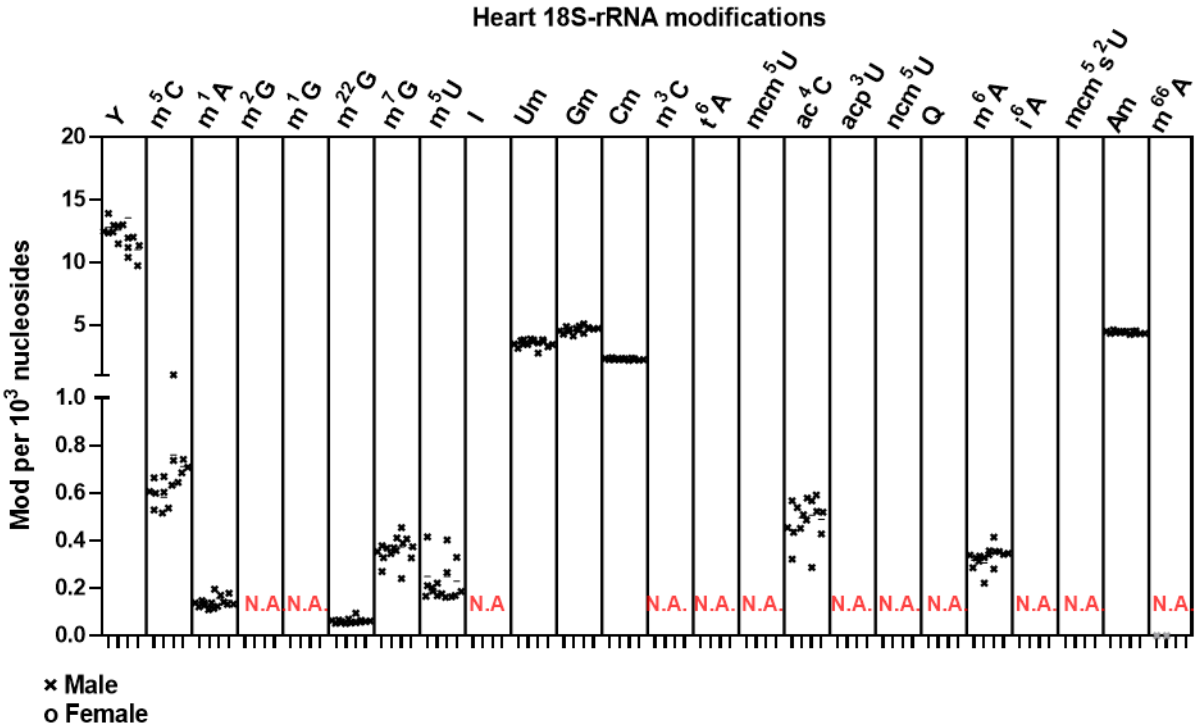
Heart 18S-rRNA modifications
Ψ
m5C
m1A
m2G
m1G
m22G
m7G
m5U
I
Um
Gm
Cm
m3C
t6A
mcm5U
ac4C
acp3U
ncm5U
Q
m6A
i6A
mcm5s2U
Am
m66A
Mod per 10^3 nucleosides
20
15
10
5
1.0
0.8
0.6
0.4
0.2
0.0
N.A.
× Male
o Female

2. Lung (A)

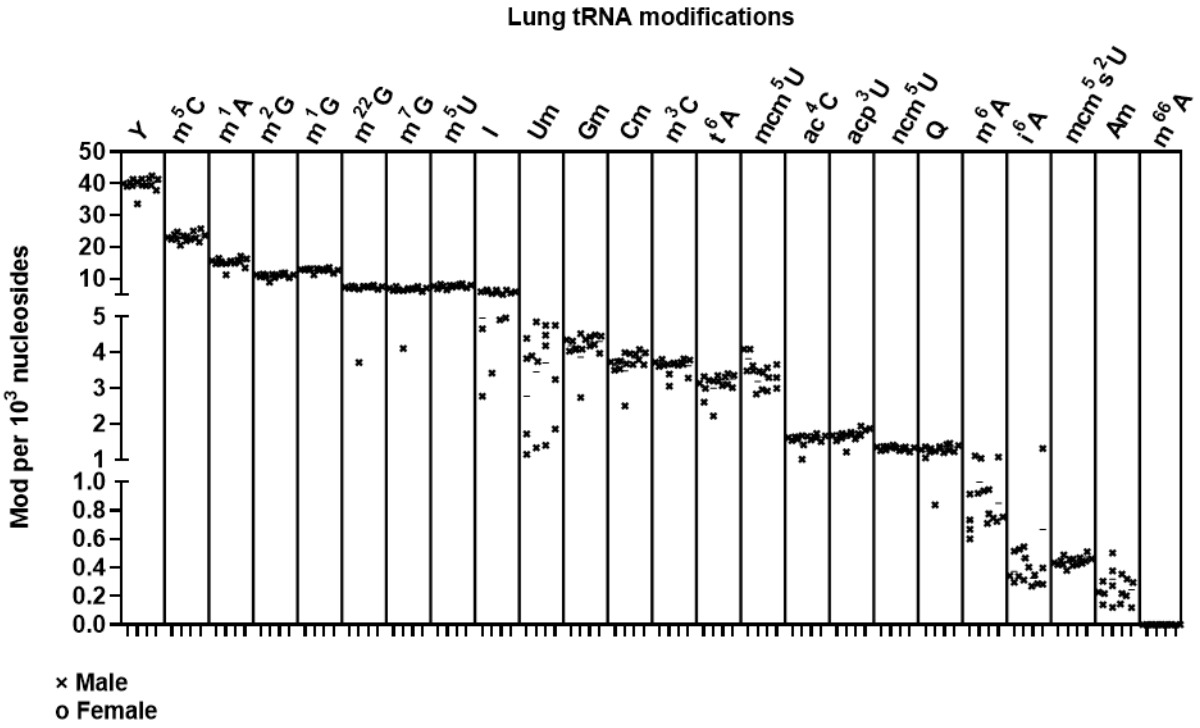
Lung tRNA modifications
Y
m5C
m1A
m2G
m1G
m22G
m7G
m5U
I
Um
Gm
Cm
m3C
t6A
mcm5U
ac4C
acp3U
ncm5U
Q
m6A
i6A
mcm5s2U
Am
m66A
Mod per 10^3 nucleosides
50
40
30
20
10
5
4
3
2
1
1.0
0.8
0.6
0.4
0.2
0.0
× Male
o Female

(B)

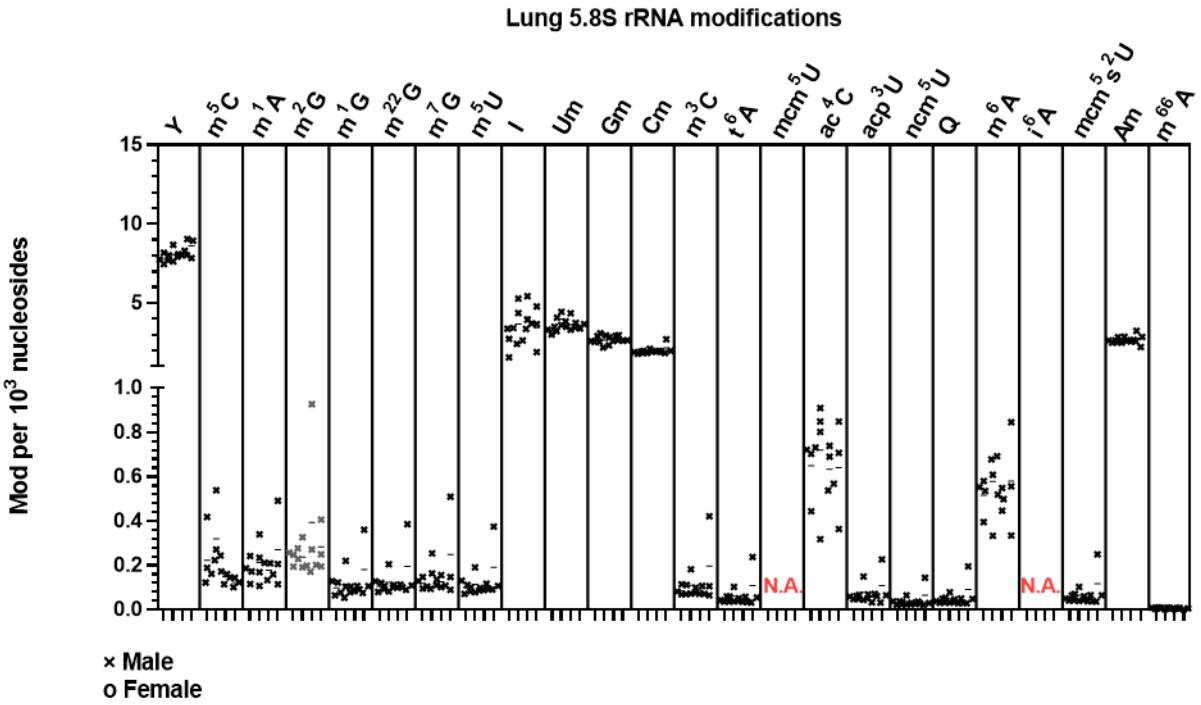
Lung 5.8S rRNA modifications
Y
m5C
m1A
m2G
m1G
m22G
m7G
m5U
I
Um
Gm
Cm
m3C
t6A
mcm5U
ac4C
acp3U
ncm5U
Q
m6A
i6A
mcm5s2U
Am
m66A
N.A.
N.A.
Mod per 10^3 nucleosides
15
10
5
1.0
0.8
0.6
0.4
0.2
0.0
× Male
o Female

(C)

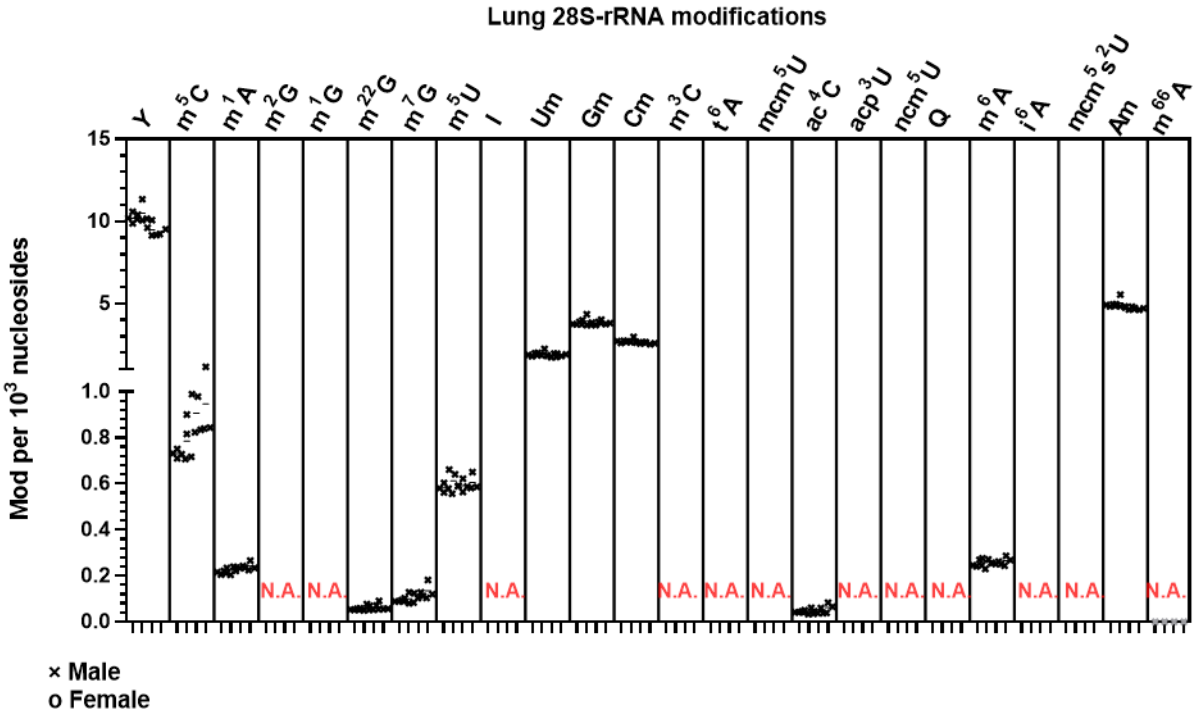
Lung 28S-rRNA modifications
Mod per 10^3 nucleosides
Ψ
m5C
m1A
m2G
m1G
m22G
m7G
m5U
I
Um
Gm
Cm
m3C
t6A
mcm5U
ac4C
acp3U
ncm5U
Q
m6A
i6A
mcm5s2U
Am
m66A
N.A.
× Male
o Female

(D)

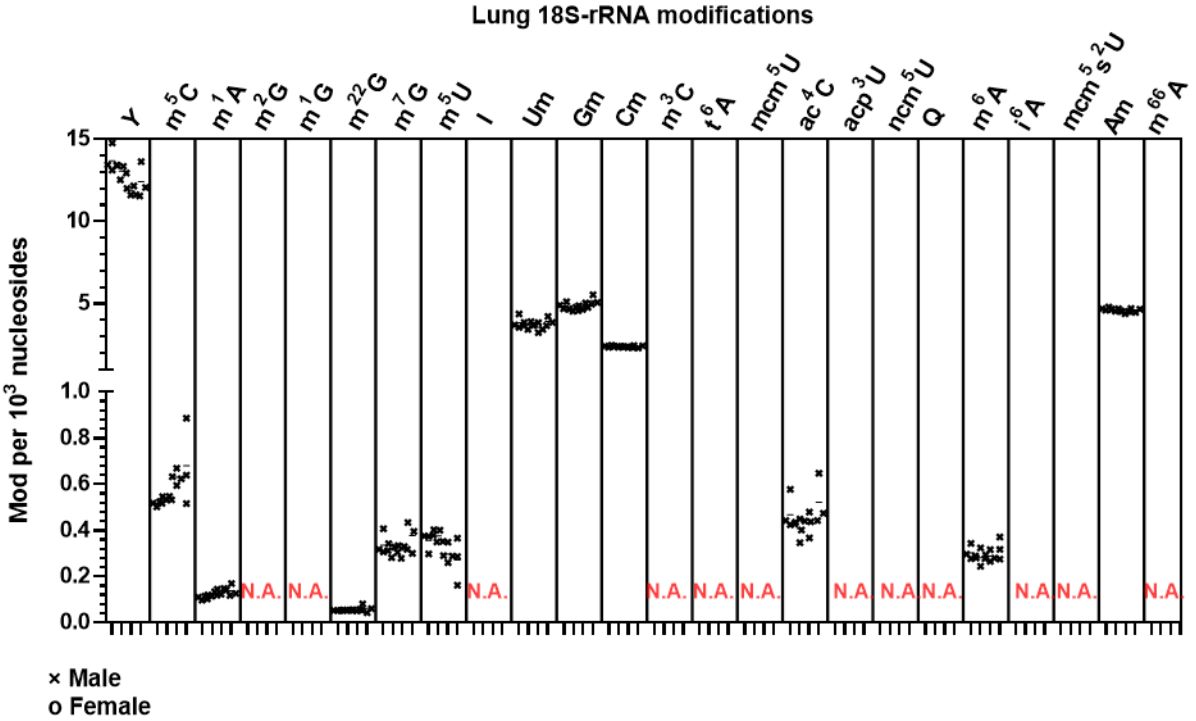
Lung 18S-rRNA modifications
Mod per 10^3 nucleosides
Ψ
m5C
m1A
m2G
m1G
m22G
m7G
m5U
I
Um
Gm
Cm
m3C
t6A
mcm5U
ac4C
acp3U
ncm5U
Q
m6A
i6A
mcm5s2U
Am
m66A
N.A.
× Male
o Female

3. Cortex (A)

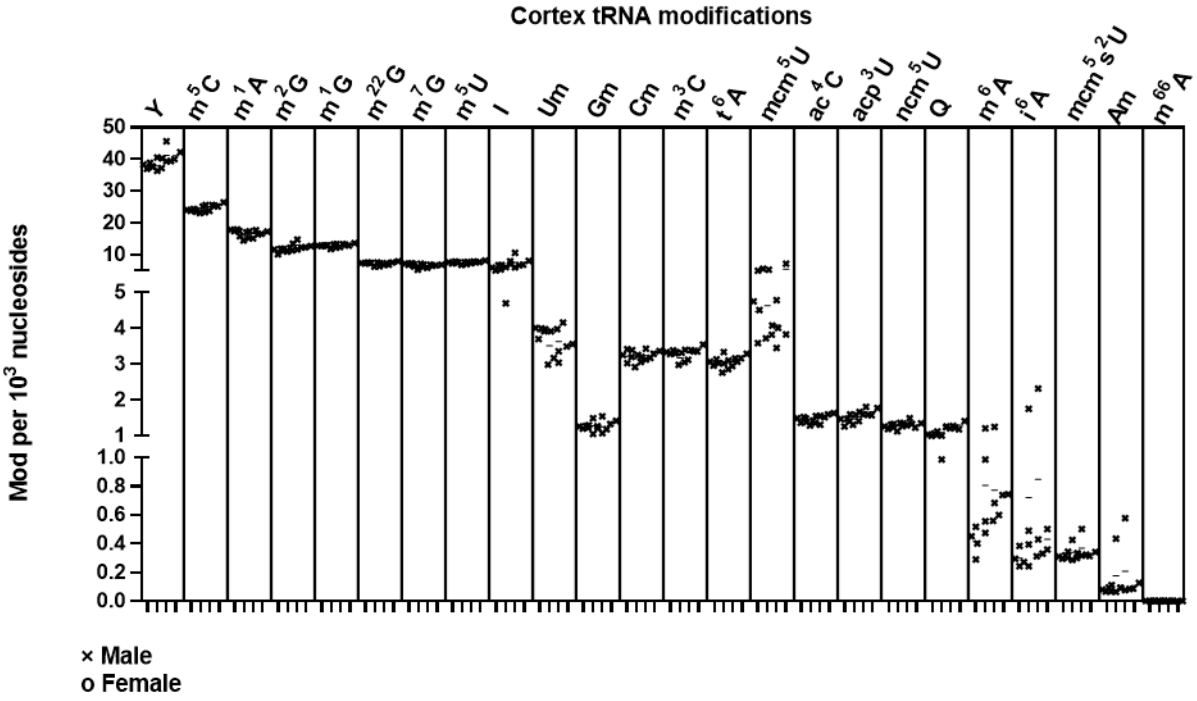
Cortex tRNA modifications
Mod per 10^3 nucleosides
Ψ
m5C
m1A
m2G
m1G
m22G
m7G
m5U
I
Um
Gm
Cm
m3C
t6A
mcm5U
ac4C
acp3U
ncm5U
Q
m6A
i6A
mcm5s2U
Am
m66A
× Male
o Female

(B)

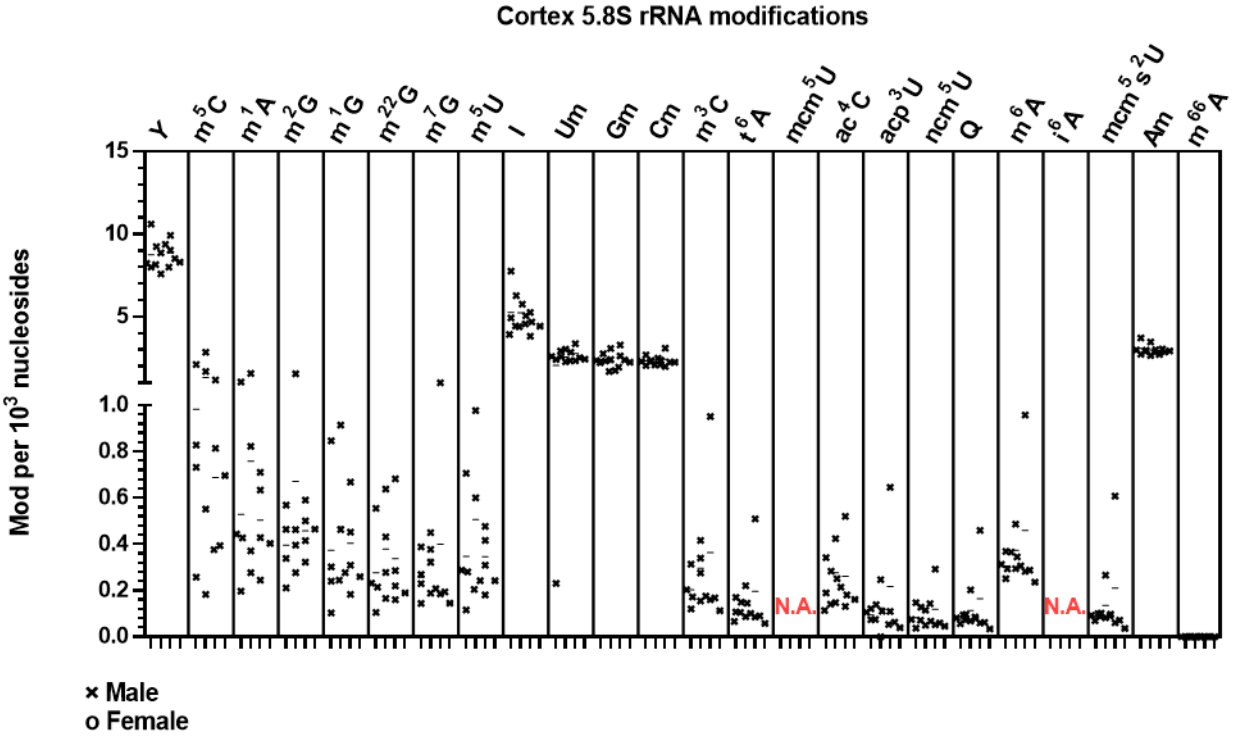
Cortex 5.8S rRNA modifications
Mod per 10^3 nucleosides
Ψ
m5C
m1A
m2G
m1G
m22G
m7G
m5U
I
Um
Gm
Cm
m3C
t6A
mcm5U
ac4C
acp3U
ncm5U
Q
m6A
i6A
mcm5s2U
Am
m66A
N.A.
N.A.
× Male
o Female

(C)

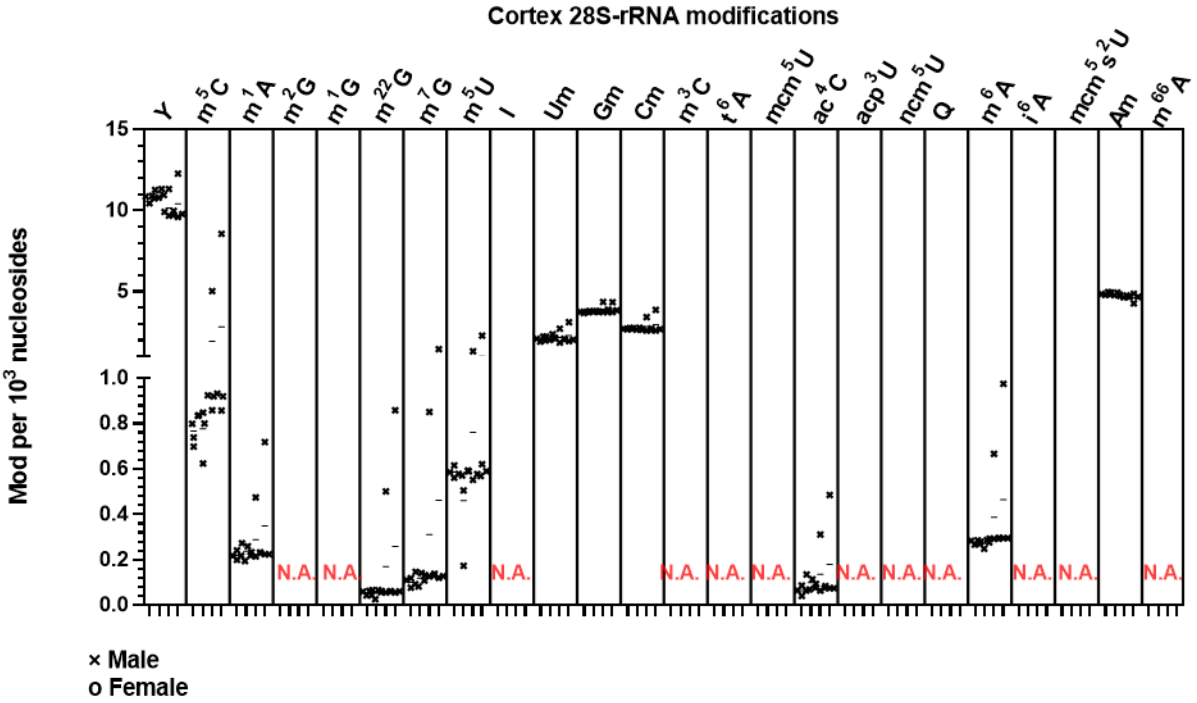
Cortex 28S-rRNA modifications
Mod per 10^3 nucleosides
Ψ m5C m1A m2G m1G m22G m7G m5U I Um Gm Cm m3C t6A mcm5U ac4C acp3U ncm5U Q m6A i6A mcm5s2U Am m66A
N.A.
× Male
o Female

(D)

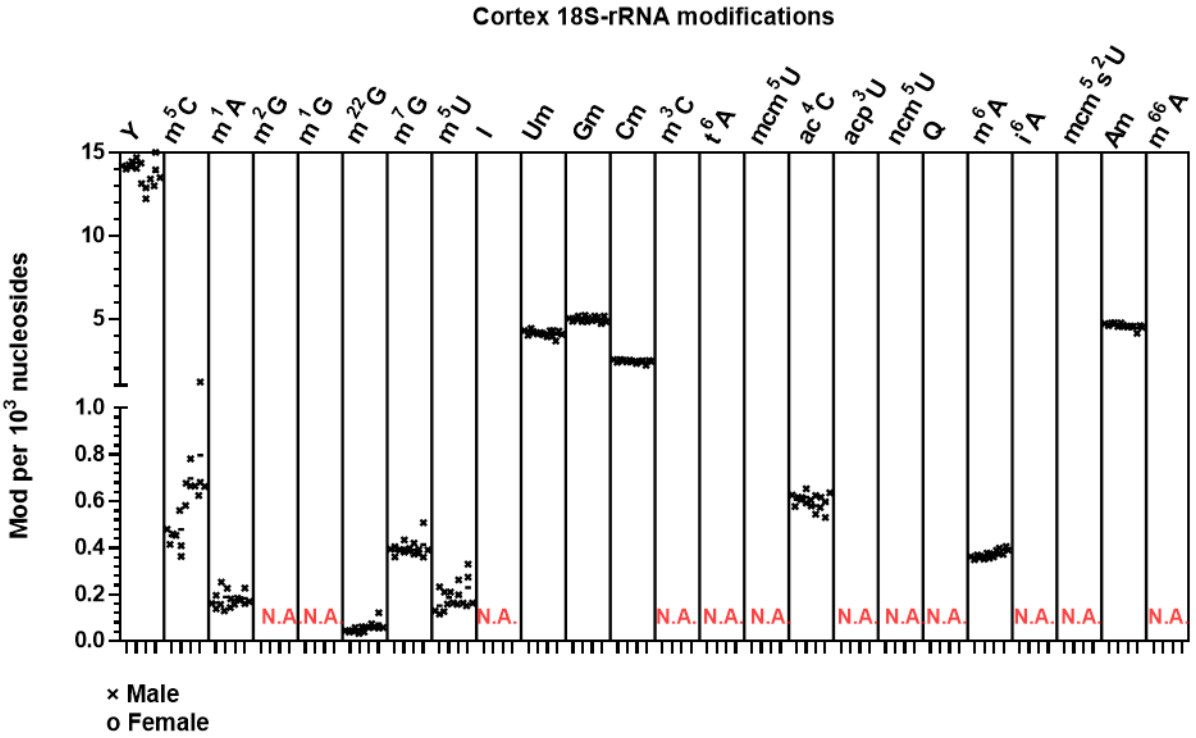
Cortex 18S-rRNA modifications
Mod per 10^3 nucleosides
Ψ m5C m1A m2G m1G m22G m7G m5U I Um Gm Cm m3C t6A mcm5U ac4C acp3U ncm5U Q m6A i6A mcm5s2U Am m66A
N.A.
× Male
o Female

4. Spleen (A)

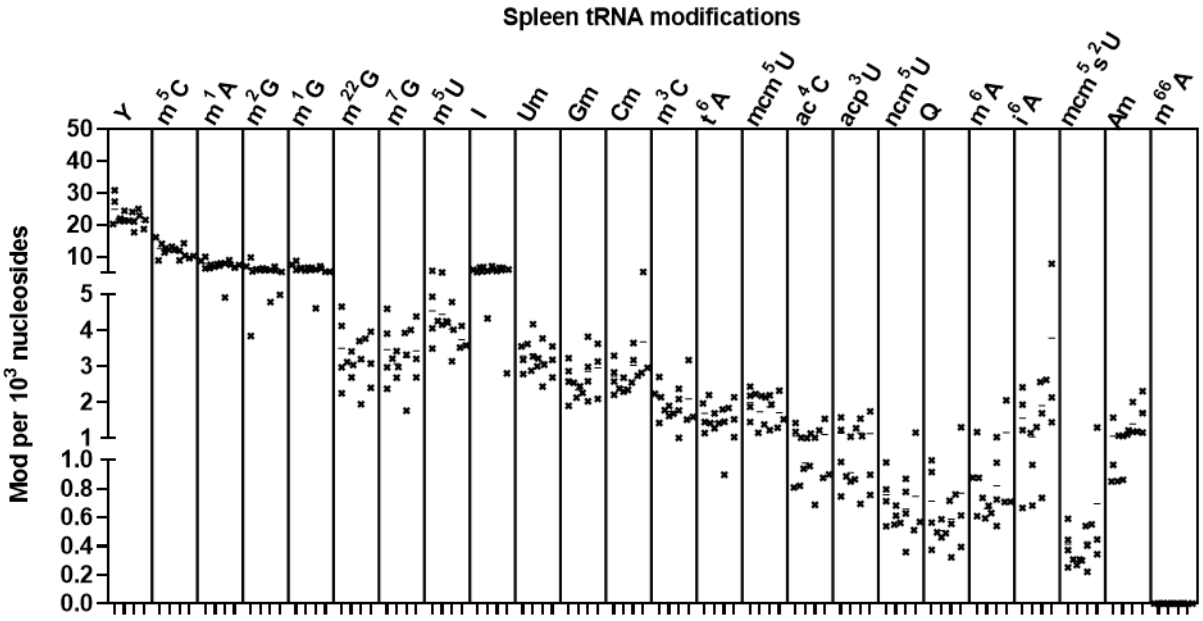
Spleen tRNA modifications
Mod per 10^3 nucleosides
Y
m5C
m1A
m2G
m1G
m22G
m7G
m5U
I
Um
Gm
Cm
m3C
t6A
mcm5U
ac4C
acp3U
ncm5U
Q
m6A
i6A
mcm5s2U
Am
m66A

(B)

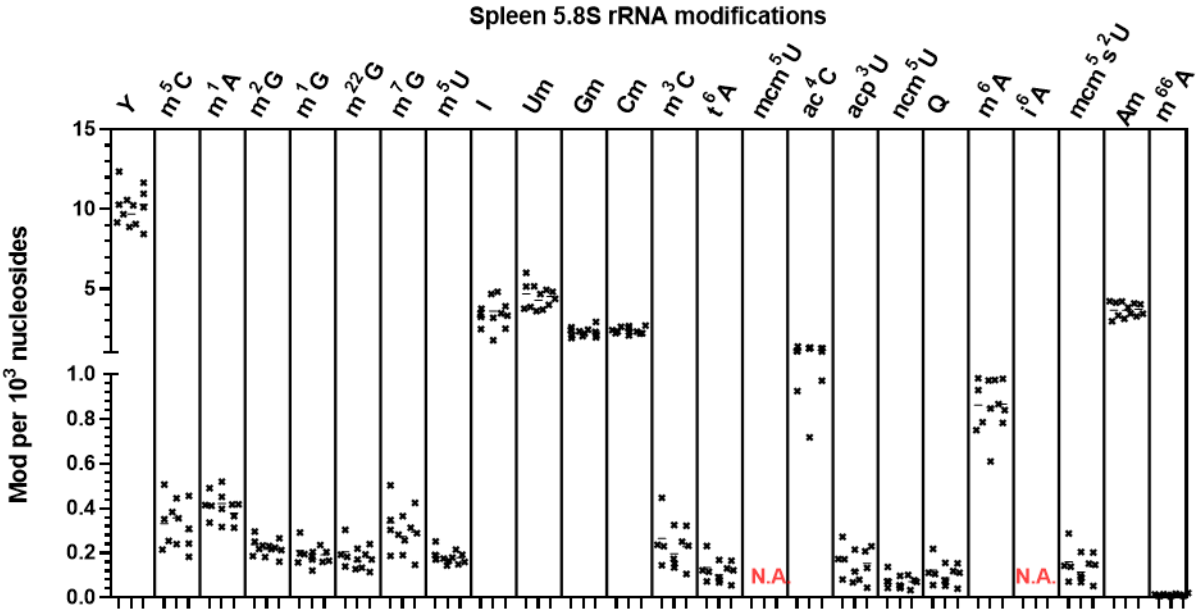
Spleen 5.8S rRNA modifications
Mod per 10^3 nucleosides
Y
m5C
m1A
m2G
m1G
m22G
m7G
m5U
I
Um
Gm
Cm
m3C
t6A
mcm5U
ac4C
acp3U
ncm5U
Q
m6A
i6A
mcm5s2U
Am
m66A
N.A.
N.A.

(C)

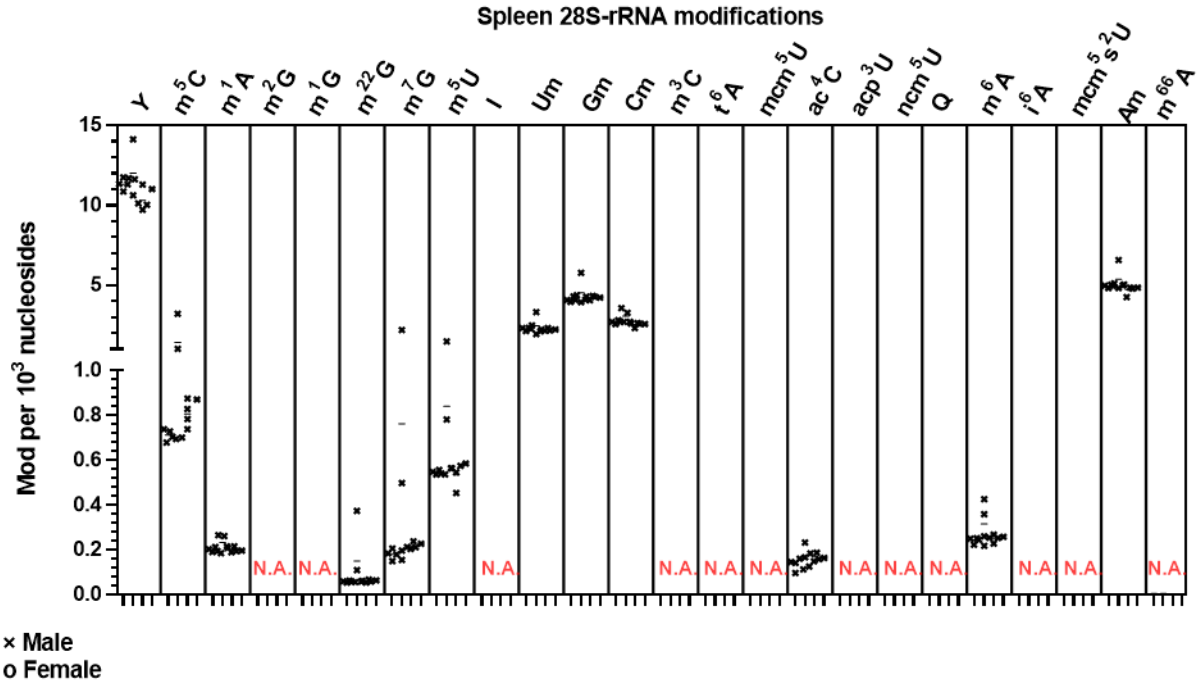
Spleen 28S-rRNA modifications
Ψ
m5C
m1A
m2G
m1G
m22G
m7G
m5U
I
Um
Gm
Cm
m3C
t6A
mcm5U
ac4C
acp3U
ncm5U
Q
m6A
i6A
mcm5s2U
Am
m66A
Mod per 10^3 nucleosides
15
10
5
1.0
0.8
0.6
0.4
0.2
0.0
N.A.
× Male
o Female

(D)

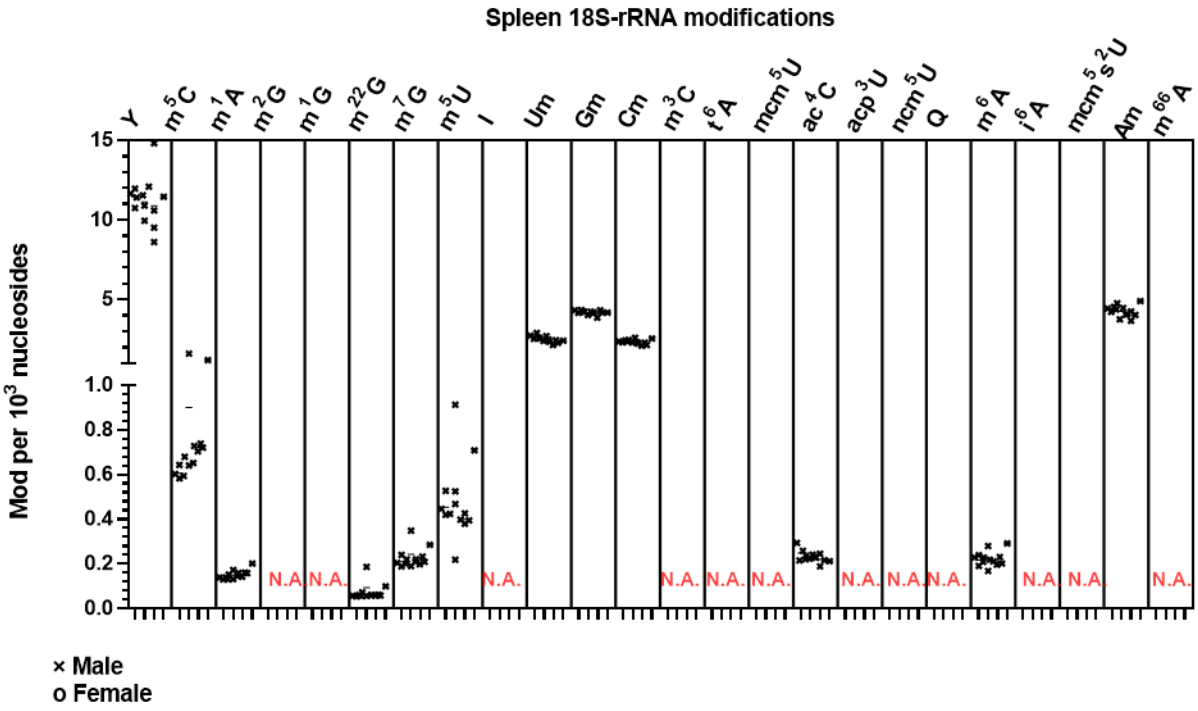
Spleen 18S-rRNA modifications
Ψ
m5C
m1A
m2G
m1G
m22G
m7G
m5U
I
Um
Gm
Cm
m3C
t6A
mcm5U
ac4C
acp3U
ncm5U
Q
m6A
i6A
mcm5s2U
Am
m66A
Mod per 10^3 nucleosides
15
10
5
1.0
0.8
0.6
0.4
0.2
0.0
N.A.
× Male
o Female

5. Olfactory bulb (A)

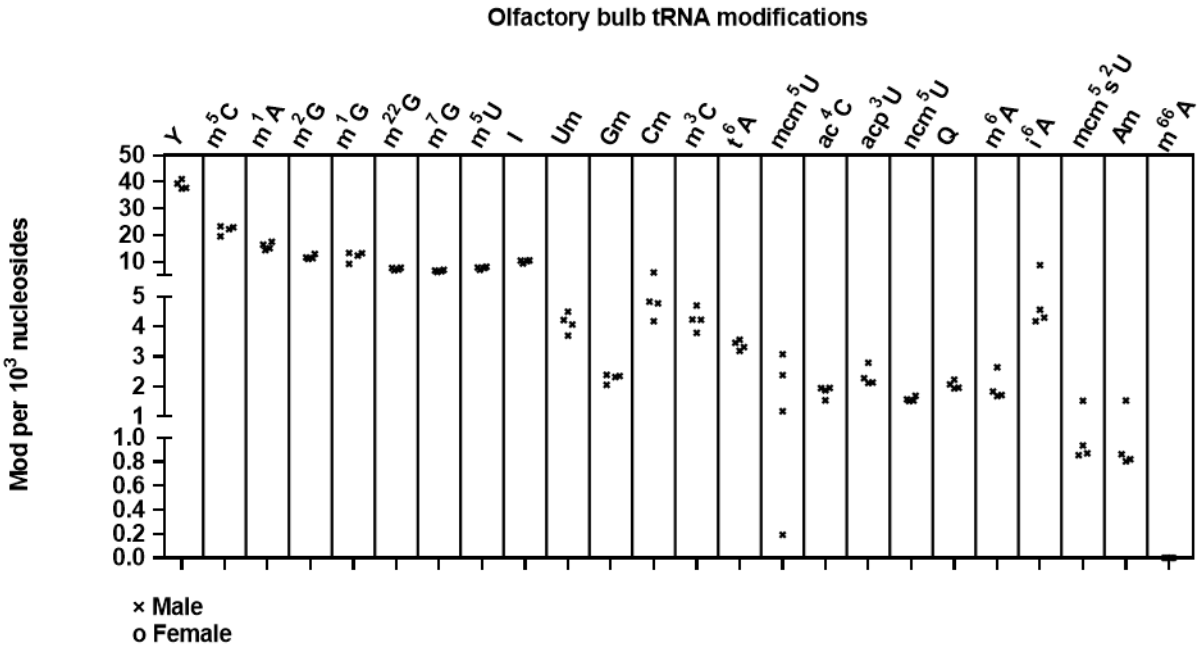

(B)

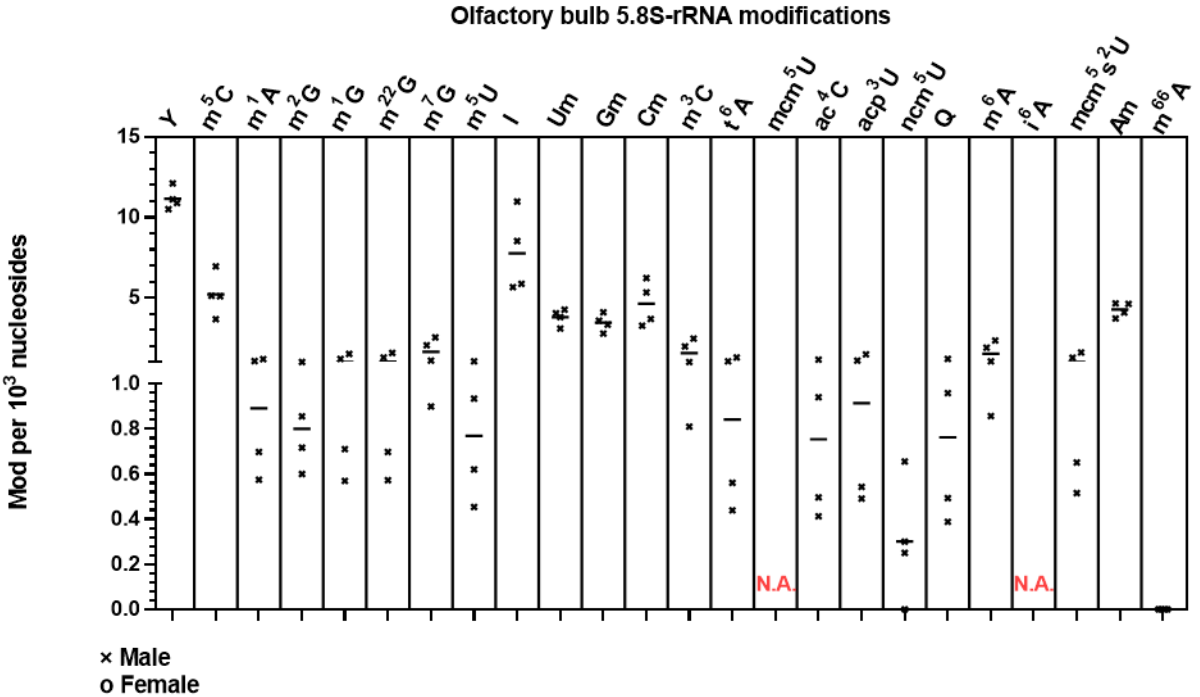

6. kidney (A)

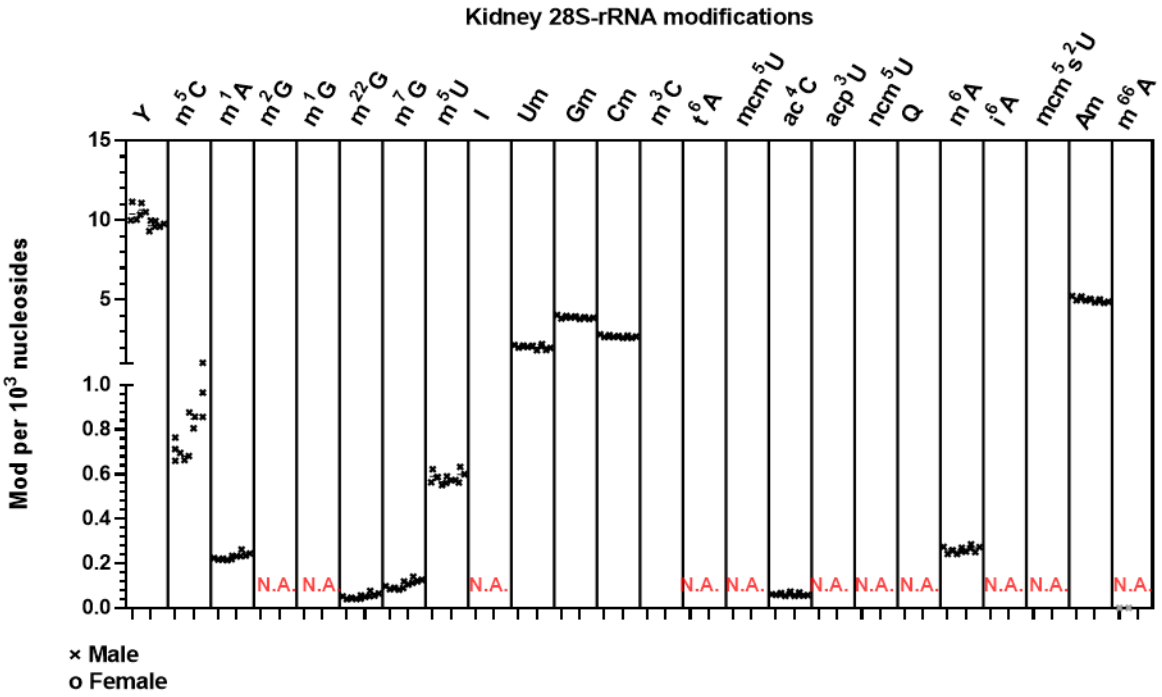
Kidney 28S-rRNA modifications
Ψ
m5C
m1A
m2G
m1G
m22G
m7G
m5U
I
Um
Gm
Cm
m3C
t6A
mcm5U
ac4C
acp3U
ncm5U
Q
m6A
i6A
mcm5s2U
Am
m66A
Mod per 10^3 nucleosides
15
10
5
1.0
0.8
0.6
0.4
0.2
0.0
N.A.
× Male
o Female

(B)

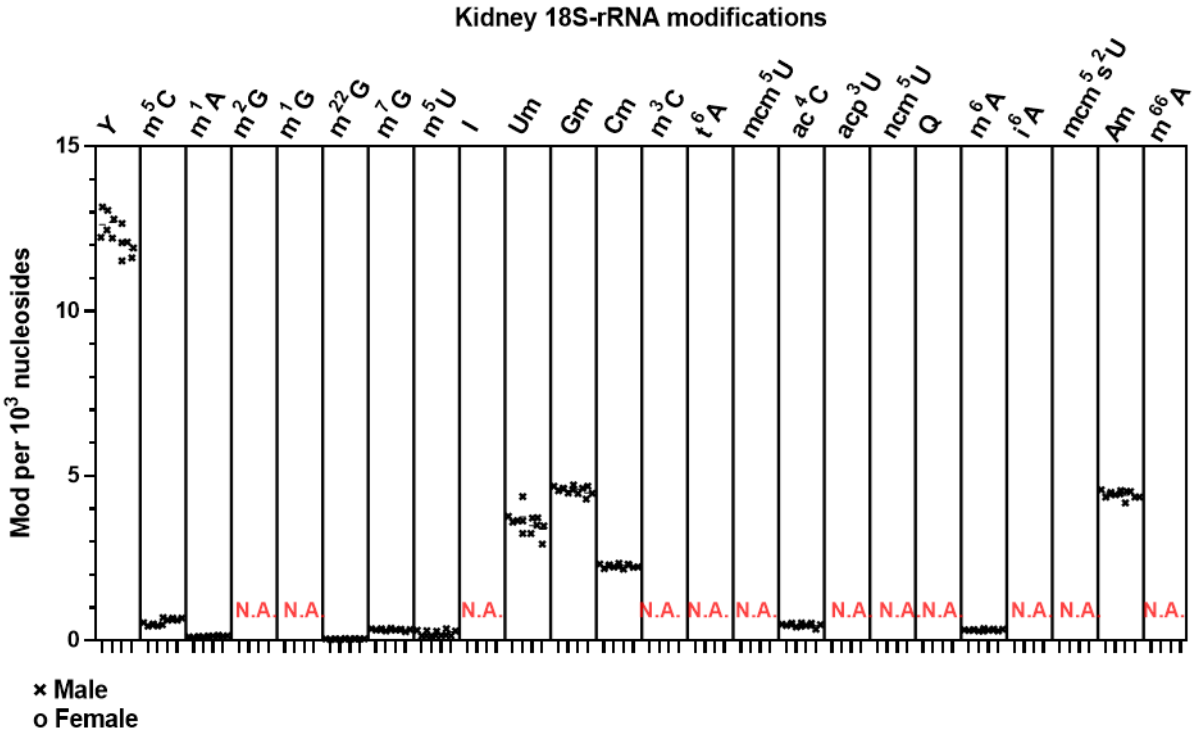
Kidney 18S-rRNA modifications
Ψ
m5C
m1A
m2G
m1G
m22G
m7G
m5U
I
Um
Gm
Cm
m3C
t6A
mcm5U
ac4C
acp3U
ncm5U
Q
m6A
i6A
mcm5s2U
Am
m66A
Mod per 10^3 nucleosides
15
10
5
0
N.A.
× Male
o Female

Supplementary figure 2 Overlaid graphs of absolute quantified RNA modifications from mouse organs: (A) Heart, **(B)** lung, **(C)** cortex, **(D)** Spleen, **(E)** olfactory bulb and **(F)** kidney.

(A)

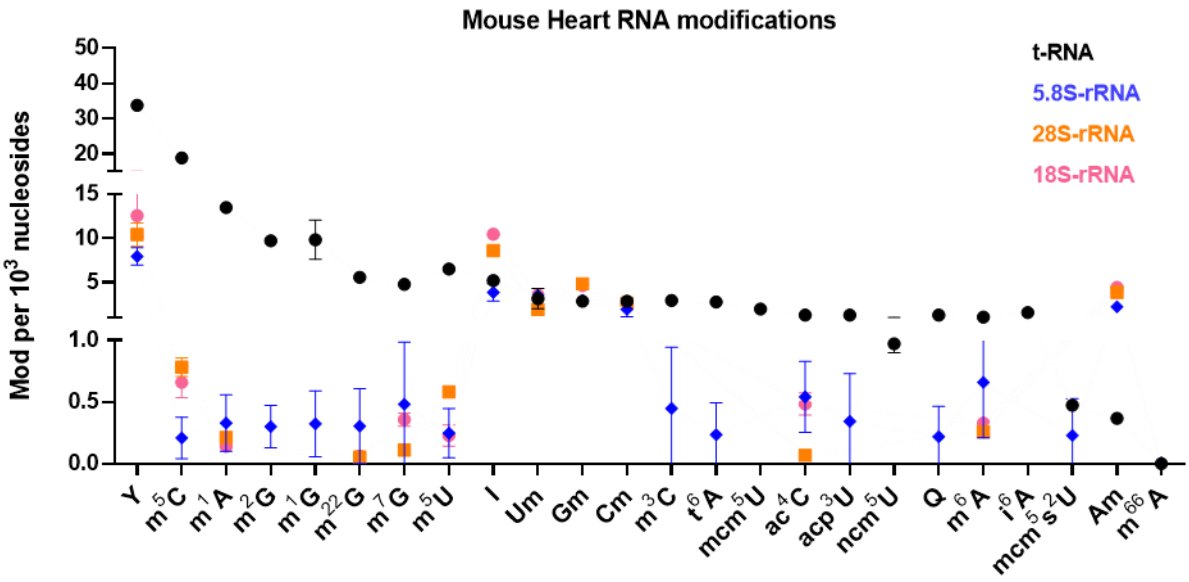

(B)

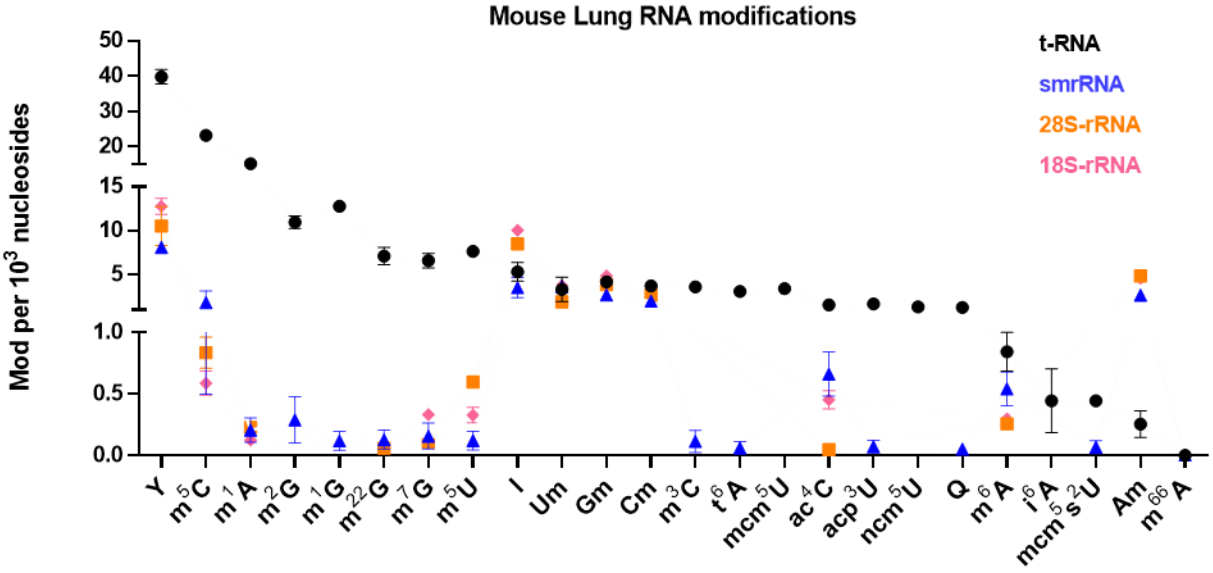

(C)

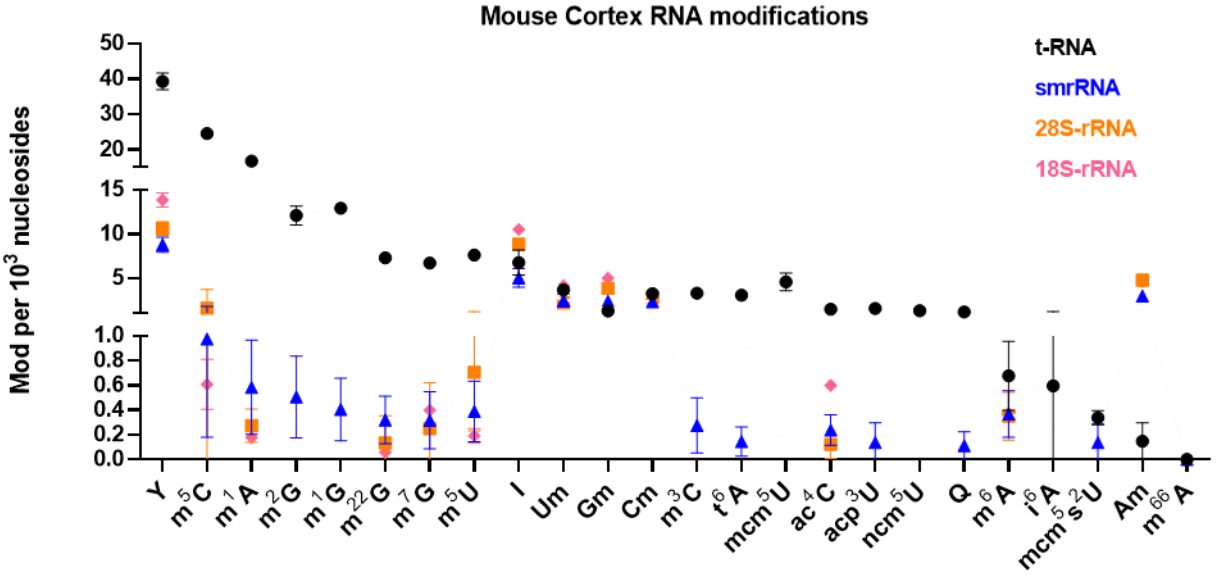
Mouse Cortex RNA modifications
t-RNA
smrRNA
28S-rRNA
18S-rRNA
Mod per 10^3 nucleosides
50
40
30
20
15
10
5
1.0
0.8
0.6
0.4
0.2
0.0
Y
m5C
m1A
m2G
m1G
m22G
m7G
m5U
I
Um
Gm
Cm
m3C
t6A
mcm5U
ac4C
acp3U
ncm5U
Q
m6A
i6A
mcm5s2U
Am
m66A

(D)

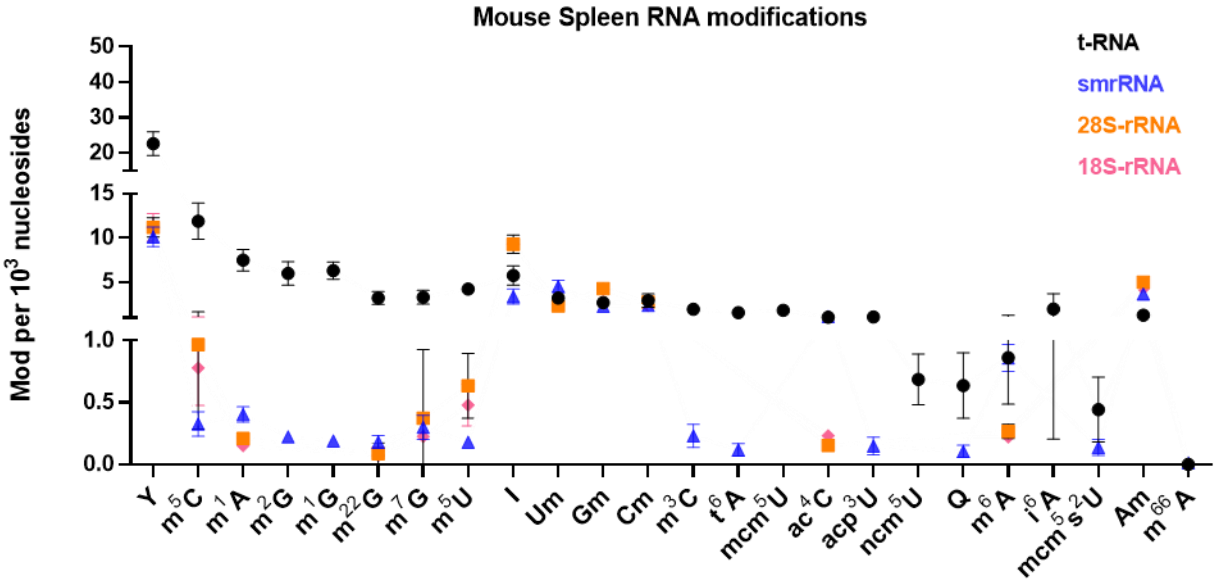
Mouse Spleen RNA modifications
t-RNA
smrRNA
28S-rRNA
18S-rRNA
Mod per 10^3 nucleosides
50
40
30
20
15
10
5
1.0
0.5
0.0
Y
m5C
m1A
m2G
m1G
m22G
m7G
m5U
I
Um
Gm
Cm
m3C
t6A
mcm5U
ac4C
acp3U
ncm5U
Q
m6A
i6A
mcm5s2U
Am
m66A

(E)

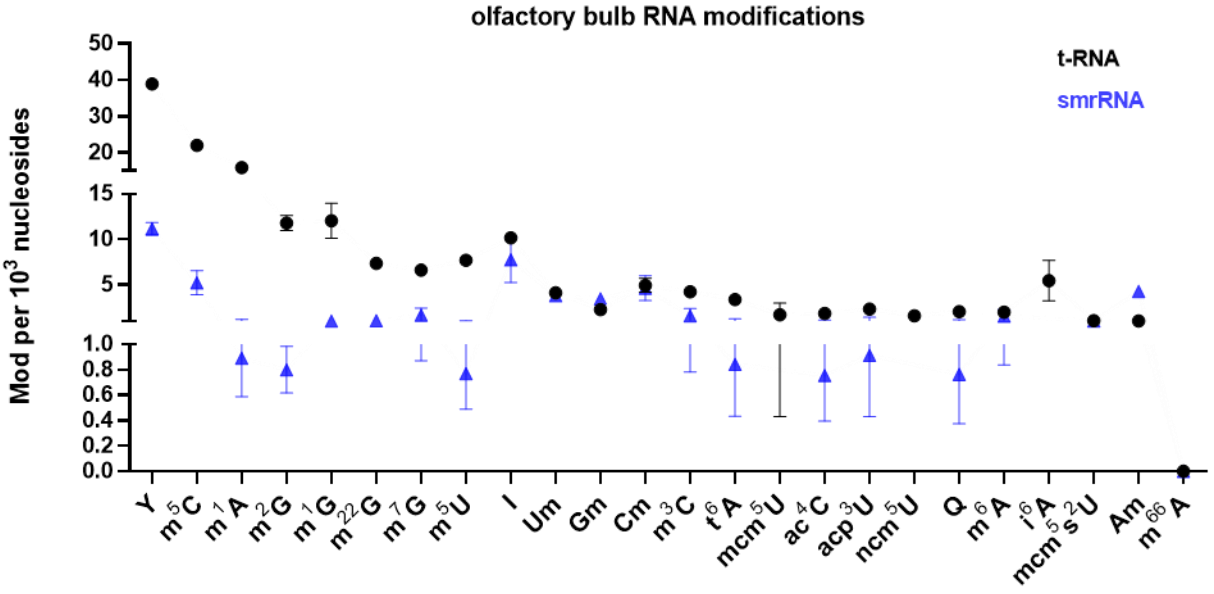
olfactory bulb RNA modifications
t-RNA
smrRNA
Mod per 10^3 nucleosides
50
40
30
20
15
10
5
1.0
0.8
0.6
0.4
0.2
0.0
Y
m5C
m1A
m2G
m1G
m22G
m7G
m5U
I
Um
Gm
Cm
m3C
t6A
mcm5U
ac4C
acp3U
ncm5U
Q
m6A
i6A
mcm5s2U
Am
m66A

(F)

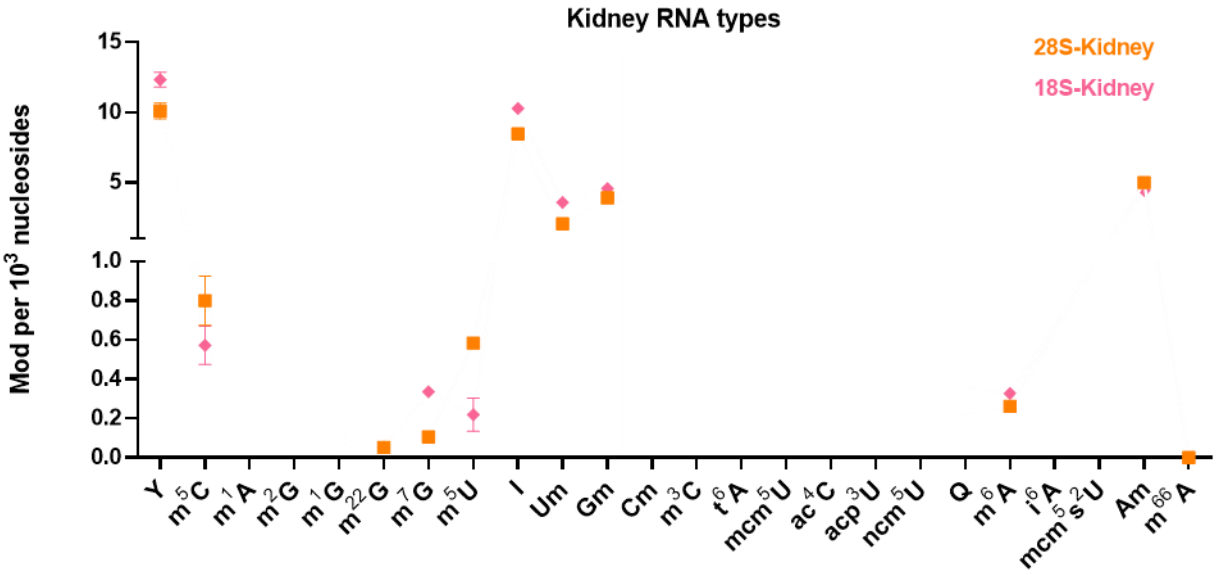
Kidney RNA types
28S-Kidney
18S-Kidney
Mod per 10^3 nucleosides
15
10
5
1.0
0.8
0.6
0.4
0.2
0.0
Y
m5C
m1A
m2G
m1G
m22G
m7G
m5U
I
Um
Gm
Cm
m3C
t6A
mcm5U
ac4C
acp3U
ncm5U
Q
m6A
i6A
mcm5s2U
Am
m66A

6.2. List of figures

6.3. List of tables

7. References

1. Higgs PG, Lehman N. The RNA World: molecular cooperation at the origins of life. *Nat Rev Genet*. **2015**;16(1):7-17.
2. Watson JD, Crick FH. Molecular structure of nucleic acids; a structure for deoxyribose nucleic acid. *Nature*. **1953**;171(4356):737-8.
3. Crick F. Central dogma of molecular biology. *Nature*. **1970**;227(5258):561-3.
4. Starr JL, Sells BH. Methylated ribonucleic acids. *Physiol Rev*. **1969**;49(3):623-69.
5. Brenner S, Jacob F, Meselson M. An unstable intermediate carrying information from genes to ribosomes for protein synthesis. *Nature*. **1961**;190:576-81.
6. Chapeville F, Lipmann F, Von Ehrenstein G, Weisblum B, Ray WJ, Jr., Benzer S. On the role of soluble ribonucleic acid in coding for amino acids. *Proc Natl Acad Sci U S A*. **1962**;48(6):1086-92.
7. Grunberger D, Weinstein IB, Jacobson KB. Codon recognition by enzymatically mischarged valine transfer ribonucleic acid. *Science*. **1969**;166(3913):1635-7.
8. Rich A, RajBhandary UL. Transfer RNA: molecular structure, sequence, and properties. *Annu Rev Biochem*. **1976**;45:805-60.
9. Mattick JS, Makunin IV. Small regulatory RNAs in mammals. *Hum Mol Genet*. **2005**;14 Spec No 1:R121-32.
10. Wyatt JR, Puglisi JD, Tinoco I, Jr. RNA folding: pseudoknots, loops and bulges. *Bioessays*. **1989**;11(4):100-6.
11. Gros F, Hiatt H, Gilbert W, Kurland CG, Risebrough RW, Watson JD. Unstable ribonucleic acid revealed by pulse labelling of Escherichia coli. *Nature*. **1961**;190:581-5.
12. Baer BW, Kornberg RD. The protein responsible for the repeating structure of cytoplasmic poly(A)-ribonucleoprotein. *J Cell Biol*. **1983**;96(3):717-21.
13. Yehudai-Resheff S, Hirsh M, Schuster G. Polynucleotide phosphorylase functions as both an exonuclease and a poly(A) polymerase in spinach chloroplasts. *Mol Cell Biol*. **2001**;21(16):5408-16.
14. Roeder RG, Rutter WJ. Multiple forms of DNA-dependent RNA polymerase in eukaryotic organisms. *Nature*. **1969**;224(5216):234-7.
15. Wierzbicki AT, Haag JR, Pikaard CS. Noncoding transcription by RNA polymerase Pol IVb/Pol V mediates transcriptional silencing of overlapping and adjacent genes. *Cell*. **2008**;135(4):635-48.

16. von Hippel PH. An integrated model of the transcription complex in elongation, termination, and editing. *Science*. **1998**;281(5377):660-5.
17. Boccaletto P, Stefaniak F, Ray A, Cappannini A, Mukherjee S, Purta E, et al. MODOMICS: a database of RNA modification pathways. 2021 update. *Nucleic Acids Res*. **2022**;50(D1):D231-d5.
18. Slobodin B, Han R, Calderone V, Vrielink J, Loayza-Puch F, Elkon R, et al. Transcription Impacts the Efficiency of mRNA Translation via Co-transcriptional N6-adenosine Methylation. *Cell*. **2017**;169(2):326-37.e12.
19. de Crécy-Lagard V, Boccaletto P, Mangleburg CG, Sharma P, Lowe TM, Leidel SA, et al. Matching tRNA modifications in humans to their known and predicted enzymes. *Nucleic Acids Res*. **2019**;47(5):2143-59.
20. Tuorto F, Legrand C, Cirzi C, Federico G, Liebers R, Müller M, et al. Queuosine-modified tRNAs confer nutritional control of protein translation. *Embo j*. **2018**;37(18).
21. Schaefer MR. The Regulation of RNA Modification Systems: The Next Frontier in Epitranscriptomics? *Genes (Basel)*. **2021**;12(3).
22. Lewis CJ, Pan T, Kalsotra A. RNA modifications and structures cooperate to guide RNA-protein interactions. *Nat Rev Mol Cell Biol*. **2017**;18(3):202-10.
23. Secrist JA, 3rd. Nucleoside and nucleotide nomenclature. *Curr Protoc Nucleic Acid Chem*. **2001**;Appendix 1:Appendix 1D.
24. Cohn WE, Volkin E. Nucleoside-5′-phosphates from ribonucleic acid. *Nature*. **1951**;167:483-4.
25. Delaunay S, Pascual G, Feng B, Klann K, Behm M, Hotz-Wagenblatt A, et al. Mitochondrial RNA modifications shape metabolic plasticity in metastasis. *Nature*. **2022**;607(7919):593-603.
26. Suzuki T, Yashiro Y, Kikuchi I, Ishigami Y, Saito H, Matsuzawa I, et al. Complete chemical structures of human mitochondrial tRNAs. *Nat Commun*. **2020**;11(1):4269.
27. Bilbille Y, Gustilo EM, Harris KA, Jones CN, Lusic H, Kaiser RJ, et al. The human mitochondrial tRNAMet: structure/function relationship of a unique modification in the decoding of unconventional codons. *J Mol Biol*. **2011**;406(2):257-74.
28. Sloan KE, Warda AS, Sharma S, Entian KD, Lafontaine DLJ, Bohnsack MT. Tuning the ribosome: The influence of rRNA modification on eukaryotic ribosome biogenesis and function. *RNA Biol*. **2017**;14(9):1138-52.

29. Berg MD, Giguere DJ, Dron JS, Lant JT, Genereaux J, Liao C, et al. Targeted sequencing reveals expanded genetic diversity of human transfer RNAs. *RNA Biol*. **2019**;16(11):1574-85.
30. Crothers DM, Seno T, Söll G. Is there a discriminator site in transfer RNA? *Proc Natl Acad Sci U S A*. **1972**;69(10):3063-7.
31. Auffinger P, Westhof E. An extended structural signature for the tRNA anticodon loop. *Rna*. **2001**;7(3):334-41.
32. Grosjean H, Cedergren RJ, McKay W. Structure in tRNA data. *Biochimie*. **1982**;64(6):387-97.
33. Noller HF, Hoffarth V, Zimniak L. Unusual resistance of peptidyl transferase to protein extraction procedures. *Science*. **1992**;256(5062):1416-9.
34. Ramakrishnan V, White SW. Ribosomal protein structures: insights into the architecture, machinery and evolution of the ribosome. *Trends Biochem Sci*. **1998**;23(6):208-12.
35. Wilson DN, Doudna Cate JH. The structure and function of the eukaryotic ribosome. *Cold Spring Harb Perspect Biol*. **2012**;4(5).
36. Selmer M, Dunham CM, Murphy FVt, Weixlbaumer A, Petry S, Kelley AC, et al. Structure of the 70S ribosome complexed with mRNA and tRNA. *Science*. **2006**;313(5795):1935-42.
37. Jenner LB, Demeshkina N, Yusupova G, Yusupov M. Structural aspects of messenger RNA reading frame maintenance by the ribosome. *Nat Struct Mol Biol*. **2010**;17(5):555-60.
38. Leung EK, Suslov N, Tuttle N, Sengupta R, Piccirilli JA. The mechanism of peptidyl transfer catalysis by the ribosome. *Annu Rev Biochem*. **2011**;80:527-55.
39. Wilson DN. On the specificity of antibiotics targeting the large ribosomal subunit. *Ann N Y Acad Sci*. **2011**;1241:1-16.
40. Jackson RJ, Hellen CU, Pestova TV. The mechanism of eukaryotic translation initiation and principles of its regulation. *Nat Rev Mol Cell Biol*. **2010**;11(2):113-27.
41. Frank J, Zhu J, Penczek P, Li Y, Srivastava S, Verschoor A, et al. A model of protein synthesis based on cryo-electron microscopy of the E. coli ribosome. *Nature*. **1995**;376(6539):441-4.
42. Ban N, Nissen P, Hansen J, Moore PB, Steitz TA. The complete atomic structure of the large ribosomal subunit at 2.4 A resolution. *Science*. **2000**;289(5481):905-20.

43. Wilson DN, Beckmann R. The ribosomal tunnel as a functional environment for nascent polypeptide folding and translational stalling. *Curr Opin Struct Biol*. **2011**;21(2):274-82.
44. Berndt U, Oellerer S, Zhang Y, Johnson AE, Rospert S. A signal-anchor sequence stimulates signal recognition particle binding to ribosomes from inside the exit tunnel. *Proc Natl Acad Sci U S A*. **2009**;106(5):1398-403.
45. Pool MR. A trans-membrane segment inside the ribosome exit tunnel triggers RAMP4 recruitment to the Sec61p translocase. *J Cell Biol*. **2009**;185(5):889-902.
46. Hinnebusch AG. Molecular mechanism of scanning and start codon selection in eukaryotes. *Microbiol Mol Biol Rev*. **2011**;75(3):434-67, first page of table of contents.
47. Martin F, Ménétret JF, Simonetti A, Myasnikov AG, Vicens Q, Prongidi-Fix L, et al. Ribosomal 18S rRNA base pairs with mRNA during eukaryotic translation initiation. *Nat Commun*. **2016**;7:12622.
48. Zaher HS, Green R. Fidelity at the molecular level: lessons from protein synthesis. *Cell*. **2009**;136(4):746-62.
49. Bouadloun F, Donner D, Kurland CG. Codon-specific missense errors in vivo. *Embo j*. **1983**;2(8):1351-6.
50. Wada M, Ito K. A genetic approach for analyzing the co-operative function of the tRNA mimicry complex, eRF1/eRF3, in translation termination on the ribosome. *Nucleic Acids Res*. **2014**;42(12):7851-66.
51. Jackson RJ, Hellen CU, Pestova TV. Termination and post-termination events in eukaryotic translation. *Adv Protein Chem Struct Biol*. **2012**;86:45-93.
52. Mignone F, Gissi C, Liuni S, Pesole G. Untranslated regions of mRNAs. *Genome Biol*. **2002**;3(3):Reviews0004.
53. Galloway A, Cowling VH. mRNA cap regulation in mammalian cell function and fate. *Biochim Biophys Acta Gene Regul Mech*. **2019**;1862(3):270-9.
54. Dominissini D, Nachtergaele S, Moshitch-Moshkovitz S, Peer E, Kol N, Ben-Haim MS, et al. The dynamic N(1)-methyladenosine methylome in eukaryotic messenger RNA. *Nature*. **2016**;530(7591):441-6.
55. Li X, Xiong X, Yi C. Epitranscriptome sequencing technologies: decoding RNA modifications. *Nat Methods*. **2016**;14(1):23-31.
56. Frye M, Blanco S. Post-transcriptional modifications in development and stem cells. *Development*. **2016**;143(21):3871-81.

57. García-Vílchez R, Sevilla A, Blanco S. Post-transcriptional regulation by cytosine-5 methylation of RNA. *Biochim Biophys Acta Gene Regul Mech*. **2019**;1862(3):240-52.
58. Czudnochowski N, Wang AL, Finer-Moore J, Stroud RM. In human pseudouridine synthase 1 (hPus1), a C-terminal helical insert blocks tRNA from binding in the same orientation as in the Pus1 bacterial homologue TruA, consistent with their different target selectivities. *J Mol Biol*. **2013**;425(20):3875-87.
59. Carlile TM, Rojas-Duran MF, Zinshteyn B, Shin H, Bartoli KM, Gilbert WV. Pseudouridine profiling reveals regulated mRNA pseudouridylation in yeast and human cells. *Nature*. **2014**;515(7525):143-6.
60. Jia G, Fu Y, Zhao X, Dai Q, Zheng G, Yang Y, et al. N6-methyladenosine in nuclear RNA is a major substrate of the obesity-associated FTO. *Nat Chem Biol*. **2011**;7(12):885-7.
61. He L, Li H, Wu A, Peng Y, Shu G, Yin G. Functions of N6-methyladenosine and its role in cancer. *Mol Cancer*. **2019**;18(1):176.
62. Arango D, Sturgill D, Alhusaini N, Dillman AA, Sweet TJ, Hanson G, et al. Acetylation of Cytidine in mRNA Promotes Translation Efficiency. *Cell*. **2018**;175(7):1872-86.e24.
63. Jin G, Xu M, Zou M, Duan S. The Processing, Gene Regulation, Biological Functions, and Clinical Relevance of N4-Acetylcytidine on RNA: A Systematic Review. *Mol Ther Nucleic Acids*. **2020**;20:13-24.
64. Choi J, Indrisiunaite G, DeMirci H, Ieong KW, Wang J, Petrov A, et al. 2'-O-methylation in mRNA disrupts tRNA decoding during translation elongation. *Nat Struct Mol Biol*. **2018**;25(3):208-16.
65. El Yacoubi B, Bailly M, de Crécy-Lagard V. Biosynthesis and function of posttranscriptional modifications of transfer RNAs. *Annu Rev Genet*. **2012**;46:69-95.
66. Grosjean H, Söll DG, Crothers DM. Studies of the complex between transfer RNAs with complementary anticodons. I. Origins of enhanced affinity between complementary triplets. *J Mol Biol*. **1976**;103(3):499-519.
67. Urbonavicius J, Qian Q, Durand JM, Hagervall TG, Björk GR. Improvement of reading frame maintenance is a common function for several tRNA modifications. *Embo j*. **2001**;20(17):4863-73.
68. Ge J, Yu YT. RNA pseudouridylation: new insights into an old modification. *Trends Biochem Sci*. **2013**;38(4):210-8.

69. Arnez JG, Steitz TA. Crystal structure of unmodified tRNA(Gln) complexed with glutaminyl-tRNA synthetase and ATP suggests a possible role for pseudo-uridines in stabilization of RNA structure. *Biochemistry*. **1994**;33(24):7560-7.

70. Hayrapetyan A, Seidu-Larry S, Helm M. Function of modified nucleosides in RNA stabilization. *Structure, Mechanism, Functions, Cellular Interactions and Evolution*. **2009**:550-63.

71. Tomikawa C. 7-Methylguanosine Modifications in Transfer RNA (tRNA). *Int J Mol Sci*. **2018**;19(12).

72. Chen Y, Sierzputowska-Gracz H, Guenther R, Everett K, Agris PF. 5-Methylcytidine is required for cooperative binding of Mg2+ and a conformational transition at the anticodon stem-loop of yeast phenylalanine tRNA. *Biochemistry*. **1993**;32(38):10249-53.

73. Yue D, Kintanar A, Horowitz J. Nucleoside modifications stabilize Mg2+ binding in Escherichia coli tRNA(Val): an imino proton NMR investigation. *Biochemistry*. **1994**;33(30):8905-11.

74. Hayrapetyan A, Grosjean H, Helm M. Effect of a quaternary pentamine on RNA stabilization and enzymatic methylation. *Biol Chem*. **2009**;390(9):851-61.

75. Motorin Y, Helm M. tRNA stabilization by modified nucleotides. *Biochemistry*. **2010**;49(24):4934-44.

76. Sørensen MA, Elf J, Bouakaz E, Tenson T, Sanyal S, Björk GR, et al. Over expression of a tRNA(Leu) isoacceptor changes charging pattern of leucine tRNAs and reveals new codon reading. *J Mol Biol*. **2005**;354(1):16-24.

77. Eargle J, Black AA, Sethi A, Trabuco LG, Luthey-Schulten Z. Dynamics of Recognition between tRNA and elongation factor Tu. *J Mol Biol*. **2008**;377(5):1382-405.

78. Ohira T, Suzuki T. Retrograde nuclear import of tRNA precursors is required for modified base biogenesis in yeast. *Proc Natl Acad Sci U S A*. **2011**;108(26):10502-7.

79. Kotelawala L, Grayhack EJ, Phizicky EM. Identification of yeast tRNA Um(44) 2'-O-methyltransferase (Trm44) and demonstration of a Trm44 role in sustaining levels of specific tRNA(Ser) species. *Rna*. **2008**;14(1):158-69.

80. Noon KR, Guymon R, Crain PF, McCloskey JA, Thomm M, Lim J, et al. Influence of temperature on tRNA modification in archaea: Methanococcoides burtonii (optimum growth temperature [Topt], 23 degrees C) and Stetteria hydrogenophila (Topt, 95 degrees C). *J Bacteriol*. **2003**;185(18):5483-90.

81. Chan CT, Dyavaiah M, DeMott MS, Taghizadeh K, Dedon PC, Begley TJ. A quantitative systems approach reveals dynamic control of tRNA modifications during cellular stress. *PLoS Genet*. **2010**;6(12):e1001247.
82. Reichle VF, Petrov DP, Weber V, Jung K, Kellner S. NAIL-MS reveals the repair of 2-methylthiocytidine by AlkB in E. coli. *Nat Commun*. **2019**;10(1):5600.
83. Persson BC. Modification of tRNA as a regulatory device. *Mol Microbiol*. **1993**;8(6):1011-6.
84. Golovina AY, Dzama MM, Osterman IA, Sergiev PV, Serebryakova MV, Bogdanov AA, et al. The last rRNA methyltransferase of E. coli revealed: the yhiR gene encodes adenine-N6 methyltransferase specific for modification of A2030 of 23S ribosomal RNA. *Rna*. **2012**;18(9):1725-34.
85. Taoka M, Nobe Y, Hori M, Takeuchi A, Masaki S, Yamauchi Y, et al. A mass spectrometry-based method for comprehensive quantitative determination of post-transcriptional RNA modifications: the complete chemical structure of Schizosaccharomyces pombe ribosomal RNAs. *Nucleic Acids Res*. **2015**;43(18):e115.
86. Georgeson J, Schwartz S. The ribosome epitranscriptome: inert-or a platform for functional plasticity? *Rna*. **2021**;27(11):1293-301.
87. Sergiev PV, Aleksashin NA, Chugunova AA, Polikanov YS, Dontsova OA. Structural and evolutionary insights into ribosomal RNA methylation. *Nat Chem Biol*. **2018**;14(3):226-35.
88. Piekna-Przybylska D, Przybylski P, Baudin-Baillieu A, Rousset JP, Fournier MJ. Ribosome performance is enhanced by a rich cluster of pseudouridines in the A-site finger region of the large subunit. *J Biol Chem*. **2008**;283(38):26026-36.
89. King TH, Liu B, McCully RR, Fournier MJ. Ribosome structure and activity are altered in cells lacking snoRNPs that form pseudouridines in the peptidyl transferase center. *Mol Cell*. **2003**;11(2):425-35.
90. Ayadi L, Galvanin A, Pichot F, Marchand V, Motorin Y. RNA ribose methylation (2'-O-methylation): Occurrence, biosynthesis and biological functions. *Biochim Biophys Acta Gene Regul Mech*. **2019**;1862(3):253-69.
91. Incarnato D, Anselmi F, Morandi E, Neri F, Maldotti M, Rapelli S, et al. High-throughput single-base resolution mapping of RNA 2′-O-methylated residues. *Nucleic Acids Res*. **2017**;45(3):1433-41.
92. Gongadze GM. 5S rRNA and ribosome. *Biochemistry (Mosc)*. **2011**;76(13):1450-64.

93. Abou Elela S, Nazar RN. Role of the 5.8S rRNA in ribosome translocation. *Nucleic Acids Res*. **1997**;25(9):1788-94.
94. Richter F, Plehn JE, Bessler L, Hertler J, Jörg M, Cirzi C, et al. RNA marker modifications reveal the necessity for rigorous preparation protocols to avoid artifacts in epitranscriptomic analysis. *Nucleic Acids Res*. **2022**;50(8):4201-15.
95. Charette M, Gray MW. Pseudouridine in RNA: what, where, how, and why. *IUBMB Life*. **2000**;49(5):341-51.
96. Liu J, Yue Y, Han D, Wang X, Fu Y, Zhang L, et al. A METTL3-METTL14 complex mediates mammalian nuclear RNA N6-adenosine methylation. *Nat Chem Biol*. **2014**;10(2):93-5.
97. Schwartz S, Mumbach MR, Jovanovic M, Wang T, Maciag K, Bushkin GG, et al. Perturbation of m6A writers reveals two distinct classes of mRNA methylation at internal and 5' sites. *Cell Rep*. **2014**;8(1):284-96.
98. Shi H, Wei J, He C. Where, When, and How: Context-Dependent Functions of RNA Methylation Writers, Readers, and Erasers. *Mol Cell*. **2019**;74(4):640-50.
99. Zhao X, Yang Y, Sun BF, Shi Y, Yang X, Xiao W, et al. FTO-dependent demethylation of N6-methyladenosine regulates mRNA splicing and is required for adipogenesis. *Cell Res*. **2014**;24(12):1403-19.
100. Wei CM, Gershowitz A, Moss B. Methylated nucleotides block 5' terminus of HeLa cell messenger RNA. *Cell*. **1975**;4(4):379-86.
101. Wei J, Liu F, Lu Z, Fei Q, Ai Y, He PC, et al. Differential m(6)A, m(6)A(m), and m(1)A Demethylation Mediated by FTO in the Cell Nucleus and Cytoplasm. *Mol Cell*. **2018**;71(6):973-85.e5.
102. Luo J, Liu H, Luan S, He C, Li Z. Aberrant Regulation of mRNA m⁶A Modification in Cancer Development. *Int J Mol Sci*. **2018**;19(9).
103. Zheng G, Dahl JA, Niu Y, Fedorcsak P, Huang CM, Li CJ, et al. ALKBH5 is a mammalian RNA demethylase that impacts RNA metabolism and mouse fertility. *Mol Cell*. **2013**;49(1):18-29.
104. Tang C, Klukovich R, Peng H, Wang Z, Yu T, Zhang Y, et al. ALKBH5-dependent m6A demethylation controls splicing and stability of long 3'-UTR mRNAs in male germ cells. *Proc Natl Acad Sci U S A*. **2018**;115(2):E325-e33.
105. Zheng Q, Hou J, Zhou Y, Li Z, Cao X. The RNA helicase DDX46 inhibits innate immunity by entrapping m(6)A-demethylated antiviral transcripts in the nucleus. *Nat Immunol*. **2017**;18(10):1094-103.

106. Zhao BS, Roundtree IA, He C. Post-transcriptional gene regulation by mRNA modifications. *Nat Rev Mol Cell Biol*. **2017**;18(1):31-42.
107. Zhou B, Liu C, Xu L, Yuan Y, Zhao J, Zhao W, et al. N(6) -Methyladenosine Reader Protein YT521-B Homology Domain-Containing 2 Suppresses Liver Steatosis by Regulation of mRNA Stability of Lipogenic Genes. *Hepatology*. **2021**;73(1):91-103.
108. Chen Y, Wang J, Xu D, Xiang Z, Ding J, Yang X, et al. m(6)A mRNA methylation regulates testosterone synthesis through modulating autophagy in Leydig cells. *Autophagy*. **2021**;17(2):457-75.
109. Berulava T, Buchholz E, Elerdashvili V, Pena T, Islam MR, Lbik D, et al. Changes in m6A RNA methylation contribute to heart failure progression by modulating translation. *Eur J Heart Fail*. **2020**;22(1):54-66.
110. Liu T, Wei Q, Jin J, Luo Q, Liu Y, Yang Y, et al. The m6A reader YTHDF1 promotes ovarian cancer progression via augmenting EIF3C translation. *Nucleic Acids Res*. **2020**;48(7):3816-31.
111. Chen YS, Yang WL, Zhao YL, Yang YG. Dynamic transcriptomic m(5) C and its regulatory role in RNA processing. *Wiley Interdiscip Rev RNA*. **2021**;12(4):e1639.
112. Hamma T, Ferré-D'Amaré AR. Pseudouridine synthases. *Chem Biol*. **2006**;13(11):1125-35.
113. Hamma T, Ferré-D'Amaré AR. The box H/ACA ribonucleoprotein complex: interplay of RNA and protein structures in post-transcriptional RNA modification. *J Biol Chem*. **2010**;285(2):805-9.
114. Sakurai M, Ueda H, Yano T, Okada S, Terajima H, Mitsuyama T, et al. A biochemical landscape of A-to-I RNA editing in the human brain transcriptome. *Genome Res*. **2014**;24(3):522-34.
115. Bass BL. RNA editing by adenosine deaminases that act on RNA. *Annu Rev Biochem*. **2002**;71:817-46.
116. Higuchi M, Maas S, Single FN, Hartner J, Rozov A, Burnashev N, et al. Point mutation in an AMPA receptor gene rescues lethality in mice deficient in the RNA-editing enzyme ADAR2. *Nature*. **2000**;406(6791):78-81.
117. Xu B, Liu D, Wang Z, Tian R, Zuo Y. Multi-substrate selectivity based on key loops and non-homologous domains: new insight into ALKBH family. *Cell Mol Life Sci*. **2021**;78(1):129-41.
118. Kataoka H, Yamamoto Y, Sekiguchi M. A new gene (alkB) of Escherichia coli that controls sensitivity to methyl methane sulfonate. *J Bacteriol*. **1983**;153(3):1301-7.

119. Welford RW, Kirkpatrick JM, McNeill LA, Puri M, Oldham NJ, Schofield CJ. Incorporation of oxygen into the succinate co-product of iron(II) and 2-oxoglutarate dependent oxygenases from bacteria, plants and humans. *FEBS Lett*. **2005**;579(23):5170-4.
120. Fedeles BI, Singh V, Delaney JC, Li D, Essigmann JM. The AlkB Family of Fe(II)/α-Ketoglutarate-dependent Dioxygenases: Repairing Nucleic Acid Alkylation Damage and Beyond. *J Biol Chem*. **2015**;290(34):20734-42.
121. Liu F, Clark W, Luo G, Wang X, Fu Y, Wei J, et al. ALKBH1-Mediated tRNA Demethylation Regulates Translation. *Cell*. **2016**;167(3):816-28.e16.
122. Ma CJ, Ding JH, Ye TT, Yuan BF, Feng YQ. AlkB Homologue 1 Demethylates N(3)-Methylcytidine in mRNA of Mammals. *ACS Chem Biol*. **2019**;14(7):1418-25.
123. Zhang M, Yang S, Nelakanti R, Zhao W, Liu G, Li Z, et al. Mammalian ALKBH1 serves as an N(6)-mA demethylase of unpairing DNA. *Cell Res*. **2020**;30(3):197-210.
124. Haag S, Sloan KE, Ranjan N, Warda AS, Kretschmer J, Blessing C, et al. NSUN3 and ABH1 modify the wobble position of mt-tRNAMet to expand codon recognition in mitochondrial translation. *Embo j*. **2016**;35(19):2104-19.
125. Li X, Xiong X, Wang K, Wang L, Shu X, Ma S, et al. Transcriptome-wide mapping reveals reversible and dynamic N(1)-methyladenosine methylome. *Nat Chem Biol*. **2016**;12(5):311-6.
126. Chen Z, Qi M, Shen B, Luo G, Wu Y, Li J, et al. Transfer RNA demethylase ALKBH3 promotes cancer progression via induction of tRNA-derived small RNAs. *Nucleic Acids Res*. **2019**;47(5):2533-45.
127. Ueda Y, Ooshio I, Fusamae Y, Kitae K, Kawaguchi M, Jingushi K, et al. AlkB homolog 3-mediated tRNA demethylation promotes protein synthesis in cancer cells. *Sci Rep*. **2017**;7:42271.
128. Ougland R, Zhang CM, Liiv A, Johansen RF, Seeberg E, Hou YM, et al. AlkB restores the biological function of mRNA and tRNA inactivated by chemical methylation. *Mol Cell*. **2004**;16(1):107-16.
129. Chen H, Zhou L, Li J, Hu K. ALKBH family members as novel biomarkers and prognostic factors in human breast cancer. *Aging (Albany NY)*. **2022**;14(16):6579-93.
130. Esteve-Puig R, Bueno-Costa A, Esteller M. Writers, readers and erasers of RNA modifications in cancer. *Cancer Lett*. **2020**;474:127-37.

131. Wagner A, Hofmeister O, Rolland SG, Maiser A, Aasumets K, Schmitt S, et al. Mitochondrial Alkbh1 localizes to mtRNA granules and its knockdown induces the mitochondrial UPR in humans and C. elegans. *J Cell Sci*. **2019**;132(19).
132. Yamato I, Sho M, Shimada K, Hotta K, Ueda Y, Yasuda S, et al. PCA-1/ALKBH3 contributes to pancreatic cancer by supporting apoptotic resistance and angiogenesis. *Cancer Res*. **2012**;72(18):4829-39.
133. Spinola M, Galvan A, Pignatiello C, Conti B, Pastorino U, Nicander B, et al. Identification and functional characterization of the candidate tumor suppressor gene TRIT1 in human lung cancer. *Oncogene*. **2005**;24(35):5502-9.
134. He Y, Hu H, Wang Y, Yuan H, Lu Z, Wu P, et al. ALKBH5 Inhibits Pancreatic Cancer Motility by Decreasing Long Non-Coding RNA KCNK15-AS1 Methylation. *Cell Physiol Biochem*. **2018**;48(2):838-46.
135. Kwok CT, Marshall AD, Rasko JE, Wong JJ. Genetic alterations of m(6)A regulators predict poorer survival in acute myeloid leukemia. *J Hematol Oncol*. **2017**;10(1):39.
136. Zhang S, Zhao BS, Zhou A, Lin K, Zheng S, Lu Z, et al. m(6)A Demethylase ALKBH5 Maintains Tumorigenicity of Glioblastoma Stem-like Cells by Sustaining FOXM1 Expression and Cell Proliferation Program. *Cancer Cell*. **2017**;31(4):591-606.e6.
137. Zhang C, Samanta D, Lu H, Bullen JW, Zhang H, Chen I, et al. Hypoxia induces the breast cancer stem cell phenotype by HIF-dependent and ALKBH5-mediated m^{6}A-demethylation of NANOG mRNA. *Proc Natl Acad Sci U S A*. **2016**;113(14):E2047-56.
138. Cui Q, Shi H, Ye P, Li L, Qu Q, Sun G, et al. m(6)A RNA Methylation Regulates the Self-Renewal and Tumorigenesis of Glioblastoma Stem Cells. *Cell Rep*. **2017**;18(11):2622-34.
139. Zhou S, Bai ZL, Xia D, Zhao ZJ, Zhao R, Wang YY, et al. FTO regulates the chemo-radiotherapy resistance of cervical squamous cell carcinoma (CSCC) by targeting β-catenin through mRNA demethylation. *Mol Carcinog*. **2018**;57(5):590-7.
140. Su R, Dong L, Li C, Nachtergaele S, Wunderlich M, Qing Y, et al. R-2HG Exhibits Anti-tumor Activity by Targeting FTO/m(6)A/MYC/CEBPA Signaling. *Cell*. **2018**;172(1-2):90-105.e23.
141. Yang S, Wei J, Cui YH, Park G, Shah P, Deng Y, et al. m(6)A mRNA demethylase FTO regulates melanoma tumorigenicity and response to anti-PD-1 blockade. *Nat Commun*. **2019**;10(1):2782.
142. Xu D, Shao W, Jiang Y, Wang X, Liu Y, Liu X. FTO expression is associated with the occurrence of gastric cancer and prognosis. *Oncol Rep*. **2017**;38(4):2285-92.

143. Tan A, Dang Y, Chen G, Mo Z. Overexpression of the fat mass and obesity associated gene (FTO) in breast cancer and its clinical implications. *Int J Clin Exp Pathol*. **2015**;8(10):13405-10.
144. Delaunay S, Rapino F, Tharun L, Zhou Z, Heukamp L, Termathe M, et al. Elp3 links tRNA modification to IRES-dependent translation of LEF1 to sustain metastasis in breast cancer. *J Exp Med*. **2016**;213(11):2503-23.
145. Liu M, Chen F, Liu T, Chen F, Liu S, Yang J. The role of oxidative stress in influenza virus infection. *Microbes Infect*. **2017**;19(12):580-6.
146. Klaunig JE. Oxidative Stress and Cancer. *Curr Pharm Des*. **2018**;24(40):4771-8.
147. Moloney JN, Cotter TG. ROS signalling in the biology of cancer. *Semin Cell Dev Biol*. **2018**;80:50-64.
148. Ding W, Higgins DP, Yadav DK, Godbole AA, Pukkila-Worley R, Walker AK. Stress-responsive and metabolic gene regulation are altered in low S-adenosylmethionine. *PLoS Genet*. **2018**;14(11):e1007812.
149. Radi E, Formichi P, Battisti C, Federico A. Apoptosis and oxidative stress in neurodegenerative diseases. *J Alzheimers Dis*. **2014**;42 Suppl 3:S125-52.
150. Li Z, Wu J, Deleo CJ. RNA damage and surveillance under oxidative stress. *IUBMB Life*. **2006**;58(10):581-8.
151. Daiber A, Kröller-Schön S, Oelze M, Hahad O, Li H, Schulz R, et al. Oxidative stress and inflammation contribute to traffic noise-induced vascular and cerebral dysfunction via uncoupling of nitric oxide synthases. *Redox Biol*. **2020**;34:101506.
152. Suzuki T. The expanding world of tRNA modifications and their disease relevance. *Nat Rev Mol Cell Biol*. **2021**;22(6):375-92.
153. Wollen KL, Hagen L, Vågbø CB, Rabe R, Iveland TS, Aas PA, et al. ALKBH3 partner ASCC3 mediates P-body formation and selective clearance of MMS-induced 1-methyladenosine and 3-methylcytosine from mRNA. *J Transl Med*. **2021**;19(1):287.
154. Ovejero S, Soulet C, Moriel-Carretero M. The Alkylating Agent Methyl Methanesulfonate Triggers Lipid Alterations at the Inner Nuclear Membrane That Are Independent from Its DNA-Damaging Ability. *Int J Mol Sci*. **2021**;22(14).
155. Aas PA, Otterlei M, Falnes PO, Vågbø CB, Skorpen F, Akbari M, et al. Human and bacterial oxidative demethylases repair alkylation damage in both RNA and DNA. *Nature*. **2003**;421(6925):859-63.

156. Tsao N, Brickner JR, Rodell R, Ganguly A, Wood M, Oyeniran C, et al. Aberrant RNA methylation triggers recruitment of an alkylation repair complex. *Mol Cell*. **2021**;81(20):4228-42.e8.
157. Ma C, Chang M, Lv H, Zhang ZW, Zhang W, He X, et al. RNA m(6)A methylation participates in regulation of postnatal development of the mouse cerebellum. *Genome Biol*. **2018**;19(1):68.
158. Fu H, Feng J, Liu Q, Sun F, Tie Y, Zhu J, et al. Stress induces tRNA cleavage by angiogenin in mammalian cells. *FEBS Lett*. **2009**;583(2):437-42.
159. Thompson DM, Parker R. Stressing out over tRNA cleavage. *Cell*. **2009**;138(2):215-9.
160. Lee SR, Collins K. Starvation-induced cleavage of the tRNA anticodon loop in Tetrahymena thermophila. *J Biol Chem*. **2005**;280(52):42744-9.
161. Thompson DM, Lu C, Green PJ, Parker R. tRNA cleavage is a conserved response to oxidative stress in eukaryotes. *Rna*. **2008**;14(10):2095-103.
162. Yamasaki S, Ivanov P, Hu GF, Anderson P. Angiogenin cleaves tRNA and promotes stress-induced translational repression. *J Cell Biol*. **2009**;185(1):35-42.
163. Haussecker D, Huang Y, Lau A, Parameswaran P, Fire AZ, Kay MA. Human tRNA-derived small RNAs in the global regulation of RNA silencing. *Rna*. **2010**;16(4):673-95.
164. Hsieh LC, Lin SI, Shih AC, Chen JW, Lin WY, Tseng CY, et al. Uncovering small RNA-mediated responses to phosphate deficiency in Arabidopsis by deep sequencing. *Plant Physiol*. **2009**;151(4):2120-32.
165. Li Y, Luo J, Zhou H, Liao JY, Ma LM, Chen YQ, et al. Stress-induced tRNA-derived RNAs: a novel class of small RNAs in the primitive eukaryote Giardia lamblia. *Nucleic Acids Res*. **2008**;36(19):6048-55.
166. Gebetsberger J, Zywicki M, Künzi A, Polacek N. tRNA-derived fragments target the ribosome and function as regulatory non-coding RNA in Haloferax volcanii. *Archaea*. **2012**;2012:260909.
167. Hoang TT, Raines RT. Molecular basis for the autonomous promotion of cell proliferation by angiogenin. *Nucleic Acids Res*. **2017**;45(2):818-31.
168. Saxena SK, Rybak SM, Davey RT, Jr., Youle RJ, Ackerman EJ. Angiogenin is a cytotoxic, tRNA-specific ribonuclease in the RNase A superfamily. *J Biol Chem*. **1992**;267(30):21982-6.
169. Rybak SM, Vallee BL. Base cleavage specificity of angiogenin with Saccharomyces cerevisiae and Escherichia coli 5S RNAs. *Biochemistry*. **1988**;27(7):2288-94.

170. Shapiro R, Riordan JF, Vallee BL. Characteristic ribonucleolytic activity of human angiogenin. *Biochemistry*. **1986**;25(12):3527-32.
171. Peebles CL, Gegenheimer P, Abelson J. Precise excision of intervening sequences from precursor tRNAs by a membrane-associated yeast endonuclease. *Cell*. **1983**;32(2):525-36.
172. Thompson LD, Brandon LD, Nieuwlandt DT, Daniels CJ. Transfer RNA intron processing in the halophilic archaebacteria. *Can J Microbiol*. **1989**;35(1):36-42.
173. Chan PP, Lowe TM. GtRNAdb 2.0: an expanded database of transfer RNA genes identified in complete and draft genomes. *Nucleic Acids Res*. **2016**;44(D1):D184-9.
174. Schmidt CA, Matera AG. tRNA introns: Presence, processing, and purpose. *Wiley Interdiscip Rev RNA*. **2020**;11(3):e1583.
175. Chen Q, Zhang X, Shi J, Yan M, Zhou T. Origins and evolving functionalities of tRNA-derived small RNAs. *Trends Biochem Sci*. **2021**;46(10):790-804.
176. Peng H, Shi J, Zhang Y, Zhang H, Liao S, Li W, et al. A novel class of tRNA-derived small RNAs extremely enriched in mature mouse sperm. *Cell Res*. **2012**;22(11):1609-12.
177. Cole C, Sobala A, Lu C, Thatcher SR, Bowman A, Brown JW, et al. Filtering of deep sequencing data reveals the existence of abundant Dicer-dependent small RNAs derived from tRNAs. *Rna*. **2009**;15(12):2147-60.
178. Reinsborough CW, Ipas H, Abell NS, Nottingham RM, Yao J, Devanathan SK, et al. BCDIN3D regulates tRNAHis 3' fragment processing. *PLoS Genet*. **2019**;15(7):e1008273.
179. Nechooshtan G, Yunusov D, Chang K, Gingeras TR. Processing by RNase 1 forms tRNA halves and distinct Y RNA fragments in the extracellular environment. *Nucleic Acids Res*. **2020**;48(14):8035-49.
180. Kikuchi Y, Sasaki N, Ando-Yamagami Y. Cleavage of tRNA within the mature tRNA sequence by the catalytic RNA of RNase P: implication for the formation of the primer tRNA fragment for reverse transcription in copia retrovirus-like particles. *Proc Natl Acad Sci U S A*. **1990**;87(20):8105-9.
181. Su Z, Wilson B, Kumar P, Dutta A. Noncanonical Roles of tRNAs: tRNA Fragments and Beyond. *Annu Rev Genet*. **2020**;54:47-69.
182. Shabalina SA, Koonin EV. Origins and evolution of eukaryotic RNA interference. *Trends Ecol Evol*. **2008**;23(10):578-87.

183. Tuorto F, Liebers R, Musch T, Schaefer M, Hofmann S, Kellner S, et al. RNA cytosine methylation by Dnmt2 and NSun2 promotes tRNA stability and protein synthesis. *Nat Struct Mol Biol*. **2012**;19(9):900-5.

184. Schaefer M, Pollex T, Hanna K, Tuorto F, Meusburger M, Helm M, et al. RNA methylation by Dnmt2 protects transfer RNAs against stress-induced cleavage. *Genes Dev*. **2010**;24(15):1590-5.

185. Wang X, Matuszek Z, Huang Y, Parisien M, Dai Q, Clark W, et al. Queuosine modification protects cognate tRNAs against ribonuclease cleavage. *Rna*. **2018**;24(10):1305-13.

186. Müller M, Hartmann M, Schuster I, Bender S, Thüring KL, Helm M, et al. Dynamic modulation of Dnmt2-dependent tRNA methylation by the micronutrient queuine. *Nucleic Acids Res*. **2015**;43(22):10952-62.

187. Barraud P, Gato A, Heiss M, Catala M, Kellner S, Tisné C. Time-resolved NMR monitoring of tRNA maturation. *Nat Commun*. **2019**;10(1):3373.

188. Rashad S, Han X, Sato K, Mishima E, Abe T, Tominaga T, et al. The stress specific impact of ALKBH1 on tRNA cleavage and tiRNA generation. *RNA Biol*. **2020**;17(8):1092-103.

189. Cosentino C, Toivonen S, Diaz Villamil E, Atta M, Ravanat JL, Demine S, et al. Pancreatic β-cell tRNA hypomethylation and fragmentation link TRMT10A deficiency with diabetes. *Nucleic Acids Res*. **2018**;46(19):10302-18.

190. Vitali P, Kiss T. Cooperative 2'-O-methylation of the wobble cytidine of human elongator tRNA(Met)(CAT) by a nucleolar and a Cajal body-specific box C/D RNP. *Genes Dev*. **2019**;33(13-14):741-6.

191. Saikia M, Jobava R, Parisien M, Putnam A, Krokowski D, Gao XH, et al. Angiogenin-cleaved tRNA halves interact with cytochrome c, protecting cells from apoptosis during osmotic stress. *Mol Cell Biol*. **2014**;34(13):2450-63.

192. Emara MM, Ivanov P, Hickman T, Dawra N, Tisdale S, Kedersha N, et al. Angiogenin-induced tRNA-derived stress-induced RNAs promote stress-induced stress granule assembly. *J Biol Chem*. **2010**;285(14):10959-68.

193. Lyons SM, Achorn C, Kedersha NL, Anderson PJ, Ivanov P. YB-1 regulates tiRNA-induced Stress Granule formation but not translational repression. *Nucleic Acids Res*. **2016**;44(14):6949-60.

194. Sanadgol N, König L, Drino A, Jovic M, Schaefer MR. Experimental paradigms revisited: oxidative stress-induced tRNA fragmentation does not correlate with stress

granule formation but is associated with delayed cell death. *Nucleic Acids Res*. **2022**;50(12):6919-37.

195. Drino A, Oberbauer V, Troger C, Janisiw E, Anrather D, Hartl M, et al. Production and purification of endogenously modified tRNA-derived small RNAs. *RNA Biol*. **2020**;17(8):1104-15.
196. Zamore PD, Tuschl T, Sharp PA, Bartel DP. RNAi: double-stranded RNA directs the ATP-dependent cleavage of mRNA at 21 to 23 nucleotide intervals. *Cell*. **2000**;101(1):25-33.
197. Gavrilov K, Saltzman WM. Therapeutic siRNA: principles, challenges, and strategies. *Yale J Biol Med*. **2012**;85(2):187-200.
198. Aagaard L, Rossi JJ. RNAi therapeutics: principles, prospects and challenges. *Adv Drug Deliv Rev*. **2007**;59(2-3):75-86.
199. Behlke MA. Progress towards in vivo use of siRNAs. *Mol Ther*. **2006**;13(4):644-70.
200. Gao Y, Liu XL, Li XR. Research progress on siRNA delivery with nonviral carriers. *Int J Nanomedicine*. **2011**;6:1017-25.
201. Stark R, Grzelak M, Hadfield J. RNA sequencing: the teenage years. *Nat Rev Genet*. **2019**;20(11):631-56.
202. Lu K, Miyazaki Y, Summers MF. Isotope labeling strategies for NMR studies of RNA. *J Biomol NMR*. **2010**;46(1):113-25.
203. Longhini AP, LeBlanc RM, Becette O, Salguero C, Wunderlich CH, Johnson BA, et al. Chemo-enzymatic synthesis of site-specific isotopically labeled nucleotides for use in NMR resonance assignment, dynamics and structural characterizations. *Nucleic Acids Res*. **2016**;44(6):e52.
204. Yoluç Y, Ammann G, Barraud P, Jora M, Limbach PA, Motorin Y, et al. Instrumental analysis of RNA modifications. *Crit Rev Biochem Mol Biol*. **2021**;56(2):178-204.
205. Wilkinson DJ. Historical and contemporary stable isotope tracer approaches to studying mammalian protein metabolism. *Mass Spectrom Rev*. **2018**;37(1):57-80.
206. Nikonowicz EP, Sirr A, Legault P, Jucker FM, Baer LM, Pardi A. Preparation of 13C and 15N labelled RNAs for heteronuclear multi-dimensional NMR studies. *Nucleic Acids Res*. **1992**;20(17):4507-13.
207. Liu Y, Sousa R, Wang YX. Specific labeling: An effective tool to explore the RNA world. *Bioessays*. **2016**;38(2):192-200.
208. Liu Y, Yu P, Dyba M, Sousa R, Stagno JR, Wang YX. Applications of PLOR in labeling large RNAs at specific sites. *Methods*. **2016**;103:4-10.

209. Kellner S, Neumann J, Rosenkranz D, Lebedeva S, Ketting RF, Zischler H, et al. Profiling of RNA modifications by multiplexed stable isotope labelling. *Chem Commun (Camb)*. **2014**;50(26):3516-8.
210. Kellner S, Ochel A, Thüring K, Spenkuch F, Neumann J, Sharma S, et al. Absolute and relative quantification of RNA modifications via biosynthetic isotopomers. *Nucleic Acids Res*. **2014**;42(18):e142.
211. Heiss M, Reichle VF, Kellner S. Observing the fate of tRNA and its modifications by nucleic acid isotope labeling mass spectrometry: NAIL-MS. *RNA Biol*. **2017**;14(9):1260-8.
212. Thakur CS, Luo Y, Chen B, Eldho NV, Dayie TK. Biomass production of site selective 13C/15N nucleotides using wild type and a transketolase E. coli mutant for labeling RNA for high resolution NMR. *J Biomol NMR*. **2012**;52(2):103-14.
213. Nikonowicz EP, Pardi A. Three-dimensional heteronuclear NMR studies of RNA. *Nature*. **1992**;355(6356):184-6.
214. Dumelin CE, Chen Y, Leconte AM, Chen YG, Liu DR. Discovery and biological characterization of geranylated RNA in bacteria. *Nat Chem Biol*. **2012**;8(11):913-9.
215. Dal Magro C, Keller P, Kotter A, Werner S, Duarte V, Marchand V, et al. A Vastly Increased Chemical Variety of RNA Modifications Containing a Thioacetal Structure. *Angew Chem Int Ed Engl*. **2018**;57(26):7893-7.
216. Waghmare SP, Dickman MJ. Characterization and quantification of RNA post-transcriptional modifications using stable isotope labeling of RNA in conjunction with mass spectrometry analysis. *Anal Chem*. **2011**;83(12):4894-901.
217. Popova AM, Williamson JR. Quantitative analysis of rRNA modifications using stable isotope labeling and mass spectrometry. *J Am Chem Soc*. **2014**;136(5):2058-69.
218. Miranda-Santos I, Gramacho S, Pineiro M, Martinez-Gomez K, Fritz M, Hollemeyer K, et al. Mass isotopomer analysis of nucleosides isolated from RNA and DNA using GC/MS. *Anal Chem*. **2015**;87(1):617-23.
219. Paulines MJ, Limbach PA. Comparative Analysis of Ribonucleic Acid Digests (CARD) by Mass Spectrometry. *Methods Mol Biol*. **2017**;1562:19-32.
220. Paulines MJ, Limbach PA. Stable Isotope Labeling for Improved Comparative Analysis of RNA Digests by Mass Spectrometry. *J Am Soc Mass Spectrom*. **2017**;28(3):551-61.
221. Kung AW, Kilby PM, Portwood DE, Dickman MJ. Quantification of dsRNA using stable isotope labeling dilution liquid chromatography/mass spectrometry. *Rapid Commun Mass Spectrom*. **2018**;32(7):590-6.

222. Borland K, Diesend J, Ito-Kureha T, Heissmeyer V, Hammann C, Buck AH, et al. Production and Application of Stable Isotope-Labeled Internal Standards for RNA Modification Analysis. *Genes (Basel)*. **2019**;10(1).
223. Asadi-Atoi P, Barraud P, Tisne C, Kellner S. Benefits of stable isotope labeling in RNA analysis. *Biol Chem*. **2019**;400(7):847-65.
224. McLuckey SA, Van Berkel GJ, Glish GL. Tandem mass spectrometry of small, multiply charged oligonucleotides. *J Am Soc Mass Spectrom*. **1992**;3(1):60-70.
225. Limbach PA, Crain PF, McCloskey JA. Characterization of oligonucleotides and nucleic acids by mass spectrometry. *Curr Opin Biotechnol*. **1995**;6(1):96-102.
226. Calderisi G, Glasner H, Breuker K. Radical Transfer Dissociation for De Novo Characterization of Modified Ribonucleic Acids by Mass Spectrometry. *Angew Chem Int Ed Engl*. **2020**;59(11):4309-13.
227. Kowalak JA, Pomerantz SC, Crain PF, McCloskey JA. A novel method for the determination of post-transcriptional modification in RNA by mass spectrometry. *Nucleic Acids Res*. **1993**;21(19):4577-85.
228. Thakur P, Estevez M, Lobue PA, Limbach PA, Addepalli B. Improved RNA modification mapping of cellular non-coding RNAs using C- and U-specific RNases. *Analyst*. **2020**;145(3):816-27.
229. Lobue PA, Yu N, Jora M, Abernathy S, Limbach PA. Improved application of RNAModMapper - An RNA modification mapping software tool - For analysis of liquid chromatography tandem mass spectrometry (LC-MS/MS) data. *Methods*. **2019**;156:128-38.
230. Wein S, Andrews B, Sachsenberg T, Santos-Rosa H, Kohlbacher O, Kouzarides T, et al. A computational platform for high-throughput analysis of RNA sequences and modifications by mass spectrometry. *Nat Commun*. **2020**;11(1):926.
231. Jiang T, Yu N, Kim J, Murgo JR, Kissai M, Ravichandran K, et al. Oligonucleotide Sequence Mapping of Large Therapeutic mRNAs via Parallel Ribonuclease Digestions and LC-MS/MS. *Anal Chem*. **2019**;91(13):8500-6.
232. Li F, Su X, Bäurer S, Lämmerhofer M. Multiple heart-cutting mixed-mode chromatography-reversed-phase 2D-liquid chromatography method for separation and mass spectrometric characterization of synthetic oligonucleotides. *J Chromatogr A*. **2020**;1625:461338.

233. Li F, Lämmerhofer M. Impurity profiling of siRNA by two-dimensional liquid chromatography-mass spectrometry with quinine carbamate anion-exchanger and ion-pair reversed-phase chromatography. *J Chromatogr A*. **2021**;1643:462065.
234. Fountain KJ, Gilar M, Gebler JC. Analysis of native and chemically modified oligonucleotides by tandem ion-pair reversed-phase high-performance liquid chromatography/electrospray ionization mass spectrometry. *Rapid Commun Mass Spectrom*. **2003**;17(7):646-53.
235. Apffel A, Chakel JA, Fischer S, Lichtenwalter K, Hancock WS. Analysis of Oligonucleotides by HPLC-Electrospray Ionization Mass Spectrometry. *Anal Chem*. **1997**;69(7):1320-5.
236. Chen B, Bartlett MG. Evaluation of mobile phase composition for enhancing sensitivity of targeted quantification of oligonucleotides using ultra-high performance liquid chromatography and mass spectrometry: application to phosphorothioate deoxyribonucleic acid. *J Chromatogr A*. **2013**;1288:73-81.
237. Basiri B, Murph MM, Bartlett MG. Assessing the Interplay between the Physicochemical Parameters of Ion-Pairing Reagents and the Analyte Sequence on the Electrospray Desorption Process for Oligonucleotides. *J Am Soc Mass Spectrom*. **2017**;28(8):1647-56.
238. Lobue PA, Jora M, Addepalli B, Limbach PA. Oligonucleotide analysis by hydrophilic interaction liquid chromatography-mass spectrometry in the absence of ion-pair reagents. *J Chromatogr A*. **2019**;1595:39-48.
239. MacNeill R, Hutchinson T, Acharya V, Stromeyer R, Ohorodnik S. An oligonucleotide bioanalytical LC-SRM methodology entirely liberated from ion-pairing. *Bioanalysis*. **2019**;11(12):1157-69.
240. Pomerantz SC, McCloskey JA. Analysis of RNA hydrolyzates by liquid chromatography-mass spectrometry. *Methods Enzymol*. **1990**;193:796-824.
241. Crain PF. Preparation and enzymatic hydrolysis of DNA and RNA for mass spectrometry. *Methods Enzymol*. **1990**;193:782-90.
242. Jora M, Borland K, Abernathy S, Zhao R, Kelley M, Kellner S, et al. Chemical Amination/Imination of Carbonothiolated Nucleosides During RNA Hydrolysis. *Angew Chem Int Ed Engl*. **2021**;60(8):3961-6.
243. Kaiser S, Byrne SR, Ammann G, Asadi Atoi P, Borland K, Brecheisen R, et al. Strategies to Avoid Artifacts in Mass Spectrometry-Based Epitranscriptome Analyses. *Angew Chem Int Ed Engl*. **2021**;60(44):23885-93.

244. Karas M, Hillenkamp F. Laser desorption ionization of proteins with molecular masses exceeding 10,000 daltons. *Anal Chem*. **1988**;60(20):2299-301.
245. Douthwaite S, Kirpekar F. Identifying modifications in RNA by MALDI mass spectrometry. *Methods Enzymol*. **2007**;425:3-20.
246. Fenn JB, Mann M, Meng CK, Wong SF, Whitehouse CM. Electrospray ionization for mass spectrometry of large biomolecules. *Science*. **1989**;246(4926):64-71.
247. Kirpekar F, Nordhoff E, Kristiansen K, Roepstorff P, Lezius A, Hahner S, et al. Matrix assisted laser desorption/ionization mass spectrometry of enzymatically synthesized RNA up to 150 kDa. *Nucleic Acids Res*. **1994**;22(19):3866-70.
248. Nordhoff E, Kirpekar F, Karas M, Cramer R, Hahner S, Hillenkamp F, et al. Comparison of IR- and UV-matrix-assisted laser desorption/ionization mass spectrometry of oligodeoxynucleotides. *Nucleic Acids Res*. **1994**;22(13):2460-5.
249. Gehrke CW, Kuo KC. Ribonucleoside analysis by reversed-phase high-performance liquid chromatography. *J Chromatogr*. **1989**;471:3-36.
250. Nordhoff E, Kirpekar F, Roepstorff P. Mass spectrometry of nucleic acids. *Mass Spectrom Rev*. **1996**;15(2):67-138.
251. Su D, Chan CT, Gu C, Lim KS, Chionh YH, McBee ME, et al. Quantitative analysis of ribonucleoside modifications in tRNA by HPLC-coupled mass spectrometry. *Nat Protoc*. **2014**;9(4):828-41.
252. Urban PL. Quantitative mass spectrometry: an overview. *Philos Trans A Math Phys Eng Sci*. **2016**;374(2079).
253. Traube FR, Schiffers S, Iwan K, Kellner S, Spada F, Müller M, et al. Isotope-dilution mass spectrometry for exact quantification of noncanonical DNA nucleosides. *Nat Protoc*. **2019**;14(1):283-312.
254. Meyer KD, Jaffrey SR. The dynamic epitranscriptome: N6-methyladenosine and gene expression control. *Nat Rev Mol Cell Biol*. **2014**;15(5):313-26.
255. Heiss M, Borland K, Yoluç Y, Kellner S. Quantification of Modified Nucleosides in the Context of NAIL-MS. *Methods Mol Biol*. **2021**;2298:279-306.
256. Iwata R, Ido T, Takahashi T, Nakanishi H, Iida S. Optimization of [11C]HCN production and no-carrier-added [1-11C]amino acid synthesis. *Int J Rad Appl Instrum A*. **1987**;38(2):97-102.
257. Gkatza NA, Castro C, Harvey RF, Heiß M, Popis MC, Blanco S, et al. Cytosine-5 RNA methylation links protein synthesis to cell metabolism. *PLoS Biol*. **2019**;17(6):e3000297.

258. Meyer KD, Saletore Y, Zumbo P, Elemento O, Mason CE, Jaffrey SR. Comprehensive analysis of mRNA methylation reveals enrichment in 3' UTRs and near stop codons. *Cell*. **2012**;149(7):1635-46.
259. Hebras J, Krogh N, Marty V, Nielsen H, Cavaillé J. Developmental changes of rRNA ribose methylations in the mouse. *RNA Biol*. **2020**;17(1):150-64.
260. Brandmayr C, Wagner M, Brückl T, Globisch D, Pearson D, Kneuttinger AC, et al. Isotope-based analysis of modified tRNA nucleosides correlates modification density with translational efficiency. *Angew Chem Int Ed Engl*. **2012**;51(44):11162-5.
261. Hagelskamp F, Kellner S. Analysis of the epitranscriptome with ion-pairing reagent free oligonucleotide mass spectrometry. *Methods Enzymol*. **2021**;658:111-35.
262. Yoluç Y, van de Logt E, Kellner-Kaiser S. The Stress-Dependent Dynamics of Saccharomyces cerevisiae tRNA and rRNA Modification Profiles. *Genes (Basel)*. **2021**;12(9).
263. Sharma S, Entian KD. Chemical Modifications of Ribosomal RNA. *Methods Mol Biol*. **2022**;2533:149-66.
264. Decatur WA, Schnare MN. Different mechanisms for pseudouridine formation in yeast 5S and 5.8S rRNAs. *Mol Cell Biol*. **2008**;28(10):3089-100.
265. Johansson MJ, Esberg A, Huang B, Björk GR, Byström AS. Eukaryotic wobble uridine modifications promote a functionally redundant decoding system. *Mol Cell Biol*. **2008**;28(10):3301-12.
266. Laten H, Gorman J, Bock RM. Isopentenyladenosine deficient tRNA from an antisuppressor mutant of Saccharomyces cerevisiae. *Nucleic Acids Res*. **1978**;5(11):4329-42.
267. Powell CA, Minczuk M. TRMT2B is responsible for both tRNA and rRNA m(5)U-methylation in human mitochondria. *RNA Biol*. **2020**;17(4):451-62.
268. Levanon EY, Hallegger M, Kinar Y, Shemesh R, Djinovic-Carugo K, Rechavi G, et al. Evolutionarily conserved human targets of adenosine to inosine RNA editing. *Nucleic Acids Res*. **2005**;33(4):1162-8.
269. Boccaletto P, Machnicka MA, Purta E, Piatkowski P, Baginski B, Wirecki TK, et al. MODOMICS: a database of RNA modification pathways. 2017 update. *Nucleic Acids Res*. **2018**;46(D1):D303-d7.
270. Droogmans L, Grosjean H. 2'-O-methylation and inosine formation in the wobble position of anticodon-substituted tRNA-Phe in a homologous yeast in vitro system. *Biochimie*. **1991**;73(7-8):1021-5.

271. Mercer TR, Neph S, Dinger ME, Crawford J, Smith MA, Shearwood AM, et al. The human mitochondrial transcriptome. *Cell*. **2011**;146(4):645-58.
272. Barchiesi A, Vascotto C. Transcription, Processing, and Decay of Mitochondrial RNA in Health and Disease. *Int J Mol Sci*. **2019**;20(9).
273. Lander ES, Linton LM, Birren B, Nusbaum C, Zody MC, Baldwin J, et al. Initial sequencing and analysis of the human genome. *Nature*. **2001**;409(6822):860-921.
274. Su AI, Wiltshire T, Batalov S, Lapp H, Ching KA, Block D, et al. A gene atlas of the mouse and human protein-encoding transcriptomes. *Proc Natl Acad Sci U S A*. **2004**;101(16):6062-7.
275. Yu CH, Dang Y, Zhou Z, Wu C, Zhao F, Sachs MS, et al. Codon Usage Influences the Local Rate of Translation Elongation to Regulate Co-translational Protein Folding. *Mol Cell*. **2015**;59(5):744-54.
276. Nedialkova DD, Leidel SA. Optimization of Codon Translation Rates via tRNA Modifications Maintains Proteome Integrity. *Cell*. **2015**;161(7):1606-18.
277. Goffena J, Lefcort F, Zhang Y, Lehrmann E, Chaverra M, Felig J, et al. Elongator and codon bias regulate protein levels in mammalian peripheral neurons. *Nat Commun*. **2018**;9(1):889.
278. Sun B, Lorang C, Qin S, Zhang Y, Liu K, Li G, et al. Mouse Organ-Specific Proteins and Functions. *Cells*. **2021**;10(12).
279. Yu P, Zhou S, Gao Y, Liang Y, Guo W, Wang DO, et al. Dynamic landscapes of tRNA transcriptomes and translatomes in diverse mouse tissues. *Genomics Proteomics Bioinformatics*. **2022**.
280. Geiger T, Velic A, Macek B, Lundberg E, Kampf C, Nagaraj N, et al. Initial quantitative proteomic map of 28 mouse tissues using the SILAC mouse. *Mol Cell Proteomics*. **2013**;12(6):1709-22.
281. Towbin H, Staehelin T, Gordon J. Electrophoretic transfer of proteins from polyacrylamide gels to nitrocellulose sheets: procedure and some applications. *Proc Natl Acad Sci U S A*. **1979**;76(9):4350-4.
282. Taylor SC, Berkelman T, Yadav G, Hammond M. A defined methodology for reliable quantification of Western blot data. *Mol Biotechnol*. **2013**;55(3):217-26.
283. Rivera Del Rio A, Keppler JK, Boom RM, Janssen AEM. Protein acidification and hydrolysis by pepsin ensure efficient trypsin-catalyzed hydrolysis. *Food Funct*. **2021**;12(10):4570-81.

284. Dong MW. Tryptic mapping by reversed phase liquid chromatography. *Adv Chromatogr*. **1992**;32:21-51.
285. Rawlings ND, Barrett AJ. Families of serine peptidases. *Methods Enzymol*. **1994**;244:19-61.
286. Moritz CP. Tubulin or Not Tubulin: Heading Toward Total Protein Staining as Loading Control in Western Blots. *Proteomics*. **2017**;17(20).
287. Heiss M, Hagelskamp F, Marchand V, Motorin Y, Kellner S. Cell culture NAIL-MS allows insight into human tRNA and rRNA modification dynamics in vivo. *Nat Commun*. **2021**;12(1):389.
288. Chong ZX, Yeap SK, Ho WY. Transfection types, methods and strategies: a technical review. *PeerJ*. **2021**;9:e11165.
289. Dango S, Mosammaparast N, Sowa ME, Xiong LJ, Wu F, Park K, et al. DNA unwinding by ASCC3 helicase is coupled to ALKBH3-dependent DNA alkylation repair and cancer cell proliferation. *Mol Cell*. **2011**;44(3):373-84.
290. Juszkiewicz S, Chandrasekaran V, Lin Z, Kraatz S, Ramakrishnan V, Hegde RS. ZNF598 Is a Quality Control Sensor of Collided Ribosomes. *Mol Cell*. **2018**;72(3):469-81.e7.
291. Reichle VF, Weber V, Kellner S. NAIL-MS in E. coli Determines the Source and Fate of Methylation in tRNA. *Chembiochem*. **2018**;19(24):2575-83.
292. Motorin Y, Seidu-Larry S, Helm M. DNA and RNA Pyrimidine Nucleobase Alkylation at the Carbon-5 Position. *Adv Exp Med Biol*. **2016**;945:19-33.
293. Reichle VF, Kaiser S, Heiss M, Hagelskamp F, Borland K, Kellner S. Surpassing limits of static RNA modification analysis with dynamic NAIL-MS. *Methods*. **2019**;156:91-101.
294. Petrov A, Wu T, Puglisi EV, Puglisi JD. RNA purification by preparative polyacrylamide gel electrophoresis. *Methods Enzymol*. **2013**;530:315-30.
295. Sprinzl M, Horn C, Brown M, Ioudovitch A, Steinberg S. Compilation of tRNA sequences and sequences of tRNA genes. *Nucleic Acids Res*. **1998**;26(1):148-53.
296. Kawai G, Yamamoto Y, Kamimura T, Masegi T, Sekine M, Hata T, et al. Conformational rigidity of specific pyrimidine residues in tRNA arises from posttranscriptional modifications that enhance steric interaction between the base and the 2'-hydroxyl group. *Biochemistry*. **1992**;31(4):1040-6.

297. Judge AD, Sood V, Shaw JR, Fang D, McClintock K, MacLachlan I. Sequence-dependent stimulation of the mammalian innate immune response by synthetic siRNA. *Nat Biotechnol*. **2005**;23(4):457-62.